UNIVERSITÀ DEGLI STUDI DI SALERNO

UNIVERSITY OF SALERNO
Pharmacy Department

PhD program
in **Drug Discovery and Development**
Ciclo XXXVIII

PhD thesis in

Sustainable recovery of bioactive and functional compounds from natural sources

PhD student
Doctor *Simona Serio*

Tutor
Prof. *Anna Lisa Piccinelli*

Co-tutor
Prof. *Daniel Granato*

PhD program supervisor**: Prof. Alessandra Tosco**

List of abbreviations

AChE: Acetylcholinesterase;
AOC: Antioxidant capacity;
BBD: Box-Behnken design;
BChE: Butyrylcholinesterase;
CLS: Chronological Lifespan;
CSL: *Ceratonia siliqua* leaves;
DoE: Design of Experiment;
EE: Extraction Efficiency;
EY: Extraction Yield;
FGs: Flavonol glycosides;
Fs: Flavanones;
GGL: *Glycyrrhiza glabra* leaves;
GGs: N-galloylated glucosides;
Gla: Glabranin;
Lic: Licoflavanone;
Myr: Myricitrin;
NBFC: National Biodiversity Future Center;
NCDs: Non-communicable diseases;
P: Extraction purity;
PHWE: Pressurized Hot Water Extraction;
Pin: Pinocembrin;
Probe-UAE: Ultrasound Probe-Assisted Extraction;
RSM: Response Surface Methodology;
$ScCO_2$: Supercritical CO_2 extraction;
SDGs: Sustainable Development Goals;
SFE: Supercritical Fluid Extraction;
Sil: Siliquapyranone;
SLE: Solid-Liquid Extraction;
SLR: Solid-Liquid Ratio;
So: Soxhlet extraction;
TEAC: Trolox equivalent Antioxidant Capacity;
TeGG: 1,2,3,6-Tetragalloyl glucose;
TPC: Total Phenolic Content;
UAE: Ultrasound Assisted Extraction;
α-AMY: α-amylase;
α-GLU: α-glucosidase.

Chapter 1

Sustainable recovery of health-promoting from natural sources

1.1 Introduction

Healthy food and botanicals can make a significant contribution to health and well-being. The relationships between diet and disease are more widely understood and there is increased consumers awareness of “healthy eating” as they prefer products containing natural ingredients instead of artificially synthetized ones because natural products are usually considered as safer and with lower environmental impact [1]. This recent awareness is bringing new insights into the development of novel foods, functional foods and food supplements, containing “sustainable functional compounds”, bioactive compounds that could be recovered or biotechnologically produced from renewable resources providing health benefits to the consumers and at the same time being more eco-friendly. Therefore, a major turn toward natural ingredient will provide the consumers’ demand for healthier products and simultaneously a lower environmental impact during their production [2]. Within this frame the industry is increasing the development of novel foods to produce functional food items, food additives, dietary supplements and herbal products as well as pharmaceutical and cosmetic industries are increasing their interest in natural compounds as a source for product formulation or lead compounds. Actually, compounds derived from natural sources, mainly specialized metabolites, have played a key role in drug discovery for their link with the prevention or reduced progression of many non-communicable diseases, such as cardiovascular disease, cancer, diabetes and neurodegenerative diseases. Their use in traditional medicine may provide insights regarding efficacy and safety [3]. The term functional and/or bioactive compound is used to denote natural compounds that possess biological activities. These compounds occur naturally as plant and/or microbial metabolites and the plant-based foods are rich source of them. Health-promoting and -protective properties of bioactives from foods are the tangible example of Hippocrates’ saying, “*Let food be your medicine*” [2]. Thus, the interest for value-added food is constantly flourishing as an equally increasing number of studies proves or highlights their benefits to human health. Accordingly, if a food has claimed on improving health and is frequently being associated with holistic therapies, such food can be termed

as a functional food. Some foods considered to be functional are fruits, vegetables, cereals, seaweed, and herbal products. Agricultural by-products are also becoming very popular due to their high content of bioactive compounds and the development of a circular economy that converts waste into eco-sustainable products [4].

Nowadays, the recovery and enrichment processes of bioactive compounds from different food or vegetal sources represents a challenging step, with problems related to costs, efficiency, selectivity, environmental sustainability and which should also respect the 12 principles of the “Green chemistry”, a set of criteria and guidelines for developing sustainable processes [5,6]. Traditional extraction methods, such as Soxhlet extractions, distillation, maceration are time and energy consuming as well as requires huge amount of solvents, often toxic or polluting [7]. Instead, new green extraction techniques are based on processes with low energy consumption, which allow the use of alternative solvents or non-toxic solvents, renewable raw material, and yield safe and high-quality extracts/products [8]. The compressed fluids techniques can satisfy many of the green extraction principles, depending on the solvents and conditions used for extracting the natural compounds [9].

They are usually designed to be more sustainable and environment friendly in order to achieve the targets of Sustainable Development Goals (SDGs) designed by United Nations General Assembly and the principles of the green chemistry [7].

The apparent simplicity of this concept conceals a series of substantial challenges that the modern processing industry must overcome. In the current sustainability-driven era, the recovery of bioactive compounds from natural matrices cannot rely solely on efficiency or yield: it must also ensure that the entire process poses no risk to human health or to the environment [2].

1.2. Sustainable Development Goals of United Nations

In this study, the selection of plant matrices and their subsequent exploitation for the recovery of bioactive compounds using innovative extraction technologies is aligned with the guiding principles of the SDGs, a set of 17 global objectives adopted as part of the 2030 Agenda for Sustainable Development (Fig. 1.1). These goals constitute a shared international framework aimed at addressing the major social, environmental, and economic challenges threatening global sustainability [Sitography 1].

Figure 1.1. *17 SDGs of EU United Nations.*

Among the 17 SDGs, three goals, SDG 3 (Good Health and Well-Being), SDG 12 (Responsible Consumption and Production), and SDG 2 (Zero Hunger), are particularly relevant for the matrix selection in this research project. These goals emphasize the importance of promoting human health through natural and safe resources (SDG 3), ensuring sustainable and ethical production systems (SDG 12), and valorizing plant biodiversity to enhance food security and nutritional quality (SDG 2).

The SDG 3, which aims to ensure healthy lives and promote well-being for all, highlights the importance of dietary strategies that support human health. In this context, functional foods (foods that provide benefits beyond basic nutrition) play a relevant role, as they contribute to maintaining physiological

balance and reducing risk factors associated with non-communicable diseases[10]. Since ancient times, edible and medicinal plants have been used across cultures for their health-promoting properties, and they continue to represent rich sources of bioactive compounds with demonstrated potential to support metabolic, cognitive, and antioxidant functions [11,12]. Investing in the study and valorization of food matrices rich in such compounds is therefore aligned with SDG 3, as it provides opportunities to develop ingredients capable of contributing to overall well-being and long-term health maintenance.

The SDG 12 aims to use environmentally friendly production methods and reduce the amount of waste. To pursue this goal the huge amount of fruit and vegetable wastes generated by agro-food industries could be use as raw material potentially rich in bioactive compounds. According to various scientific evidence these wastes could constitute a source of bioactive substances, and their valorization could lead to a circular economy in which industry and society could benefit [13]. The linear economy model traditionally adopted by food companies is based on a “take – produce – consume - discard” logic, which leads to the generation of substantial amounts of waste and contributes significantly to environmental degradation and climate change. In contrast, the circular economy promotes a more efficient and regenerative use of resources: waste streams are reconsidered as valuable inputs, and cost optimization is achieved through strategies that extend product life cycles without compromising consumer demand. Companies embracing circular principles adopt a “produce – use – recover – reprocess - recycle” framework, effectively reducing the volume of waste and by-products generated and mitigating the pressure on natural resources[10].

In addition, the SDG2 (Zero Hunger) intends to achieve food security and promote sustainable agriculture. Agricultural diversification is a formidable tool for achieving the SDG2, and all the crops that are relatively “underutilized” could be a good source of micronutrients, protein, energy and fibers which make them attractive for possible research, Research studies proved that the underutilized plant crops and food processing residues are the gold mines of functional ingredients which have the potential to provide nutritional, biological and technological functionalities.

Sustainability is not only about choosing plant matrices, but also, selecting the most appropriate extraction techniques for recovering functional metabolites. Three SDGs are particularly relevant in guiding the assessment of the best technological choices: SDG 7 (Affordable and Clean Energy), SDG 12 (Responsible Consumption and Production), and SDG 13 (Climate Action).

SDG 12 promotes sustainable and responsible production models, requiring extraction processes that minimize environmental impact and the production of waste. This involves replacing petrochemical solvents with biodegradable, non-toxic, and recyclable alternatives, as well as reducing waste and post-processing steps. Innovative unconventional extraction techniques, such as supercritical fluid extraction, pressurized liquid extraction, ultrasound-assisted extraction, and microwave-assisted extraction, are consistent with the sustainable production of green extracts and principles of green chemistry.

The link with SDG 13, relating to climate action, is equally direct. The use of non-petroleum-based solvents and processes that promote high energy efficiency helps to reduce the carbon footprint of extraction processes. Furthermore, the possibility of scaling up many innovative techniques without proportionally increasing the environmental industrial impact ensures greater sustainability of the production cycle [14].

Finally, SDG 7 emphasizes the need to reduce energy consumption and increase the efficiency of industrial processes. Compared to conventional techniques, emerging extraction techniques are generally characterized by lower energy requirements, shorter cycles and therefore shorter overall times. These SDGs provide a clear strategic framework for guiding the selection of plant matrices in a perspective of sustainable functional compounds recovery. Consequently, choosing a sustainable matrix must be accompanied by its exploitation through equally sustainable extraction technologies, methods that are efficient, scalable, and genuinely environmentally responsible, to obtain high-value functional ingredients while minimizing environmental impact.

1.3. Green extraction of natural products

A key challenge in developing sustainable extraction protocols is the careful selection of operating parameters, as these significantly influence the effectiveness of the process. The optimization of operating conditions is essential to maximize the recovery of target compounds, improve the valorization of raw materials and product quality, and reduce environmental impact [15,16]. In recent years, the growing focus on sustainability and the circular economy has highlighted the need to apply the principles of green chemistry to the extraction of natural products. Twenty-five years ago, Anastas and Warner introduced the 12 principles of green chemistry, emphasizing the importance of reducing the use and generation of hazardous substances [17]. The six principles of green extraction of natural products [6,8,17], which represent the extension of green chemistry to the recovery of natural compounds, fit into this context (Fig.1.2).

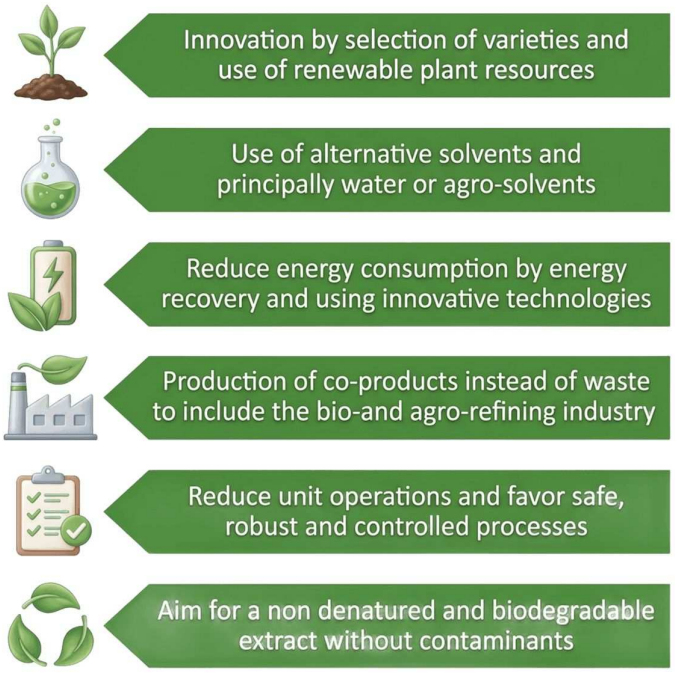

Figure 1.2. *The six principles of green extraction of natural products [6,17].*

The first principle concerns the conscious selection of matrices, favoring sustainable or underutilized biomasses rich in bioactive secondary metabolites and often derived from agri-food waste, in line with the objectives of the circular bioeconomy [17]. Environmental protection is essential; history shows that the overexploitation of plants can lead to species becoming rare or causing their extinction, so biodiversity conservation is crucial for future generations. Key strategies for preventing the loss of endemic species include the use of renewable resources, plant breeding and innovative biotechnological processes [8]. The second principle concerns the choice of solvents: in addition to environmental safety, it is essential to ensure safety in use (flammability, volatility), favoring water or alternative solvents such as ILs, DES, supercritical fluids, surfactants, or edible oils, which represent greener solutions compared to traditional organic solvents [18] and meet both technological and economical demands. Less use of hazardous solvents is also one of the EU environmental policy and legislation priorities for 2010-2050 [8]. The third principle emphasizes the need to reduce energy consumption: since many traditional extraction processes are energy-intensive, the sustainable approach involves optimization of extraction parameters, energy recovery, and the adoption of renewable technologies that increase yield without requiring high energy inputs [18]. The fourth principal fits into the concept of biorefinery, in which biomass is converted into multiple value-added products while minimizing waste production, according to the fundamentals of the circular bioeconomy [6,17]. The fifth principle concerns the simplification of the process chain (Process Intensification): reducing unit operations means reducing costs, consumption, and environmental impact. Techniques such as supercritical CO_2 extraction represent optimal choices as they integrate multiple stages into a single clean and easily scalable process [6]. Finally, in the sixth principle the concept of naturalness is established. A sustainable green extract must be natural, safe (absence of contaminants), traceable, high quality and functionality with active and non-denatured compounds and with a low environmental footprint in accordance with specific legislation concerning the application sector [8].

Chapter 2

Selection of valuable matrices as source of health-promoting compounds

Part of this work was conducted in collaboration with:
[1] Professor Paola Coccetti research group – University of Milano Bicocca (Italy)

2.1. Introduction

Biodiversity represents one of the planet's greatest resources and a fundamental heritage for life on Earth, encompassing economic, ecological, scientific, ethical, and cultural dimensions. Safeguarding biodiversity is essential for maintaining the stability and resilience of ecosystems, and beyond its ecological role, it also contributes to human physical and mental wellness [19]. The Mediterranean basin is one of the world's most important biodiversity hotspots, and Italy, with its diverse geology, climate, and topography, boasts one of the richest flora heritages in Europe, characterized by exceptional species richness and endemism. Currently, biodiversity is increasingly threatened by habitat destruction, pollution, climate change, overexploitation of natural resources, and the spread of alien species[20].

To address the ongoing biodiversity crisis, and in line with the EU 2020-2030 Biodiversity Strategy and the SDGs, Italy has adopted a new national strategy aimed at protecting and enhancing its biological heritage. A major milestone in this process was reached in February 2022, when the protection of the environment, biodiversity, and ecosystems was incorporated into the fundamental principles of the Italian Constitution, marking a historic shift toward an ethic of environmental responsibility. In the same year, the National Biodiversity Future Center (NBFC) was established. Funded through the National Recovery and Resilience Plan (PNRR) within the Next Generation EU framework, NBFC is the first Italian research center entirely dedicated to the monitoring, conservation, restoration, and valorization of biodiversity. The Center is articulated into eight Spokes, each comprising several research activities.

Within NBFC Spoke 6 "Biodiversity and Human Wellbeing", this research project is focused on the valorization of Italian flora biodiversity through a large-scale bioprospecting strategy (Figure 2.1).

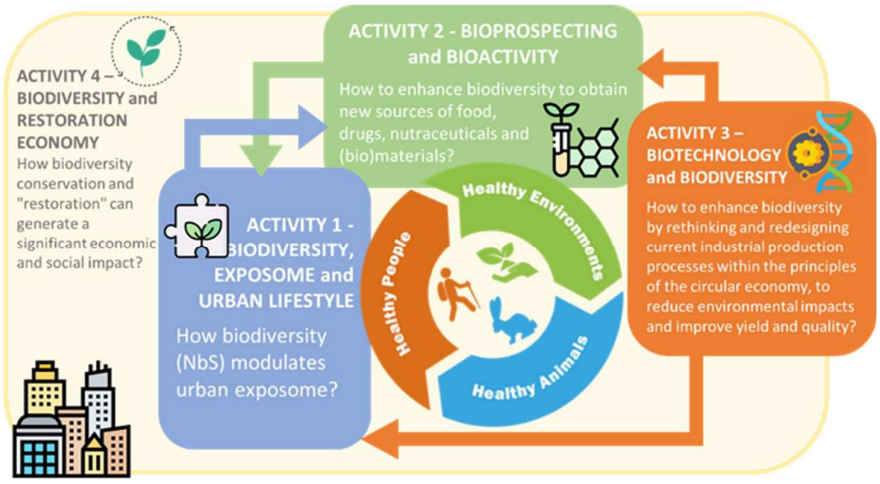

Figure 2.1. *Research activities of NBFC spoke 6 (Biodiversity and Human Wellbeing).*

Hence, a bioprospecting platform was established to explore the extensive phytochemical diversity of Italian vascular and non-vascular flora (over 11,000 species). Approximately 700 species were selected on a phylogenetic basis, ensuring a representative collection of all major Italian plant families [21]. A subset of these plant extracts (112) was subjected to an integrated screening platform combining software-assisted metabolomic profiling (UHPLC-DAD-HRMS/MS) with *in vitro* bioactivity assays targeting mechanisms relevant to non-communicable diseases (NCDs). Like in a funnel-shaped diagram, the most interesting plant were matched with literature, value of agri-food supply chain, and "environmental preservation" and "resource optimization" criteria to select the most promising natural sources for the sustainable recovery of bioactive and functional compounds through green extraction processes. In this frame, the recovery and restoration of biodiversity not only preserve Italian ecosystem integrity but also open new opportunities for bioprospecting, enabling the discovery of plants and phytochemicals with promising applications. By unlocking this natural chemical diversity, biodiversity-centered research can support the development of new drugs, nutraceuticals, dietary supplements, functional foods, cosmetics, and more sustainable agricultural products, thereby transforming Italian rich biological heritage into a driver of innovation and human well-being.

The main objectives achieved in this study were:

- Implementation of a **software-assisted untargeted UHPLC-HRMS/MS procedure** for the rapid and semi-automated profiling of Italian flora plant extracts;
- High-throughput screening of antioxidant, neuroprotective and hypoglycemic potential of Italian flora plant extracts by ***in vitro* assays**;
- **Selection of the most valuable sources** for the recovery of bioactive compounds through sustainable extraction methods.

2.2. Bioprospecting studies on Italian flora biodiversity

In accordance with the NBFC project, a bioprospecting campaign was conducted across Italian areas of high biodiversity. Approximately 700 plant species belonging to the main Italian botanical families were selected based on phylogenetic diversity, habitat variability (alpine, mediterranean and insular), chemodiversity, traditional safety of use, and the limited phytochemical characterization available. Two major plant groups were considered: species collected from botanical gardens and commercial nurseries (~75% Angiosperms, 15% Bryophytes, 10% Gymnosperms and Pteridophytes); species not commercially available, sampled directly in natural habitats.

For each species, aerial parts (mainly leaves and stems, and reproductive organs when present) were collected following a pooled design: three independent pools per species, each consisting of 5-10 individual plants to minimize inter-individual variability. Sampling was performed during predefined seasonal windows (2022-2024), depending on species phenology. Species identity was validated by a systematic botanist, and voucher material was deposited for herbarium and genotype barcoding.

For the first three sampling campaigns, 112 plant extracts, selected as part of the bioprospecting study from University of Verona, were analyzed with the aim of evaluating potential health-promoting activities and profiling secondary metabolites. Table A1 reports the species investigated, their botanical families, traditional uses [Sitography 2] and their inclusion in Belfrit list. All plant extracts were profiled through an untargeted metabolomic approach to identify key specialized metabolite classes and the main compounds. To evaluate their biological relevance, a set of rapid *in vitro* assays was chosen to efficiently discriminate extracts with antioxidant, neuroprotective, and antihyperglycemic potential. The selection of these assays was guided by the global impact of NCDs, including cardiovascular diseases, diabetes, atherosclerosis, neurodegenerative disorders, cancer, and chronic respiratory diseases, which represent the leading cause of mortality worldwide and account for nearly 70% of deaths in both Europe and Italy [Sitography 3]. Among the multiple causes

of NCDs, many are directly linked to enzyme dysfunction, whether deficiency or overexpression, making enzyme inhibition a key strategy to slow disease progression [11]. Considering the importance of medicinal plants as natural enzyme inhibitors and the exceptional richness of Italian plant biodiversity, this section highlights plant species with inhibitory activity against clinically relevant enzymes and their antioxidant *in vitro* potential. The investigation focused on acetylcholinesterase (AChE) and α-glucosidase (α-GLU) inhibition, complemented by antioxidant capacity (AOC) assessment through the ABTS assay. All bioactivity data were integrated with software-assisted metabolomic profiling to correlate chemical composition with biological effects, identify key metabolites or active chemical classes, and highlight the most promising species for future in-depth studies.

2.2.1. Software assisted untargeted UHPLC-HRMS/MS profiling

The initial step of this research involved the set-up of a software-assisted untargeted UHPLC-DAD-HRMS/MS procedure, enabling the high throughput profiling of secondary metabolites from a substantial number of extracts. This screening phase acts as a starting point for the evaluation and characterization of natural sources distinguished by a peculiar and rich bioactive profile, which can be the focus of further in-depth investigations.

A single chromatographic method suitable for the separation of a wide range of molecules with high diversity of chemical classes and polarity range (phenolic compounds, flavonoids, saponins, terpens, alkaloids) was optimized. For untargeted HRMS detection, a data-dependent acquisition mode (Full HRMS/dd-MS2, m/z 150-1500), covering the broad range of molecular masses of specialized metabolites, and the simultaneous acquisition in both positive and negative ion modes were used to obtain complementary information that simplifies and accelerates the compound characterization. A tailored workflow was created for the characterization of a wide range of secondary metabolites. This workflow managed to perform retention time alignment, unknown compound detection, elemental composition prediction for all compounds and chemical background hiding. High-confidence matching was achieved using

an in-house mzVault spectral library comprising 120 reference standards (level 1 of identification) and 184 MS/MS spectra acquired under the same chromatographic and MS conditions used for plant extract screening. Where available, both positive and negative ionization spectra were included to obtain complementary fragmentation information. For each compound, the corresponding retention time, precursor ion (m/z), collision energy, molecular formula and structural data were added. Additional identification layers were provided by mzCloud for MS/MS-based spectral matching, Predict Compositions and ChemSpider. Since Mass List and ChemSpider lack MS/MS spectra, their annotations were refined through mzLogic and Apply Spectral Distance Filter, ensuring spectral and structural consistency. In addition, UHPLC-HRMS/MS data of compounds tentatively identified by online libraries and chemotaxonomic data (level 2 of identification) were exported in in-house library, with the aim of broadening our experimental library after identifying compounds in the analyzed plants. When reference MS/MS data were not available, a tentative structure was assigned to the detected molecule based on the fragmentation patterns and spectra of structurally analogous molecules and using CD additional tools, such as the FISh Scoring and Similar Compound functions (Level 3 of identification).

This procedure enabled rapid, robust, and semi-automated annotation, providing a tailored and comprehensive screening of secondary metabolites and their main chemical classes in 112 investigated plant extracts. Further in-depth characterization studies were subsequently conducted on the extracts from plant species that showed the most promising biological and phytochemical profiles.

2.2.2 AOC and Phytochemical Correlation[1]

Antioxidant potential of the plant extracts was evaluated through the ABTS radical-scavenging assay, as it is recognized as one of the most widely used AOC methods in research laboratories. It is experimentally simple, cost-effective, and provides rapid and highly reproducible results. Its extensive use in the literature also offers a substantial advantage: data generated with the

ABTS method can be easily compared with previously published studies, ensuring broader interpretability and methodological consistency [22]. Trolox was used as the positive control, and the antioxidant activity of each extract was expressed as Trolox Equivalent Antioxidant Capacity (TEAC), a standardized and widely adopted unit that allows robust comparison of AOC across different studies and laboratories.

In this study, the extracts were initially tested at 1 mg mL^{-1}, and only those extracts showing > 50% inhibition of ABTS radical absorbance were further analyzed to determine TEAC (mmol Trolox equivalent g^{-1} extract) using a multi-level calibration curve. Quercetin, a natural compound recognized for its strong antioxidant activity, was used as a positive control (10.0 ± 0.5 mM TE mM^{-1}).

For AOC, three levels of activity were defined, based on TEAC values: low (< 2), medium (2 - 4), and high (> 4 mmol TE g^{-1} extract). The TEAC values obtained for all 112 screened plant extracts are reported in Table A2 and showed in heatmap (Fig. 2.2).

Preliminary analysis identified 30 species with medium-high AOC (TEAC > 2). All of them show a high total polyphenol content (160 - 466 mg GAE g^{-1} extract). A strong correlation between TEAC and TPC (Pearson correlation coefficient, r = 0.85) confirms the role of polyphenols in antioxidant activity, while no significant correlation emerges with Total Flavonoid Content and Proanthocyanidin Content (data not shown). This is consistent with the evidence that overall AOC depends primarily on the total pool of phenolic constituents rather than on specific subclasses of secondary metabolites.

Among the 30 active species, 15 show high antioxidant power (TEAC > 4 mmol TE/g): *Aeonium arboreum*, *Carissa macrocarpa*, *Ceratonia siliqua*, *Cistus laurifolius*, *Euphorbia pithyusa*, *Filipendula ulmaria*, *Glycyrrhiza glabra*, *Gratiola officinalis*, *Heuchera sanguinea*, *Inula salicina*, *Juniperus oxycedrus*, *Lythrum salicaria*, *Phoenix dactylifera*, *Rosa canina*, and *Trapa natans*. UHPLC-HRMS/MS profiling of these extracts shows that the most represented classes, and presumably those responsible for the observed activity, include hydrolyzable tannins (ellagitannins and gallotannins), flavan-3-ols (catechins, gallocatechins, and their polymers), and flavonols (quercetin, myricetin, and

kaempferol glycosides). These phenolic groups are recognized in literature data as some of the most potent natural antioxidants [23–25].

To confirm the chemical antioxidant screening results, the most active extracts were evaluated in a model of humanized yeast cells overexpressing α-synuclein, a condition known to induce elevated intracellular ROS levels and severe oxidative stress, by Prof.ssa Paola Coccetti of University of Milano Bicocca research group. Among the tested extracts, five of them (*Aeonium arboretum*, *Glycyrrhiza glabra*, *Gratiola officinalis*, *Inula salicina* and *Rosa canina*) showed a particularly strong antioxidant response (Fig. 2.2), reducing intracellular ROS by 51-87%.

2.2.3. AChE Inhibitory Activity and Phytochemical Correlation

Alzheimer's disease (AD), the most common neurodegenerative disorder in the elderly, is characterized by marked cognitive decline largely attributable to cholinergic dysfunction, in particular the progressive loss of cholinergic neurons and the resulting reduction in acetylcholine (ACh) levels. As the disease progresses, the activity of AChE, which is initially predominant, tends to decrease, particularly in areas affected by amyloid deposits, contributing to cholinergic deficiency [26]. For this reason, the search for inhibitors that are active against AChE represents a promising strategy for increasing ACh levels in the synaptic cleft and improving cognitive functions.

The AChE inhibitory activities of 112 plant extracts were evaluated using a fluorescent procedure developed by Sanchez-Martínez et al. [27] to overcome the drawbacks of colorimetric Ellman's method in analyzing plant extracts (absorbance measured at 412 nm). The commonly used drug galantamine (IC_{50}= 2.6 ± 0.1 μM) was used as positive control.

For this assay, inhibitory potency of plant species was defined according to the cutoff values proposed by Dos Santos et al. [28] for plant extracts, which define three ranges: extracts with IC_{50} > 200 μg mL^{-1} are considered to have low activity, those with IC_{50} between 200 and 20 μg mL^{-1} have medium activity, while IC_{50} < 20 μg mL^{-1} identifies extracts with high inhibitory potency. Hence, in this study extracts were initially screened at a final well concentration of 200

µg mL^{-1}. Only those exhibiting > 50% inhibition were subsequently selected for IC_{50} determination, expressed in µg mL^{-1}, using a dose-response inhibition curve.

The results of the AChE inhibition assays (Table A2) are summarized in the heatmap (Fig. 2.2) and revealed five highly active plants, with values ranging from 5.6 to 18.9 µg mL^{-1}: *Carissa macrocarpa*, *Ceratonia siliqua*, *Euphorbia pithyusa*, *Juniperus oxycedrus*, and *Sternbergia lutea*. UHPLC-HRMS/MS profiling of these extracts revealed several classes of secondary metabolites, including alkaloids, terpenes, flavonols, proanthocyanidins, and hydrolyzable tannins, all known for their neuroprotective and antioxidant potential.

The data obtained for *S. lutea* (IC_{50} = 8.1 µg mL^{-1}) are fully consistent with the literature; the *Amaryllidaceae* family is known for producing specific alkaloids with a wide range of physiological effects, particularly on the central nervous system, often mediated by the inhibition of AChE and BChE. Alkaloids such as galantamine, emantamine, lycorine, and pancratistatin are considered lead molecules in research into new therapies for AD, and interest in this class has grown, especially since galantamine FDA approval in 2001 for the treatment of mild to moderate AD [29].

In addition to alkaloids, phenolic compounds also play an important role. In the case of *C. macrocarpa* (IC_{50} = 5.6 µg mL^{-1}), the data are consistent with the review by Ghanem et al. [30], which reports an AChE IC_{50} of 4.0 ± 0.2 µg mL^{-1} for the methanolic extract of the aerial parts (leaves and stems), compared to 0.074 ± 0.004 µg mL^{-1} for donepezil (positive control). The authors attribute this activity to the interactions of phenolic functional groups with the enzyme site, which can induce denaturation and reduction of catalytic activity. For *C. siliqua* (IC_{50} = 18.9 µg mL^{-1}), a research study showed that the pulp extract of pods has high inhibitory activity against AChE (IC_{50} = 13.19 µg mL^{-1}) [31]. This inhibitory capacity has been attributed to the high abundance of phenolic compounds, a class of metabolites widely recognized for their cholinesterase-inhibiting properties; this is consistent with our results, which show gallotannins and other phenols in *C. siliqua*, probably responsible for the observed activity.

In the case of *E. pithyusa* (IC_{50} = 10.2 µg mL^{-1}), one of the main secondary metabolites identified is a sulfated derivative of ellagic acid, extensively studied

for its potential to reduce oxidative stress and for its significant neuroprotective activity, linked to its free radical scavenging action. The low IC_{50} reported for ellagic acid (45.6 µM; [32]) is consistent with the strong inhibitory activity observed for *E. pithyusa* extracts, in which this compound represents one of the major constituents. For *J. oxycedrus*, our results (IC_{50} = 7.1 µg mL^{-1}), are consistent with Tavares et al. [33] studies on the leaves of four species of *Juniperus* (*J. navicularis*, *J. oxycedrus*, *J. phoenicea*, and *J. turbinata*) which contain a wide range of phenolic compounds with significant inhibitory activity against AChE and a marked ability to scavenge intracellular radicals in neuronal models subjected to oxidative stress.

2.2.4. α-GLU Inhibitory Activity and Phytochemical Correlation

Postprandial hyperglycemia is a key pathological feature of diabetes mellitus and a major driver in the onset and progression of type 2 diabetes (T2DM) and its complications, including cardiovascular disease, nephropathy, and neuropathy [34,35]. A well-established therapeutic strategy to control postprandial glucose levels is the inhibition of the digestive enzymes α-amylase (α-AMY) and α-GLU, which slows carbohydrate absorption. Numerous plant-derived compounds have demonstrated potent and often safer inhibitory activity toward these enzymes, highlighting their potential in the management of T2DM [36].

For this assay, activity ranges were defined using an approach analogous to that adopted for AChE, integrating literature data [34,35,37] and the experimental IC_{50} of quercetin (4.8 µg mL^{-1}), a selective natural α-GLU inhibitor stronger than acarbose, to establish the activity thresholds. Three cut-offs were determined multiplying quercetin IC_{50} by a factor of 10: IC_{50} > 200 µg mL^{-1} (low activity), 200-50 µg mL^{-1} (medium activity), and < 50 µg mL^{-1} (high activity). Also, for α-GLU inhibitory assay, extracts were initially screened at a final well concentration of 200 µg mL^{-1}. Only those exhibiting > 50% inhibition were subsequently selected for IC_{50} determination, expressed in µg mL^{-1}, using a dose-response inhibition curve.

The α-GLU inhibition screening (Table A2) revealed 34 highly active plant species (IC_{50} < 50 μg mL^{-1}), with values ranging from 0.1 to 44.9 μg mL^{-1}. The best-performing species, divided by botanical family, are shown in the heatmap (Fig. 2.2). Some families proved to be particularly rich in enzyme inhibitors, including *Apocynaceae* (2/4), *Cistaceae* (2/2), *Crassulaceae* (3/3), *Cupressaceae* (4/4), *Fabaceae* (3/6), *Lythraceae* (2/2), *Rosaceae* (5/6), and *Saxifragaceae* (2/2). UHPLC-HRMS/MS profiles show that plant extracts of these species are mainly characterized by proanthocyanidins, tannins (gallotannins and ellagitannins), flavonoids, and their derivatives, classes widely recognized for their ability to modulate postprandial glucose levels.

Proanthocyanidins, widely represented in many of the active species, are among the most studied classes for their beneficial effects on glycemic homeostasis. Although known for their very low bioavailability, they exert their action mainly inhibiting intestinal α-GLU, favorably modulating the microbiota, protecting the intestinal barrier, and reducing postprandial hyperglycemia. Their antioxidant, hypoglycemic, and anti-inflammatory properties further contribute to the prevention and management of type 2 diabetes and its complications [38].

Moving on to tannins, the predominant metabolites in *Cistaceae*, *Lythraceae*, *Rosaceae* and *Crassulaceae*, show high inhibitory potency against α-GLU. As reported by Dirir et al. [34], several tannins exhibit IC_{50} values between 2.9 and 68.4 μM, substantially lower than that of acarbose (174 μM), with procyanidin A2 standing out as one of the most potent inhibitors (IC_{50} = 0.47 μM). Above all, gallotannins were the main metabolites of the most active species, such as *Ceratonia siliqua*, *Diospyros kaki*, *Heuchera sanguinea*, *Kalanchoë daigremontiana*, and *Trapa natans*. In the study by Liu et al. [39], it was demonstrated that the inhibitory activity of gallotannins increases proportionally to the number of galloyl groups, thanks to their ability to form hydrogen bonds and hydrophobic interactions with the enzyme. Furthermore, both pentagalloylglucose and tannic acid have shown hypoglycemic effects equal to or greater than those of acarbose in *in vitro* and *in vivo* tests, significantly reducing postprandial blood glucose in diabetic mice in sucrose, maltose, and starch tolerance tests.

Flavonoids are also reported as good inhibitors, with documented activity for numerous subclasses: isoflavonoids, flavanones, flavanols, flavonols, and flavones. Different flavonoids show greater efficacy than acarbose [34]. Among flavanols, catechin, occurring in several active species, including *Aeonium arboreum*, *Cydonia oblonga*, *Cistus laurifolius*, and *Cistus monspeliensis*, has demonstrated a competitive inhibitory mechanism against α-GLU, with efficacy comparable to that of acarbose [35].

Flavonols such as quercetin, kaempferol, and myricetin, widely distributed in the *Apocynaceae*, *Cistaceae*, *Crassulaceae*, *Cupressaceae*, and *Fabaceae* families, are among the most studied natural inhibitors of α-GLU and are reported to be more potent than acarbose according to many experimental findings [35].

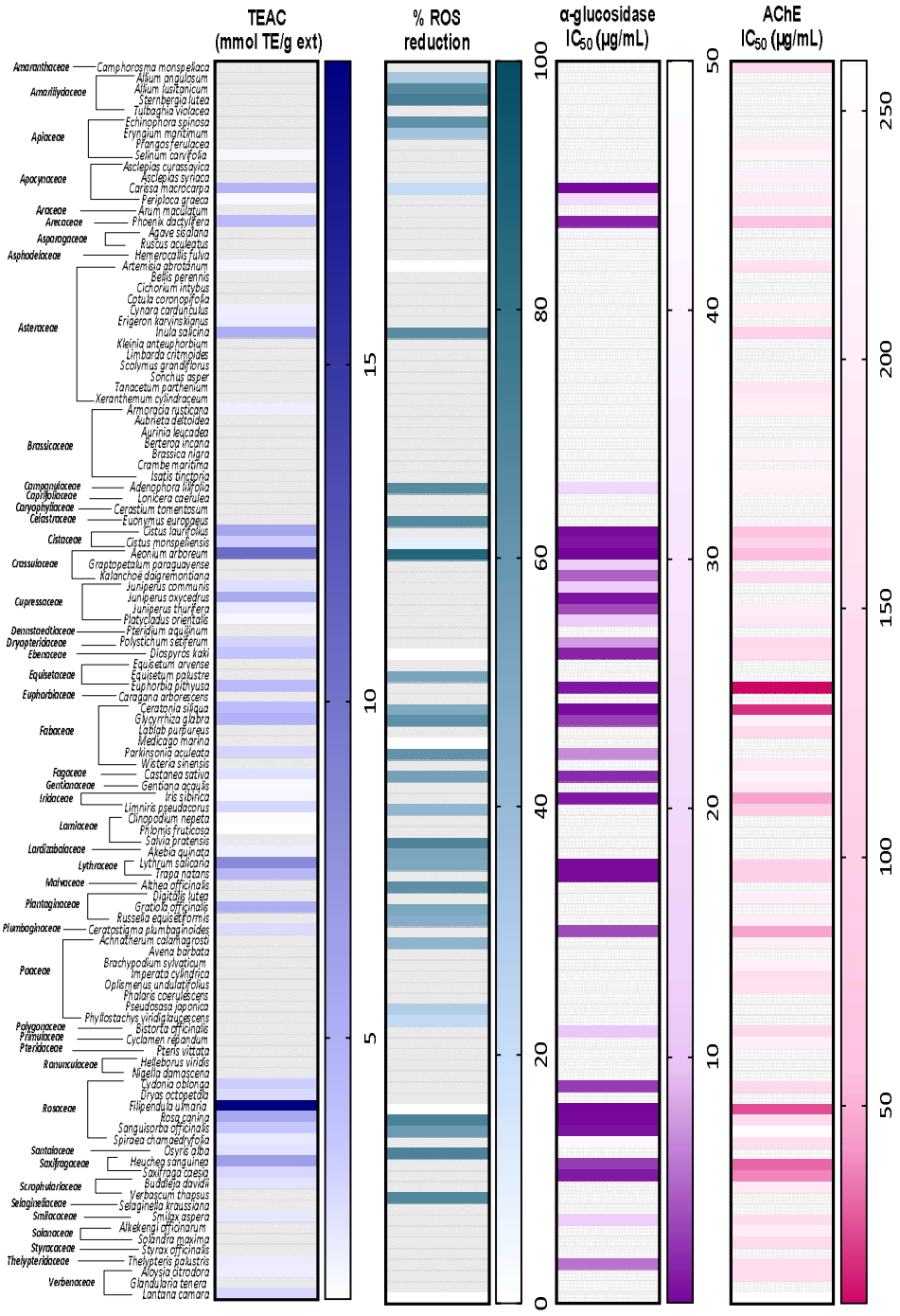

Figure 2.1 *Heatmap of antioxidant screening assays (ABTS* and *ROS reduction) and enzyme inhibition assays (α-GLU and AChE) of 112 investigated extracts from Italian flora.*

2.3. Selection of the most valuable matrices

Like in a funnel-shaped diagram, chemical profiling data and *in vitro* bioactivity results, including AOC and AChE/α-GLU inhibitory assays, were integrated with literature evidence, agro-food supply chain relevance, and criteria related to environmental preservation and resource optimization. This multilevel integration allowed the identification of the most promising natural matrices for the sustainable recovery of bioactive and functional compounds through green extraction strategies.

Among the aerial-part extracts screened, representing 47 botanical families, two species emerged as particularly valuable due to their distinctive phytochemical profile, potential *in vitro* activities, and strategic importance within the agro-food sector: *Ceratonia siliqua* (CSL) and *Glycyrrhiza glabra* leaves (GGL).

These plants belong to the Fabaceae, one of the largest and most chemically diverse plant families, comprising about 745 genera and more than 19,500 species worldwide. This family is well known for its broad spectrum of bioactive specialized metabolites, including isoflavonoids, alkaloids, terpenoids, and phenolic acids [34].

In the preliminary screening, the leaves of both species displayed a remarkable biological potential, showing marked AOC (TEAC = 3.9 and 4.7 mmol TE g^{-1} CSL and GGL extract, respectively), a result validated in a yeast α-synuclein model (% ROS reduction = 49 and 63% for CSL and GGL extract, respectively) and strong enzymatic inhibitory activity, with *C. siliqua* active against AChE (IC_{50} = 18.9 μg mL^{-1}) and both active against α-GLU (IC_{50} = 0.4 and 3.0 μg mL^{-1} of CSL and GGL extract, respectively). UHPLC-HRMS/MS profiling revealed highly characteristic marker metabolites: siliquapyranone and tetragalloylglucose in CSL, and pinocembrin together with several prenylated flavanones in GGL. These compounds are not ubiquitous in the plant kingdom; hence this finding contributes to the biotechnological interest of these species.

In addition, the chemical and biological data obtained for carob (*C. siliqua*) and licorice (*G. glabra*) leaves highlight their relevance, supporting the valorization

of the epigeal biomass as a substantial added-value source for their supply chains. *C. siliqua* is mainly cultivated for its pods, which are used in the production of flour, syrups, and baked goods, while *G. glabra* is historically associated with the use of its roots and rhizomes (licorice), typically exploited in the confectionery and bakery industry. In both cases, the leaves are an underutilized resource that could potentially be transformed into nutraceuticals or functional ingredients with high added value.

From a geographical point of view, both species are native to the Mediterranean area and widely distributed in southern Italy. Calabrian *G. glabra* is recognized at European level through the PDO "Liquirizia di Calabria," while *C. siliqua* has recently gained strategic importance in agroforestry restoration programs, exemplified by the use of the *Amele* variety to help restore agricultural areas in the Apulian region damaged by *Xylella fastidiosa.* The sustainable exploitation of their biomass therefore offers a concrete opportunity to promote Italian biodiversity, strengthen local supply chains, and develop new products with biological activity, in line with the principles of the circular bioeconomy and responsible management of plant resources.

2.4. Materials and Methods

2.4.1. Chemicals and standards

Analytical-grade methanol and ethanol, 6-hydroxy-2,5,7,8-tetramethylchroman-2-carboxylic acid (Trolox), 2,2′-azino-bis(3-ethylbenzothiazoline-6-sulphonic acid) (ABTS), potassium persulfate ($K_2S_2O_8$), acetylcholinesterase from *Electrophorus electricus* (EC 3.1.1.7, Type V-S, lyophilized powder, 200-1000 U mg^{-1} protein), Trizma hydrochloride (Tris-HCl), acetylthiocholine iodide (ACht), 4-Fluoro-7-sulfamoylbenzofurazan (ABD-F), galantamine hydrobromide, α-glucosidase from *Saccharomyces cerevisiae* (EC 3.2.1.20, Type I, ≥10 U mg^{-1} protein), 4-nitrophenyl-β-D-glucopyranoside (pNPG), and acarbose were all purchased from Merck (Milan, Italy). Sodium phosphate dibasic (Na_2HPO_4), sodium carbonate (Na_2CO_3), and

potassium phosphate monobasic (K_2HPO_4) were obtained from J.T. Baker (Deventer, The Netherlands).

2.4.2. Sampling and extraction

The sampling and plant extraction were conducted within the framework of the NBFC project under the coordination of the University of Verona, led by Prof. Flavia Guzzo. Aerial parts (mainly leaves and stems) were collected for all species, within predefined seasonal windows between 2022 and 2024, according to the natural phenology of each species. A three-pool design in which each pool consisted of material collected from multiple individual plants, was adopted to minimize intra-population variability. Plant material was immediately frozen in liquid nitrogen, finely ground using an A11 basic analytical mill (IKA-Werke, Staufen, Germany), and stored at -80 °C until extraction. Approximately 1 g of frozen powder was extracted with 10 volumes (w/v) of LC-MS grade methanol using a standardized ultrasound-assisted protocol: samples were vortexed for 30 s, sonicated on ice for 10 min in a 40 kHz ultrasonic bath, and centrifuged at 14,000 x g for 10 min at 4 °C. The resulting supernatants were aliquoted into 1.5 mL tubes (1 mL extract corresponding to 100 mg fresh material), dried either under vacuum (SpeedVac) or under a nitrogen stream. Extraction yield was determined gravimetrically and expressed as mg extract per 100 mg fresh weight. Dried extracts were dissolved in ethanol, centrifuged, and appropriately diluted in MeOH 20% for UHPLC-DAD-HRMS/MS analysis and with PBS, Tris-HCl, or water depending on the requirements of the *in vitro* assays.

2.4.3. Untargeted UHPLC-DAD-HRMS/MS procedure

UHPLC-DAD-HRMS profiles of plant extracts were acquired with a Vanquish Flex UHPLC system interfaced to a double detector, a Diode Array Detector FG and an Orbitap Exploris 120 mass spectrometer, equipped with a heated electrospray ionization source, HESI-II (Thermo Fisher Scientific, Milano, Italy). The chromatographic separations were performed using a Kinetex C18 column (2.1 × 100 mm, 1.6 µm; Phenomenex, Bologna, Italy) protected by a

C18 Guard Cartridge (2.1 mm I.D.) and thermostated at 25 °C, and a binary gradient of H_2O (A) and MeCN (B), both containing 0.1 % formic acid (injection volume, 5 µL). The elution method was as follows: 0-3 min, 2 % B; 3-5 min,2-13% B;5-9min, 13 %B ;9-12 min 13-18 %B; 12-13 18%B ;13-17min,18-30%B ;17-20 min, 30 % B; 20-30 min, 30-40 % B; 30-38 min, 40-60%B; 38-39 min, 60-98%B; 39-42 min, 98%B; 42-43 min, 98-2%B; 43-48 min, 2%B. UV-Vis spectra were acquired in the range of 200-600 nm and HRMS data were acquired simultaneously in positive and negative ionization modes. A Full MS data-dependent MS/MS (Full MS/dd-MS2) acquisition mode was used, with the resolution of Full MS scan (scan range *m/z* 150-1500) and dd-MS^2 scan set at 60000 and 30000 FWHM, respectively. A stepped HCD collision energy (20, 40, and 60) was applied for fragmentation to obtain representative fragmentation profiles suitable for the annotation of structurally diverse metabolites, which may fragment optimally at different collision energies. Instrument control and spectra acquisition were carried out using Xcalibur software version 4.6 (Thermo Fisher Scientific).

Raw UHPLC-DAD-HRMS/MS chromatograms and spectra were processed in Compound Discoverer (Thermo Fisher Scientific) using a customized workflow specifically optimized for untargeted secondary-metabolite profiling. The workflow began with Select Spectra, restricting chromatographic data to the 0-35 min retention time range to exclude the washing step, followed by Align Retention Time, which corrected chromatographic shifts using a mass tolerance of 5 ppm. Mass traces were generated through Create Mass Trace, including all signals within ± 5 ppm of theoretical m/z in both ionization modes, maximizing chemical coverage. Compound detection relied on Detect Compounds, applying a minimum intensity threshold of 100,000 and considering an extended set of adducts. Redundant features were consolidated using Merge Features with 5 ppm mass and 0.1 min RT tolerances, and Group Compounds produced a unified feature table.

Compound annotation integrated several identification sources via Assign Compound Annotations: an in-house mzVault spectral library comprising 120 reference standards and 184 MS/MS spectra, mzCloud for MS/MS-based spectral matching, an in-house Mass List, Predict Compositions (formula

generation within C1-C100, H1-H150, N0-N4, O0-O90, S0-S1), and ChemSpider. Since Mass List and ChemSpider lack MS/MS spectra their annotations were refined through mzLogic and Apply Spectral Distance Filter, ensuring spectral and structural consistency.

To explore chemical relationships, identified features were organized into clusters through Generate Molecular Network, grouping metabolites sharing similar MS/MS fragmentation and allowing recognition of commonly occurring modifications, including manually defined plant-specific substituents. Signal consistency across samples was ensured using Fill Gaps, linked to Mark Background Compounds to remove features detected in blanks. Characteristic fragmentation signatures were further investigated using Search Neutral Losses. Post-processing refinements included manual annotation via the Structure Proposal Sheet and validation through FISh Scoring, an *in-silico* fragmentation approach that evaluates the consistency between predicted (theoretical) fragment ions and the experimental MS/MS spectra. Level 1 was assigned for mzVault matches, Level 2 for annotations from external databases, and Level 3 for tentative MS/MS-based structural proposals.

2.4.4. Antioxidant assay

The antioxidant capacities (AOCs) of the extracts were evaluated using ABTS scavenging capacity assay according to Celano et al., [40]. A multimode microplate reader Varioskan LUX was employed for the assays. Quercetin was used as positive control and Trolox calibration curves (2.5–25 µM) were used to calculate AOC. Results were expressed as Trolox equivalent antioxidant capacity (TEAC) per g of extract (mmol TE g^{-1}, mean ± SD of three analysis replicates).

In ABTS assay, extracts were dissolved in methanol and appropriately diluted with 5 mM PBS (pH 7.4) at a concentration of 1 mg mL^{-1}. Only the extracts showing > 50% inhibition were further analyzed to determine TEAC using a multi-level calibration curve. 5 µL of diluted extracts or PBS (control) were added to 500 µL of ABTS•+ solution (0.1 mM) and the mixtures were incubated in the dark at 30 °C for 60 min. The absorbances were measured at 734 nm.

Curves of Trolox and extracts were obtained by plotting concentration against the % Inhibition of radical absorbance.

2.4.5. Determination of the total phenolic content (TPC)

The total phenolic content (TPC) of CSL extracts was determined using the Folin-Ciocalteu colorimetric method according to Celano et al. [40]. Briefly, 20 µL of diluted samples and 50 µL of diluted FC reagent (10 % v/v aqueous solution) were added to 100 µL of ultrapure water in a 96-well microplate. Then 30 µL of Na_2CO_3 (20 %, *w*/*v*) were added, and the mixtures were incubated at 25 ◦C for 45 min. The absorbances were read at 725 nm with a multimode microplate reader Varioskan LUX (Thermo Fisher Scientific). TPC was estimated from the calibration curve of gallic acid (GA) (range 5–200 µg mL^{-1}) and the data were expressed as GA equivalents per g of extracts (mg GAE g^{-1} extract, mean ± SD of three extraction replicates).

2.4.6. In vitro AChE inhibitory assays

The AChE inhibitory activities of the extracts were evaluated using a fluorescent procedure developed by Sanchez-Martínez et al. [27] to overcome the drawbacks of colorimetric Ellman's method in analyzing plant extracts. Galantamine (0.5-30 µM, well concentration) was used as positive control and a 150 mM Tris-HCl solution (pH = 8) was used to dilute the enzymes and ABD-F reagent to working concentrations. Stock solutions of inhibitors and substrates (ATCI) were diluted with H_2O.

In brief, each well was filled with 100 µL of H_2O (negative control) or inhibitors at various concentrations, 100 µL of buffer, and 25 µL of AChE (0.8 U mL^{-1}). After incubation for 10 min at 37 °C, the reaction was initiated by adding 25 µL of ABD-F (125 µM) and 50 µL of ATCI at concentrations corresponding to KM (Michaelis–Menten constant) values (approximately 1.6 mM) [27]. Fluorescence readings (λexcitation /λemission = 389/513 nm) were recorded every minute for 15 min at 37 °C with microplate reader Varioskan LUX. Kinetic determinations were conducted to determine the average enzymatic velocity (Vmean), which was used to calculate the percentage of inhibition

$$\%\ Inhibition = (Vmean\ neg\ control - Vmean\ sample) / Vmean\ neg\ control$$

Extracts were initially screened at a well concentration of 200 µg mL^{-1}. Only those exhibiting > 50% inhibition were subsequently selected for IC_{50} determination, expressed in µg mL^{-1}, using a dose-response inhibition curve, at least five different concentrations. Results were reported as IC_{50} ± SD of three replicates

2.4.7. In vitro α-GLU inhibitory assay

The inhibitory activity of α-GLU was evaluated according to the method reported by Chen et al. [41]. Acarbose (0.05–1 mM, well concentration) and quercetin (2–50 µM, well concentration) were used as positive controls, and a 50 mM phosphate buffer solution (pH = 6.8) was employed for dilutions.

Briefly, 10 µL of α-GLU (0.25 U mL^{-1}) was added to 145 µL of buffer (negative control) or diluted solutions of inhibitor (extracts, acarbose and quercetin) and incubated at 37 °C for 10 min. Then, 45 µL of the substrate pNPG (1 mM) was added, and the mixture was further incubated at 37 °C for 20 min. Finally, 50 µL of 0.1 M Na_2CO_3 was added to each well. Enzymatic activity was evaluated by measuring absorbance at 405 nm using microplate reader Varioskan LUX. % Inhibition was calculated using absorbance. Extracts were initially screened at a final well concentration of 200 µg mL^{-1}. Only those exhibiting > 50% inhibition were subsequently selected for IC_{50} determination, expressed in µg mL^{-1}, using a dose-response inhibition curve, at least five different concentrations.

2.5. Appendix

Table A1. *Name, code, botanical families, traditional uses [Sitography 2] and inclusion in Belfrit list of 112 species of Italian flora.*

Plant	CODE	Family	Uses	BELFRIT list
Camphorosma monspeliaca	CAMO	Amaranthaceae	medicinal	✓
Allium angulosum	ALAN	Amaryllidaceae	none	other spp
Allium lusitanicum	ALLU	Amaryllidaceae	medicinal	other spp
Sternbergia lutea	SL	Amaryllidaceae	toxic	-
Tulbaghia violacea	TUVI	Amaryllidaceae	ornamental/medicinal	-
Echinophora spinosa	ECSP	Apiaceae	edible	-
Eryngium maritimum	ERMA	Apiaceae	none	other spp
Prangos ferulacea	PRFE	Apiaceae	none	other spp (F)
Selinum carvifolia	SECA	Apiaceae	none	✓ (F)
Asclepias curassavica	ASCU	Apocynaceae	medicinal/ornamental	-
Asclepias syriaca	ASSY	Apocynaceae	nectarifer	-
Carissa macrocarpa	CAMA	Apocynaceae	ornamental	other spp (F)
Periploca graeca	PEGR	Apocynaceae	ornamental	-
Arum maculatum	ARMA	Araceae	toxic/medicinal	-
Phoenix dactylifera	PHDA	Arecaceae	edible/medicinal	✓ (F)
Agave sisalana	AGSI	Asparagaceae	none	✓
Ruscus aculeatus	RUAC	Asparagaceae	edible/medicinal	✓
Hemerocallis fulva	HEFU	Asphodelaceae	edible	-
Artemisia abrotanum	ARAB	Asteraceae	medicinal	✓
Bellis perennis	BEPE	Asteraceae	edible/medicinal	✓
Cichorium intybus	CIIN	Asteraceae	edible/medicinal	✓
Cotula coronopifolia	COCO	Asteraceae	none	-
Cynara cardunculus	CYCA	Asteraceae	edible/medicinal	✓
Erigeron karvinskianus	ERKA	Asteraceae	none	other spp
Inula salicina	INSA	Asteraceae	medicinal	other spp
Kleinia anteuphorbium	KLAN	Asteraceae	none	-
Limbarda critmoides	LICR	Asteraceae	edible	-
Scolymus grandiflorus	SCGR	Asteraceae	edible	-
Sonchus asper	SOAS	Asteraceae	edible/medicinal	-
Tanacetum parthenium	TAPA	Asteraceae	edible/medicinal	✓
Xeranthemum cylindraceum	XECY	Asteraceae	none	other spp
Armoracia rusticana	ARRU	Brassicaceae	edible/medicinal	✓
Aubrieta deltoidea	AUDE	Brassicaceae	ornamental	-
Aurinia leucadea	AULE	Brassicaceae	none	-
Berteroa incana	BEIN	Brassicaceae	none	-
Brassica nigra	BRNI	Brassicaceae	edible/medicinal	✓
Crambe maritima	CRMA	Brassicaceae	none	✓ (F)
Isatis tinctoria	ISTI	Brassicaceae	toxic/medicinal	✓
Adenophora lilifolia	ADLI	Campanulaceae	none	-
Lonicera caerulea	LOCA	Caprifoliaceae	medicinal	other spp
Cerastium tomentosum	CETO	Caryophyllaceae	none	-
Euonymus europaeus	EUEU	Celastraceae	forest	-
Cistus laurifolius	CILA	Cistaceae	medicinal	other spp
Cistus monspeliensis	CIMO	Cistaceae	medicinal	other spp
Aeonium arboreum	AEAR	Crassulaceae	none	-
Graptopetalum paraguayense	GRPA	Crassulaceae	none	-
Kalanchoë daigremontiana	KADA	Crassulaceae	none	-

Plant	CODE	Family	Uses	BELFRIT list
Juniperus communis	JUCO	Cupressaceae	edible/medicinal	✓
Juniperus oxycedrus	JUOX	Cupressaceae	toxic/medicinal	other spp
Juniperus thurifera	JUTH	Cupressaceae	forestale	other spp
Platycladus orientalis	PLOR	Cupressaceae	medicinal/ornamental	-
Pteridium aquilinum	PTAQ	Dennstaedtiaceae	toxic/medicinal	-
Polystichum setiferum	POSE	Dryopteridaceae	none	other spp
Diospyros kaki	DK	Ebenaceae	none	✓
Equisetum arvense	EQAR	Equisetaceae	edible/medicinal	✓
Equisetum palustre	EQPA	Equisetaceae	none	other spp
Euphorbia pithyusa	EUPI	Euphorbiaceae	medicinal/artigianale	other spp
Caragana arborescens	CAAR	Fabaceae	ornamental	-
Ceratonia siliqua	CESI	Fabaceae	edible/medicinal	✓ (F)
Lablab purpureus	LAPU	Fabaceae	none	-
Glycyrrhiza glabra	GLGL	Fabaceae	edible/medicinal	✓ (R)
Medicago marina	MEMA	Fabaceae	none	other spp
Parkinsonia aculeata	PA	Fabaceae	forest	-
Wisteria sinensis	WISI	Fabaceae	edible	-
Castanea sativa	CASA	Fagaceae	edible	✓
Gentiana acaulis	GEAC	Gentianaceae	medicinal	✓
Iris sibirica	IRSI	Iridaceae	medicinal	-
Limniris pseudacorus	LIPS	Iridaceae	medicinal	-
Clinopodium nepeta	CLNE	Lamiaceae	edible/medicinal	✓
Phlomis fruticosa	PHFR	Lamiaceae	medicinal	-
Salvia pratensis	SP	Lamiaceae	edible/medicinal	✓
Akebia quinata	AQ	Lardizabalaceae	none	-
Lythrum salicaria	LYSA	Lythraceae	edible/medicinal	✓
Trapa natans	TRNA	Lythraceae	edible/medicinal	-
Althea officinalis	AO	Malvaceae	edible/medicinal	✓
Digitalis lutea	DILU	Plantaginaceae	toxic/medicinal	-
Gratiola officinalis	GROF	Plantaginaceae	medicinal	-
Russelia equisetiformis	RUEQ	Plantaginaceae	none	-
Ceratostigma plumbaginoides	CEPL	Plumbaginaceae	none	-
Achnatherum calamagrosti	ACCA	Poaceae	none	-
Avena barbata	AVBA	Poaceae	edible	other spp
Brachypodium sylvaticum	BRSY	Poaceae	none	-
Imperata cylindrica	IMCY	Poaceae	none	-
Oplismenus undulatifolius	OPUN	Poaceae	none	-
Phalaris coerulescens	PHCO	Poaceae	none	-
Pseudosasa japonica	PJ	Poaceae	none	-
Phyllostachys viridiglaucescens	PV	Poaceae	none	-
Bistorta officinalis	BIOF	Polygonaceae	edible/medicinal	✓
Cyclamen repandum	CYRE	Primulaceae	toxic/medicinal	-
Pteris vittata	PTVI	Pteridaceae	none	-
Helleborus viridis	HEVI	Ranunculaceae	toxic/medicinal	-
Nigella damascena	NIDA	Ranunculaceae	toxic/medicinal	other spp
Cydonia oblonga	CYOB	Rosaceae	edible/medicinal	✓ (F)
Dryas octopetala	DROC	Rosaceae	medicinal	-
Filipendula ulmaria	FIUL	Rosaceae	medicinal	✓
Rosa canina	ROCA	Rosaceae	edible/medicinal	✓
Sanguisorba officinalis	SO	Rosaceae	edible/medicinal	✓
Spiraea chamaedryfolia	SPCH	Rosaceae	forest	-
Osyris alba	OSAL	Santalaceae	none	-
Heuchea sanguinea	HS	Saxifragaceae	none	-
Saxifraga caesia	SACA	Saxifragaceae	none	other spp

Plant	CODE	Family	Uses	BELFRIT list
Buddleja davidii	BUDA	Scrophulariaceae	forest	-
Verbascum thapsus	VT	Scrophulariaceae	medicinal	✓
Selaginella kraussiana	SEKR	Selaginellaceae	none	✓
Smilax aspera	SMAS	Smilacaceae	edible/medicinal	✓
Alkekengi officinarum	ALOF	Solanaceae	edible/medicinal	✓ (F)
Solandra maxima	SOMA	Solanaceae	none	-
Styrax officinalis	STOF	Styracaceae	edible/medicinal	✓
Thelypteris palustris	THPA	Thelypteridaceae	ornamental	-
Aloysia citrodora	ALCI	Verbenaceae	edible/medicinal	✓
Glandularia tenera	GLTE	Verbenaceae	none	other spp
Lantana camara	LACA	Verbenaceae	none	-

F: fruit; R: root.

Table A2. *Antioxidant (ABTS and TPC) and enzyme inhibition assays (α-GLU and AChE) data of 112 investigated extracts from Italian flora.*[a]

CODE	Family	TPC (mg GAE g^{-1}) ±SD	TEAC (mmol TE g^{-1}) ±SD	IC_{50} α-GLU (μg mL^{-1}) ±SD	IC50 AChe (μg mL^{-1}) ±SD
CAMO	Amaranthaceae	25.0±3.7	-	> 200	141.1±13.6
ALAN	Amaryllidaceae	51.1±0.7	-	60.25±1.04	> 200
ALLU	Amaryllidaceae	17.1±1.1	-	> 200	> 200
SL	Amaryllidaceae	11.3±1.5	-	> 200	8.1±0.9
TUVI	Amaryllidaceae	4.4±0.4	-	> 200	> 200
ECSP	Apiaceae	5.1±0.2	-	> 200	> 200
ERMA	Apiaceae	4.8±0.4	-	> 200	> 200
PRFE	Apiaceae	41.0±0.6	-	> 200	197.9±3.4
SECA	Apiaceae	107.9±4.4	1.45±0.01	> 200	214.2±7.9
ASCU	Apocynaceae	42.6±3.4	-	> 200	> 200
ASSY	Apocynaceae	36.6±0.3	-	> 200	207.4±4.8
CAMA	Apocynaceae	173.1±3	4.54±0.01	0.26±0.01	5.6±0.3
PEGR	Apocynaceae	69.7±2.1	1.32±0.01	22.99±1.28	187.8±7.3
ARMA	Araceae	14.3±1.2	-	> 200	> 200
PHDA	Arecaceae	159.6±3.6	4.16±0.06	1.45±0.01	64.8±0.5
AGSI	Asparagaceae	4.7±3.8	-	> 200	> 200
RUAC	Asparagaceae	19.8±1.0	-	> 200	> 200
HEFU	Asphodelaceae	24.6±0.3	-	> 200	> 200
ARAB	Asteraceae	89.6±2.3	1.49±0.05	> 200	161.9±7.6
BEPE	Asteraceae	38.7±20.6	-	> 200	> 200
CIIN	Asteraceae	98.8±26.9	-	> 200	> 200
COCO	Asteraceae	32.6±2.6	-	> 200	> 200
CYCA	Asteraceae	132.7±1.9	1.77±0.03	> 200	200.2±24.8
ERKA	Asteraceae	155.1±3.3	1.90±0.04	> 200	> 200
INSA	Asteraceae	289.1±18.4	5.03±0.10	> 200	111.7±6.9
KLAN	Asteraceae	30.0±0.5	-	> 200	> 200
LICR	Asteraceae	10.0±0.9	-	> 200	> 200

CODE	Family	TPC (mg GAE g^{-1}) ±SD	TEAC (mmol TE g^{-1}) ±SD	IC_{50} α-GLU (µg mL^{-1}) ±SD	IC50 AChe (µg mL^{-1}) ±SD
SCGR	Asteraceae	35.2±1.4	-	> 200	> 200
SOAS	Asteraceae	32.0±1.5	-	> 200	> 200
TAPA	Asteraceae	91.4±1.8	-	> 200	176.2±7.2
XECY	Asteraceae	64.6±1.7	-	> 200	195.8±4.6
ARRU	Brassicaceae	29.1±5.2	1.75±0.03	> 200	201.1±2.3
AUDE	Brassicaceae	25.6±2.4	-	> 200	> 200
AULE	Brassicaceae	24.3±0.5	-	> 200	> 200
BEIN	Brassicaceae	15.9±1.0	-	> 200	> 200
BRNI	Brassicaceae	13.5±5.7	-	> 200	215.4±3.1
CRMA	Brassicaceae	30.2±5.6	-	> 200	> 200
ISTI	Brassicaceae	97.1±5.8	-	> 200	214.4±1.9
ADLI	Campanulaceae	39.4±2.2	-	18.99±2.72	213.3±5.3
LOCA	Caprifoliaceae	42.5±0.5	-	> 200	> 200
CETO	Caryophyllaceae	8.1±0.3	-	> 200	> 200
EUEU	Celastraceae	34.3±1.5	-	> 200	> 200
CILA	Cistaceae	206.7±7.1	5.85±0.12	0.39±0.01	59.8±4.5
CIMO	Cistaceae	164.9±0.6	3.11±0.07	0.83±0.05	117.8±7.4
AEAR	Crassulaceae	461.6±1.4	10.46±0.11	0.13±0.01	49.5±0.8
GRPA	Crassulaceae	23.5±0.6	-	11.35±0.25	> 200
KADA	Crassulaceae	122.8±23.6	-	4.68±0.03	137.9±2.5
JUCO	Cupressaceae	108.9±23.3	2.39±0.01	11.38±0.56	> 200
JUOX	Cupressaceae	176.1±1.6	5.47±0.17	0.81±0.01	7.1±0.3
JUTH	Cupressaceae	73.0±6.0	1.99±0.02	3.65±0.13	202.8±14.4
PLOR	Cupressaceae	49.9±0.6	1.42±0.01	11.02±0.96	188.3±2.0
PTAQ	Dennstaedtiaceae	43.5±2.1	-	> 200	> 200
POSE	Dryopteridaceae	226.9±14.8	2.81±0.03	7.63±0.07	127.0±4.2
DK	Ebenaceae	110.9±0.4	3.50±0.04	1.54±0.09	150.0±1.1
EQAR	Equisetaceae	18.6±2.0	-	> 200	> 200
EQPA	Equisetaceae	6.7±1.0	-	> 200	> 200
EUPI	Euphorbiaceae	229.4±23.6	4.12±0.03	1.02±0.93	10.2±0.1
CAAR	Fabaceae	43.1±5.5	-	> 200	> 200
CESI	Fabaceae	224.6±15.2	3.92±0.05	0.37±0.01	18.9±0.3

CODE	Family	TPC (mg GAE g^{-1}) ±SD	TEAC (mmol TE g^{-1}) ±SD	IC_{50} α-GLU (µg mL^{-1}) ±SD	IC50 AChe (µg mL^{-1}) ±SD
GLGL	Fabaceae	72.4±3.8	4.70±0.11	3.01±0.25	> 200
LAPU	Fabaceae	38.7±9.8	-	> 200	137.1±14.2
MEMA	Fabaceae	1.4±0.1	-	> 200	> 200
PA	Fabaceae	120.2±19.7	2.86±0.02	6.76±0.63	> 200
WISI	Fabaceae	69.3±7.8	-	83.54±46.18	178.8±10.2
CASA	Fagaceae	121.8±9.7	2.40±0.02	1.95±0.08	214.1±11.9
GEAC	Gentianaceae	69.5±1.9	1.40±0.01	> 200	189.8±1.5
IRSI	Iridaceae	107.9±2.9	1.47±0.01	1.05±0.03	44.3±0.5
LIPS	Iridaceae	125.0±3.0	2.75±0.02	> 200	92.3±1.1
CLNE	Lamiaceae	126.4±3.7	1.25±0.01	> 200	> 200
PHFR	Lamiaceae	110.6±7.4	1.12±0.01	> 200	> 200
SP	Lamiaceae	39.5±2.5	-	> 200	> 200
AQ	Lardizabalaceae	88.7±10.6	1.75±0.01	> 200	> 200
LYSA	Lythraceae	301.1±18.9	8.01±0.23	0.37±0.01	105.0±2.8
TRNA	Lythraceae	236.1±6.1	4.50±0.05	0.31±0.01	103.3±3.8
AO	Malvaceae	29.7±4.6	-	> 200	> 200
DILU	Plantaginaceae	118.6±1.6	-	> 200	203.9±0.8
GROF	Plantaginaceae	352.7±10.5	4.96±0.02	> 200	> 200
RUEQ	Plantaginaceae	165.0±7.2	-	> 200	> 200
CEPL	Plumbaginaceae	196.6±1.4	2.53±0.02	3.6±0.14	44.3±2.6
ACCA	Poaceae	34.1±2.9	-	> 200	212.2±0.6
AVBA	Poaceae	6.1±0.1	-	> 200	> 200
BRSY	Poaceae	18.5±5.3	-	> 200	212.5±6.5
IMCY	Poaceae	81.9±2.3	-	> 200	150.2±2.3
OPUN	Poaceae	29.8±1.2	-	> 200	158.1±8.1
PHCO	Poaceae	19.1±3.8	-	> 200	> 200
PV	Poaceae	31.4±0.9	-	> 200	> 200
PJ	Poaceae	35.9±2.2	-	> 200	> 200
BIOF	Polygonaceae	72.8±2.1	-	9.75±0.63	129.5±6.8
CYRE	Primulaceae	17.2±2.3	-	> 200	213.1±8.5
PTVI	Pteridaceae	33.8±1.6	-	> 200	> 200
HEVI	Ranunculaceae	38.3±0.3	-	> 200	> 200

CODE	Family	TPC (mg GAE g^{-1}) ±SD	TEAC (mmol TE g^{-1}) ±SD	IC_{50} α-GLU (µg mL^{-1}) ±SD	IC50 AChe (µg mL^{-1}) ±SD
NIDA	Ranunculaceae	24.9±1.1	-	> 200	> 200
CYOB	Rosaceae	170.1±12.8	3.10±0.05	2.81±0.21	135.4±2.6
DROC	Rosaceae	139.9±7.4	2.58±0.07	53.03±4.79	> 200
FIUL	Rosaceae	465.7±26.1	19.51±2.01	0.21±0.01	25.2±0.8
ROCA	Rosaceae	192.9±9	5.67±0.39	0.25±0.01	140.2±16.3
SO	Rosaceae	195.3±4.6	3.35±0.02	0.74±0.02	254.1±0.4
SPCH	Rosaceae	118.1±8.9	2.02±0.01	44.94±1.63	151.4±16.3
OSAL	Santalaceae	110.2±3.3	2.24±0.03	196.96±7.92	> 200
HS	Saxifragaceae	258.7±8.5	6.42±0.1	2.91±0.02	30.6±0.1
SACA	Saxifragaceae	123.2±8.3	2.72±0.01	1.07±0.01	37.4±0.8
BUDA	Scrophulariaceae	127.5±18.3	2.19±0.04	> 200	189.2±7.4
VT	Scrophulariaceae	77.1±2.7	-	> 200	> 200
SEKR	Selaginellaceae	15.5±0.6	-	> 200	> 200
SMAS	Smilacaceae	168.1±7.1	2.10±0.02	12.41±0.24	149.4±0.5
ALOF	Solanaceae	69.8±3.3	-	> 200	196.9±19.5
SOMA	Solanaceae	105.7±6.8	-	> 200	136.1±6.4
STOF	Styracaceae	60.4±1.4	-	> 200	> 200
THPA	Thelypteridaceae	86.9±5.7	1.86±0.01	5.49±0.01	150.0±5.5
ALCI	Verbenaceae	78.5±1.5	1.83±0.01	> 200	148.6±3.6
GLTE	Verbenaceae	32.6±1.6	-	> 200	> 200
LACA	Verbenaceae	171.9±29.1	2.67±0.06	> 200	> 200

[a] *Values are expressed as mean ± SD.*

Chapter 3

Ceratonia siliqua leaves (CSL)

Part of this work was conducted in the laboratory of:
[1] Professor Daniel Granato – University of Limerick (Ireland)
Part of this work was conducted in collaboration with:
[2] Professor Francesca Sansone – Pharmaceutical Technology group, University of Salerno (DiFarma)

Adapted from:
S. Serio, V. Santoro, R. Celano, D. Fiore, M. C. Proto, F. Corbo, M. L. Clodoveo, R. Tardugno, A. L. Piccinelli, L. Rastrelli. Carob (*Ceratonia siliqua*) leaves: A comprehensive analysis of bioactive profile and health-promoting potential of an untapped resource. *Food Chemistry*, **2025**, 468, 142392

S. Serio, V. Santoro, A. L. Piccinelli, R. Celano, L. Rastrelli. Advanced extraction techniques for sustainable recovery of health-promoting compounds from Carob leaves. *Ultrasonics sonochemistry*, **2026**, 124, 107710.

3.1. Introduction

Carob plant (*Ceratonia siliqua* L.), belonging to the Fabaceae family, is an evergreen perennial tree, native to the Mediterranean and also widespread in North and South America, Africa, and Australia. It has been used by humans since ancient times for its economic and nutritional value; various parts of the plant, such as the leaves, bark and pods, have been widely used in traditional medicine to treat conditions including diarrhea, diabetes and hypertension [42]. Carob has recently been rediscovered due to high nutritional value and potential beneficial effects on health of its fruits, commonly known as carob pods [42–44]. Pods are the primary valuable plant parts used in industrial sectors to produce a variety of food products, as they contain high levels of sugar, dietary fiber, micronutrients, inositols (D-pinitol) and phenolic compounds (phenolic acids, gallotannins and flavonoids). The seeds, containing galactomannans, are primarily processed to obtain locust bean gum (food additive E410), while the carob pulp is used in the production of powder, flour, and syrup. These carob pulp products are increasingly recognized as functional ingredients in healthy food products due to their high dietary fiber content, pinitol and phenolic compounds, and their beneficial effects on gastrointestinal diseases, diabetes, hyperlipidemia, inflammation, and oxidative stress [42–44].

In addition to high nutritional and health promoting values, the carob tree is notable for its environmental resilience. It is considered a highly drought-resistant species, capable of adapting morphologically and physiologically to conditions of severe water scarcity, and of growing in marginal and poor soils. These ecological advantages make it particularly valuable in regions characterized by prolonged warm temperatures and droughts, thereby enhancing food security and the local economies and contributing to the achievement of some United Nations SDGs in the Mediterranean region [42,44].

A concrete exemplification of this potential can be found today in Puglia, one of the regions most affected by olive grove decline caused by *Xylella fastidiosa* subsp. *pauca.* Here, the carob tree, and particularly the native *Amele* variety,

has been chosen as a strategic crop for the redevelopment of agricultural landscapes and the recovery of devastated areas, particularly in the areas of Ostuni, Fasano, and Monopoli. In this sense, the *Amele* variety not only provides an agronomic solution to the loss of monumental olive groves but also creates an opportunity to enhance the agri-food legacy of southern Italy, strengthening local identity and creating new economic opportunities linked to healthy, sustainable products rooted in Mediterranean tradition [Sitography 4]. The renewed interest in carob-based products highlights how this traditional crop can serve as a source of innovative and functional ingredients, mainly derived from the nutritional potential of its pods [45]. Yet, the potential of the carob tree extends far beyond its fruits: its leaves and other underutilized parts of the plant are increasingly recognized as valuable sources of bioactive compounds. This growing awareness is part of a broader trend in which plant leaves are being re-evaluated as functional ingredients. To harness this potential, the extraction and characterization of bioactive compounds from these underutilized matrices become essential steps in translating natural resources into functional and sustainable applications.

Traditional extraction methods such as maceration, distillation, and Soxhlet extraction, while still commonly used, present several limitations: they are time-consuming, solvent-intensive, and energy-demanding, often yielding low extraction efficiency and generating substantial waste [7]. To overcome these drawbacks, the concept of green extraction rooted in the twelve principles of green chemistry and engineering and condensed into six guiding eco-extraction principles [8], has emerged. These principles promote energy-efficient processes, the use of renewable and safer solvents, and the production of high-quality extracts, making sustainability and process intensification the core of modern extraction technologies. Among these, Pressurized Hot Water Extraction (PHWE) and Ultrasound-Assisted Extraction (UAE) have emerged as efficient and sustainable alternatives [17]. PHWE uses water in subcritical conditions, which at high temperatures and moderate pressures changes its polarity, becoming an efficient solvent for polar and semi-polar compounds. UAE, on the other hand, is a non-thermal method, using ultrasonic energy to break down cell walls and accelerate mass transfer,

enabling rapid extraction with less solvent use and higher yields [7]. Optimizing the operating parameters in these techniques is crucial to maximize the recovery of target compounds, reduce environmental impact and ensure high-quality extracts [15,16].

Based on the previously discussed selection criteria, which identified CSL as a promising matrix, their remarkable adaptability and ecological and economic importance in the Mediterranean region further support their value as a sustainable resource for the recovery of bioactive compounds. In this context, developing efficient and eco-friendly extraction methods enables the production of high-quality extracts that can be used to create functional ingredients for nutraceutical, pharmaceutical, and food applications. Their actual functional potential, however, must be verified through biological evaluation. For a more realistic assessment of bioactivity, preliminary chemical screenings should be complemented by cell-based assays, to confirm whether the metabolites retain their activity under physiologically relevant conditions, and by *in vitro* bioaccessibility studies, to determine their stability and ability to reach target sites [46]. This integrated approach offers a complete workflow, from the comprehensive characterization of a natural biomass to the development of a finished product with potential health-promoting properties.

The main objectives achieved in this study were:

- **Comprehensive analysis** of bioactive profile and health-promoting potential of CSL;
- **Green extraction approaches** for the recovery of CSL bioactive compounds aimed at the production of enriched and high-quality extracts;
- **Evaluation of the biological potential and bioaccessibility** of the optimized extracts through integrated chemical, enzymatic, and cell-based assays.

3.2. Comprehensive analysis of bioactive profile and health-promoting potential of CSL

The use of unconventional plant matrices and underutilized biomass, such as CSL, represents a promising strategy for the development of new functional ingredients in the food and nutraceutical sectors. However, their use is currently limited due to a lack of in-depth scientific knowledge regarding the chemical composition and biological properties of these resources. Some preliminary studies have reported interesting activities of infusions and alcoholic extracts of leaves, including antioxidant [47], hypoglycemic [48], anti-obesity [49] and neuroprotective [50]. However, the phytochemicals responsible for these properties have yet to be definitively identified. Furthermore, the chemical investigations conducted so far have mainly relied on colorimetric methods to estimate total phenolic or flavonoid content [47], or on HPLC-UV analyses [51] targeting a few known compounds, without providing a complete characterization of the phytocomplex. To fill this gap, systematic studies are needed to characterize the secondary metabolites and evaluate their potential applications, with a view to promoting their use on an industrial scale as natural ingredients. In this perspective, the identification and isolation of CSL markers using advanced techniques (HRMS, NMR) are an essential step in linking chemical composition to biological effects, allowing activity to be attributed to individual compounds.

In this context, this study aims to deepen our knowledge of CSL, and particular attention was paid to the Apulian *Amele* variety, which plays a strategic role in the redevelopment of areas affected by *Xylella fastidiosa* and is now an agricultural resource of growing interest. The study involved an integrated approach, in which the quali-quantitative characterization of exhaustive extracts of CSL using UHPLC-DAD-HRMS/MS was conducted in parallel with the evaluation of cell free *in vitro* biological activities, including antioxidant, anticholinesterase, and carbohydrate-hydrolyzing enzyme inhibition activities. The research was conducted on CSL samples collected from the Amele variety between the two flowering phases (from May to September). The combined analysis of chemical and biological data allowed the identification of the most

relevant bioactive compounds, which were subsequently isolated and characterized using advanced techniques (HRMS and NMR). The optimal harvesting period to obtain biomass rich in functional molecules was also defined. This enhances a resource that is still untapped but promising for the development of innovative nutraceutical and pharmaceutical ingredients.

3.2.1 Quali-quantitative profiling of CSL

3.2.1.1 Untargeted UHPLC-HRMS/MS analysis

The profile of specialized metabolites in CSL exhaustive extracts (UAE with EtOH: H2O 7:3, v/v) obtained during five different harvesting months (May-September) was analyzed using an untargeted approach with UHPLC-DAD-HRMS/MS. The chromatographic conditions were optimized to ensure good resolution and peak separation within reduced analysis times. Among the ionization modes tested, the negative mode proved to be the most sensitive and diagnostic and was therefore adopted for characterization. Full scan and data-dependent MS/MS (ddMS^2) modes were used for mass analysis to acquire both the precursor ions and the diagnostic fragments, enabling a more accurate identification of the structure. Metabolite assignment was performed by combining UV spectra, HRMS data, and MS/MS fragmentation profiles with information from literature, public databases, and chemotaxonomic considerations; reference standards were also used, where available

A total of 40 specialized metabolites were tentatively identified and grouped mainly into two classes: N-galloylated glucosides (GGs) and flavonol glycosides (FGs). The identification of six compounds was definitively confirmed by direct comparison with commercial standards or purified molecules. A representative UHPLC chromatogram of CSL is shown in Fig. 3.1, while the list of identified compounds, numbered according to elution order, is reported in Table 3.1.

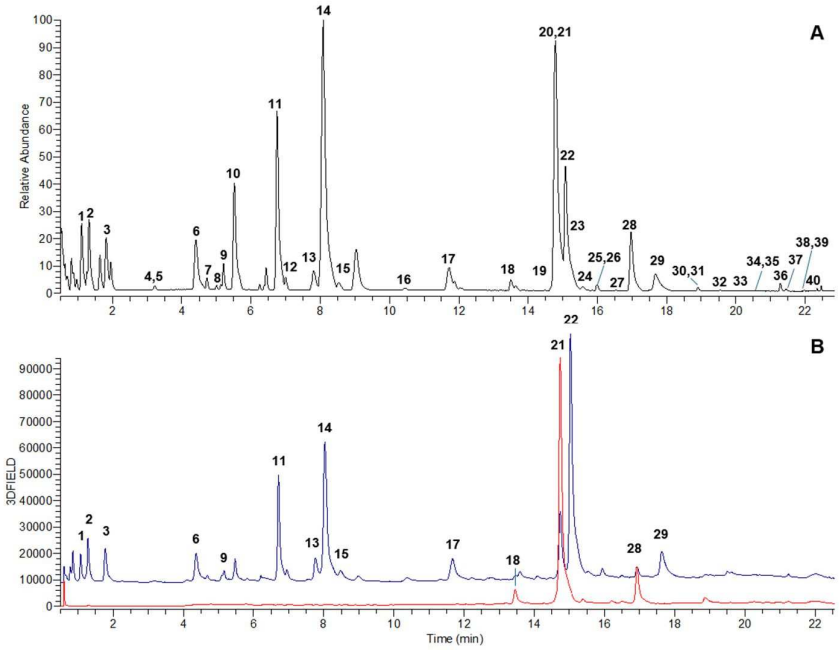

Figure 3.1. *Profile of CSL: A. UHPLC-(-)-HRMS chromatogram (m/z 100–1000), B. UHPLC-UV chromatograms (280 nm-blue line, 350 nm red line).*

Among the metabolites identified, GGs represent the most abundant class. These molecules consist of a sugar moiety (usually glucose) esterified with one or more units of gallic acid. Based on accurate masses and fragmentation profiles, two mono-GGs (1 and 5), four di-GGs (3, 6, 8, and 12), three tri-GGs (13, 15, and 17), two tetra-GGs (22 and 25), and one penta-galloylglucose (29) were detected. In the (-)-HRMS^2 spectra, these compounds showed the typical fragmentation pattern of GGs, characterized by progressive or simultaneous losses of gallic acid units (m/z 152.0104, $C_7H_4O_4$) starting from the precursor ion (Table 3.1). In addition to the usual GGs, several derivatives have been observed, including hydroxycinnamoyl-GGs (24, 27, 32 and 33), as well as species-specific compounds such as siliquapyranone (Sil, 14) and its analogues (7, 9, 11 and 26). These molecules stand out as potential chemical markers of the plant. Indeed, up to now, Sil has been isolated only from CSL [52] and tentatively identified in carob pods [45,53].

Table 3.1. *UHPLC-(-)-HRMS data of compounds detected in CSL* [a] *according to metabolomics standards initiative (MSI).*

N°	Rt (min)	Compound	Formula	[M-H]$^-$ (m/z)	Error (ppm)	Diagnostic product ion (m/z)	MSI Level [a]
1	1.11	Galloyl glucose	$C_{13}H_{16}O_{10}$	331.0673	0.8	169.0145, 125.0246	2
2	1.32	Gallic acid	$C_7H_6O_5$	169.0143	0.6	125.0246	1
3	1.82	Digalloyl glucose	$C_{20}H_{20}O_{14}$	483.0778	-0.4	331.0674, 169.0144, 125.0245	2
4	3.16	Galloyl dihexoside	$C_{19}H_{26}O_{15}$	493.1201	0.3	313.0568, 271.0464, 169.0144	2
5	3.22	Galloyl glucose	$C_{13}H_{16}O_{10}$	331.0673	0.8	169.0143, 125.0245	2
6	4.41	Digalloyl glucose	$C_{20}H_{20}O_{14}$	483.0779	-0.3	331.0675, 169.0144, 125.0246	2
7	4.73	Galloyl parasorboside acid form	$C_{19}H_{26}O_{13}$	461.1301	0.1	331.0676, 309.1194, 169.0144	3
8	5.13	Digalloyl glucose	$C_{20}H_{20}O_{14}$	483.0779	-0.3	331.0675, 169.0144, 125.0246	2
9	5.20	Galloyl parasorboside	$C_{19}H_{24}O_{12}$	443.1193	-0.4	331.0676, 313.0566, 169.0144, 125.0245	3
10	5.52	Methyl gallate	$C_8H_8O_5$	183.0299	-0.2	168.0066, 124.0167	2
11	6.75	Siliquapyranone acid form (**Sil-A**)	$C_{26}H_{30}O_{17}$	613.1406	-0.8	483.0783, 461.1302, 331.0674, 169.0144	3
12	7.00	Digalloyl glucose	$C_{20}H_{20}O_{14}$	483.0780	-0.1	313.0569, 271.0463, 169.0144	2
13	7.81	Trigalloyl glucose	$C_{27}H_{24}O_{18}$	635.0889	0.1	465.0678, 313.0569, 169.0144	2
14	8.08	Siliquapyranone (**Sil**)	$C_{26}H_{28}O_{16}$	595.1301	-0.6	483.0784, 443.1196, 331.0671, 169.0144	1
15	8.53	Trigalloyl glucose	$C_{27}H_{24}O_{18}$	635.0889	0.1	465.0677, 313.0568, 169.0143	2
16	10.44	Gallocatechin gallate	$C_{22}H_{18}O_{11}$	457.0776	0.1	305.0668, 169.0143	1
17	11.72	Trigalloyl glucose	$C_{27}H_{24}O_{18}$	635.0889	0.1	465.0677, 313.0569, 169.0143	2
18	13.50	Myricetin 3-*O*-hexoside	$C_{21}H_{20}O_{13}$	479.0830	-0.2	316.0226, 271.0250, 178.9987, 151.0038, 137.0245	2
19	14.48	Catechin 3-*O*-gallate	$C_{22}H_{18}O_{10}$	441.0825	-0.5	289.0720, 169.0143	2
20	14.67	Myricetin 3-*O*-pentoside	$C_{20}H_{18}O_{12}$	449.0725	-0.2	316.0226, 271.0250, 178.9987, 151.0038, 137.0246	2
21	14.79	Myricitrin (**Myr**)	$C_{21}H_{20}O_{12}$	463.0877	-1.0	316.0226, 271.0250, 178.9986, 151.0037, 137.0245	1
22	15.08	1,2,3,6-Tetragalloyl glucose (**TeGG**)	$C_{34}H_{28}O_{22}$	787.0990	-1.2	617.0789, 465.0674, 313.0567, 169.0144	1
23	15.38	Quercetin *O*-hexoside	$C_{21}H_{20}O_{12}$	463.0880	-0.4	300.0277, 270.0250, 178.9986, 151.0038, 121.0296	2
24	15.85	Coumaroyl galloyl glucose	$C_{22}H_{22}O_{12}$	477.1038	-0.1	331.0667, 169.0143	2
25	15.96	Tetragalloyl glucose	$C_{34}H_{28}O_{22}$	787.0996	0.3	617.0790, 465.0675, 313.0569, 169.0144	2
26	15.98	Trigalloyl parasorboside	$C_{33}H_{32}O_{20}$	747.1414	0.1	635.0896, 465.0676	3
27	16.54	Galloyl feruloyl glucose	$C_{23}H_{24}O_{13}$	507.1147	0.7	355.1034, 193.0507, 169.0144	2
28	16.97	Quercetin *O*-deoxyhexoside	$C_{21}H_{20}O_{11}$	447.0929	0.4	300.0278, 271.0251, 178.9987, 151.0038, 121.0296	2
29	17.69	Pentagalloyl glucose	$C_{41}H_{32}O_{26}$	939.1111	0.9	787.0992, 617.0786, 465.0673,313.0567, 169.0144	2
30	18.90	Kaempferol *O*-deoxyhexoside	$C_{21}H_{20}O_{10}$	431.0892	1.0	285.0405, 255.0300, 163.0039, 151.0037	2
31	18.97	Myricetin *O*-galloyl deoxyhexoside	$C_{28}H_{24}O_{16}$	615.0994	1.2	463.0883, 317.0305, 178.9987, 151.0038, 137.0245, 169.0144	2
32	19.47	Coumaroyl trigalloyl glucose	$C_{36}H_{30}O_{20}$	781.1260	1.0	617.0790, 465.0674, 313.0569, 169.0144	2
33	19.90	Cinnamoyl galloyl glucose	$C_{22}H_{22}O_{11}$	461.1091	1.2	313.0565, 169.0144	2
34	20.33	Quercetin *O*-galloyl deoxyhexoside	$C_{28}H_{24}O_{15}$	599.1048	0.9	447.0931, 301.0356, 178.9987, 151.0038, 121.0296	2
35	20.97	Methyl quercetin	$C_{16}H_{12}O_7$	315.0515	1.5	300.0278, 271.0250	2
36	21.28	Dimethoxy flavone hexoside	$C_{24}H_{26}O_{13}$	521.1300	-0.1	313.0720, 298.0484, 283.0250	3
37	21.45	Genistein	$C_{15}H_{10}O_5$	269.0457	0.5	241.0505, 133.0296	1
38	21.97	Trihydroxy-octadecadienoic acid	$C_{18}H_{32}O_5$	327.2180	1.0	229.1446, 211.1341	2
39	22.07	Trihydroxy-octadecadienoic acid	$C_{18}H_{32}O_5$	327.2180	1.0	229.1446, 211.1341	2
40	22.33	Trihydroxy-octadecenoic acid	$C_{18}H_{34}O_5$	329.2337	1.0	229.1446, 211.1341	2

In the (-)-HRMS^2 spectrum of Sil, diagnostic ions were detected at m/z 443.1196, 331.0671, 169.0144, and 483.0784, attributable respectively to the sequential loss of galloyl ($C_7H_4O_4$, m/z 152.0104), pyranone ($C_6H_8O_2$, m/z 112.0519), a hexose unit ($C_6H_{10}O_5$, m/z 162.0523), and the ion [M–H–$C_6H_8O_2$]$^-$, supporting the putative identification of Sil, which was subsequently confirmed by purification and NMR analysis. Compounds 7, 9, 11, and 26 were classified as Sil analogues based on the similarity in fragmentation patterns. For example, in compound 7, proposed as the acid form of siliquapyranone (Sil-A), the ions at m/z 483.0783 and 331.0674 correspond to the loss of a pyranone unit plus a water molecule ([M–H–$C_6H_{10}O_3$]$^-$ and [M–H–$C_7H_4O_4$–$C_6H_{10}O_3$]$^-$).

The second main class of metabolites of CSL extracts is FGs. Among these, myricitrin (21) was found to be the predominant compound. In total, nine FGs (18, 20, 21, 23, 28, 30, 31, 34, and 35) were tentatively identified based on diagnostic ions obtained in (−)-HRMS^2 spectra, attributable to neutral sugar losses, retro-Diels–Alder fragmentations (1,3A$^-$, 1,2A$^-$, and 1,2B$^-$), and other characteristic dissociations of the flavonol skeleton [54].

Thus, UHPLC-HRMS/MS analysis has enabled the comprehensive phytochemical profiling of CSL, distinguished by the presence of GGs, FGs, and peculiar markers such as Sil, Sil-A, TeGG and Myr (Fig. 3.2).

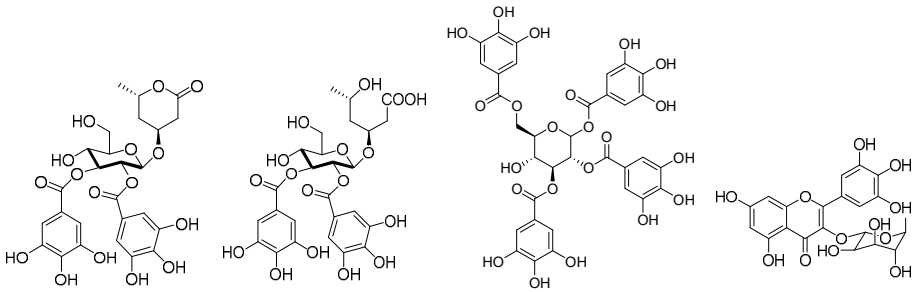

Figure 3.2. *Main marker compounds of CSL.*

Similar qualitative profiles were also observed in CSL sampled in various Italian regions (Fig. 3.3), including Veneto (Padova Botanical Garden), Campania (University of Salerno), and Puglia, where the *Amele* variety

coexists with the wild variety, confirming the presence of the main metabolites as markers of the plant and the dominant chemical classes.

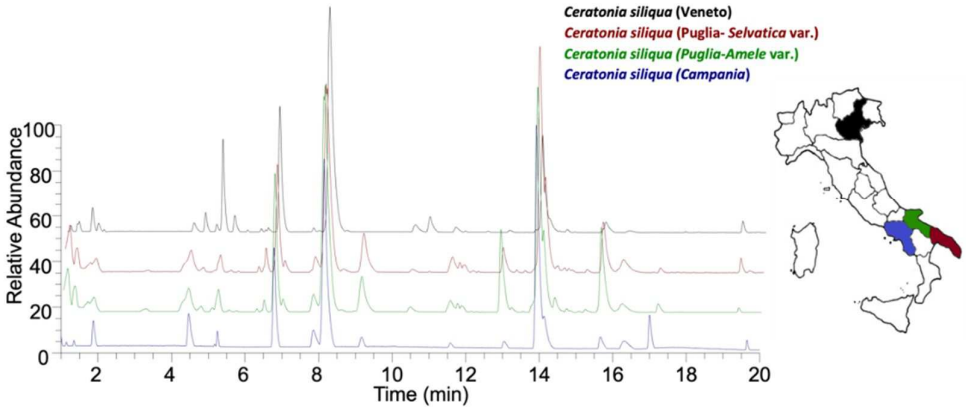

Figure 3.3. *UHPLC-UV chromatograms (280 nm) of CSL collected in different Italian regions (Veneto black line, Selvatica variety collected in Puglia red line, Amele variety collected in Puglia green line and Campania blue line).*

3.2.1.2 Isolation of major CSL compounds

The main compounds in the CSL extracts were isolated in their pure form using automated flash chromatography on a C18 reverse phase column. The isolation focused on two metabolites of interest: Sil and TeGG, which were selected based on their relative abundance, the absence of commercial standards and the limited knowledge of their structures, justifying their isolation for further study.

This process enabled the purification of Sil, TeGG and Myr with a purity greater than 95%, as determined by UHPLC-DAD. The structures were clarified by NMR experiments, which confirmed the identity of Sil (Fig. 3.2) and allowed the correct assignment of the position of the galloyl units on the glycosidic skeleton of TeGG, identified as 1,2,3,6-tetragalloylglucose (Fig. 3.2).

3.2.1.3 Quantitative analysis

Untargeted UHPLC-HRMS analysis showed that the qualitative profiles of CSL extracts remained comparable throughout the entire sampling period. To further investigate these observations, the main metabolites were then

quantified using the UHPLC-UV method with external standards. The compounds selected as quantitative markers (1–3, 6, 9–11, 13–15, 17, 18, 21, 22, 28 and 29; Fig. 3.1B) were quantified in all the extracts between May and September (Table 3.2).

Table 3.2. *Level of main CSL compounds according to the harvesting period.*

	Quantitative data [1]				
Compounds (mg g^{-1} extract)	**May**	**June**	**July**	**August**	**September**
Galloyl glucose [2]	1.9 ± 0.1 [b]	7.7 ± 0.1 [d]	3.0 ± 0.1 [c]	2.9 ± 0.1 [c]	1.6 ± 0.1 [a]
Gallic acid	3.9 ± 0.2 [a]	5.1 ± 0.2 [b]	6.0 ± 0.2 [c]	6.2 ± 0.1 [c]	5.1 ± 0.2 [b]
Digalloyl glucoses [2]	3.1 ± 0.1 [a]	5.3 ± 0.1 [c]	5.5 ± 0.2 [c]	4.6 ± 0.1 [b]	4.4 ± 0.1 [b]
Digalloyl glucose [2]	3.4 ±0.1 [a]	5.8 ± 0.1 [c]	6.0 ± 0.2 [c]	4.8 ± 0.1 [b]	4.8 ± 0.1 [b]
Galloyl parasorboside [2]	2.1 ± 0.1 [d]	1.9 ± 0.1 [b]	1.9 ± 0.1 [b]	2.0 ± 0.1 [c]	1.8 ± 0.1 [a]
Methyl gallate [2]	3.8 ± 0.4 [a]	3.4 ± 0.5 [a]	4.2 ± 0.5 [a]	4.0 ± 0.4 [a]	4.3 ± 0.4 [a]
Siliquapyranone acid form [3]	17.4 ± 0.6 [a]	22.8 ± 0.4 [b]	28.8 ± 1.2 [c]	21.9 ± 0.4 [b]	22.6 ± 0.4 [b]
Trigalloyl glucoses [2]	1.6 ± 0.1 [a]	4.0 ± 0.1 [c]	3.9 ±0.2 [c]	2.5 ± 0.1 [b]	2.5 ± 0.1 [b]
Siliquapyranone	39.1 ± 0.2 [a]	55.4 ± 1.0 [d]	56.3 ± 1.6 [d]	51.8 ± 0.8 [c]	47.6 ± 0.7 [b]
Trigalloyl glucose [2]	1.3 ±0.1 [ab]	1.2 ± 0.1 [a]	1.7 ± 0.1 [c]	1.3 ± 0.1 [b]	1.4 ± 0.1 [b]
Trigalloyl glucose [2]	4.6 ± 0.1 [a]	4.6 ± 0.1 [a]	6.4 ± 0.6 [c]	5.4 ± 0.1 [b]	5.1 ± 0.1 [ab]
Myricitin 3-*O*-hexoside [4]	2.4 ± 0.1 [a]	4.3 ± 0.1 [c]	2.9 ± 0.1 [b]	2.9 ± 0.1 [b]	2.4 ± 0.1 [a]
Myricitrin	27.0 ± 0.6 [a]	31.5 ± 0.9 [b]	32.8 ± 1.1 [b]	33.0 ± 0.5 [b]	32.0 ± 0.6 [b]
1,2,3,6-Tetragalloyl glucose	46.5 ± 2.3 [a]	52.5± 1.9 [b]	69.4 ± 3.2 [d]	58.9 ± 1.5 [c]	52.3 ± 1.4 [b]
Quercetin 3-*O*-deoxyhexoside[5]	6.4 ± 0.1 [c]	5.6 ± 0.1 [b]	5.7 ± 0.4 [b]	4.7 ± 0.1 [a]	4.2 ± 0.2 [a]
Pentagalloyl glucose [2]	4.1 ±0.5 [ab]	4.5 ± 0.5 [ab]	7.1 ± 0.5 [c]	5.0 ± 0.4 [b]	3.5± 0.6 [a]
Galloylglucosides (GGs)	132.7±3.4 [a]	174.1 ± 3.7 [c]	200.2 ± 7.7 [d]	171.4 ± 1.8 [c]	156.9 ± 2.2 [b]
flavonol glycosides (FGs)	35.7±0.7 [a]	41.4 ± 0.8 [c]	41.3 ± 1.2 [c]	40.5 ± 0.7 [bc]	38.5± 0.4 [b]
Total	168.4 ± 4.1 [a]	215.4 ± 4.5 [c]	241.6 ± 8.9 [d]	211.8 ± 2.4 [c]	195.4 ± 2.6 [b]

[1] different superscript letters in the same raw indicate significantly different values ($p \leq 0.05$ by a Tukey's HSD test); [2] gallic acid equivalent; [3] siliquapyranone equivalent; [4] myricitrin equivalent; [5] quercetin-3-O-glucoside equivalent.

The results showed a total metabolite content ranging from 168 to 242 mg g^{-1} of extract. The most abundant metabolite class was GGs, which constituted 79–83% of the total. The predominant GGs were Sil and TeGG (28–32% and 30–35% of GGs, respectively). Among FGs, Myr was the main metabolite, constituting 75–83% of this class. The concentrations of key metabolites, Sil (39–56 mg g^{-1}), Sil-A (17–29 mg g^{-1}), TeGG (46–69 mg g^{-1}), and Myr (27–33 mg g^{-1}), as well as the total contents of GGs (133–200 mg g^{-1}) and FGs (36–41 mg g^{-1}) retained similar ranges during the period considered (Fig. 3.4). However, significantly lower levels were observed in the spring harvest ($p < 0.05$), followed by a gradual increase in summer, with a peak at the end of July, before declining in September. No statistically significant variations emerged for FGs between June and September (Table 3.2). Based on this evidence, the optimal harvesting period is between July and August, coinciding with fruit

harvesting. This is a key benefit, as harvesting the leaves during the same time frame would not lead to extra costs, enhancing the efficiency of the entire production chain.

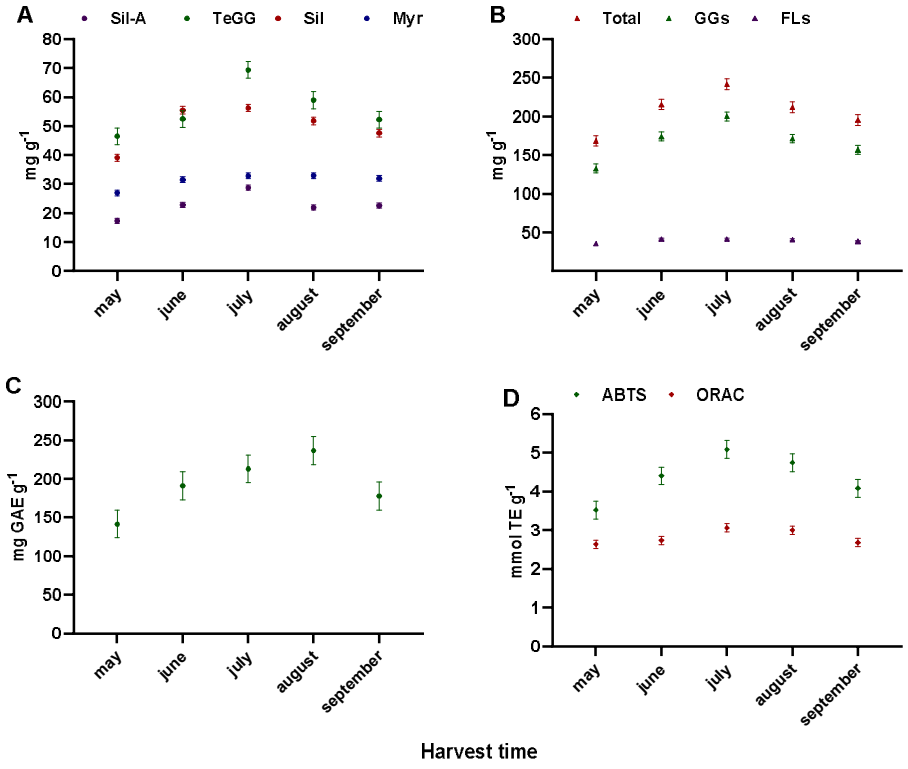

Fig. 3.4. *Means plot of (A) main compounds, (B) metabolite classes, (C) TPC and (D) AOC (ABTS and ORAC assays) of CSL according to harvesting time.*
Bars display the Tukey's HSD confidence intervals.

3.2.1.4 Total Phenolic Content (TPC)

UHPLC analysis showed that phenolic compounds are the predominant constituents of CSL, making TPC a rapid and effective indicator for characterizing this unexploited biomass. The TPC values (Table 3.3) obtained from the exhaustive extracts showed a consistent trend with the quantitative profile of bioactive metabolites (Fig. 3.4), with the highest levels detected in samples collected in July (213 mg GAE g^{-1}) and August (237 mg GAE g^{-1}). These data confirm that the summer months are the most favourable harvesting period for maximizing metabolic content. Furthermore, the TPC values recorded far exceed those reported for mature carob pods from various

producing countries (18–41 mg GAE g^{-1}, extracted in alcoholic solvent) [55] and are in line with the range described for leaves (65–162 mg GAE g^{-1}) [48]. Overall, these results demonstrate that carob leaves are a particularly rich source of phenolic compounds, even more concentrated than pods, highlighting their potential as an alternative source of bioactive molecules.

3.2.2 Cell free in vitro assays

Food and medicinal plants are now recognized as valuable sources of bioactive molecules that are useful for preventing and managing chronic diseases such as diabetes, cardiometabolic disorders, cancer and Alzheimer's disease. Plant extracts and isolated compounds have demonstrated an impressive ability to modulate key enzymes involved in these processes, generating increasing interest in natural products thanks to their biocompatibility and minimal side effects [11]. Based on these findings, CSL extracts, and its main metabolites were evaluated using *in vitro* assays to characterize their functional potential, expanding the preliminary knowledge available on carob leaves. The selected activities were based on preliminary research conducted on carob leaves.

3.2.2.1 AOC (ABTS and ORAC assays) of CSL extracts and its main compounds

The *in vitro* antioxidant capacities (AOC) of CSL extracts and the main isolated compounds (TeGG, Sil, and Myr) were evaluated using ORAC and ABTS assays (Fig. 3.4, Table 3.3). The exhaustive extracts showed significant activity in both tests (3.5–5.1 and 2.6–3.1 mmol TE g^{-1}, respectively), with higher values in samples collected at the end of July, in line with higher metabolic content and TPC, suggesting a correlation between antioxidant activity and polyphenol content. Despite limitations in comparison with the literature due to different methods of expressing results, our data are in line with the only value available for carob leaves (ABTS, 3.3 mmol TE g^{-1}) [47] and significantly higher than those reported for pods (ABTS, 0.1–0.2; ORAC, 0.3–0.4 mmol TE g^{-1}) [56,57]. Compared to the leaves of other fruit trees, CSL exhibited higher ABTS values (3.5–5.1 mmol TE g^{-1}) than apricots (0.7–1.7), apples (0.4–0.6),

pears (0.8–0.9) and quinces (0.8–0.9), and values similar to those of pomegranates (3.9–4.0). However, in the ORAC test, CSL values (2.6–3.1 mmol TE g^{-1}) were slightly lower than those reported for the same matrices (apricot: 3.0–4.1; apple: 3.6–4.9; pear: 3.4–5.0; quince: 4.6–5.9) [47,58].

Table 3.3. *AOC of CSL extracts and its main compounds*

Index [1]	May	June	July	August	September
TPC (mg GAE g^{-1} extract)	141.6 ± 9.3^{a}	191.2 ± 4.0^{b}	212.9 ± 8.4^{bc}	236.6 ± 0.1^{c}	177.6 ± 26.8^{b}
ABTS (mmol TE g^{-1} extract)	3.5 ± 0.1^{a}	4.4 ± 0.^{bc}	5.1 ± 0.3^{d}	4.7 ± 0.2^{cd}	4.1 ± 0.1^{b}
ORAC (mmol TE g^{-1} extract)	2.6 ± 0.1^{a}	2.7 ± 0.1^{a}	3.1 ± 0.1^{b}	3.0 ± 0.1^{b}	2.7 ± 0.1^{a}

	TeGG	Sil	Myr	Quercetin
ABTS (µmol TE $µmol^{-1}$)	9.9 ± 0.1	7.3 ± 0.4	5.7 ± 0.2	10.0 ± 0.6
ORAC (µmol TE $µmol^{-1}$)	1.6 ± 0.1	2.2 ± 0.03	2.2 ± 0.1	5.1 ± 0.1

[1] Data were expressed as mean ± SD of three assay replicates. Different superscript letters in the same raw indicate significantly different values ($p \leq 0.05$ by a Tukey's HSD test).

AOC strongly correlated with TPC and levels of the main compounds. ABTS exhibited the highest correlations (Pearson's correlation coefficient $r > 0.86$, $p < 0.001$), particularly with TeGG and Sil, whose antioxidant activity was highly comparable to quercetin, a natural antioxidant reference (Table 3.3). In the ORAC assay, TeGG, Sil, and Myr exhibited a good activity (Table 3.3), although lower than quercetin. ORAC showed a closer relationship with UHPLC quantitative data, especially for the total content of quantified compounds ($r = 0.83$, $p < 0.001$), GGs ($r = 0.83$) and Sil ($r = 0.81$). Interestingly, these differences reflect the nature of the two methods. ABTS combines SET (Single electron transfer) and HAT (Hydrogen atom transfer) mechanisms to evaluate overall AOC using an artificial radical. In contrast, ORAC is based exclusively on HAT and peroxyl radicals and more closely replicates biological oxidative mechanisms. This difference helps clarify why the values are not the same and makes the combined use of the two tests especially informative.

Overall, the results confirm that carob leaves are a promising source of antioxidants, with TeGG and Sil being the main contributors to the observed activity.

3.2.2.2 α-GLU and α-AMY inhibitory activities of CSL extracts and its main compounds

Postprandial hyperglycemia is one of the most significant symptoms of diabetes mellitus (DM) and a determining factor in the development of type 2 diabetes mellitus (T2DM) and its complications, including cardiovascular disease, nephropathy, neuropathy and angiopathy. A well-established strategy to delay its onset is to reduce intestinal carbohydrate absorption by inhibiting the digestive enzymes α-AMY and α-GLU [35]. α-AMY begins the digestion of complex carbohydrates by breaking starch into smaller molecules, α-GLU then completes the process by converting oligosaccharides and disaccharides into absorbable monosaccharides, such as glucose. Therefore, identifying new sources, particularly natural ones, that can modulate the activity of both enzymes is crucial [59].

CSL extracts and the main isolated compounds (TeGG, Sil, and Myr) were tested *in vitro* to see how they affected enzyme inhibition. The results were then compared with those of acarbose (A), a drug used to treat diabetes, and quercetin (Q), a natural compound with potent α-GLU inhibitory activity. In addition to IC_{50} values, activity was expressed as relative activities to positive controls (RA_A and RA_Q). RA values <1, = 1, and > 1 respectively denote a stronger, equivalent, and weaker inhibitory activity compared to A and Q [60]. Expressing the results in relation to the positive controls (A and Q) not only allows for a more direct assessment of the potential biological relevance of the data but also represents a useful approach for standardizing measurements between different laboratories, making comparisons between studies more consistent and easier to interpret.

CSL extracts showed poor inhibitory capacity against α-AMY (Figure 3.5 A-B, Table 3.4) (IC_{50}= 186.4 – >200 μg mL^{-1}), significantly lower than that of acarbose (RA_A = 5). Only TeGG showed moderate activity (IC_{50} = 98.2 ± 1.9 μM; RA_A = 1.6), which was still weaker than the controls (Table 3.4). In contrast, the results on α-GLU revealed a very marked dose-dependent inhibition (Figure 3.5 C-D), with IC_{50} values between 0.51 and 0.58 μg mL^{-1}, which were much lower than those of acarbose (RA_A = 0.003) and quercetin (RA_Q = 0.1) (Table 3.4). The selectivity for α-GLU over α-AMY, already observed for carob

pulp [59], is particularly interesting from a clinical point of view: selective α-GLU inhibitors are considered safer in the management of T2DM, as α-AMY inhibition can cause undesirable gastrointestinal effects related to the passage of undigested carbohydrates into the colon [35].

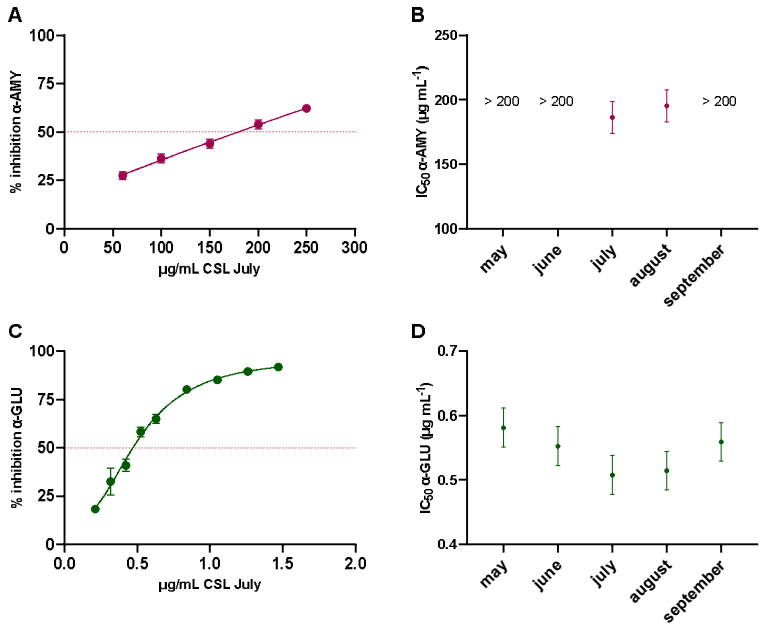

Fig.3.5. *Inhibition curves and IC_{50} means plot of α-AMY (A, B) and α-GLU (C, D) of CSL extracts according to harvesting time. Bars display the Tukey's HSD confidence intervals.*

Table 3.4. *α-GLU and α-AMY inhibition of CSL extracts and its compounds.*

Enzyme Inhibition assay [1]					
Enzyme (IC_{50})	**May**	**June**	**July**	**August**	**September**
α-GLU (μg mL^{-1})	0.58 ± 0.01 [a]	0.55 ± 0.03 [ab]	0.51 ± 0.02 [b]	0.51 ± 0.02 [b]	0.56 ± 0.03 [ab]
RA_A [2]	0.003	0.003	0.003	0.003	0.003
RA_Q [3]	0.1	0.1	0.1	0.1	0.1
α-AMY (μg mL^{-1})	> 200	> 200	186.4 ± 4.0	195.4 ± 9.0	> 200
RA_A [b]	–	–	4.9	4.6	–
	TeGG	**Sil**	**Myr**	Quercetin	Acarbose
α-GLU (μM)	0.049 ± 0.002	14.5 ± 0.6	230.7 ± 4.0	15.8 ± 0.1	295.3 ± 7.9
RA_A [2]	0.0002	0.05	0.8	–	–
RA_Q [3]	0.003	0.9	14.6	–	–
α-AMY (μM)	98.2 ± 1.9	> 500	> 500	–	62.3 ± 0.7
RA_A [2]	1.6			–	–

[1] Data were expressed as mean ± SD of three assay replicates, Different superscript letters in the same raw indicate significantly different values ($p \leq 0.05$ by a Tukey's HSD test); [2] RA_A, relative activity to acarbose; [3] RA_Q, relative activity to quercetin.

TeGG and Sil resulted as potent α-GLU inhibitors, with IC_{50} <15 μM (Table 3.4), significantly lower than those of A (RA_A = 0.0002 and 0.05, respectively). Myr, on the other hand, showed a comparable activity to the drug (IC_{50} = 230.7 ± 4.0 μM). Compared to Q, Sil demonstrated similar efficacy (RA_Q = 0.9), whereas TeGG stood out due to its significantly higher potency (RA_Q = 0.003). Correlation analysis revealed a close association between GGs and α-GLU inhibition, identifying TeGG as the main contributor to the overall inhibitory activity of the extracts ($r = -0.71$, $p < 0.01$). These data are in line with earlier evidence on gallotannins, where the number of galloyl units is linked to inhibitory activity [36,39]. Gallotannins containing 3–10 galloyl units exhibited IC_{50} values ranging from 1 to 15 μM. Pentagalloylglucose and tannic acid emerged as the most potent inhibitors, with IC_{50} values of approximately 1 μM and RA_A values of 0.004–0.006, respectively. However, the activity of 1,2,3,6-tetragalloylglucose (TeGG) had not previously been reported, making this result particularly significant.

Overall, the results demonstrate that CSL extracts, and TeGG in particular, have strong hypoglycemic potential through the selective inhibition of α-GLU, making them potential functional ingredients in the prevention and management of T2DM.

3.2.2.3 Cholinesterase (AChE and BChE) inhibitory activities of CSL extracts and its main compounds

In Alzheimer's disease, cognitive decline is linked to cholinergic dysfunction and reduced acetylcholine (ACh) levels. As the disease progresses, AChE activity decreases while butyrylcholinesterase (BChE) activity increases, both contributing to cholinergic deficiency [26]. Therefore, dual AChE/BChE inhibition represents a promising approach to enhance ACh levels and improve cognitive function.

The potential inhibitory activities of CSL extracts and their main compounds against AChE and BChE were therefore evaluated *in vitro* using galantamine as a reference drug and fluorescent enzyme kinetics [27]. Inhibitory potency was expressed as both IC_{50} values and relative activity to galantamine (RA_G) [29], enabling more immediate comparisons.

CSL extracts exhibited dose-dependent inhibition of both cholinesterase enzymes (Fig. 3.6).

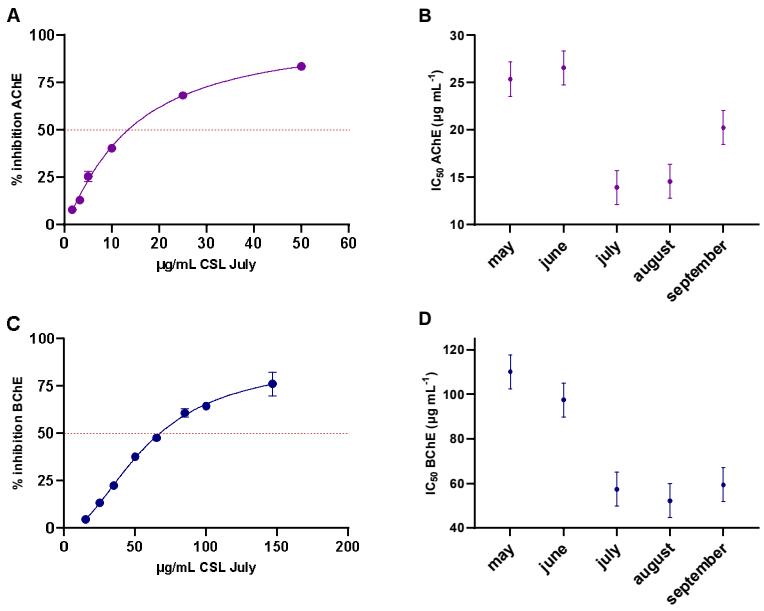

Fig.3.6. *Inhibition curves and IC_{50} means plot of AChE (A,B) and BChE (C,D) of CSL extracts according to harvesting time. Bars display the Tukey's HSD confidence intervals.*

For AChE, the IC_{50} values ranged from 13.9 to 26.6 μg mL^{-1} (Table 3.5), with significantly higher activity observed in samples collected in July and August (Fig. 3.6B). According to Dos Santos et al., [28] criteria, these extracts are highly potent inhibitors (IC_{50} < 20 μg mL^{-1}). The extracts also exhibited significant inhibitory activity against BChE (IC_{50} 52.2–110.1 μg mL^{-1}), although approximately four times lower than that observed for AChE (Table 3.5). The trend in inhibitory potency varied with the harvest period, with peak activity occurring in the summer months (Fig. 3.6B-D and Table 3.5).

Table 3.5. *AChE and BChE inhibition of CSL extracts and its compounds.*

	Enzyme Inhibition assay [1]				
Enzyme (IC_{50})	**May**	**June**	**July**	**August**	**September**
AChE (μg mL^{-1})	25.4 ± 0.7 [a]	26.6 ± 2.3 [a]	13.9 ± 0.2 [c]	14.6 ± 0.2 [c]	20.3 ± 1.5 [b]
RA_G [2]	26	28	14	15	21
BChE (μg mL^{-1})	110.1 ± 11.1 [a]	97.5 ± 3.5 [a]	57.4 ± 0.7 [b]	52.3 ± 0.8 [b]	59.4 ± 4.9 [b]
RA_G [2]	12	11	6	6	6
	TeGG	**Sil**	**Myr**	Galantamine	
AChE (μM)	65.4 ± 4.2	88.9 ± 7.0	58.6 ± 6.6	2.6 ± 0.1	
RA_G [2]	25.2	34.2	22.5	–	
BChE (μM)	24.9 ± 0.8	240.1 ± 8.1	88.9 ± 4.8	25.2 ± 0.2	
RA_G [2]	1.0	9.5	3.5	–	

[1] Data were expressed as mean ± SD of three assay replicates. Different superscript letters in the same raw indicate significantly different values ($p \leq 0.05$ by a Tukey's HSD test); [2] RA_G, relative activity to galantamine.

Unlike the extracts, the pure compounds TeGG, Sil, and Myr (Table 3.5) showed only weak activity against ChEs [61], with IC_{50} values between 20 and 100 μM for AChE and between 50 and 150 μM for BChE. The only exception was TeGG, which exhibited moderate to strong inhibition of BChE (IC_{50} 10–50 μM), comparable to galantamine (RA_G = 1.0). These results suggest that the potent inhibitory activity of CSL extracts against AChE and BChE is not solely due to the tested compounds but is likely due to the action of additional untested components or the synergistic interaction of different metabolites. As is well known, plant extracts can exhibit synergistic, additive or antagonistic activities between their constituents, resulting in a biological activity of the phytocomplex that is greater (or sometimes lower) than that of the individual compounds [62].

3.3. Green extraction techniques for sustainable recovery of CSL compounds

Comprehensive analysis of bioactive profile and health-promoting potential of CSL revealed high levels of n-galloylated glucoses (GGs) and flavonol-glycosides (FGs), with siliquapyranone (Sil), 1,2,3,6-tetragalloylglusose (TeGG) and myricitrin (Myr) as main compounds and contributors to CSL's activities [63]. The metabolites identified in CSL, along with their demonstrated *in vitro* bioactivities, confirm the great potential of this matrix as a valuable source for the recovery of bioactive compounds. Its sustainable exploitation through advanced, eco-friendly extraction technologies not only enhances the recovery and value of these metabolites but also contributes to the achievement of the SDGs [64].

Conventional extraction methods, such as solid-liquid extraction, have traditionally been considered the core unit operation in the recovery of bioactive compounds from plant matrices. However, these processes often involve multiple laborious steps and rely heavily on large amounts of organic solvents. Moreover, they are time- and energy-intensive, produce significant waste, and can compromise extract quality due to the presence of residual solvents or thermally degraded compounds. In contrast, modern green and non-conventional extraction technologies have been developed to intensify these processes. Their main objective is to achieve higher extraction efficiency and product quality while minimizing solvent use, processing time, energy demand, and environmental impact, ultimately aligning with both economic and sustainability goals and the principles of green chemistry [8]. Among them, Pressurized Liquid Extraction (PLE) enhances solvent efficiency through high temperature and pressure, allowing rapid extraction, although it may lead to the degradation of thermolabile compounds and involves high equipment costs. Its sustainable variant, PHWE, exploits the reduced dielectric constant of water under pressure and heat to improve the extraction of polar and medium-polar compounds [65]. The exclusive use of water as a solvent makes the resulting extract directly applicable for subsequent processing or formulation, eliminating the need for post-extraction steps, thereby reducing

both processing time and environmental impact. Alongside PLE, UAE is an innovative technique based on ultrasonic cavitation, which disrupts cell walls and enhances mass transfer, enabling fast and high-yield extractions with limited thermal degradation. It requires simple and energy-efficient equipment, but its reliance on organic solvents and the need for additional post-extraction steps remain the main drawbacks [15]. In both cases, the effectiveness and quality of the process depend on the optimization of the operating parameters, essential for maximizing the recovery of target compounds, reducing environmental impact, and preserving the naturalness of the extracts. Careful evaluation of the outputs (chemical profile, metabolite levels, and degradation indicators) is equally essential to ensure high-quality products [15].

This section focuses on the design and optimization of two advanced extraction techniques, PHWE and UAE, for the sustainable recovery of bioactive compounds from CSL. Both techniques were specifically tailored to extract target metabolites using mild and eco-friendly solvents (water or low % of EtOH). The overall aim was to improve extraction efficiency and extract quality while reducing processing time, solvent consumption, and environmental impact. PHWE and UAE using a probe system (probe-UAE) were explored and optimized through Response surface methodology (RSM), monitoring the quali-quantitative profile of the extracts by UHPLC-UV analysis. Optimal conditions were established to maximize the recovery and extract content of CSL markers, Sil, TeGG and Myr, while simultaneously minimizing their degradation during the processes. Finally, the performance of these extraction techniques was compared with conventional methods, specifically Soxhlet extraction and maceration.

3.3.1 Pressurized hot water extraction (PHWE)

PHWE is among the most promising green extraction techniques, enabling rapid, automated, and efficient recovery of bioactive compounds in an environmentally friendly manner. It eliminates the need for organic solvents, producing extracts suitable for direct use or further processing. In this study,

water was used as the sole extraction solvent, without the addition of modifiers, based on the chemical profile of CSL and to avoid the costs associated with solvent evaporation or recycling. Under PHWE conditions, the dielectric constant of water decreases, reducing its polarity and making it effective for extracting both polar and moderately polar compounds [66].

PHWE performance mainly depends on temperature, pressure, and extraction time, although parameters such as particle size, solid-to-liquid ratio, dispersing agent, and potential modifiers may also influence extraction yield [66,67].

Despite the advantages of this technique, prolonged exposure to high temperatures can cause thermal degradation of sensitive metabolites and loss of bioactivity. Therefore, careful optimization of operating parameters is essential to obtain high-quality extracts and prevent artefact formation [68].

3.3.1.1 Preliminary PHWE experiments

Preliminary experiments were conducted before proceeding with the setup of a Design of experiments (DoE) to define specific technical parameters and reduce the number of independent variables in the analysis. These tests enable a more precise definition of the experimental domain and the most appropriate operating conditions. In this way, chemometric optimization could focus on the most relevant factors, reducing complexity and improving the overall efficiency of the process [68].

Preliminary experiments were conducted in triplicate at 100 bar, one cycle, 10 min of static time, 50 g/L matrix/solvent ratio, 50% of cell volume rinse and 40 sec of purge, to define specific technical parameters, optimize the range of independent factors, and reduce the number of variables to be included in the chemometric analysis. The tests concerned temperature (60–175°C), matrix amount (1-3 g) and type of dispersant (diatomaceous earth, sand, glass beads).

A crucial aspect was the study of the stability of the main CSL compounds under PHWE conditions at different temperatures (60–175°C), to define the maximum operating temperature. In this range, the dielectric constant of water is reduced by about 40%, from typical values of 79 at room temperature to about 35 at 200 °C, making it a solvent with polarity comparable to methanol

[66]. This variation increases the solubility and therefore the extraction of medium-polar compounds. However, high temperatures can trigger undesirable reactions, such as degradation or hydrolysis of thermolabile metabolites and formation of Maillard products.

UHPLC-DAD-HRMS data (Fig. 3.7) showed that Myr increases up to 135°C, in contrast to Sil and TeGG, which begin to decrease at temperatures above 120°C. Gallic acid (GA) starts to increase at 90°C, a phenomenon attributable to the hydrolysis of the ester bonds of GGs. A similar temperature-dependent hydrolytic effect on galloylated compounds has been observed in pistachio hulls[69] chestnut shells [69] and winery by-products [70] subjected to SWE at high temperatures. In these studies, the release of gallic acid during extraction was attributed to the hydrolysis of hydrolyzable tannins and galloylated procyanidins.

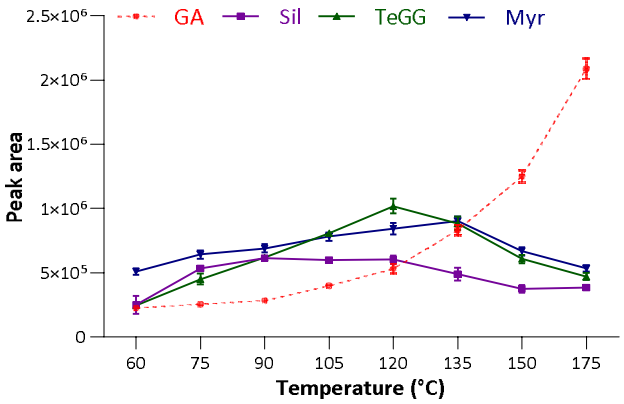

Fig. 3.7. *Temperature-trend of main CSL compounds (Sil, TeGG and Myr) and hydrolysis indicator (GA).*

Furthermore, gallic acid may undergo thermal decarboxylation to pyrogallol at elevated temperatures, as reported in the literature [69]. This phenomenon was observed only at 135°C in our data. Moreover, previous studies suggest the formation of 5-hydroxymethylfurfual (HMF) as an undesirable product of Maillard and/or caramelization reactions [71]. In our conditions only small traces of HMF were detected at 150°C. Therefore, the maximum operating temperature was set at 140°C, a compromise between extraction efficiency and prevention of degradation or artifacts.

Concerning matrix amount, 1.5 g was established as the optimal quantity to ensure efficient analyte recovery. The dispersing agents (diatomaceous earth, sand, and glass beads) showed comparable performance in terms of analyte recovery, but with different effects on the quality and clarity of the extract Diatomaceous earths produced extracts containing suspended solid material, likely released from dispersant under the applied conditions. Glass beads instead proved to be the most sustainable solution, as they are washable and reusable, and therefore more suitable from a green perspective.

3.3.1.2 Optimization of PHWE by RSM

Insights from preliminary experiments highlighted temperature as a critical factor influencing CSL extract quality, which is primarily determined by the content of active compounds and the absence of denatured molecules or extraction artefacts [66]. Increasing temperature enhances the solubility of other matrix components, reducing extraction selectivity, and can cause degradation of thermolabile compounds and chemical reactions, such as caramelization and Maillard reactions [66]. Moreover, extraction time also plays a crucial role in the stability of labile compounds, as prolonged exposure to high temperatures can further promote degradation [69]. Consequently, simultaneous optimization of temperature and extraction time in PHWE is essential to achieve a balance between extraction efficiency and bioactive compound stability.

In light of these considerations, PHWE optimization was conducted using RSM with a Box-Behnken design (BBD), evaluating the effects of temperature (A), static time (B), and number of cycles (C) (Table 3.6). Key response variables included extraction efficiency (EE, mg g^{-1} leaf) and extract content (P, g 100 g^{-1} extract) for the target compounds, while GA content was monitored as an indicator of the hydrolytic degradation of TeGG and Sil and considered a response to be minimized. In addition, for comparative analysis, extraction yield (EY) and TPC, were included. This strategy allowed the identification of optimal operating conditions to maximize the recovery of main metabolites, while ensuring the stability of the most sensitive compounds and the overall quality of the extract.

Table 3.6. *Independent PHWE factors and their levels[a].*

Independent factors	Units	Level		
		− 1	**0**	**1**
A. Temperature	°C	60	100	140
B. Static time	min	5	8	11
C. cycle	n	1	2	3

[a]Fixed factors: extraction solvent, water; pressure, 100 bar; purge, 40 sec; rinse, 50% cell volume.

The results for all these variables, obtained under different BBD experimental conditions, are reported in Table 3.7. The highest levels of Sil, TeGG and Myr were consistent with previously data for CSL exhaustive extracts (3.9-5.6, 5.2-6.9 and 2.7-3.3 g 100–1 extract, respectively for Sil, TeGG and Myr). These results indicate that PHWE can achieve complete recovery of target analytes from the matrix.

The analysis of the effects of experimental factors A–C, their interactions, and their statistical significance was conducted using ANOVA (Table 3.8), while the standardized contributions to the response variables are shown in the Pareto charts (Fig. 3.8). The results showed that temperature (A) and number of cycles (C) are the most influential factors for all responses considered. Moreover, the quadratic term of temperature (AA) and its interactions with static time (AB) and number of cycles (AC) have a significant role. In contrast, static time (B) showed a direct influence only on EY, Sil, and GA (Table 3.8). Furthermore, temperature and its interaction and quadratic terms produced contrasting effects on Sil and TeGG compared to GA (Fig. 3.8), suggesting that GA resulted in a key indicator of the hydrolytic degradation phenomena affecting these compounds.

The quadratic models (Table 3.8, Table 3.9), constructed by including only statistically significant terms ($p < 0.05$), were found to be very robust overall. In all cases, the p-value associated with the model was< 0.001, showing clear statistical significance and indicating that the findings are not the result of chance.

Table 3.7. *BBD matrix, target response values and predicted and experimental results obtained under optimal PHWE conditions.*

run	block	A (°C)	B (min)	C (n)	EE_Sil	EE_TeGG (mg g^{-1} CSL)	EE_Myr	P_Sil	P_TeGG (g 100 g^{-1} ex)	P_Myr	EE_GA (mg g^{-1} CSL)	TPC (mg GAE g^{-1})	yield (g 100 g^{-1})
1	1	100	8	2	11.5	11.3	8.9	4.8	3.9	2.7	4.3	56.9	30.5
2	1	140	5	2	7.7	11.0	9.5	2.6	3.3	2.5	7.3	74.1	33.9
3	1	140	8	3	4.6	8.8	9.0	1.1	2.2	2.2	13.9	113.9	41.3
4	1	60	8	1	7.2	3.6	5.3	4.1	1.8	2.3	2.1	28.2	21.6
5	1	100	11	3	10.0	11.1	9.0	4.3	4.3	2.9	5.0	70.0	30.8
6	1	100	5	3	12.3	12.8	9.6	5.6	4.5	3.0	4.1	66.8	30.4
7	1	60	5	2	9.1	4.0	6.2	4.5	2.0	2.6	2.4	34.2	23.1
8	1	140	11	2	4.6	7.9	9.2	0.8	2.0	2.2	13.6	107.2	38.9
9	1	100	5	1	11.1	7.9	7.3	5.7	3.4	2.7	2.7	38.9	24.7
10	1	100	11	1	9.9	10.4	8.1	4.3	3.8	2.7	3.6	50.5	28.1
11	1	60	8	3	10.4	6.1	8.0	5.1	2.8	3.0	2.9	45.3	25.9
12	1	100	8	2	11.4	12.4	9.3	4.4	4.2	2.8	4.7	65.5	29.4
13	1	60	11	2	10.2	5.4	7.3	5.3	2.5	2.9	2.9	39.0	25.1
14	1	140	8	1	5.3	9.9	8.7	1.6	3.2	2.6	7.8	75.0	33.7
15	1	100	8	2	10.4	10.6	8.5	4.8	4.5	3.0	3.7	63.2	29.9
16	2	100	8	2	11.4	13.3	9.5	4.5	4.5	2.9	4.1	68.6	29.1
17	2	140	5	2	8.4	13.1	10.0	2.5	3.8	2.6	7.3	82.3	35.1
18	2	140	8	3	5.7	11.8	9.5	1.1	2.7	2.1	11.9	109.9	41.7
19	2	60	8	1	8.1	4.0	5.7	3.9	2.0	2.4	2.3	28.1	22.3
20	2	100	11	3	9.6	12.4	9.1	3.5	4.1	2.7	5.2	69.7	30.9
21	2	100	5	3	12.2	13.3	9.3	4.9	4.7	2.9	4.3	66.3	30.6
22	2	60	5	2	9.9	4.8	6.6	4.4	2.1	2.4	2.5	34.7	23.8
23	2	140	11	2	4.7	8.7	8.6	0.9	2.3	2.1	12.3	97.4	38.9
24	2	100	5	1	10.8	8.7	7.4	5.3	3.7	2.8	2.7	45.3	24.7
25	2	100	11	1	8.8	10.0	7.6	3.8	3.9	2.7	3.8	46.4	27.0
26	2	60	8	3	10.7	6.1	7.9	4.8	2.6	2.8	3.1	41.8	26.2
27	2	100	8	2	11.0	12.7	9.1	4.5	4.5	2.9	4.2	62.4	28.8
28	2	60	11	2	10.3	5.8	7.5	4.6	2.5	2.7	3.0	38.6	25.0
29	2	140	8	1	5.9	11.7	8.9	1.8	3.5	2.6	7.8	76.2	32.2
30	2	100	8	2	10.5	12.3	8.8	4.4	4.3	2.8	4.1	63.2	28.4
Optimum		**°C**	**min**	**n**	**EE_Sil**	**EE_TeGG**	**EE_Myr**	**P_Sil**	**P_TeGG**	**P_Myr**	**EE_GA**	**TPC**	**yield**
Predicted values		**98**	**5**	**3**	11.9	13.2	9.2	5.3	4.4	2.9	3.9	65.3	30.4
95% confidence interval					11.5 - 12.4	11.9 - 14.4	8.9 - 9.5	5.0 - 5.5	4.2 - 4.7	2.8 - 3.0	3.3 - 4.6	61.0 - 69.5	29.4 - 31.3
Desirability		**0.90**			0.96	0.93	0.84	0.92	0.92	0.86	0.84	0.41	0.45
Experimental value (n = 6)					12.2 ± 0.2	13.8 ± 0.4	9.1 ± 0.1	5.2 ± 0.1	4.6 ± 0.3	2.9 ± 0.3	4.1 ± 0.2	60.0 ± 3.0	29.60 ± 0.7
95% confidence interval					12.0 - 12.4	13.8 - 13.9	9.0 - 9.2	5.1 - 5.3	4.4 - 4.8	2.6 - 3.1	3.9 - 4.2	60.3 - 61.4	28.8 - 30.1

Table 3.8. *Analysis of Variance (ANOVA) for response variables of PHWE.*

	Sil (mg/g leaf)		TeGG (mg/g leaf)		Myr (mg/g leaf)		GA (mg/g leaf)		Sil (% extract)		TeGG (% extract)		Myr (% extract)		Extraction yield		TPC (mgGAE/g)	
	F-value	*p-value*	*F-value*	*p-value*	*F-value*	*p-value*	*F-value*	*p-value*	*F-value*	*p-value*	*F-value*	*p-value*	*F-value*	*p-value*	*F-value*	*p-value*	*F-value*	*p-value*
A: Temperature	183.36	0.0002	219.91	0.0001	157.59	0.0002	1794.4	0.0000	1302.55	0.0000	26.72	0.0067	22.69	0.0089	3090.03	0.0000	438.29	0.0000
B: static time	39.15	0.0033	1.85	0.2452	0.11	0.7565	126.24	0.0004	141.18	0.0003	5.33	0.0821	1.69	0.2638	99.19	0.0006	0.34	0.0085
C: cycle number	15.38	0.0172	31.12	0.0051	67.84	0.0012	150.86	0.0003	0.02	0.8891	8.18	0.0459	3.00	0.1583	554.37	0.0000	2.55	0.0002
AA	253.25	0.0001	202.19	0.0001	27.56	0.0063	328.57	0.0001	627.86	0.0000	366.85	0.0000	58.50	0.0016	96.39	0.0006	2.25	0.0478
AB	30.04	0.0054	23.32	0.0085	12.08	0.0255	103.33	0.0005	85.41	0.0008	33.12	0.0045	18.37	0.0128	18.38	0.0128	1.21	0.0241
AC	19.57	0.0115	7.47	0.0522	14.12	0.0198	72.04	0.0011	42.40	0.0029	27.97	0.0061	37.50	0.0036	46.41	0.0024	5.94	0.0201
BB	1.19	0.3373	7.43	0.0526	1.63	0.2702	1.48	0.2905	8.96	0.0402	3.31	0.1432	0.35	0.5879	10.23	0.0329	1.94	0.0526
BC	1.26	0.3244	9.60	0.0363	2.86	0.1661	0.04	0.8532	0.18	0.6960	4.74	0.0950	0.37	0.5734	14.65	0.0187	4.59	0.6140
CC	11.24	0.0285	4.52	0.1005	8.96	0.0402	0.55	0.4989	1.55	0.2813	1.88	0.2426	0.35	0.5879	5.71	0.0752	1.36	0.1481
Lack of fit	0.71	0.7219	1.70	0.3237	0.41	0.9087	5.01	0.0653	3.30	0.1288	1.34	0.4243	0.55	0.8211	3.32	0.1274	15.81	0.5243
Lack of fit [a]	0.77	0.6905	2.45	0.1996	0.62	0.7804	4.29	0.0841	3.01	0.1475	1.65	0.3369	0.52	0.8521	3.47	0.1187	1.99	0.3853
Model		0.0000		0.0000		0.0000		0.0000		0.0000		0.0000		0.0000		0.0000		0.0047
R2		97.42		94.57		96.63		97.03		97.67		95.20		92.11		98.65		98.06
adjusted R2		96.07		91.71		94.85		95.47		96.45		92.67		87.96		97.95		97.03
R2 [a]		96.99		91.15		95.13		96.96		97.60		93.29		91.46		98.51		97.07
adjusted R2 [a]		95.85		88.33		93.27		95.99		96.68		91.16		88.74		97.84		96.14

[a] *not significant terms excluded (p > 0.05).*

Table 3.9. *Regression equations of the fitted models and corresponding optimal levels of PHWE factors.*

Response variable (Y)	Regression equation [a]	Optimum factors		
		Temperature	Time	N cycle
Sil (mg/g leaf)	$-16.631 + 0.4600\times A + 0.585\times B + 5.326\times C - 0.002\times A^2 - 0.009\times A\times B - 0.021\times A\times C - 0.677\times C^2$	92	5	3
TeGG (mg/g leaf)	$-32.367 + 0.613\times A + 1.480\times B + 3.132\times C - 0.002\times A^2 - 0.010\times A\times B - 0.265\times B\times C$	121	5	3
Myr (mg/g leaf)	$-7.325 + 0.1745\times A + 0.3958\times B + 3.6289\times C - 0.0004\times A^2 - 0.0039\times A\times B - 0.0125\times A\times C - 0.4010\times C^2$	140	5	2
Sil (g/100 g extract)	$-4.2450 + 0.2113\times A - 0.0485\times B + 0.9625\times C - 0.0010\times A^2 - 0.0046\times A\times B - 0.0097\times A\times C + 0.0213\times B^2$	82	5	3
TeGG (g/100 g ex)	$-11.6474 + 0.2573\times A + 0.3417\times B + 1.2250\times C - 0.0010\times A^2 - 0.0039\times A\times B - 0.0106\times A\times C$	104	5	3
Myr (g/100 g extract)	$-1.2604 + 0.0609\times A + 0.1333\times B + 0.6750\times C - 0.0002\times A^2 - 0.0015\times A\times B - 0.0063\times A\times C$	64	11	3
GA (mg/g leaf)	$18.6766 - 0.3457\times A - 0.7375\times B - 1.5875\times C + 0.0015\times A^2 + 0.0107\times A\times B + 0.0269\times A\times C$	88	5	1
TPC (mg GAE/g leaf)	$40.3557 - 0.464479\times A - 2.52708\times B - 0.86875\times C + 0.00285547\times A^2 + 0.0411458\times A\times B + 0.130625\times A\times C$	140	11	3
Yield	$18.425 - 0.154\times A + 1.128\times B + 1.604\times C + 0.001\times A^2 + 0.006\times A\times B + 0.028\times A\times C - 0.057\times B^2 - 0.208\times B\times C$	140	11	3

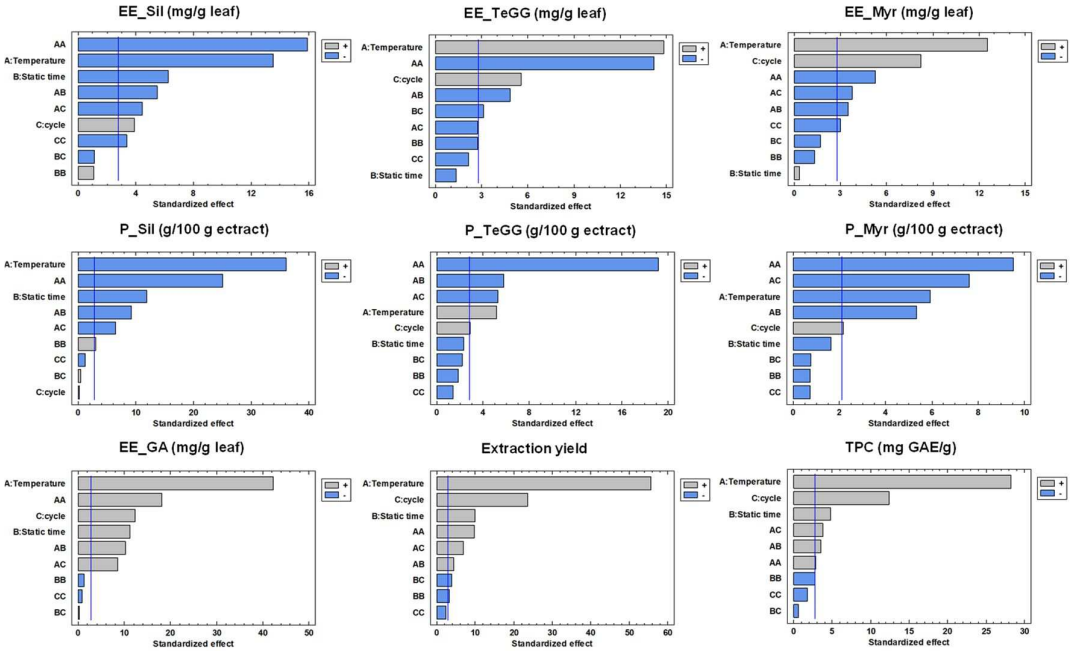

Fig. 3.8. *Pareto charts of standardized effects of PHWE factors (BBD) on EE of Sil, TeGG, Myr, and GA, P of Sil, TeGG, and Myr, EY, and TPC.*
The vertical line marks significance at the 95% confidence level.

Analysis of the F-values (Table 3.8) showed that temperature is the main factor, both in its linear form and in the quadratic term with low p-values, indicating a strong influence of the factor on the responses considered. The adequacy of the models was assessed through the lack-of-fit test giving favourable results, with p-values > 0.5 (Table 3.8), suggesting that the models fit well the experimental data without systematic deviations. In terms of predictive ability, R squared (R^2) ranged between 92% and 99% (Table 3.8), demonstrating that almost all the observed variability is explained by the models, while the adjusted R^2 values, ranging between 88% and 98% (Table 3.8), confirm that the high degree of explanation is not the result of an excess of parameters introduced. Overall, these results demonstrate the accuracy and robustness of the models developed and provide a reliable statistical basis for interpreting the combined effects of PHWE factors.

As evidenced by the response surfaces (Fig. 3.9-10), temperature exerted a pronounced influence on all responses.

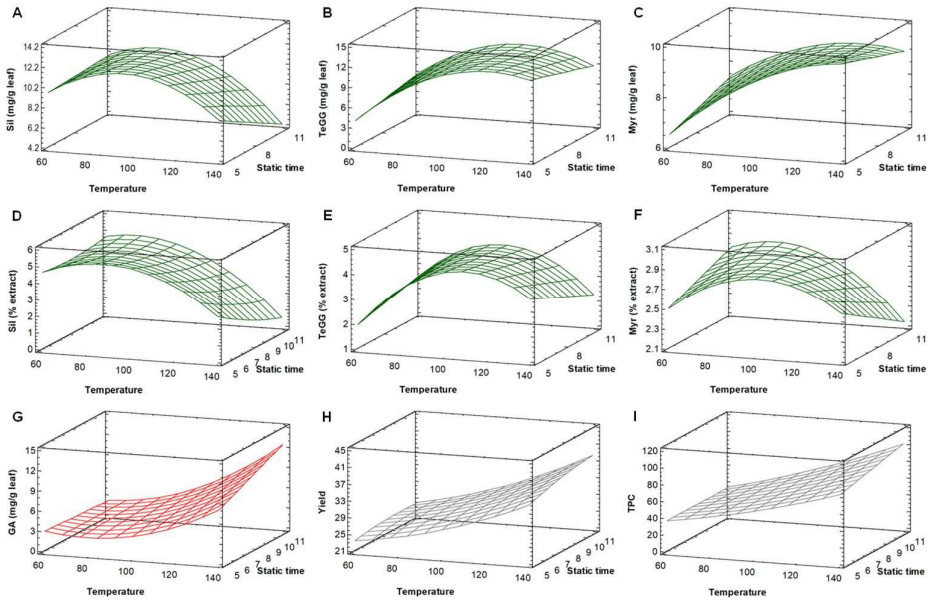

Fig 3.9. *Response surfaces of EE of Sil (A), TeGG (B), Myr (C), and GA (G); P of Sil (D), TeGG (E), and Myr (F); EY (H); and TPC (I) as a function of T and ST in PHWE of CSL.*

Cycle number fixed at the center point (n = 2). Only statistically significant effects are shown.

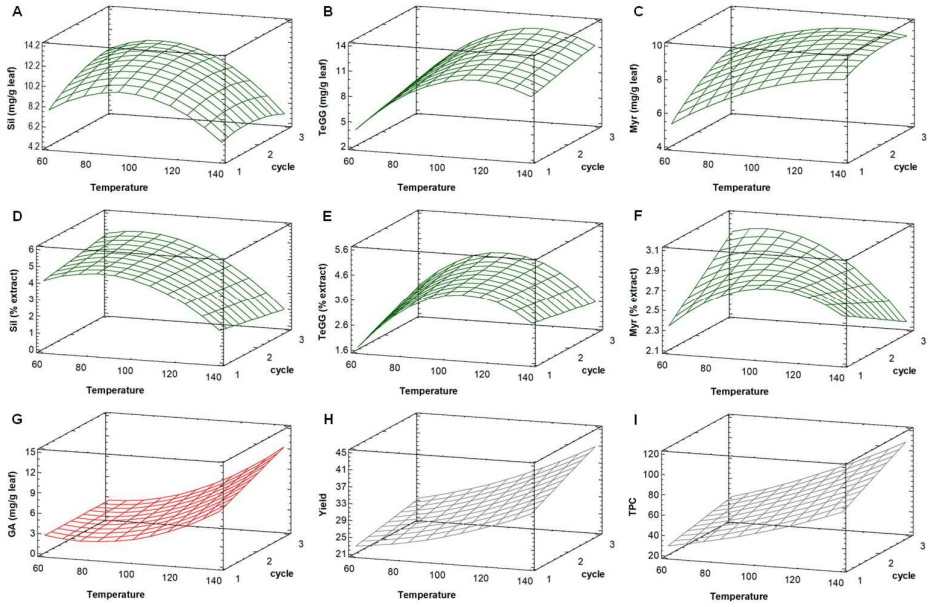

Fig 3.10. *Response surfaces of EE of Sil (A), TeGG (B), Myr (C), and GA (G); P of Sil (D), TeGG (E), and Myr (F); EY (H); and TPC (I) as a function of T and C in PHWE of CSL. Static time fixed at the center point (8 min). Only statistically significant effects are shown.*

EE of Sil and TeGG showed a non-linear trend: values increased up to approximately 90°C and 120°C, respectively, and then decreased at higher temperatures (Fig. 3.9A-B, Table 3.9). This behaviour is consistent with the results obtained for GA, whose levels increased progressively with increasing temperature (Fig. 3.9G), suggesting that Sil and TeGG are sensitive to ester bond hydrolysis under more drastic conditions.

The static time had a secondary but still significant impact. A prolonged static time further reduced the stability of Sil, leading to a decrease in its recovery and a corresponding increase in GA (Fig. 3.9A and 3.9G). In contrast, the number of extraction cycles had a more favourable effect: dividing the total time into several cycles attenuating the degradation of Sil, reducing the hydrolytic impact observed with long static times (Fig. 3.10A).

Temperature, both independently and in combination with static time (AB) and cycle number (AC), also exhibited a marked impact on the purity of target compounds, which declined beyond 65-100°C (Fig. 3.9D-F and Table 3.9). This trend likely reflects co-extraction of matrix components under more intensive PHWE conditions, reducing the target compound content in the extract. Indeed, the response surface for EY (Fig. 3.9H and Fig. 3.10H) showed an upward trend with increasing temperature, static time and number of cycles. The response of TPC to PHWE factors (Fig. 3.9I and Fig. 3.10I) closely resembled that of EY.

Overall, these findings highlight that temperature and its interactions with static time and number of cycles are key parameters in PHWE for thermolabile compounds, as it influences both EE and hydrolysis of Sil and TeGG. For this reason, a multiple response analysis was applied to simultaneously maximize the recovery of main compounds and produce enriched extracts (EE and P of Sil, TeGG and Myr), while minimizing the formation of degradation products (EE of GA). Using the desirability function (BBD, Fig. 3.11), the optimal conditions were identified as 98 °C and three extraction cycles lasting 5 minutes each, with a desirability index of 0.90. These conditions were experimentally validated (n=6), and the results obtained aligned with the predicted ranges (Table 3.7), confirming the predictive power and the reliability of the model.

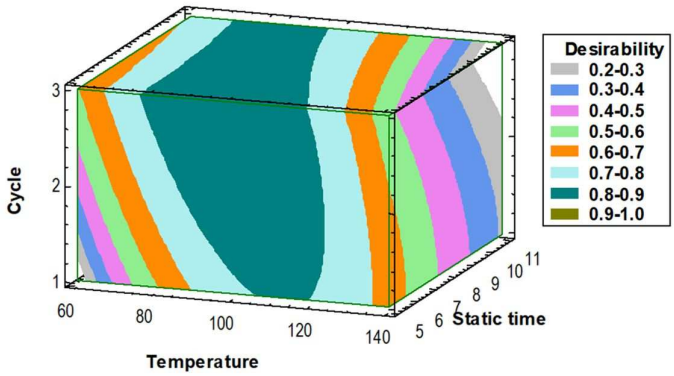

Fig 3.11. *Desirability plot of PHWE optimization*

If PHWE optimization prioritized TPC and EY, predicted optimal PHWE conditions corresponded to the maximum values of the considered factors (140°C, three cycles of 11 min). However, as shown in PHWE extract profiles (Fig. 3.12) for the two different optimized conditions, the more intense conditions led to extensive hydrolysis of Sil and TeGG, along with higher GA levels. Moreover, the degradation product pyrogallol was formed under the PHWE conditions optimized based on TPC and EY (6 mg g^{-1} extract). This suggests that, although TPC and EY are commonly used to optimize phenolic compound extraction in experimental designs, relying solely on these responses does not guarantee the naturalness of extract, as demonstrated by various studies [69,71,72].

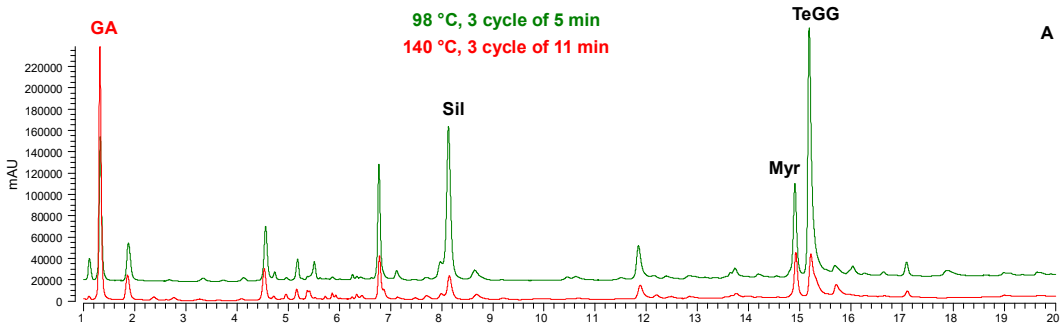

Fig 3.12. *UHPLC-UV profiles at 280 nm of PHWE extract obtained under optimal conditions (green line) or based on EY and TPC (red line).*

3.3.2 Ultrasound probe assisted extraction (probe-UAE)

Unlike PHWE, a heat-dependent extraction technique, UAE relies on mechanical acoustic energy rather than temperature to promote mass transfer and cell disruption. Its main advantages lie in the speed of the process, reduced energy consumption, and the possibility of operating at low temperatures, while ensuring high-quality extracts. In this study, a probe-based system was selected over a bath system due to its higher ultrasonic intensity, reproducibility, and suitability for large-scale applications. A constant low frequency (24 kHz) was employed as various studies indicate that it produces fewer cavitation bubbles with larger diameters, thereby enhancing the cavitation effect [73–75].

Regarding extraction solvent, water and aqueous ethanol mixtures were evaluated. Ethanol–water mixtures are widely proposed for extracting phenolic compounds from plant matrices due to its high affinity for these bioactive compounds [15,74,75]. Additionally, ethanol is widely used for its affordability, renewable origin, and classification as a GRAS solvent. However, the efficiency of UAE does not depend solely on the choice of solvent but requires the control and optimization of numerous operating parameters, including power, frequency, time, temperature, duty cycles, liquid/solid ratio, which significantly influence both the yield and purity of the extract. So, the study specifically focused on the optimization of these variables, with the aim of maximizing the recovery of bioactive compounds from CSL.

3.3.2.1 Preliminary probe-UAE experiments

Preliminary tests were carried out to assess the individual influence of the main UAE parameters and to define the experimental domain and the most appropriate operating conditions. All tests conducted in triplicate, were performed with a solid/liquid ratio (SLR) of 25 $g \cdot L^{-1}$, 24kHz frequency, 30°C and a 3 mm sonotrode. Kinetic curves of CSL compounds were obtained by UHPLC-UV analysis of UAE extracts collected at different time intervals (2–30 minutes).

Preliminary trials compared intermittent (50%) and continuous (100%) duty cycles. The pulsed mode effectively minimized overheating and energy use, without compromising extraction efficiency. In the next phase, the most suitable solvent mixture was evaluated by keeping the duty cycle (50%), amplitude (60%) and the other experimental parameters (reported above) constant. Three solvent mixtures were tested: water; 20% EtOH; and 50% EtOH. As shown in Fig. 3.13, EE increased with the organic fraction and only 50% EtOH ensured reproducible Sil recovery (Fig. 3.13A). CSL profiles revealed an inverse trend in diGG levels as function of % EtOH (Fig. 3.13B), suggesting the possible conversion of Sil to diGG following loss of its pyranone moiety in aqueous media.

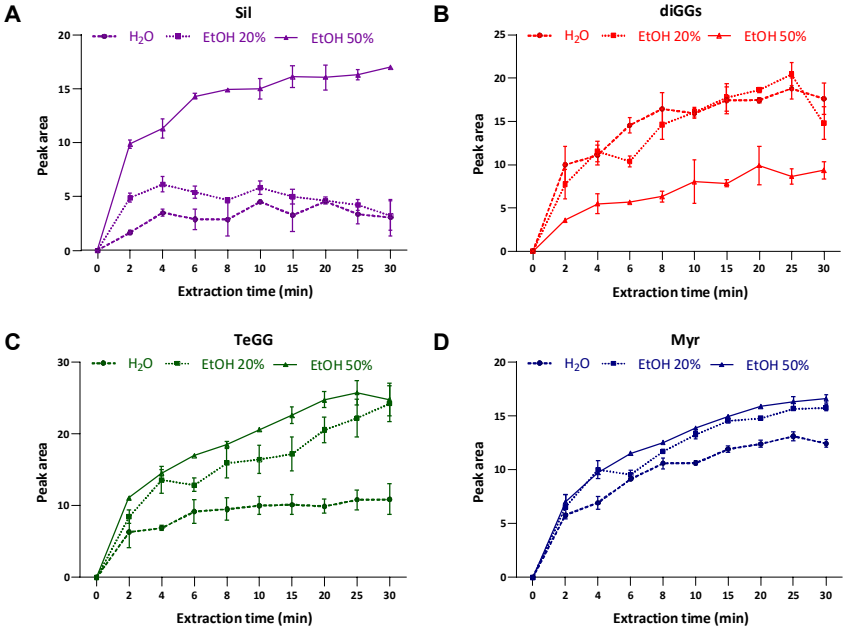

Fig. 3.13. *Extraction kinetics of main CSL compounds (A, Sil; C, TeGG; D, Myr) and Sil degradation indicator (B, diGGs).*

Two main hypotheses were considered to understand the nature of this transformation: chemical degradation by reactive radicals generated during the implosion of cavitation bubbles [74,75] or an enzymatic reaction triggered by the release of vacuolar enzymes after cells rupture [76].To discriminate between these two possibilities, the liquid extract was treated again under the same operating UAE conditions and no significant change in Sil concentrations

was observed, thus excluding the involvement of radicals during acoustic cavitation. Consequently, the observed Sil hydrolysis can be attributed to the action of vacuolar enzymes released into the media after cell disruption [76], promoting the formation of diGGs. Therefore, the minimum percentage of ethanol was set at 30% (the lower limit of the experimental domain).

Under optimal solvent conditions, amplitude (A) tests were carried out. This parameter represents the maximum mechanical oscillation of sonotrode during the propagation of ultrasonic waves in the liquid medium. The amplitude is expressed as a percentage of the maximum power output of the ultrasonic device. Three intensities (30%, 60%, and 100%) were tested to evaluate the metabolites responses. UHPLC-UV analysis showed no significant variations, so 60% A was chosen as a compromise between EE and energy consumption. Finally, kinetic tests showed that maximum recovery of Sil, Myr, and TeGG is achieved within the first 20 minutes. Accordingly, 20 min was defined as the maximum time considered in the DOE, since no further changes were observed beyond this point.

3.3.2.2 Optimization of probe-UAE by RSM

Probe-UAE conditions were then optimized by RSM using the same approach as for PHWE, considering the individual and combined effects of the solvent type (A), the extraction time (B) and SLR (C) (Table 3.10). Such factors directly influence acoustic cavitation, compound solubility, and mass transfer between the matrix and solvent. Their correct combination maximizes EE while avoiding the excessive energy consumption.

Table 3.10 *Independent variables and their levels for Probe-UAE*

Independent factors	Units	Level		
		− 1	**0**	**1**
A. % EtOH	v/v	30	50	70
B. Extraction time	min	10	15	20
C. Solid-liquid ratio (SLR)	g L^{-1}	20	60	100

Fixed factors: solvent volume, 20 mL; frequency, 24 kHz; amplitude, 60%; duty cycles, 50%.

The response variables considered were the same as for PHWE (EE and P of Sil, TeGG and Myr), along with the ethanol volume (L per kg matrix).

Additionally, diGGs levels were used to monitor Sil degradation. The results of the probe-UAE experiments performed under different BBD conditions are reported in Table 3.11. Similarly to PHWE, Probe-UAE was an effective technique for exhaustively extracting CSL bioactive compounds, as evidenced by the high levels of Sil, TeGG and Myr in the extracts.

ANOVA analysis (Table 3.12 and Fig. 3.14) showed that factors A-C, the quadratic terms of EtOH percentage (AA) and SLR (CC) significantly affected EY and the EEs of TeGG and Myr ($p < 0.001$). However, the EEs of Sil and diGGs were strongly influenced by the % EtOH and its quadratic term (A and AA) but exhibited an opposite extraction tendency (Table 3.12). Extraction time (B and AB) also had a significant effect on these responses, while less pronounced. The content of the target compounds in the extracts was negatively affected by the % EtOH quadratic term (AA, $p < 0.05$) (Fig. 3.14).

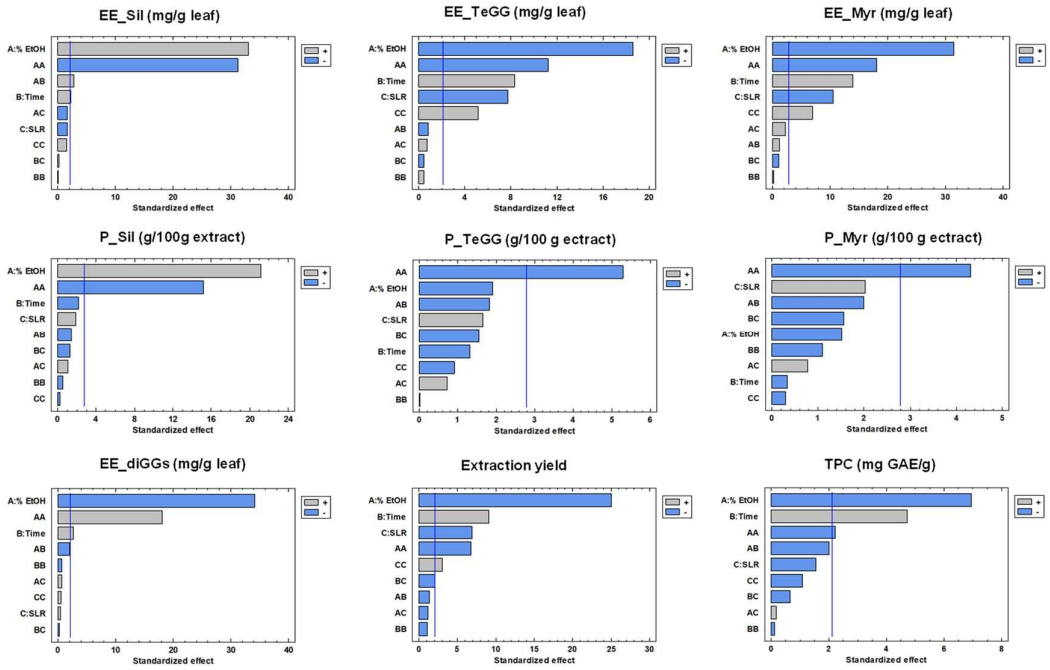

Fig. 3.14. *Pareto charts of standardized effects of Probe-UAE factors (BBD) on EE of Sil, TeGG, Myr, and GA, P of Sil, TeGG, and Myr, EY, and TPC.*

The vertical line marks significance at the 95% confidence level.

The regression model equations (Table 3.13) resulting from the removal of statistically no significant terms ($p > 0.05$, 95% confidence level), accurately describe the relationship between the experimental factors and the response variables.

Table 3.11. *BBD matrix, target response values. predicted and experimental results obtained under optimal UAE conditions*

run	block	A (v/v)	B (min)	C (g L^{-1})	EE_Sil	EE_TeGG (mg g^{-1} CSL)	EE_Myr	P_Sil	P_TeGG (g 100 g^{-1} ext)	P_Myr	EE_GA (mg g^{-1} CSL)	TPC (mg GAE g^{-1})	yield (g 100 g^{-1})
1	1	50	10	02	12.0	12.8	7.8	4.6	5.2	2.9	3.3	81.1	25.4
2	1	70	20	60	11.2	10.6	6.7	4.4	4.4	2.6	3.1	78.7	21.2
3	1	70	15	20	11.5	11.2	6.9	4.1	3.9	2.5	2.8	77.5	23.0
4	1	30	20	60	2.3	14.1	8.6	0.8	5.0	2.9	10	94.8	29.4
5	1	30	15	100	2.8	12.7	7.9	1.0	4.9	3.0	9.9	90.1	27.8
6	1	50	15	60	12.3	13.1	8.2	4.3	4.9	2.9	3.7	92.3	25.5
7	1	70	15	100	10.7	9.9	6.2	4.8	4.6	2.8	2.9	72.0	20.8
8	1	50	20	100	13.1	13.9	8.6	4.8	5.4	3.1	3.7	95.8	27.2
9	1	50	15	60	12.3	13.0	8.1	5.1	5.5	3.4	3.5	92.6	26.5
10	1	50	10	100	11.9	12.1	7.5	5.2	5.6	3.3	3.5	83.1	24.9
11	1	30	10	60	4.2	12.7	7.9	1.5	5.2	3.0	8.8	87.0	27.2
12	1	50	15	60	12.2	12.6	7.9	5.1	5.6	3.3	3.5	92.1	26.3
13	1	50	20	20	12.9	14.3	8.9	4.8	5.4	3.2	3.5	97.8	29.2
14	1	70	10	60	10.1	9.5	5.9	5.4	5.2	3.1	2.9	72.1	20.2
15	1	30	15	20	2.7	14.5	9.1	0.9	4.9	3.0	11.0	93.8	30.2
16	2	50	10	20	12.0	13.6	8.1	4.0	4.9	2.6	3.5	83.1	24.9
17	2	70	20	60	10.7	10.0	6.4	3.7	4.1	2.3	3.0	78.9	21.7
18	2	70	15	20	11.9	11.4	6.8	4.8	4.9	2.8	2.5	78.5	23.3
19	2	30	20	60	1.9	13.8	8.5	0.7	5.1	2.9	9.9	129.1	29.0
20	2	30	15	100	2.0	12.5	7.8	0.7	4.9	2.9	9.6	89.9	27.5
21	2	50	15	60	11.7	12.6	7.9	4.7	5.4	3.2	3.7	91.4	26.6
22	2	70	15	100	10.0	9.4	5.9	5.1	5.1	3.0	2.9	72.9	19.8
23	2	50	20	100	12.8	13.7	8.6	4.6	5.1	3.1	3.8	87.8	26.2
24	2	50	15	60	12.0	12.8	8.0	4.7	5.4	3.0	3.7	90.7	25.5
25	2	50	10	100	11.9	12.7	7.9	4.9	5.6	3.2	3.6	83.5	24.0
26	2	30	10	60	1.8	12.0	7.7	0.7	4.9	2.7	8.6	84.2	26.1
27	2	50	15	60	12.2	12.8	8.0	5.0	5.8	3.2	3.7	91.8	25.2
28	2	50	20	20	12.9	15.3	9.3	4.5	5.4	3.0	3.9	97.8	28.9
29	2	70	10	60	9.6	8.8	5.3	4.9	4.8	2.7	2.8	67.6	19.6
30	2	30	15	20	2.5	14.7	9.2	0.9	4.6	2.7	8.8	95.4	28.8
Optimum		**°C**	**min**	**n**	**EE_Sil**	**EE_TeGG**	**EE_Myr**	**P_Sil**	**P_TeGG**	**P_Myr**	**EE_GA**	**TPC**	**yield**
Predicted values		**52**	**20**	**100**	12.9	13.4	8.4	4.9	5.4	3.1	3.6	96.7	26.5
95% confidence interval					12.4 – 13.3	13.1 - 13.8	8.2 – 8.6	4.7 - 5.1	5.2 – 5.5	3.0 - 3.2	3.3 – 3.9	92.0 – 101.4	25.8 – 27.1
Desirability			**0.83**		0.98	0.71	0.77	0.89	0.78	0.72	0.87	0.47	0.62
Experimental value (n = 6)					12.5 ± 0.7	13.9 ± 0.6	8.6 ± 0.2	5.2 ± 0.5	5.1 ± 0.5	3.1 ± 0.3	3.9 ± 0.1	97.0 ± 4.9	27.8 ± 0.6
95% confidence interval					11.7 - 12.9	13.2 - 14.3	8.3 – 8.7	4.9 - 5.5	4.8 – 5.4	2.9 - 3.3	3.8 - 4.0	93.6 – 100.3	27.3 – 28.3

Table 3.12. *Analysis of Variance (ANOVA) for response variables of Probe-UAE.*

	Sil (mg/g leaf)		TeGG (mg/g leaf)		Myr (mg/g leaf)		diGGs (mg/g leaf)		Sil (% extract)		TeGG (% extract)		Myr (% extract)		Extraction yield		TPC (mgGAE/g)	
	F-value	*p*-value	*F*-value	*p*-value	*F*-value	*p*-value	*F*-value	*p*-value	*F*-value	*p*-value	*F*-value	*p*-value	*F*-value	*p*-value	*F*-value	*p*-value	*F*-value	*p*-value
A: % EtOH	1095.30	0.0000	346.34	0.0000	988.08	0.0000	1164.9	0.0000	449.94	0.0000	3.65	0.1288	2.28	0.2059	625.31	0.0000	48.25	0.0000
B: Time	4.86	0.0415	68.72	0.0000	193.61	0.0002	7.13	0.0162	4.61	0.0984	1.72	0.2593	0.11	0.7533	82.62	0.0000	22.20	0.0002
C: SLR	2.81	0.1119	59.77	0.0000	111.75	0.0005	0.21	0.6538	3.55	0.1327	2.70	0.1756	4.08	0.1135	47.89	0.0000	2.38	0.1411
AA	975.84	0.0000	126.66	0.0000	326.17	0.0001	326.58	0.0000	230.88	0.0001	27.98	0.0061	18.59	0.0125	45.32	0.0000	4.89	0.0410
AB	8.05	0.0114	0.72	0.4070	1.35	0.3098	3.82	0.0673	1.97	0.2335	3.28	0.1442	3.97	0.1171	1.72	0.2072	4.00	0.0618
AC	2.85	0.1096	0.49	0.4933	4.81	0.0934	0.38	0.5443	1.11	0.3523	0.53	0.5062	0.60	0.4811	1.39	0.2545	0.03	0.8563
BB	0.00	0.9503	0.20	0.6640	0.06	0.8183	0.46	0.5089	0.30	0.6125	0.00	0.9904	1.19	0.3359	1.14	0.3014	0.01	0.9105
BC	0.03	0.8596	0.20	0.6583	1.29	0.3195	0.00	0.8806	1.62	0.2723	2.40	0.1961	2.41	0.1957	4.23	0.0553	0.43	0.5213
CC	2.50	0.1326	26.64	0.0001	48.11	0.0023	0.24	0.6317	0.05	0.8287	0.81	0.4192	0.09	0.7816	9.31	0.0072	1.15	0.2977
Lack of fit	2.48	0.0963	2.46	0.0978	3.47	0.1189	1.39	0.2793	0.88	0.6211	0.84	0.6434	0.62	0.7795	2.02	0.1498	0.77	0.5254
Lack of fit [a]	1.60	0.2107	1.29	0.3150	3.14	0.1383	2.08	0.1083	0.32	0.7291	0.63	0.5407	0.22	0.8008	2.08	0.1037	1.50	0.2314
Model		0.0000		0.0000		0.0000		0.0000		0.0000		0.0001		0.0002		0.0000		0.0000
R-squared		98.86		96.33		96.81		98.62		97.58		71.93		72.90		97.27		81.12
adjusted R-squared		98.34		94.68		95.12		97.99		96.31		59.29		58.64		96.04		72.63
R-squared [a]		98.47		96.09		96.38		98.28		95.74		52.67		47.52		96.27		73.31
adjusted R-squared [a]		98.23		95.27		95.43		98.10		95.25		47.21		41.47		95.49		70.23

[a] *not significant terms excluded (p > 0.05).*

Table 3.13. *Regression equations of the fitted models and corresponding optimal levels of probe-UAE factors.*

Response variable (Y)	Regression equation [a]	Optimum factors		
		% EtOH	Time	SLR
Sil (mg/g leaf)	$-30.4756 + 1.5485\times A - 0.1926\times B - 0.01142\times A^2 + 0.0049A\times B$	58	20	95
TeGG (mg/g leaf)	$8.1178 + 0.2848\times A + 0.1465\times B - 0.0671\times C - 0.0037\times A^2 + 0.0004\times C^2$	39	20	20
Myr (mg/g leaf)	$4.9794 + 0.1696\times A + 0.0931\times B - 0.0345\times C - 0.0022\times A^2 + 0.0002\times C^2$	38	20	20
Sil (g/100 g extract)	$-12.2283 + 0.5852\times A - 0.0049\times A^2$	60	11	24
TeGG (g/100g extract)	$2.0092 + 0.1417\times A - 0.0015\times A^2$	48	16	63
Myr (g/100 g extract)	$1.3580 + 0.0739\times A - 0.0008\times A^2$	48	15	63
diGGs (mg/g leaf)	$27.6095 - 0.8242\times A + 0.0526\times B + 0.0066\times A^2$	63	10	100
TPC (mg GAE/g leaf)	$65.1469 + 0.6696\times A + 1.4500\times B - 0.0120\times A^2$	30	20	60
Yield	$25.0486 + 0.1686\times A + 0.2561\times B - 0.0731\times C - 0.0034\times A^2 + 0.0004\times C^2$	33	20	20

Specifically, the EE of Sil (Fig. 3.15A) primarily varied as a function of %EtOH, with maximum effects occurring at 58% EtOH (Table 3.13). No relevant variations attributable to extraction time or SLR were observed for Sil recovery. The contrasting effects of %EtOH on Sil and diGGs support the hypothesis that Sil is converted into diGGs by enzymatic hydrolysis at EtOH percentages below 50%. Above this threshold, enzymatic activity appears to be inhibited as a consequence of enzyme denaturation caused by the increased organic solvent content, since most natural enzymes are known to be highly sensitive and easily inactivated in such conditions [77]. In contrast to Sil, the recoveries of TeGG (Fig. 3.15B and Fig. 3.16B) and Myr (Fig. 3.15C and Fig. 3.16C), as well as EY (Fig. 3.15H and Fig. 3.16H) and TPC (Fig. 3.15I and Fig. 3.16I), were significantly affected by all three independent factors. However, beyond 38% EtOH (Table 3.13), the EE of TeGG and Myr decreased due to the solvent's lower dielectric constant. Regarding the content of bioactive compounds in the extract, % EtOH was the only significant factor affecting these response variables (Fig. 3.15D–F and Fig. 3.16D–F). The levels of Sil, TeGG and Myr in the extract peaked at an intermediate % EtOH (48–60%) before declining. These results highlight that solvent selection in ultrasound assisted systems depend primarily on the solubility and polarity of the target compounds. In this case, the main CSL compounds were more effectively extracted using low to medium ethanol content. As reported in previous studies [74], aqueous ethanol mixtures enhance the yield of phenolic compounds up to a certain % EtOH. After this point, high ethanol content may cause plant tissue dehydration, protein denaturation or the solubilization of additional matrix components due to the solvent's increased extracting power [74].

In conclusion, the ethanol content was the predominant factor influencing both probe-UAE efficiency and the quality of the extract. Multiple response analysis was used to simultaneously optimize the three studied factors, identifying an aqueous EtOH solution of 52% v/v, an SLR of 100 g L^{-1} and 20 minutes extraction time (with a desirability score of 0.83) as the optimal probe-UAE conditions (Fig. 3.17) for maximizing CSL compound recovery and producing enriched extracts (EE and P of Sil, TeGG and Myr), while avoiding Sil hydrolysis.

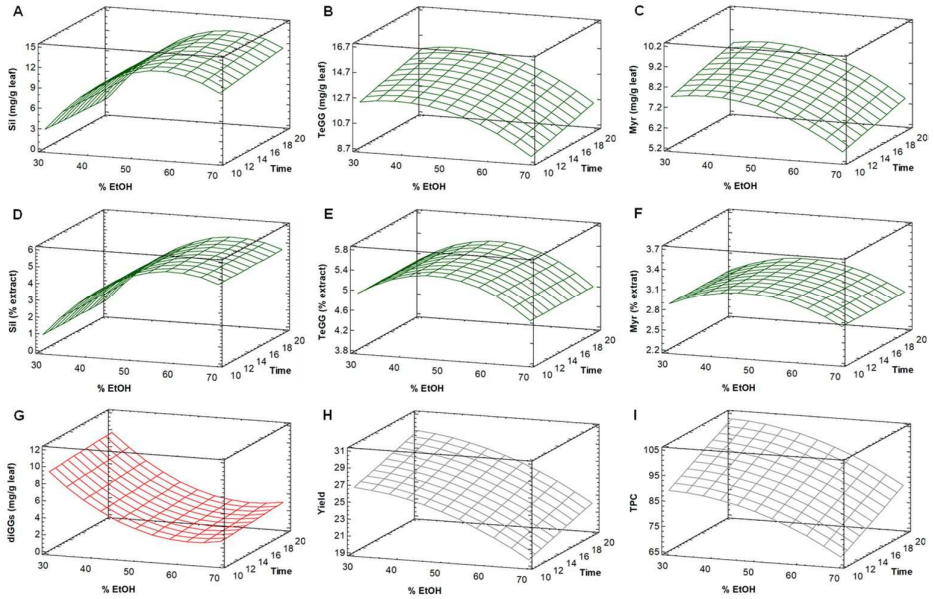

Fig 3.15. *Response surfaces of EE of Sil (A), TeGG (B), Myr (C), and diGGs (G); P of Sil (D), TeGG (E), and Myr (F); EY (H); and TPC (I) as a function of %EtOH and extraction time in probe-UAE of CSL.*

SLR fixed at the center point (60 g L^{-1}). Only statistically significant effects are shown.

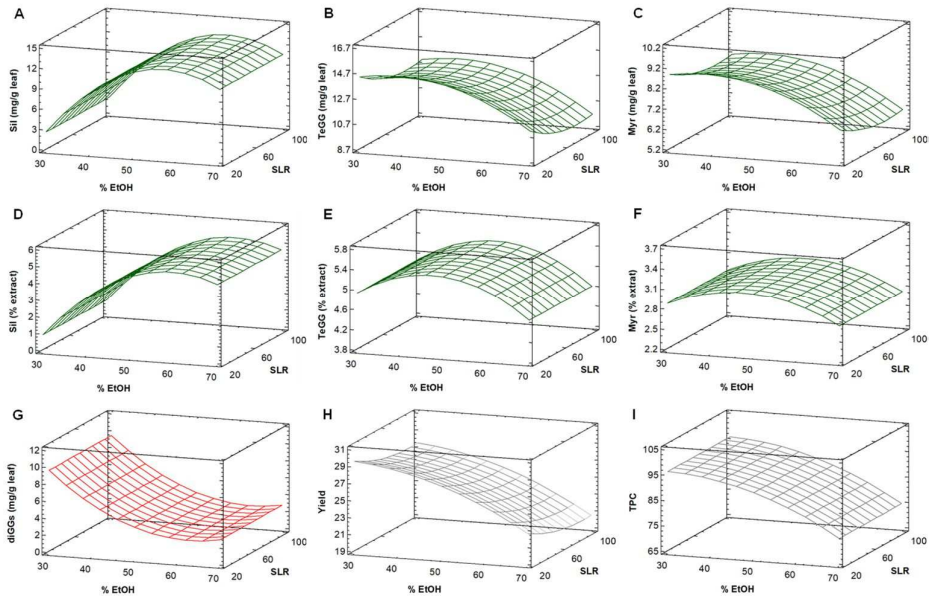

Fig 3.16. *Response surfaces of EE of Sil (A), TeGG (B), Myr (C), and diGGs (G); P of Sil (D), TeGG (E), and Myr (F); EY (H); and TPC (I) as a function of %EtOH and SLR in probe-UAE of CSL. Extraction time fixed at the center point (15 min). Only statistically significant effects are shown.*

The predictive capacity of the model was successful, as demonstrated that all experimental responses remained within the 95% confidence interval of the predicted values (Table 3.11).

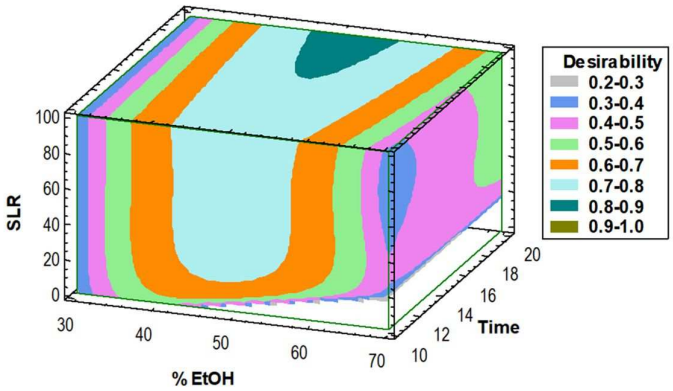

Fig 3.17. *Desiderability plot of Probe-UAE optimization.*

However, even for UAE, optimal conditions based solely on TPC and EY (30% EtOH v/v, 65 g L^{-1}, 20 min, desirability of 0.79) resulted in extracts full of artifacts. As shown in the chromatographic profiles (Fig. 3.18), the lower percentage of ethanol resulted in Sil conversion into diGGs. This further reinforces the importance of optimizing extraction conditions based on specific target compound levels using chromatographic methods rather than less selective spectrophotometric methods to ensure high-quality extracts with undenatured compounds [78].

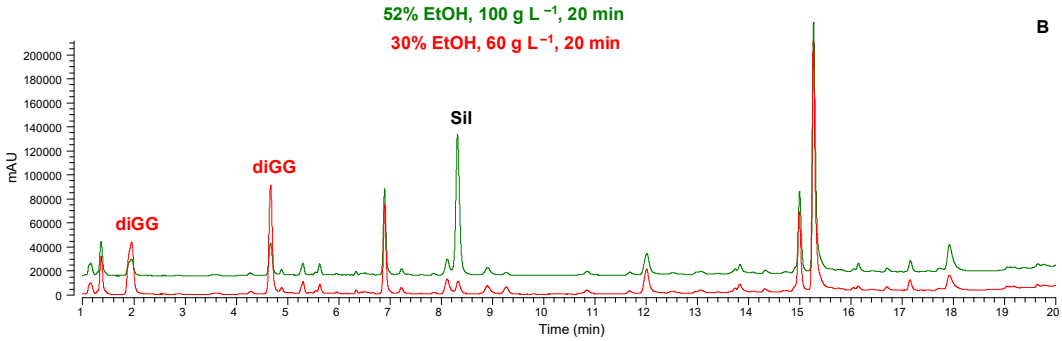

Fig 3.18. *UHPLC-UV profiles at 280 nm of and probe-UAE extract obtained under optimal conditions (green line) or based on EY and TPC (red line).*

3.3.3 PHWE and probe-UAE performance vs conventional methods

Conventional extraction techniques, including maceration and Soxhlet extraction, have long been considered the “gold standard” for the recovery of bioactive compounds from plant matrices. Although reliable and well-documented, their practical applicability is limited by long extraction times, high solvent and energy consumption, and the potential degradation of heat-sensitive metabolites [8,79]. Furthermore, the large use of organic solvents, often toxic or flammable [8], the poor selectivity, batch-to-batch variability, and limited compatibility with industrial scale contrasts with the principles of green chemistry and make these methods unsuitable for efficient and sustainable extraction of secondary metabolites [80].

Magnetic stirring-assisted maceration (SLE) and Soxhlet extraction (So) were used in this study as a benchmark to evaluate the efficiency and sustainability of PHWE and probe-UAE. The extraction efficiency of both techniques was quantitatively assessed by UHPLC-UV and compared with SLE, So and the exhaustive extraction described in Section 3.1.1.1. First, the product recovery (the amount of bioactive compounds recovered from the matrix) of the two techniques were determined. Both the optimized techniques achieved the complete recovery of the main bioactive compounds from CSL (88–108%), with no statistically significant differences between them ($p > 0.05$) (Table 3.14). These results demonstrate that both optimized techniques ensure the exhaustive recovery of target compounds

The sustainability of the extraction processes was evaluated according to the six principles of eco-extraction proposed [8,17] and compared with So and SLE. In line with this approach, six key parameters were considered to describe the green performance of each method: raw material consumption (Principle 1, g of matrix per g of extract), use of organic solvents (Principle 2, volume of EtOH per g of extract), energy consumption (Principle 3, kWh per extraction), waste production (Principle 4, g of solid residue and spent solvent per g of extract), extraction time (Principle 5, h per extraction), and recovery efficiency (Principle 6, % of target compounds recovered) (Table 3.14).

Table 3.14. *Extraction performance of optimized PHWE and probe-UAE compared with conventional techniques.*

	PHWE	probe-UAE	Soxhlet	Maceration
Extract yield (g 100 g^{-1} leaf)	29.6 ± 0.7 [a]	27.8 ± 0.6 [b]	20.3 ± 0.2 [c]	16.0 ± 0.8 [d]
Sil recovery (%)	87.6 ± 1.7 [a]	89.6 ± 4.8 [a]	68.0 ± 6.0 [b]	55.4 ± 3.0 [c]
TeGG recovery (%)	103.3 ± 2.6 [a]	103.5 ± 4.5 [a]	78.0 ± 5.0 [b]	71.4 ± 3.8 [b]
Myr recovery (%)	107.9 ± 3.0 [a]	101.9 ± 2.8 [a]	74.8 ± 5.3 [b]	57.2 ± 3.0 [c]
α-GLU (IC_{50}, µg mL^{-1})	0.47 ± 0.07 [a]	0.44 ± 0.06 [a]	0.48 ± 0.06 [a]	0.46 ± 0.04 [a]
Green extraction principle	**PHWE**	**probe-UAE**	**Soxhlet**	**Maceration**
1. Raw material (g g^{-1} extract)	3.4	3.6	4.9	6.2
2. Ethanol volume (L g^{-1} extract)	0.00	0.02	0.07	0.09
3. Energy consumption (Wh per cycle)	125	40	1200	400
4. Waste (g g^{-1} extract)	2.4	18.3	59.8	75.9
5. Extraction time (h per cycle)	0.25	0.3	8	24
6. Product recovery (%)	98.3	97.7	73.4	61.8

Different superscript letters in same row indicate significantly different values ($p \leq 0.05$, Tukey's HSD test).

These six indicators, already widely adopted in the literature for assessing the sustainability of extraction processes, integrate environmental, energy, economic, and analytical aspects, allowing for the comparison of different techniques on a quantitative and objective basis [80–82].

The comparative results, illustrated in the radar chart (Fig. 3.19) show that the values closest to the center of the diagram correspond to greater overall sustainability of the process. PHWE showed the most favourable profile, followed by probe-UAE, while So and SLE showed significantly lower performance in all parameters considered. Specifically, PHWE and probe-UAE required lower amounts of raw material and no ethanol (PHWE) or reduced ethanol volume (probe-UAE 4-5-fold less) to yield 1 g of extract, compared to So and SLE (Table 3.14). This contributed to a lower waste output, in terms of solvent and spent residue, with PHWE generating approximately 19-25 times less waste than the conventional techniques, due to the exclusive use of water as the extraction solvent. Moreover, So and SLE failed to achieve full recovery of the target compounds (Table 3.14), resulting in partially exhausted residues with 27–38% of bioactive compounds retained. Another clear advantage of PHWE and probe-UAE over conventional methods was the markedly reduced extraction times, achieving a 24–32 and 73–96 times faster extraction than So and SLE, respectively. These shorter extraction times strongly impact the energy demands; probe-UAE emerged as the most energy-efficient option,

with energy consumption 30-, 6- and 3-fold lower than So, SLE and PHWE, respectively (Table 3.14). Although PHWE is the most energy-intensive among the evaluated techniques, it still required 10 times less energy than So, due to its fast extraction duration.

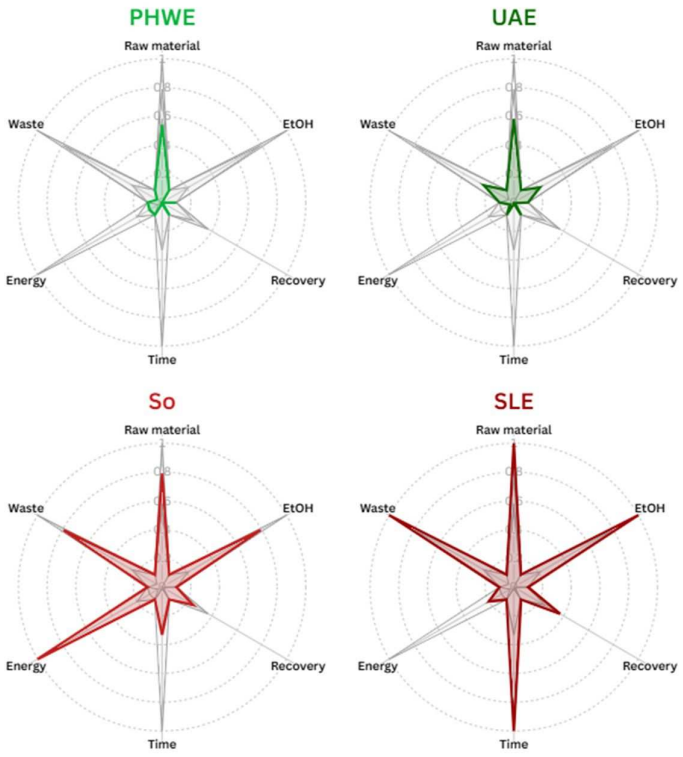

Fig 3.19. *Process assessment of PHWE, probe-UAE and conventional methods according to the six green extraction principles.*
Data are normalized on a 0–1 scale. Lower values indicate better performance.

In accordance with the principles of eco-extraction, both PHWE and probe-UAE are examples of process intensification compared to conventional methods. Both techniques have demonstrated high eco-efficiency, reduced solvent and energy use, significantly shorter extraction times, higher recovery yields, and lower waste production.

Among the two, probe-UAE stood out as the most advantageous solution from an energy and operational standpoint, thanks to the operational simplicity, low investment costs, and high extraction efficiency. However, this technique requires additional post-treatment steps (filtration, evaporation, or solvent

recycling), which can affect the overall sustainability of the process. In contrast, PHWE, while requiring more complex and expensive equipment, has the advantage of eliminating the use of organic solvents, allowing to produce aqueous extracts easily usable for direct applications or further formulations. The exclusive use of water, universally recognized as the safest and most sustainable solvent, makes this technique a significant step towards greener chemistry, promoting the principles of environmental sustainability and the circular economy in the recovery of high-value bioactive compounds.

3.4. *In vitro* evaluation of CSL extract safety, cellular bioactivity, and gastrointestinal bioaccessibility[1,2]

In vitro chemical assays represent only a preliminary screening tool useful for identifying the potential bioactivity of extracts, providing limited insight into their actual biological behaviour and offering only initial indications of their efficacy [83]. First, these methods offer a chemical index rather than a real biological response, and are strongly influenced by experimental conditions (pH, reaction times, reagent concentrations) that do not always reflect human physiology [83,84]. As numerous human intervention studies have shown, compounds with high *in vitro* antioxidant activity (e.g., isoflavones, curcumin) may show weak or negligible *in vivo* effects due to poor bioavailability and low plasma levels [84,85].

Optimized CSL extracts were evaluated through ABTS assay showing strong AOC (mmol TE g^{-1} ext =4.7 ± 0.3 for PHWE and 4.8 ± 0.4 for probe-UAE). Since the exclusive use of chemical assays is considered misleading and conceptually inadequate, further investigations were performed on cell-based models to confirm their antioxidant activity. Human cell cultures represent the experimental model closest to real physiological conditions, allowing confirmation of biological activity and safety. The use of specific cell models, both healthy (erythrocytes, fibroblasts, enterocytes) and cancer cell lines (HepG2, Caco-2), allows evaluation of the antioxidant selectivity and more realistic simulation of physiological responses across different target tissues [86].

In addition to their antioxidant potential, the optimized CSL extracts demonstrated strong and selective α-GLU inhibitory activity (IC_{50} μg mL^{-1} = 0.47 ± 0.07 for PHWE and 0.44 ± 0.06 for probe-UAE), in line with their main bioactive compounds. Among these, TeGG and Sil were particularly effective (IC_{50} < 15 μM), far outperforming acarbose, while Myr exhibited comparable inhibition. These potential bioactivities were consistent with the composition data for the PHWE and probe-UAE extracts (Tables 3.7 and 3.11), which showed no significant differences in terms of Sil, TeGG and Myr content compared to the exhaustive extract (5.5, 5.2 and 3.3 g per 100 g of extract,

respectively, Table 3.2). These data confirm that the bioactivity of CSL is primarily attributed to its main compounds, as was previously demonstrated [63].

Although confirmation of α-GLU inhibition requires *in vivo* validation [39], *in vitro* gastrointestinal digestion provides valuable complementary insight, as the biological relevance of an extract ultimately depends on the stability and bioavailability of its active compounds at their physiological target sites [87]. This is particularly crucial for α-GLU inhibitors, since the enzyme exhibits its highest activity in the proximal duodenum and jejunum, corresponding to the early stages of the simulated digestion [88]. By integrating *in vitro* cell-based, and bioaccessibility data, this section aims to achieve a comprehensive understanding of the functional potential of CSL extracts and toward the development of a formulated product containing a defined percentage of the PHWE extract paving the way for its potential use in functional applications.

3.4.1 In Vitro Cytotoxicity Testing of CSL Extracts[1]

In view of CSL extracts potential hypoglycemic and antioxidant properties and the prospective applications in food and nutraceutical products, a thorough evaluation of its safety at the gastrointestinal and hepatic levels is essential, as these organs represent the primary sites of absorption, metabolism, and potential toxicity of bioactive compounds. This analysis is therefore an essential prerequisite for the future use of the extract as a functional ingredient or dietary supplement. *In vitro* cytotoxicity tests are the first approach to assessing the safety of natural extracts, as they are rapid, sensitive, and provide preliminary information on the interaction of metabolites with the cellular environment before moving on to *in vivo* studies. In this context, the optimized extracts obtained by PHWE and probe-UAE was tested on liver (HepG2) cells using the MTT assay, at concentrations ranging from 5 to 300 μg mL^{-1}.

As shown in Fig. 3.20, the extract showed no significant cytotoxic effects: cell viability remained above 80% even at the highest dose, with no statistically significant differences between concentrations ($p < 0.05$).

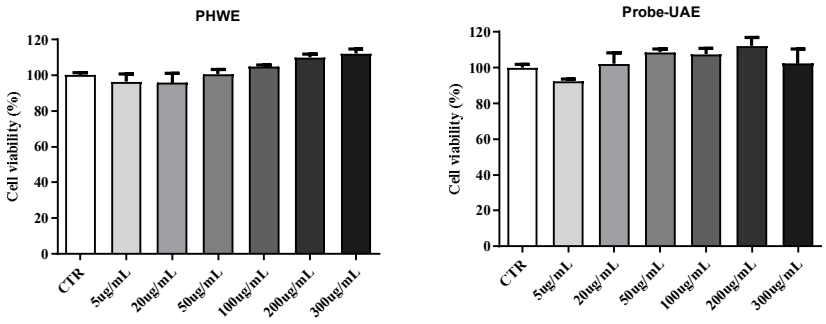

Fig. 3.20. *Effect of CSL extracts on cell viability in HepG2 cell lines, treated for 24h. Data are expressed as mean ± SD of three independent experiments. *p < 0.05 vs. control.*

These data suggest a favourable safety profile for CSL extracts in HepG2 model, with cytotoxic concentrations above the IC_{50} observed for α-GLU inhibition (≃ 0.5 μg mL^{-1}), confirming the safety of the doses intended for nutraceutical applications. Testing only HepG2 at this stage is sufficient, as the main objective is to evaluate the safety of extract concentrations that could reach the liver, a key organ for the metabolism and detoxification of bioactive compounds, and therefore a critical site for possible toxic effects or metabolic interactions [89].

3.4.2. Cell-based antioxidant assays on CSL extracts[1]

Oxidative stress is one of the main pathogenic mechanisms involved in the development and progression of chronic noncommunicable diseases (NCDs), such as type 2 diabetes, obesity, cardiovascular and neurodegenerative diseases [90]. The accumulation of reactive oxygen species (ROS) alters the cellular redox balance, promoting inflammation, biomolecular damage, and metabolic dysfunction. For this reason, the identification of natural compounds or extracts with high AOC represents a promising strategy for the management and prevention of NCDs, as they can help reduce systemic oxidative stress and restore cellular function [90].

Therefore, the antioxidant potential of CSL extracts was investigated in biologically relevant models to obtain deeper information on their bioactivity in cellular systems.

Optimized PHWE and probe-UAE extracts were tested on HepG2 cells and erythrocytes (primary red blood cells, RBCs) to assess their cellular antioxidant activity (CAA) under AAPH-induced oxidative stress. Both models are widely employed in biochemical and nutritional research to study oxidative stress responses [86]Erythrocytes are a biologically relevant model for assessing antioxidant activity, as their capacity to neutralize free radicals and ROS reflects systemic protection [91]. Their lack of a nucleus and protein repair mechanisms makes them particularly vulnerable to oxidative stress, thus suitable for evaluating the protective effects of bioactive extracts on cell membranes [92]. Concerning HepG2 cells derived from human hepatocellular carcinoma, they are a well-established model for studying metabolism and antioxidant response in the liver [41].

In HepG2 cells, both PHWE and probe-UAE extracts significantly reduced AAPH-induced ROS production in a dose-dependent manner (Fig. 3.21), exhibiting a good antioxidant activity comparable to that of quercetin.

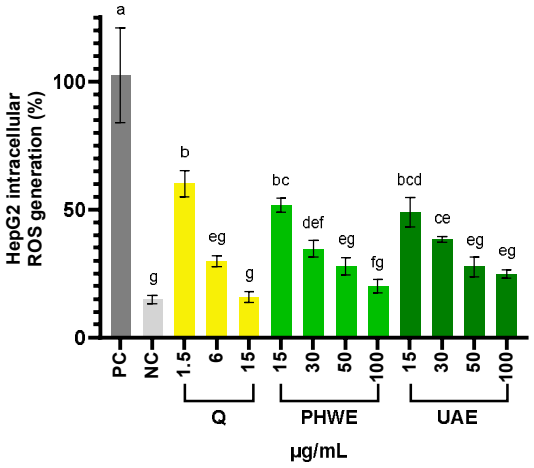

Fig. 3.21. *Effects of PHWE and probe-UAE extracts on intracellular ROS generation in HepG2 cells.*

PC = AAPH- treated cells; NC = untreated cells (PBS); Q = quercetin. Different letters represent statistically different results ($p \leq 0.05$).

Notably, even at the lowest tested concentration (15 µg mL^{-1}) a reduction of approximately 50% in intracellular ROS levels was observed compared to the

positive control. At 100 µg mL^{-1}, ROS levels reached values (20 and 25%) close to those of untreated cells (NC, 14%), indicating the high efficiency of CSL extracts in mitigating oxidative stress in this cellular model. AAPH-induced oxidative stress in erythrocytes was evaluated to further assess the antioxidant activity of optimized CSL extracts. The CAA results in RBCs (Fig. 3.22a) were consistent with those obtained in HepG2. Both PHWE and probe-UAE extracts effectively reduced intracellular ROS generation, showing greater AOC than quercetin (53% at 100 µg mL^{-1}), starting from a concentration of 30 µg mL^{-1}. At the highest tested concentration (300 µg mL^{-1}), ROS levels in pretreated RBCs (23 and 26%) were comparable to those of untreated cells (15%), confirming a strong antioxidant effect also in erythrocytes.

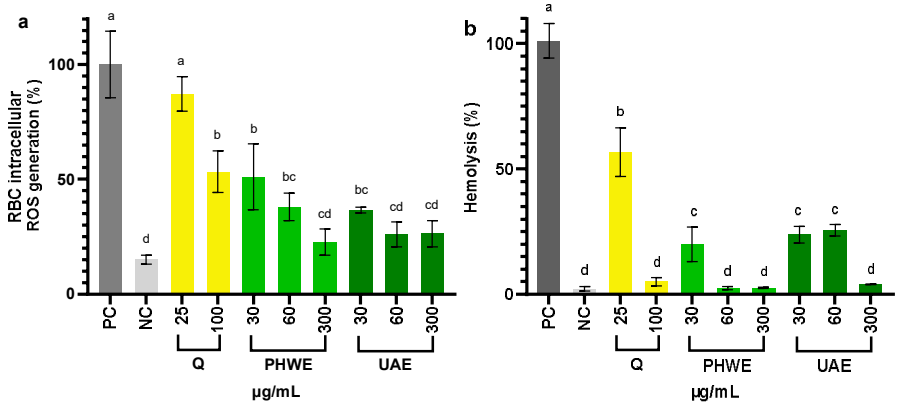

Fig. 3.22. *Effects of PHWE and probe-UAE extracts on intracellular ROS generation in RBCs (a), and their anti-haemolytic activity (b).*

PC = AAPH-treated cells; NC = untreated cells (PBS); Q = quercetin. Different letters in the same graph represent statistically different results ($p \leq 0.05$).

RBCs are particularly susceptible to free radical-induced membrane damage, which can lead to haemolysis. Therefore, haemolysis is a reliable model to evaluate membrane-protective effects of antioxidant agents [93]. As shown in Fig. 3.22b, both CSL extracts significantly inhibited the AAPH-induced haemolysis, exerting marked membrane protection. PHWE and probe-UAE extracts at 60 and 300 µg mL^{-1}, respectively, demonstrated anti-haemolytic effects (2.4 and 4.0%) comparable to untreated cells (NC, 2.1%) and to quercetin at 100 µg mL^{-1} (5.0%).

These findings demonstrate that optimized PHWE and probe-UAE extracts exert potent intracellular antioxidant effects in both HepG2 and RBC cells and

anti-haemolytic activity. Combined with their α-GLU inhibitory activity, these properties highlight the potential of CSL extracts to target interconnected mechanisms such as oxidative stress and postprandial hyperglycemia, relevant in the management of type 2 diabetes [94].

3.4.3 In Vitro digestion and Bioaccessibility of CSL-PHWE and Its Formulation

3.4.3.1 PHWE formulative study[2]

The use of raw plant extracts is often limited by chemical-physical instability, low manageability, and often unfavourable organoleptic characteristics. Thus, a formulation containing the optimized CSL extract was designed and optimized to enhance its physicochemical stability, extend compound shelf life, and improve its suitability for nutraceutical applications. Among the optimized green extraction methods, the optimized PHWE extract was chosen for its water-based and ready-to-use nature, making it directly processable through spray-drying. Dissolution tests confirmed its stability in simulated gastric fluid (pH 1.2 and 1.0), both with and without enzymes, making enteric coating unnecessary. Spray drying was selected as the microencapsulation technique due to its scalability, rapid processing, and capacity to produce amorphous, stable powders with high encapsulation efficiency [95]. Maltodextrins, though commonly used as carriers, were excluded for their low glass transition temperature (Tg) [96] and because they can act as substrates for carbohydrate-hydrolyzing enzymes, competing with the extract's active compounds for enzyme binding sites and thereby weakening the overall inhibitory effect. Instead, inulin, a linear D-fructose polysaccharide with β-(2-1) linkages, was chosen as the main carrier for its high Tg, amorphous structure, viscosity-enhancing and prebiotic properties [97]. To enhance encapsulation and microparticle formation, pectin was added as a synergistic polymer for its stabilizing and gelling effects. Several formulation conditions were studied, and the optimal composition was obtained with a 10:1 inulin/pectin ratio (3% inulin, 0.3% pectin). Spray dryer inlet temperature was set to 125 °C to balance

efficient drying with preservation of thermosensitive compounds. Outlet temperatures remained below inulin's Tg (~89 °C), avoiding crystallization.

Morphological analysis by SEM (Fig. 3.23) highlighted clear morphological differences among the powders. The lyophilized extract (Fig. 3.23a) showed heterogeneous flakes and crystalline clusters. In contrast, the spray-dried matrix without extract (Fig. 3.23b) showed spherical appearance with minor collapse. When the PHWE extract was incorporated into the formulation (Fig. 3.23c), the particles maintained their spherical morphology and exhibited smooth and slightly more pronounced surface collapse. This phenomenon is consistent with the increased viscosity (from 18.5 to 38.5 mPA*s) of the polymer-extract mixture, which leads to more particle collapses during drying due to reduced solvent evaporation rate and internal volume contraction.

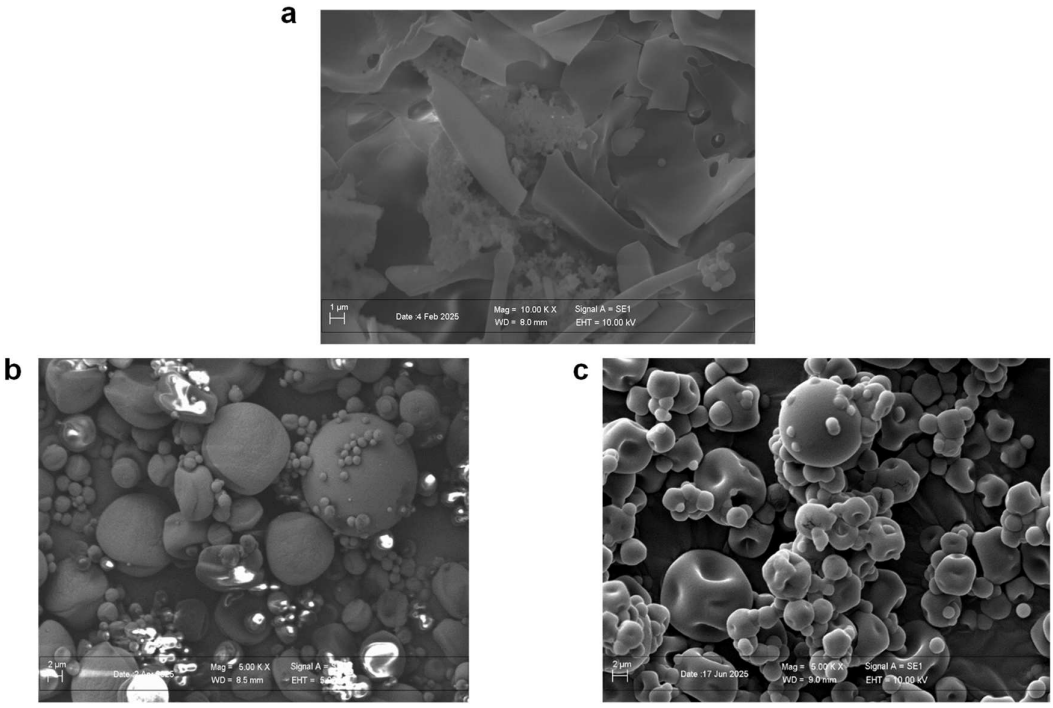

Figure 3.23.*SEM Images of lyophilized PHWE extract (a), spray-dried matrix without extract (b), and spray-dried matrix with PHWE extract (c).*

Thermal analysis (Differential Scanning Colorimetry, DSC) confirmed that all powders were in an amorphous solid state, without any signs of crystallization or degradation below 300 °C. This result indicates strong interactions between the extract and the polymeric matrix with improved technological performance,

organoleptic qualities and thermal stability, offering promising applications in the nutraceutical and food industries.

The optimized spray-dried formulation, containing a Theoretical Extract Content (TEC) of 15.4% (w/w), resulted in microparticles with good spray-drying yield (83.4%), excellent encapsulation efficiency (EnE) of the main bioactive compounds (98-102 %) and an actual total metabolite content of 3.4 g 100 g^{-1} (Table 3.15).

Table 3.15 Encapsulation efficiency (EnE) and formultion content.

	SIL	TeGG	My	TOT
EnE (%)	100.7 ± 1.6	97.7 ± 0.9	102.2 ± 1.6	101.4 ± 1.4
mg g^{-1} DW	7.0 ± 0.2	6.8 ± 0.1	5.5 ± 0.4	33.5 ± 0.7

Data are expressed as mean ± SD of three replicates

The chemical stability of both the formulation and the extract was evaluated over the first 4 weeks-storage period under ICH storage conditions (30 ± 2 °C, 65% RH (relative humidity) ± 5 % RH) by monitoring the three main CSL markers (Sil, TeGG and Myr).

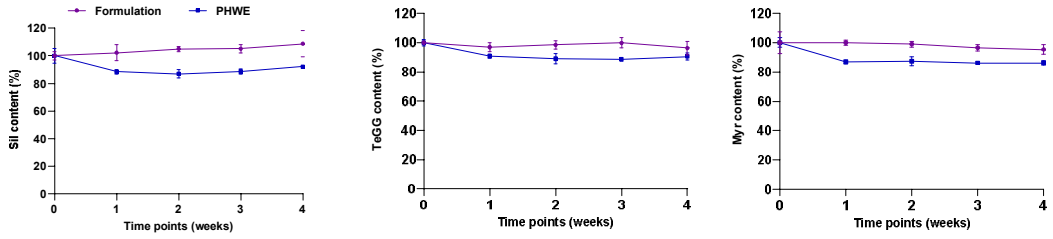

Fig. 3.24. *Stability profile of Sil (a), TeGG (b) and Myr (c) in formulation (violet line) and PHWE (blue line) evaluated under ICH conditions over 4 weeks.*

Data are expressed as mean ± SD of three replicates

The formulation retained its initial content throughout the time investigated (metabolite content expressed as percentage relative to initial content, Fig. 3.24), displaying no statistically significant variations and remaining well within the ± 5% acceptance range defined by ICH Q1A(R2). In contrast, the PHWE extract (Fig. 3.24) showed a lower metabolite (9-14%) content from the first

week and then remained stable over time; however, its variability still fell within the acceptable limits, indicating an overall satisfactory stability profile.

Preliminary solid state stability data collected over a 4-week period suggest that the formulated microparticles effectively preserve their microstructure over time. This indicates that the polymeric matrix acts as a physical barrier capable of maintaining the active compounds in a protected and stable solid-state environment. The amorphous nature of the formulation plays a key role in enhancing the physical stability of the system and minimizing potential degradation pathways. A comprehensive technological assessment is currently ongoing to evaluate the long-term retention of microstructural and functional properties, which are critical to ensuring product stability, performance, and shelf-life. These properties are directly linked to the ability of the matrix to prevent moisture uptake, inhibit recrystallization, and shield the bioactive extract from environmental stressors such as heat and humidity. Over the same period, the thermal analysis (DSC) of the PHWE extract revealed progressive structural changes (Fig. 3.25a). The thermograms exhibited a loss of the typical thermal profile associated with the lyophilized state, with a clear trend toward amorphization. These transformations were confirmed by scanning electron microscopy (SEM) images (Fig.3.25b), which showed a collapse of the original microstructure, accompanied by the emergence of particle aggregation and the onset of surface fusion among particles.

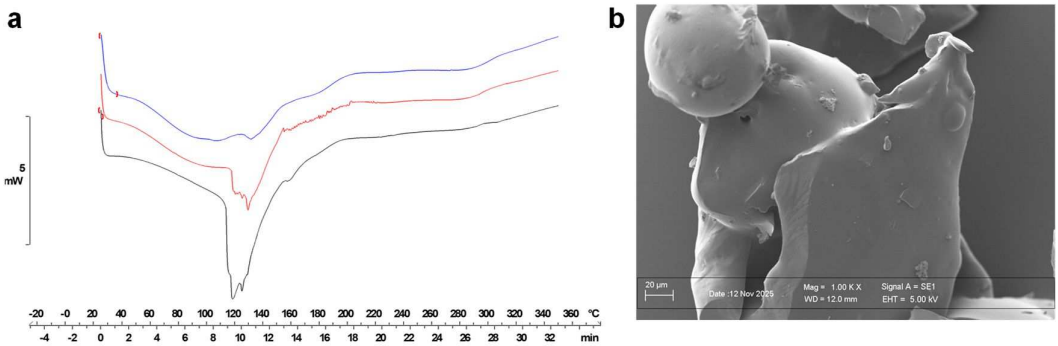

Fig. 3.25. *Differential Scanning Calorimetry (DSC) thermograms of the lyophilized PHWE at T0 (black line), after 2 weeks (red line), and after 4 weeks (blue line) of storage (a); Scanning Electron Microscopy (SEM) images at 4 weeks of storage (b).*

In contrast, the DSC profiles (Fig 3.26a) of the microencapsulated formulation remained consistent throughout the 4-week storage period. The absence of degradation peaks indicates that no thermal decomposition of the encapsulated extract occurred. Additionally, the thermal traces showed a gradual attenuation of the dehydration peak, suggesting the progressive removal of process-related residual water. SEM analysis (Fig 3.26b) further supported these findings, highlighting slight surface changes consistent with moisture migration toward the outer layer of the particles, yet without compromising the overall morphology or particle integrity. Importantly, the amorphous state of the formulation was largely preserved, with no signs of recrystallization or polymorphic transitions. The retention of this disordered structure is considered a positive indicator for the physical stability of the product, as it minimizes the risk of compound leakage or premature degradation.

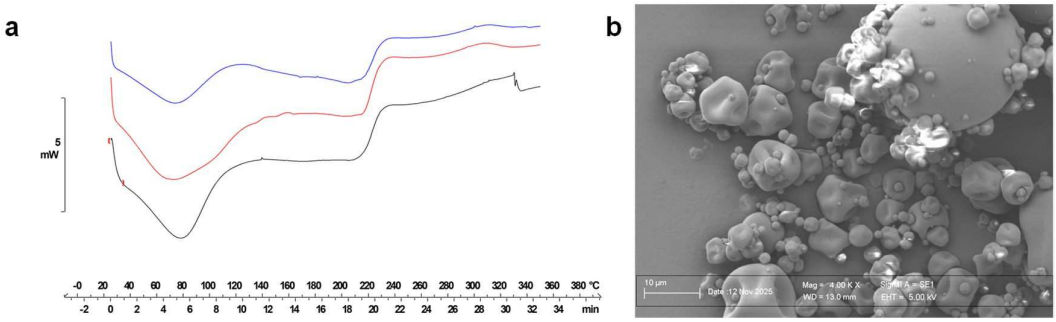

Fig. 3.26. *Differential Scanning Calorimetry (DSC) thermograms of microencapsulated formulation at T0 (black line), after 2 weeks (red line), and after 4 weeks (blue line) of storage (a); Scanning Electron Microscopy (SEM) images at 4 weeks of storage (b).*

3.4.3.2 In vitro digestion and bioaccessibility

In vitro gastrointestinal digestion simulation is a well-established approach for evaluating the stability, transformation, and bioaccessibility of bioactive compounds during digestive transit, providing predictive information on their actual biological *in vivo* potential [87]. Although carob is a recognized source of phenolic metabolites with high biological activity, studies on the digestion of leaves extracts are scattered. The available research focuses mainly on commercial products obtained from the fruit pulp [98,99], while non-edible

parts remain poorly investigated, despite their significant content of secondary metabolites.

Therefore, the INFOGEST protocol [87] was applied to both the PHWE extract and its formulation. Samples from gastric (GP) and intestinal (IP) phases were collected and analyzed in real-time by UHPLC-DAD-HRMS/MS to monitor the progress of the main metabolites during simulated digestion (Table 3.16). The metabolite release profile of the extract and the formulation was similar, indicating that the formulation can maintain the bioaccessibility (B) of active compounds over time. No significant changes were observed in the content of quantifiable metabolites during the early stages (oral and gastric phase) of simulated digestion compared to the undigested (UD) samples (Table 3.16).

Table 3.16. *Level of CSL compounds and bioaccessibility (B) of PHWE and its formulation in gastrointestinal phases.*

Compounds	PHWE UD	PHWE GP	PHWE IP	B PHWE	Formulation UD	Formulation GP	Formulation IP	B Formulation
	mg g^{-1} extract			(%)	mg g^{-1} formulation			(%)
Galloyl glucose	4.6 ± 0.1^{a}	4.7 ± 0.3^{a}	4.3 ± 0.3^{a}	93.6 ± 5.6	0.7 ± 0.1^{a}	0.7 ± 0.2^{a}	0.7 ± 0.1^{a}	99.9 ± 6.0
Gallic acid	14.2 ± 0.3^{a}	14.9 ± 1.3^{a}	3.6 ± 0.1^{b}	25.0 ± 0.5	2.4 ± 0.2^{a}	2.7 ± 0.2^{a}	0.8 ± 0.2^{b}	31.3 ± 0.6
Digalloyl glucoses	8.0 ± 0.2^{a}	8.5 ± 0.7^{a}	6.8 ± 0.2^{b}	84.5 ± 2.5	1.4 ± 0.1^{a}	1.3 ± 0.1^{ab}	1.1 ± 0.1^{b}	80.3 ± 2.4
Digalloyl glucose	10.8 ± 0.3^{a}	11.3 ± 1.2^{a}	10.0 ± 0.4^{a}	92.7 ± 3.4	1.7 ± 0.1^{a}	1.7 ± 0.2^{a}	1.6 ± 0.1^{a}	89.7 ± 3.3
Galloyl parasorboside	4.1 ± 0.2^{a}	4.1 ± 0.3^{a}	4.1 ± 0.1^{a}	100.0 ± 1.4	0.5 ± 0.1^{a}	0.5 ± 0.1^{a}	0.6 ± 0.1^{a}	113.3 ± 1.6
Siliquapyranone acid form	22.7 ± 0.3^{a}	24.2 ± 2.0^{a}	17.8 ± 0.4^{b}	78.3 ± 1.7	3.6 ± 0.1^{ab}	3.9 ± 0.3^{a}	3.1 ± 0.2^{b}	85.4 ± 1.8
Trigalloyl glucoses	4.8 ± 0.1^{b}	5.1 ± 0.1^{a}	3.2 ± 0.1^{c}	66.4 ± 0.3	0.8 ± 0.1^{a}	0.8 ± 0.0^{a}	0.6 ± 0.1^{a}	70.5 ± 0.3
Siliquapyranone	42.6 ± 0.3^{a}	44.1 ± 6.1^{a}	20.0 ± 1.1^{b}	46.9 ± 2.6	7.0 ± 0.2^{a}	7.6 ± 1.1^{a}	4.2 ± 0.2^{b}	59.5 ± 3.2
Trigalloyl glucose	8.2 ± 0.2^{a}	9.0 ± 0.6^{a}	6.2 ± 0.1^{b}	75.4 ± 0.5	1.4 ± 0.1^{a}	1.4 ± 0.1^{a}	1.1 ± 0.1^{b}	78.7 ± 0.5
Myricitin 3-*O*-hexoside	3.5 ± 0.1^{a}	3.6 ± 0.2^{a}	< LOQ	< LOQ	0.6 ± 0.1^{a}	0.6 ± 0.1^{a}	< LOQ	< LOQ
Myricitrin	31.6 ± 0.2^{a}	33.8 ± 3.0^{a}	6.6 ± 0.2^{b}	20.9 ± 0.7	5.5 ± 0.4^{a}	5.6 ± 0.5^{a}	1.5 ± 0.1^{b}	26.3 ± 0.9
1,2,3,6-TeGG	45.4 ± 0.5^{a}	47.2 ± 4.4^{a}	24.1 ± 2.1^{b}	53.1 ± 4.7	6.8 ± 0.1^{a}	6.9 ± 0.7^{a}	4.3 ± 0.2^{b}	63.2 ± 5.6
Quercetin 3-*O* deoxyhex	6.6 ± 0.1^{a}	6.9 ± 0.7^{a}	6.9 ± 0.7^{a}	105.5 ± 10.0	1.1 ± 0.1^{a}	1.2 ± 0.1^{a}	1.1 ± 0.1^{a}	100.4 ± 9.5
GGs	170.1 ± 1.3^{a}	178.3 ± 7.2^{a}	103.0 ± 2.1^{b}	60.6 ± 1.3	26.3 ± 0.3^{a}	27.7 ± 2.7^{a}	17.9 ± 0.1^{b}	69.5 ± 1.4
FGs	41.7 ± 0.1^{a}	44.2 ± 3.8^{a}	13.6 ± 0.9^{b}	32.5 ± 2.1	7.2 ± 0.4^{a}	7.4 ± 0.6^{a}	2.5 ± 0.2^{b}	37.8 ± 2.5
Total	206.9 ± 1.3^{a}	217.4 ± 1.0^{a}	113.4 ± 1.3^{b}	54.8 ± 0.6	33.5 ± 0.7^{a}	35.1 ± 3.4^{a}	20.4 ± 0.1^{b}	62.9 ± 0.7

Values represent mean ± SD (n = 3). Different superscript letters in the same row indicate significant differences between UD, GP and IP in PHWE and formulation digestion ($p \leq 0.05$, Tukey's HSD test).

According to the INFOGEST protocol, salivary amylase is only necessary for the digestion of starchy foods during the oral phase; therefore, it can be omitted in the case of matrices that do not contain starch [87]. In our case, this step, although not omitted, did not result in any appreciable changes in the content of the metabolites analyzed (data not shown). Similarly, no significant changes were found in the gastric phase confirming the stability of the CSL compounds even under acidic gastric conditions (Table 3.16). Significant losses of CSL metabolites were observed during the IP, with clear differences among the two main chemical classes. GGs retained bioaccessibility above 60%, whereas FGs showed lower stability, with values below 40%. This trend suggests that the latter compounds could be more susceptible to the intestinal environment (Table 3.16).

To understand the dynamics of this variation and monitor the behaviour of the compounds during this phase, a detailed kinetic analysis was performed, with samples collected at 30-minutes intervals (Fig. 3.27). Temporal monitoring was essential as TeGG and Sil showed marked *in vitro* inhibitory activities on α-GLU, with a much lower IC_{50} than acarbose. Since this enzyme acts in the first portions of the small intestine, the evaluation of their bioaccessibility is relevant for better understanding their potential biological effects.

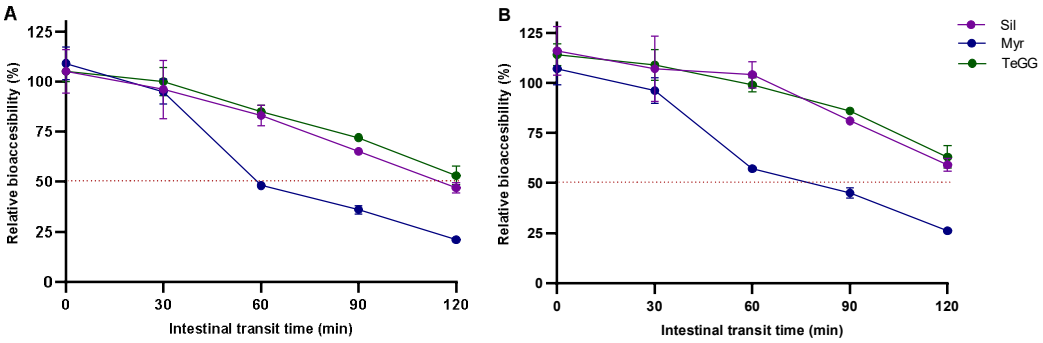

Fig 3.27. *Relative bioaccessibility (%) of main compounds from CSL-PHWE (A) and its formulation (B) over 120 min of intestinal digestion.*

Values represent mean ± SD (n = 3).

During the first half hour, metabolite concentrations remain unchanged compared to the undigested sample; the first significant reduction is observed

after 60 minutes, particularly for Myr, which decreases by about 50% (Fig. 3.27). Glycosylated flavonoids, as complex and large molecules, generally have low bioavailability, they are usually hydrolyzed by specific intestinal enzymes, resulting in the removal of the sugar part and the formation of the corresponding aglycones [100]. Hence, HRMS analysis were performed to verify the possible hydrolysis of Myr into myricetin aglycone (m/z 317.0302 $[M-H]^-$); no signal was detected, excluding the formation of relevant hydrolysis products. Within the glycosylated flavonols class (FGs), myricetin 3-O-hexoside also shows a progressive reduction trend up to 30 minutes after the start of intestinal digestion, followed by complete disappearance of the compound (Table 3.16). An opposite behaviour is observed for quercetin O-deoxyhexoside, which remains stable throughout the entire digestive process (Table 3.16). Overall, FGs show an average bioaccessibility of about 30%.

For the most abundant class (GGs), Sil and TeGG show similar behaviour, maintaining bioaccessibility above 60% for up to 90 minutes, followed by a slight reduction (~10%) at the end of the intestinal phase (120 min, Fig. 3.27). Di- and tri-galloyl glucosides, on the other hand, show an overall decrease of about 20%, suggesting possible hydrolysis of the two major compounds (Sil and TeGG) and their subsequent conversion to di- and tri-GGs (Table 3.16). In-depth HRMS analysis revealed a marked increase in ellagic acid levels in the IP samples collected at 30-minute intervals. This rise, approximately 80% relative to the initial concentrations in both the extract and the undigested formulation, may be attributed to the transformation of Sil and TeGG. Based on the degradation pathway postulated by Zannini et al., [98], gallic acid, produced by the hydrolysis of gallotannins, could first undergo dimerization into digallic acid in the intestinal juice, followed by a dehydration process leading to the formation of ellagic acid, thus justifying the increase of this molecule in this phase.

Overall, the results appear favourable for the CSL key marker metabolites, particularly Sil and TeGG. Although their bioaccessibility reach approximately 47-53% for the PHWE and 59-63% for the formulation, respectively, after 120 minutes (Fig. 3.27), Sil and TeGG maintain an almost constant concentration during the first hour of the IP. This is physiologically relevant, as intestinal α-

glucosidases exhibit their highest activity in the proximal duodenum and jejunum, corresponding to the early stages of digestion [88]. Therefore, the persistence of these α-GLU inhibitors at high levels during this period suggests that it can effectively exert its inhibitory action under physiological conditions. The observed increase in ellagic acid is particularly noteworthy, as this compound is a well-known hydrolysis product of tannins and a precursor of urolithins formation by the intestinal microbiota. Among these metabolites, urolithins A and B are the primary colonic derivatives of ellagic acid and tannins, widely recognized in both *in vitro* and *in vivo* studies for their anti-proliferative, anti-cancer, anti-inflammatory, and neuroprotective properties [100]. The observed increase in ellagic acid, together with the good bioaccessibility of the main CSL metabolites, enhances the post-digestive biological potential of both the extract and its formulation.

3.5 Conclusion and future perspectives

The research on CSL demonstrated the great potential of this untapped matrix as a sustainable source of high-value compounds. The first phase provided a comprehensive HRMS/MS profiling and biological *in vitro* screening, identifying galloylated glucoses, Sil, Sil-A, TeGG, and Myr as chemical markers of CSL and the primary contributors to the activities of the CSL extract. Notably, CSL extracts and TeGG have shown excellent performance in selectively inhibiting α-GLU.

The high content of bioactive compounds in CSL extracts marked this untapped resource as even more promising than carob pods or other fruit leaves. The optimal period to obtain the most enriched biomass coincides with fruit harvesting, thereby optimizing the production chain and promoting the sustainable utilization of this underutilized crop. For their rich metabolic profile and strong *in vitro* activities, CSL proved to be promising candidates for the development of novel functional foods and nutraceutical formulations.

Building on these findings, innovative green extraction strategies, namely PHWE and probe-UAE) were selected and carefully optimized for the sustainable and efficient recovery of CSL compounds. Through RSM and UHPLC-DAD analysis, temperature (for PHWE) and solvent (for probe-UAE) composition were identified as the key parameters affecting metabolite recovery and extraction efficiency. The optimized extraction conditions, tailored to maximize the recovery of Sil, TeGG and Myr while minimizing their degradation, enabled an exhaustive extraction of CSL bioactive compounds yielding safe and high-quality extracts and preserved functional properties. Both PHWE and probe-UAE outperformed conventional methods (Soxhlet and maceration) in terms of efficiency, purity, and environmental impact and provide a solid basis for future pilot-scale trials and potential industrial exploitation of this health-promoting natural source.

In addition, both PHWE and probe-UAE extracts retained α-GLU inhibitory activity and exhibited strong AOC against oxidative stress in cellular models, including both healthy and cancer-cell lines, confirming their functional potential. To improve its stability and applicability, the optimized PHWE extract,

chosen for its aqueous and ready-to-use nature, was successfully microencapsulated by spray drying. The formulation contributed to preserving and slightly enhancing the bioaccessibility of all key metabolites. Among them, TeGG and Sil also showed an increase in bioaccessibility, enabling its potential action against α-GLU in the upper small intestine.

Overall, this work advances the sustainable exploitation of carob leaves from a neglected biomass to a promising source of bioactive ingredients and opens various prospects for the full sustainable valorization of CSL. One potential direction for further development involves scaling up the optimized laboratory conditions to a pilot level, to assess their actual industrial applicability and their ability to maintain efficiency and recovery on larger matrix volumes.

A second area of development involves evaluating bioactive compounds during *in vitro* digestion under meal-simulated conditions. Under starch-rich meal conditions, this approach would verify whether α-GLU inhibitor compounds interact with the physiological substrate and retain their activity. The activity can be evaluated by testing the digestates in the classic *in vitro* enzyme assay.

Furthermore, according to EFSA guidelines [101], the evaluation of the extract safety profile through genotoxicity, cytotoxicity tests and other required toxicological parameters would be necessary, to support its use for human consumption. Finally, *in vivo* studies would be essential to confirm the biological *in vitro* activities and consolidate CSL extracts potential as ingredients for functional foods and formulations for human well-being.

3.6. Materials and methods

3.6.1 Chemicals and standards

MS-grade acetonitrile (MeCN) and water were supplied by Romil (Deltek, Italy). Ultrapure water (18 MΩ) was prepared by a Milli-Q purification system (Millipore, Bedford, USA). Analytical-grade methanol and ethanol, MS-grade formic acid, 6-hydroxy-2,5,7,8-tetramethyl-chromane-2-carboxylic acid (Trolox), Folin & Ciocalteu's phenol reagent (FC), 2,2′-azinobis(3-ethylbenzothiazoline-6-sulphonic acid) diammonium salt (ABTS), 2,2′-azobis(2-methylpropionamidine) dihydrochloride (AAPH), fluorescein sodium salt, potassium persulfate ($K_2S_2O_8$), Trizma hydrochloride (Tris-HCl), acetylthiocholine iodide (ATCI), Butyrylthiocoline iodide (BTCI), 4-(amino-sulfonyl)-7-fluoro-2,1,3-benzoxadiazole (ABD-F), 4-nitrophenyl-β-D-glucopyranoside (pNPG), starch from potato, 3,5-dinitrosalicylic acid (DNS), disodium hydrogen phosphate (Na_2HPO_4),potassium dihydrogen phosphate (KH_2PO_4), pyrogallol, sodium carbonate (Na_2CO_3), were obtained from Merck Chemicals (Milan, Italy). The enzymes, acetylcholinesterase from *Electrophorus electricus* (E3.1.1.7, Type V–S, lyophilized powder, 200–1000 units/mg protein; AChE), butyrylcholinesterase from equine serum (E3.1.1.8, lyophilized powder, ≥10 units/mg protein BChE), α-glucosidase from *Saccharomyces cerevisiae* (EC 3.2.1.20, Type I, lyophilized powder, ≥ 10 units/mg protein; α-GLU), and porcine pancreas α-amylase (EC 3.2.1.1, Type VI-B, ≥5 units/mg solid; α-AMY), were purchased from Merck Chemicals. Reference standards of isoquercitrin (purity ≥98 %), myricitrin (purity ≥98 %), quercetin (purity ≥98 %), gallic acid (purity ≥98 %), galantamine hydrobromide (purity ≥98 %),acarbose (purity ≥98 %) and high-degree esterified citrus pectin (DE 70–75%) and inulin were obtained from Merck Chemicals or Extrasynthese (Labservice, Anzola Emilia (BO),Italy), 1,2,3,6-Tetragalloylglucose (TeGG) and siliquapyranone (Sil) were isolated by CSL (section *3.2.1.2*). Reagents for INFOGEST protocol, Potassium chloride (KCl), potassium dihydrogen phosphate (KH_2PO_4), sodium bicarbonate ($NaHCO_3$), sodium chloride (NaCl), magnesium chloride hexahydrate ($MgCl_2{\cdot}6H_2O$),

calcium carbonate ($CaCO_3$), hydrochloric acid (HCl), and calcium chloride dihydrate ($CaCl_2 \cdot 2H_2O$) were obtained from from Merck Chemicals (Milan, Italy); the enzymes: pepsin from porcine gastric mucosa (≥400 units/mg solid), bile salts suitable for microbiology, and pancreatin from porcine pancreas (≥3× USP specifications) were purchased from Merck Chemicals (Milan, Italy). Cell culture reagents, Dulbecco's Modified Eagle Medium-low glucose (DMEM, with 1000 mg/L glucose and L-glutamine, without sodium bicarbonate and phenol red), sodium bicarbonate ($NaHCO_3$), penicillin, D-glucose, Trypsin–EDTA solution and Dulbecco's Phosphate Buffered Saline (DPBS), Hank's Balanced Salt Solution (HBSS), Roswell Park Memorial Institute (RPMI), Thiazolyl blue tetrazolium bromide (MTT) and magnesium sulfate (MgSO4) were obtained from from Merck Chemicals (Milan, Italy). Fetal bovine serum (FBS) and 2′,7′-Dichlorofluorescin diacetate (DCFH-DA) were purchased from Thermo Fisher Scientific (Waltham, MA, USA), syringe filters (CA, 0.22 µm, Ø 25 mm, sterile) were supplied by LLG-Labware (Meckenheim, Germany). Cells (HepG2) were purchased by ATCC (American Type Culture Collection, P92).

3.6.2 Sampling and exhaustive extraction of CSL

Samples of CSL, Amele variety were collected monthly from late May to late September, between the two flowering phases, from three mature (≥100 years old) trees located at the Masseria Agricola Olère in Ostuni, Puglia (40°46′06″N, 17°32′52″E, 54 m above sea level). A total of approximately 3 kg of leaves were harvested per tree. The leaves were dried in an oven at 40 °C until a constant weight was reached, then ground with a Grindomix GM 200 knife mill (Retsch, Haan, Germany) and sieved (mesh size range 300–600 µm) to obtain homogeneous powders. Exhaustive extraction was carried out in triplicate using ultrasonic-assisted solid–liquid extraction (Labsonic LBS2 ultrasonic thermostatic bath, Treviglio, Italy) with 70% aqueous ethanol (v/v) as the extraction solvent (matrix/solvent ratio 1:20, 25 °C for 30 minutes). The process was repeated three times with fresh solvent, and the exhaustive extraction was monitored by UHPLC-PDA analysis (area of main peaks <2%). The resulting supernatants were then centrifuged for 10 minutes at 13,000 g

pooled, filtered (Whatman No. 1 filter), concentrated under vacuum at 40 °C using a rotary evaporator and freeze-dried (Alpha 1-2 LD freeze dryer, Christ, Germany). The extraction yields of the samples collected in May, June, July, August, and September were 23.2 ± 0.8, 24.4 ± 0.3, 19.6 ± 0.7, 24.2 ± 0.3, and 23.4 ± 0.3 g of extract/100 g of dry matrix, respectively.

3.6.3 UHPLC-DAD-HRMS/MS analysis

The analyses were carried out using a Vanquish Flex UHPLC system interfaced to a double detector, a Diode Array Detector FG and an Orbitap Exploris 120 mass spectrometer, equipped with a heated electrospray ionization source, HESI-II (Thermo Fisher Scientific, Milano, Italy). Chromatographic separation was achieved using a Kinetex C18 column (100 × 2.1 mm I.D., 2.6 µm, Phenomenex, Bologna, Italy), operated at 30 °C with a flow rate of 500 µL min^{-1}, and a binary gradient of water (A) and MeCN (B), both containing 0.1 % formic acid (injection volume, 5 µL). The elution method was as follows: 0–3 min, 2 % B; 3–5 min,2–8%B;5–9min,8%B;9–16,8–18%B;16–17min,18%B; 17–21 min, 18–30 % B; 21–24 min, 30–98 % B. The UV spectra were acquired in the range of 200–600 nm and HRMS data were acquired in negative ionization mode. A Full MS data-dependent MS/MS (Full MS/ dd-MS2) acquisition mode was used, with the resolution of Full MS scan (scan range *m/z* 100–1000) and dd-MS^2 scan of 60,000 and 30,000 FWHM, respectively. A stepped collision energy HCD (20, 40, and 60) was applied for fragmentation. Instrument control and spectra acquisi- tion were carried out using Xcalibur software version 4.6 (Thermo Fisher Scientific). Detected compounds were characterized according to HRMS data (accurate masses, probable molecular formulas and product ions), retention times and UV spectra. The identification level was established according to metabolomics standards initiative (MSI): level 1 for compounds confirmed with reference standards, level 2 for putative identifications based on spectral data comparisons with literature sources, level 3 for assignment to a chemical class also supported by chemotaxonomic evidence, and level 4 for unidentified compounds.

3.6.4 Isolation and identification of main compounds

Major CSL compounds were isolated from the exhaustive extract by Biotage Selekt automated flash chromatography system (Biotage, Sweden AB, Uppsala, Sweden). Extract aliquots (500 mg) were dissolved in 1 mL of aqueous methanol (10 % *v*/v) and loaded onto a Biotage Sfär C18 D (100 Å, 30 µm, 12 g) column. The compounds were eluted with water (A) and methanol (B) as eluent at a flow rate of 12 mL min^{-1} according to the following gradient: 5 column volume (CV), 10 % B; 10 CV, 10–40 % B; 5 CV, 40–60 % B;2 CV, 60–95 % B. The UV spectra were acquired in the range of 200 - 400 nm. A threshold collection of 100 mAU was set at wavelength of 280 nm for Sil and TeGG and at 350 nm for Myr. The fractions corresponding to the chromatographic peaks of interest were collected, aliquoted, diluted, and analyzed preliminarily by UHPLC-DAD-HRMS/MS to verify their purity. Fractions containing the main compounds were pooled and subjected to the same purification procedure on a Biotage Sfär C18 D (100 Å, 30 µm, 6 g) column. Following this procedure, three compounds were obtained and identified by NMR and HRMS experiments as siliquapyranone (Sil) [52], 1,2,3,6-Tetragalloylglusose (TeGG) [102] and myricitrin (Myr). The purity (> 95 %) of the isolated compounds was evaluated by HPLC-PDA analysis.

3.6.5 UHPLC-UV quantitative analysis

The UHPLC-PDA system and chromatographic conditions were the same as in section 3.5.3. Two wavelengths were selected to detect target analytes based on their maximum absorbance: 280 nm for galloyl derivatives and 350 nm for flavonols. The main compounds in CSL extract were quantified using the external standards method. Calibration levels of reference standards (gallic acid, TeGG, Sil, Myr and isoquercitrin, dynamic ranges in Table 3.17) were prepared by dilution with MeOH/H_2O (1,3 *v*/v) and analyzed in triplicate. LOD and LOQ were estimated using the calibration-based approach (Table 3.17). The linearity of the calibration curves was assessed in the concentration range of 1–150 µg mL^{-1} (ten levels in triplicate). A linear model validated by

analysis of variance (ANOVA) (R^2 values >0.999) was adopted for quantitative analysis in the dynamic ranges reported in Table 3.17. Intraday repeatability was estimated for all concentration levels and coefficient of variation (CV) values of <5 % demonstrate a good method precision.

Table 3.17. *Analytical Figures-of-Merit of Calibration Models*

Compound	Dynamic range (μg mL^{-1})	R^2	LOD (mg g^{-1})	LOQ (mg g^{-1})
Gallic acid	2-150	0.9992	0.34	1.14
Siliquapyranone	2-150	0.9921	0.34	1.14
Myricitrin	1-150	0.9986	0.31	1.02
1,2,3,6-Tetragalloyl glucose	5-150	0.9966	0.81	2.70
Quercetin-3-O-glucopyranoside	1-100	0.9998	0.12	0.41

The levels of compounds for which no reference standards were available were estimated using the calibration curves of gallic acid, Myr, isoquercitrin and Sil for galloylated derivatives, myricetin glycosides, quercetin glycosides and siliquapyranone acid form, respectively. Quantitative results were expressed as mg per g of dry extracts (mg g^{-1} extract, mean ± standard deviation (SD) of three extraction replicates).

3.6.6 Determination of the TPC

TPC of CSL extracts was determined using the method explained in section 2.4.5.

3.6.7 Antioxidant assays

The antioxidant capacities (AOCs) of the exhaustive extracts and of major CSL compounds (TeGG, Sil and Myr) were evaluated using ABTS scavenging capacity and oxygen radical absorbance capacity (ORAC) assays according to Celano et al. [40]. A multimode microplate reader Varioskan LUX was employed for the assays. Quercetin was used as positive control and Trolox calibration curves (2.5–25 μM and 0.5–7.5 μM, well concentrations, for ABTS and ORAC assays, respectively) were used to calculate AOCs. Results were expressed as TEAC per g of extract (mmol TE g^{-1}, mean ± SD of three

extraction replicates) or per µmol of pure compound (µmol TE μmol^{-1}, mean ± SD of three assay replicates).

The ABTS assay was performed as described in Section 2.4.4. The tested concentration ranges for the compounds were as follows: TeGG, 0.03–0.3 mM; Sil, 0.1–0.4 mM; Myr, 0.1–1 mM. For ORAC assay, extracts and compounds were diluted with PBS 75 mM (pH 7.4) and 25 µL of solutions were added to 150 µL of fluorescein (0.01 µM) in a 96-well plate. After incubation at 37 °C for 30 min, 25 µL of AAPH (150 mM) were added to each well and the emission fluorescence intensity (λ excitation /λ emission = 485/530 nm) was recorded every minute for 1 h at 37 °C. Compounds TeGG, Sil and Myr were tested at the concentration ranged from 0.5 to 2.5 µM. The average net AUC (AUC sample – AUC control) of CSL extracts and standards was used to calculate the TEAC equivalents.

3.6.8. In vitro α-GLU inhibitory assay

The α-GLU inhibitory assay was performed as described in Section *2.4.7*. The tested concentration ranges for the compounds were as follows: TeGG, 0.02-0.2 µM; Sil, 5-50 µM; My, 50-450 µM. Results were expressed as IC_{50} (concentration of inhibitor that causes 50 % enzyme inhibition) ± SD of three replicates. Relative activity (RA) to the positive controls (ratio of the IC_{50} inhibitor relative to that of acarbose or quercetin, RA_A and RA_Q, under the same assay conditions) was also calculated to compare more accurately the results with previous studies.

3.6.9. In vitro α-AMY inhibitory assay

The inhibitory activity of α-AMY was evaluated according to Cardullo et al., [36]. The enzyme and substrate (starch) were diluted to the working concentration with 20 mM phosphate buffer (pH 6.9) containing 6.7 mM NaCl and the inhibitor stock solutions were diluted with H_2O. Acarbose (5–130 µM, well concentration) was used as positive control. Starch solution 0.5 % *w*/*v* was stirred at 90 °C for 20 min before use. For the experiments, 50 µL of diluted solutions of inhibitor or H_2O (negative control) were added to 150 µL of α-AMY

(6 U/mL) and incubated at 37 °C for 10 min. Subsequently, 150 µL of starch solution was added to microtubes and the mixture was further incubated at 37 °C for 15 min. Then, 300 µL of reagent (96 mM DNS with 30 % sodium potassium tartrate in 2 N NaOH) were added to terminate the reaction, and the mixtures were heated at 100 °C for 10 min. Finally, each mixture was diluted with 1 mL of H_2O, and the absorbance was measured at 540 nm with a microplate reader Varioskan LUX. % Inhibition was calculated using absorbance. Each inhibitor was tested in triplicate at least five different concentrations. TeGG concentration range tested was 50–150 µM. Results were expressed as IC_{50} ± SD of three replicates, and RA to acarbose (RA_A).

3.6.10. In vitro AChE and BChE inhibitory assays

Both cholinesterase inhibition assays (AChE and BChE) were performed in this study. The detailed protocol for AChE is reported in Section *2.4.6*, and the BChE assay was carried out following the same workflow, except for the specific enzyme, substrate, and inhibitor concentrations required for BChE.

In the BChE assay, galantamine was used as the positive control and tested in the 4-180 µM range. Stock solutions of BTCI (substrate) were prepared in water and added at a concentration corresponding to its Michaelis–Menten constant (Km = 1.4 mM). Each reaction well contained 25 µL of BChE (0.8 U mL^{-1}), followed by incubation for 10 min at 37 °C. The reaction was initiated by adding 25 µL ABD-F (125 µM) and 50 µL BTCI, and fluorescence was recorded under the same conditions described for the AChE assay.

Each inhibitor was tested in triplicate at least five different concentrations. The tested concentration ranges for the compounds were as follows: TeGG, 3-250 µM; Sil, 15-250 µM; Myr, 5-250 µM for AChE and TeGG, 10-80 µM; Sil, 150-700 µM; My, 30-200 µM for BChE. Results were expressed as IC_{50} ± SD of three replicates, and RA to galantamine (RA_G).

3.6.11 Conventional solid-liquid extractions

SLE and So extractions were employed as conventional solid-liquid extraction techniques using 70% ethanol/water (v/v) as extraction solvent. For Soxhlet

extraction, approximately 5 g of CSL was placed in a cellulose thimble and extracted in a Soxhlet extractor with 100 mL of solvent under reflux for 8 h. For maceration, the same amounts of sample and solvent were stirred at room temperature for 24 h. After extraction and filtration, the extracts were treated as detailed in section *3.5.2*.

3.6.12. Pressurized hot water extraction (PHWE)

PHWE was performed with an ASE 350 system (Thermo Fisher Scientific, Milano, Italy) in static extraction mode using 34 mL stainless steel cells and 250 mL collection bottles. Extraction cells, equipped with stainless steel frits and a cellulose filter at the bottom, were loaded with sample mixed with 4 mm glass beads. The fixed instrumental parameters were set as follows: distilled water as extraction solvent, pressure of 100 bar, purge of 40 sec, rinse equal to 50% cell volume, and cell preheating deactivated. For preliminary experiments, a single extraction cycle with a static time of 10 min was applied. Under optimal conditions, PHWE was performed at a temperature of 98 °C with three cycles, each with a static time of 5 min, loading 1.5 g of matrix into 34 mL cells. After cooling, PHWE extracts were diluted to a final volume of 60 mL with water. An aliquot of 1 mL was directly used for UHPLC and spectrophotometric analyses, while the remaining volume was freeze-dried to determine the EY.

3.6.13. Ultrasound-assisted extraction using probe system (probe-UAE)

Probe-UAE was conducted using an ultrasonic processor UP400St (Hielscher Ultrasonics GmbH, Teltow, Germany) equipped with a titanium sonotrode H3 (3 mm diameter, for volume from 5 to 200 mL) at a fixed working frequency of 24 kHz. CSL samples were mixed with 20 mL of solvent in a 50 mL centrifuge tube and extracted by immersing the probe 1 cm deep into the suspension at 30 °C. The temperature was continuously monitored using a thermocouple and controlled by a circulating water bath. For preliminary experiments, a SLR of 25 g L^{-1} and an extraction time of 30 min were used to assess the influence of amplitude, duty cycle, extraction solvent, and extraction kinetics.

Subsequently, the operational parameters were set to an amplitude of 60% and a duty cycle of 50%. Under optimal conditions, UAE was performed using aqueous ethanol 52% v/v, with a SLR of 100 g L^{-1} and an extraction time of 20 min. UAE extracts were filtered through a Whatman No. 1 filter paper. An aliquot of 1 mL was processed for subsequent analyses, and the remaining extract was treated as described in section *3.5.2*.

3.6.14. Experimental design and optimization

PHWE and probe-UAE conditions were optimized by Response Surface Design using a BBD quadratic model (19 degrees of freedom), consisting of two block replicates of 15 randomized experimental runs and three center points for block. The experimental design and optimization of operational conditions for each extraction process were performed using Statgraphics Centurion 18 software, provided by Statgraphics Technologies (Adalta snc, Arezzo, Italy). The independent experimental factors considered for each extraction method and their levels (-1, 0, and +1) are reported in Tables 3.6 and 3.10. Minimum and maximum levels of the independent factors were selected based on preliminary experiments. EE (mg g^{-1} leaf) and extract purity (P, g 100 g^{-1} extract) of the main CSL compounds (Sil, Myr, and TeGG) were designated as response variables to be maximized. Gallic acid (GA) and digalloylglucoses (diGGs) contents (mg g^{-1} leaf) were monitored as degradation indicators to be minimized in PHWE and probe-UAE optimization, respectively. Furthermore, EY (g extract 100 g^{-1} leaf) and TPC (mg GAE g^{-1} leaf) were considered as response variables. The experimental conditions for both designs and the corresponding response variable values are listed in Tables 3.7 (PHWE) and 3.10 (probe-UAE). A second-order polynomial equation was used to fit each dependent variable (Y) as a function of the independent factors (A-C). Mathematical models of the estimated response surfaces were defined after removing the non-significant factors and two-factor interactions identified by ANOVA ($p > 0.05$). Model adequacy and quality were verified through lack-of-fit test and regression coefficients (R2 and adjusted R2), respectively. Subsequently, simultaneous optimization of independent

factors was conducted using the desirability function aiming to maximize EEs and Ps of main CSL compounds while minimizing GA and diGGs contents. The suggested optimal conditions were experimentally validated by comparing predicted values of response variables with the experimental data of six extraction replicates (95% confidence interval).

3.6.15. UHPLC-HRMS analysis of degradation products

UHPLC-HRMS analysis was performed using the same chromatographic condition described in section *3.5.3* and the same mass acquisition parameters. Extracted ion chromatograms of pyrogallol ($[M-H]^-$ at m/z 125.0244) and 5-hydroxymethylfurfual ($[M+H]^+$ at m/z 127.0390) with a mass selection window of 3 ppm were used for their quantitation. The concentration levels of pyrogallol were estimated using solvent calibration curves (0.5-20 µg mL^{-1}).

3.6.16. Cell cultures, MTT and cellular antioxidant assays in HepG2

Human hepatocellular carcinoma (HepG2) cells were purchased from ATCC (American Type Culture Collection) and cultured in DMEM (Dulbecco's Modified Eagle Medium) low glucose, with 10 % of FBS (Fetal Bovine Serum) and 1% Pen-Strep. Cell lines were grown at 37 °C in 5 % CO_2 humidified atmosphere. Dilutions were prepared in culture medium with a final concentration of DMSO did not exceed 0.5 % (v/v). HepG2 cells were seeded into 96-well plates at a density of 1 x 10^4 cells per well in four replicates and exposed to increasing concentration (5–300 µg mL^{-1}) of the extracts for 24 h. Cell viability was assessed using the colorimetric MTT assay. To this end, after 24 h, the culture medium was removed, and 50 µL of MTT (0.5 mg mL^{-1} PBS) was added to each well and incubated for 4 h at 37 °C. Subsequently, the medium was discarded, and the formazan crystals were solubilized with 200 µL of DMSO. MTT conversion to formazan by metabolically viable cells was monitored at an optical density of 540 nm.

The protocol of cellular antioxidant assay was carried out according to the method described by Wolfe and Liu [103]. HepG2 cells were seeded at a

density of 5 × 10^4 cells per well with 100 µL of growth medium. After 24 hours, the cells were washed and incubated at 37 °C for 1 h after addition of 50 µL of DCFH-DA solution (50 µM in RPMI) and 50 µL of the extracts, or quercetin (positive control, concentration range 0.3 to 15 µg mL^{-1}), or RPMI (for controls). Subsequently, the mixture was removed, the wells were washed again with 100 µL of PBS, and 100 µL of AAPH solution (600 µM in HBSS) or RPMI (negative control) was added. Fluorescence was measured after 1h at 37 °C (λ Ex = 485 nm and λ Em = 538 nm) using a Hidex Sense plate reader (Hidex, Finland). The results were expressed as ROS generation percentage (mean ± SD).

3.6.17. Erythrocyte haemolysis and antioxidant assay

Venous blood from a healthy O^+-type donor was collected with informed consent and ethical approval from the Science and Engineering Research Ethics Committee of the University of Limerick (approval #2023_02_01_S&E). The erythrocytes were washed with PBS and isolated by centrifugation (1200 g, 5 min). PBS was used to obtain a 20 % haematocrit concentration. To evaluate erythrocyte antioxidant activity and membrane protection or damage induced by extracts, AAPH was used as a peroxyl radical generator to increase intracellular ROS and disrupt cellular homeostasis. The protocol was performed as described in Cruz et al., [91]. Briefly, 100 µL of extracts in different concentrations, quercetin (used as standard at 25 and 100 µg mL^{-1}) or PBS (for controls) was incubated with 100 µL of erythrocyte suspension (20% hematocrit) at 37 °C and 150 rpm for 20 min. Then, 200 µL of AAPH solution (200 mM in PBS) or PBS (negative control) was added, followed by gentle mixing and further incubation under the same conditions for 2 h. After incubation, tubes were centrifuged at 1200 g for 10 min to collect supernatant (SN) and precipitate (PT).

The antihaemolytic effects of the extracts was analysed using 100 µL of SN mixed with 200 µL of PBS in a 96-well plate. Absorbance was measured at the isosbestic point of hemoglobin (523 nm) (Hidex Sense). The percentage of haemolysis was calculated in relation to the total haemolysis (by replacing the

AAPH and sample by ultrapure water in the oxidation process). For intracellular ROS generation, PT was washed with 400 µL of PBS, centrifuged at 1200g for 3 min, and the resulting pellet was resuspended in 400 µL of DCFH-DA solution (10 µM) in the dark. After 20 min of incubation at 37 °C, fluorescence of 300 µL of the reaction mixture was measured (λ_{Ex} = 485 nm, λ_{Em} = 538 nm) to quantify the percentage of intracellular ROS generated [91]. The negative control contained erythrocytes with PBS (no AAPH), and the positive control contained AAPH-treated cells. Each sample was tested in four replicates, and the entire procedure was repeated twice on the same day as a biological replicate.

3.6.18. PHWE formulative study

Dissolution tests of dried PHWE extract were performed using a USP II dissolution apparatus (Sotax AT7 Smart) equipped with online UV detection (Specord 200 plus, Analytik Jena). A total of 250 mg of extract was dispersed in 250 mL of simulated gastric fluid (SGF) at pH 1.0, 1.2, and SGF with enzymes. Tests were conducted at 37 ± 0.5 °C with paddle stirring at 50 rpm for 120 minutes. Manual samples (1 mL) were collected every 15 minutes and analyzed by UHPLC-UV (section *3.5.5*). SGF solutions were prepared according to the Italian Pharmacopoeia (XII edition, 2008).

For formulation preparation, 12 g of inulin were dissolved in 290 mL of aqueous extract (0.8 g 100 mL^{-1}) at 40 °C for 30 minutes under magnetic stirring, followed by the gradual addition of 1.2 g of pectin under continuous agitation to reach a final feed volume of 400 mL. The optimized formulation contained 3% (w/w) inulin, 0.3% (w/w) pectin, and 0.6% (w/w) extract, while a control matrix without extract was prepared under identical conditions. Viscosity was measured using a rotational viscometer (Visco Basic Plus, Fungilab) with spindle L2 at 100 rpm and 25 °C, averaging five consecutive readings. Spray drying was performed using a Büchi Mini Spray Dryer S-300 under the following parameters: inlet temperature 125 °C, outlet temperature 87-89 °C, product temperature 65 °C, drying gas flow 30 m^3/h, spray gas 550 L/h, feed rate 3.0 mL/min, air pressure 6 bar, and nozzle diameter 0.7 mm. Continuous

magnetic stirring was maintained throughout the process. The morphology of lyophilized extract and spray-dried powders was examined by scanning electron microscopy (Carl Zeiss EVO MA 0) after gold coating (200-400 Å, LEICA EMSCD005). Thermal behaviour was evaluated by Differential Scanning Calorimetry (Mettler Toledo DSC 822e), analyzing 3-5 mg samples sealed in 40 µL aluminum pans, pierced, and heated from 25 °C to 350 °C at 10 °C/min.

The spray-drying yield was determined gravimetrically, comparing the recovered powder mass to the total mass of feed components:

$$Yield = \text{Powder weight} / \text{Total solids in feed} \times 100$$

The theoretical Extract Content (TEC) was calculated as the ratio between the mass of extract and the total mass of all solid components in the feed:

$$TEC\ (\%) = \text{CSL weight} / \text{Total solids in feed} \times 100$$

The Actual Extract Content (AEC) formulation powder was derived by UHPLC-DAD analysis and expressed in mg compound g^{-1} content. For the formulation and PHWE extract, 1 mg mL^{-1} solutions were prepared in MeOH 20% and analyzed.

$$AEC\ (\%) = mg\ g^{-1}\ formulation / mg\ g^{-1} PHWE \times 100$$

Encapsulation Efficiency (EE %) was derived from the ratio between AEC and TEC:

$$EnE\ (\%) = AEC / TEC \times 100$$

The chemical stability of the optimized formulation and the lyophilized PHWE extract was evaluated under intermediate storage conditions, combining elements of the long-term stability requirements outlined in ICH Topic Q1A(R2) (Agency European Medicines, 2006) with the stress conditions used for

photostability testing as described in ICH Topic Q1B. Spray-dried powders and its related extract were stored for 12 weeks in closed vials at 30 ± 2 °C, 65% RH (relative humidity) ± 5 % RH, and photo-exposed side-by-side using an EKOCHL 1500 (Steroglass S.r.l., Perugia, Italy) climatic chamber. At predetermined time points (0, 1, 2, 3, 4, 6, 8, 10, 12 weeks), samples were withdrawn and analyzed for Sil, TeGG and Myr content, used as the chemical marker of the extract. The quantification was performed by UHPLC-UV following the procedure described in 4.4.5. All analyses were conducted in triplicate. Stability was expressed as the percentage of Sil, TeGG and Myr remaining relative to the initial concentration (week 0).

3.6.19 In vitro gastro-intestinal digestion

In vitro gastro-intestinal digestion was performed by applying the INFOGEST 2.0 protocol [87]. Briefly, 3 g of CSL optimized PHWE extract, and its formulation (32 mg mL^{-1} of extract) was mixed with 2.4 mL of simulated salivary fluid containing 150 U $mL^{-1}$of salivary α-AMY. After 2 min of incubation at 37 °C in a rotating wheel (40 rpm), 4.4 mL of simulated gastric fluid was added, and the pH was corrected to 3 with HCl 6 mol L^{-1}. The gastric digestion was started by the addition of 2000 U mL^{-1} of pepsin (final concentration in the digestive system), followed by 120 min of incubation at 37 °C in a rotating wheel (40 rpm). Next, the bolus was mixed with 4.5 mL of simulated intestinal fluid. The pH was brought to 7 with concentrated NaOH, intestinal digestion was started by adding to the chyme pancreatin (final concentration in the digestive system based on trypsin activity of 200 U mL^{-1}), followed by 120 min of incubation at 37 °C in a rotating wheel (40 rpm). During the intestinal phase, aliquots were collected every 30 minutes to monitor the evolution of metabolite content throughout this stage. A control digestion with water instead of CSL samples was performed to account for the possible interferences in the assays of the digestive system. For each digestion phase, 500 µL of sample were mixed with 500 µL methanol, to precipitate enzymes. After 5 minutes the samples were centrifuged, diluted with H2O and directly analyzed by UHPLC-DAD-HRMS/MS.

3.6.20 Statistical analysis

Results are reported as mean ± standard deviation (SD) from three or six replicates. The statistical significance of UHPLC quantitative data, TPC, TEAC, IC_{50} and ROS% values were evaluated through one-way analysis of variance (ANOVA). A significance level of $p < 0.05$ was adopted, and Tukey's honestly significant difference (HSD) test was performed to determine pairwise differences between means. Statistical analyses were carried out using Statgraphics Centurion 18 software (Statgraphics Technologies), while IC_{50} values were calculated using GraphPad Prism 10.

Chapther 4

Glycyrrhiza glabra leaves (GGL)

Part of this work was conducted in collaboration with:
[1] Professor Paola Coccetti research group – University of Milano Bicocca (Italy)
Part of this work was conducted in the laboratory of:
[2] Professor Luca Campone - University of Milano Bicocca (Italy)

Adapted from:
T. Docimo, R. Celano, A. Lambiase, R. di Sanzo, **S. Serio**, V. Santoro, P. Coccetti, M. Russo, L. Rastrelli, A. L. Piccinelli. Exploring Influence of Production Area and Harvest Time on Specialized Metabolite Content of Glycyrrhiza glabra Leaves and Evaluation of Antioxidant and Anti-Aging Properties. *Antioxidants*, **2024**, 13, 93.

4.1 Introduction

Glycyrrhiza glabra L. is a perennial herbaceous plant belonging to the Fabaceae family, typical of Western Asia and the Mediterranean basin. For centuries, it has been appreciated for its many therapeutic and nutritional properties [104]. The scientific and commercial interest in licorice primarily stems from its roots and rhizomes (licorice), which are rich in secondary metabolites responsible for its sweet taste and a wide range of biological activities. Licorice is used as natural sweetener and flavour additive in the tobacco, food, pharmaceutical and beverage industries and as ingredient of functional foods and food supplements. It has been recognized for its ethnopharmacological values, and the root preparations are still widely used as expectorant and carminative, to treat gastritis and peptic ulcers, and to alleviate throat and bronchial infections [105,106]. The main constituents of the root include triterpene saponins, such as glycyrrhizic acid, and a wide range of flavonoids and chalcones. Glycyrrhizic acid is responsible for the typical sweet taste, but also for its anti-inflammatory, antiviral, hepatoprotective, and antimicrobial properties. However, excessive consumption can lead to side effects such as hypertension and water retention [107].

Among the different varieties of *Glycyrrhiza*, Calabrian licorice (*G. glabra var. typica*) occupies a prominent place due to its unique characteristics and the quality of its extracts. This variety, which grows wild and is cultivated along the coast and in the plains of Calabria, is the most appreciated for the balanced sweet-bitter taste [108]. The Calabrian territory conditions, with its mild climate, clay soils, and marine influences, determine the root's unique chemical composition and influence the concentration of its active ingredients. These distinctive characteristics have led to the recognition of the Protected Designation of Origin (PDO) for “Calabrian Licorice,” protecting the authenticity of the product and its link to the territory [108,109]. The regulations also define the areas of cultivation, harvesting methods, and processing techniques, ensuring consumers a genuine, high-quality product. “Liquirizia di Calabria DOP”, also known as “Oro Nero”, is now a hallmark of Italian excellence, a

symbol of an ancient agricultural tradition and a perfect balance between economic value, environmental sustainability, and cultural heritage.

Besides roots, this perennial plant has a vigorous vegetative aboveground biomass which is emerging as a valuable source of bioactive compounds that positively affect human well-being. However, this biomass remains underutilized, and its valorization could indirectly boost the economic value of licorice cultivation. Specialized metabolites profiling of Calabrian *G. glabra* revealed a distinctive chemical composition in the leaves compared to the roots [110]. In agreement with previous studies [111], flavanones (Fs) were identified as the most abundant class of secondary metabolites, with pinocembrin, licoflavanone, and glabranin as the major compounds. Another characteristic classes of phytochemicals are represented by flavonol glycosides (isoquercitrin and astragalin) and prenylated dihydrostilbenes, which, together with prenylated Fs, act as specific chemical markers of the aerial tissues [110]. In addition, the leaf surfaces of Calabrian *G. glabra* appear viscous and sticky and this characteristic is related to the presence of exudate, which contributes to the resistance to pathogens, herbivores, and drought [110] Leaf exudate contains mainly hydrophobic phenolic compounds such as Fs, prenylated stilbenes, isoflavones, and chalcones [110]. *G. glabra* leaves (GGL) extracts have been investigated for a wide range of biological activities, including antiproliferative, antimicrobial, antioxidant, anti-inflammatory, and α-GLU inhibitory effects [112,113].

Current PDO licorice harvesting practices take place during the autumn defoliation period, when leaves are commonly discarded or left to decompose in the soil, leading to a reduced yield and lower-quality biomass. To date, no studies have investigated how growth stage and environmental conditions influence the phytochemical content and biological activities of Calabrian GGL. Understanding these effects help define optimal harvesting practices and promote new applications for this underexploited resource, thus adding value to the Calabrian licorice supply chain.

The comprehensive chemical profiling of GGL, combined with their potential *in vitro* activity, make this matrix a valuable source for the extraction of its prenylated phenolic metabolites, to obtain enriched fractions with potential

pharmacological applications. Given their predominantly hydrophobic nature and accumulation in exudates, supercritical fluid extraction (SFE) using CO_2 as a non-polar solvent is the most suitable and sustainable approach for their selective recovery. This solvent offers several advantages, as it is inexpensive, inert, non-toxic, and easily recyclable, while allowing the selective extraction of target compounds [114]. SFE also enables the production of solvent-free, high-purity extracts avoiding the co-extraction of other matrix components [65]. Overall, SFE is an efficient, and tunable green technology for obtaining enriched extracts characterized by high quality and selectivity suitable for applications in the food, cosmetic, and pharmaceutical industries [65].

The potential of GGL metabolites and the interest in their recovery derives from the key role of prenylation, which, among the chemical modifications of specialized metabolites, strongly affects both structural diversity and biological activity. Compared with their non-prenylated counterparts, prenylated molecules exhibit higher lipid solubility, an enhanced ability to penetrate biological membranes, and a greater potential to interact with different cellular targets [115]. For this reason, prenylated phenolic compounds are promising molecules as drugs for their wide pharmacological spectrum of activities [116]. As an example, many plants within medicinal and food resources, such as *Morus alba*, *Humulus lupulus*, *Glycine max*, *Ficus carica,* and *Cannabis sativa*, accumulate prenylated phenols, and their extracts have been exploited in oncotherapy [117], metabolic disorders [118], and cardiovascular activities [119]. Regarding *Glycyrrhiza* metabolites, prenylated dihydrostilbenes and flavonoids from *G. uralensis* leaf extracts were investigated as therapeutic agents in liver fibrosis [112]. Recently, the potential of prenylated phenolics from Mulberry leaves has been also exploited for neuroprotective activity [117]. In the field of neurodegenerative diseases, accounting for a large and *increasing* health burden worldwide, drug discovery and development are urgently needed.

Neurodegenerative diseases characterized by the formation of abnormal aggregates of the presynaptic protein α-synuclein are collectively known as synucleinopathies and are the second most common group of neurodegenerative diseases [120]. In recent decades, many different models

using yeast strains that overexpress human genes associated with diseases such as Alzheimer's disease (AD), Parkinson's disease (PD) and Huntington's disease (HD) have also been exploited to understand the molecular regulation of synucleinopathies [121]. One of the most widely studied of these models concerns the expression of α-synuclein (α-syn) associated with PD [120,122,123].

As GGL are a valuable source of beneficial compounds, to harness their potential, this study investigated on:

- **Exploration** of the Influence of Production Area and Harvest Time on the Specialized Metabolite Content of GGL;
- **Evaluation** of the *in vitro* and *in vivo* Antioxidant and Anti-Aging Properties of GGL;
- **Optimization** of sc-CO_2 extraction to selectively recover exudate metabolites and produce enriched extracts.

4.2. Valorization of GGL: Identification of Optimal Harvest Time and Production Area

The main objective of this section is to enhance the value of Calabrian PDO licorice supply chain, promoting the valorization of GGL for the development of new functional products with possible applications in the food, nutraceutical, pharmaceutical and cosmetic sectors. The key objectives include both the enhancement of Calabrian biodiversity through the characterization of the ecotypes of *G. glabra* used in the production of PDO licorice, and the recovery and enhancement of agri-food waste resulting from the cultivation and processing of the plant. In this context, the epigeal parts represent a potential source of bioactive compounds of functional interest, as demonstrated by studies conducted on species of the genus *Glycyrrhiza* [111–113].

Previous studies conducted by the Food Chemistry lab (DIFARMA, UNISA) research group have shown that GGL displays a markedly different composition compared to its roots. In GGL were detected exclusively phenolic compounds, namely Fs, i.e. pinocembrin (Pin), and their prenylated derivatives, licoflavanone (Lic) and glabranin (Gla), prenylated dyhydrostilbenes, prenylisoflavones, dihydrochalcones, flavone-C-glycosides and flavonol-O-glycosides [110]. The chemical complementarity between underground and above-ground tissues reflects the different phytochemical and biological potential of the two parts. However, quantitative information on the content of the main metabolites is still lacking. To this end, an UHPLC-UV method was used to quantify the main compounds in the leaves of Calabrian *G. glabra* from three typical cultivation areas: Villapiana (A, Cosenza-Ionian coast), Castrolibero (B, Cosenza- inland Tyrrhenian area), and Scandale (C, Crotone- Ionian hinterland). The samples were collected at three different phenological stages: pre-flowering (HT-1, early May), flowering (HT-2, mid-June), and senescence (HT-3, late October). After drying according to the PDO specifications (40 °C, ventilated oven), the samples were exhaustively extracted and subjected to an in-depth investigation to assess the influence of cultivation sites and phenological stages on the content of their main metabolites, with the aim of identifying the optimal harvesting time for this

underutilized biomass. This approach not only supports the sustainable valorization of the Calabrian licorice supply chain but also provides complementary insights into root harvesting practices. Indeed, a recent study highlighted how different harvesting periods can affect the chemical profile and bioactivity of *G. glabra* roots [124,125], suggesting that an integrated evaluation of both leaves and roots could enhance the overall economic and environmental value of this crop.

4.2.1. Quantitative Profile of GGL

UHPLC-HRMS analysis [110] revealed that the qualitative profiles of the GGL extracts investigated were similar across production areas and harvesting times. The main compounds detected in the UHPLC-PDA profiles (Figure 4.1) were: the flavanones Pin (L29), Lic (L36), 8,6-prenylnaringenin (L35), Gla (L46), and a Gla isomer (L48); the flavone C-glycosides vincenin-2 (1) and isoshaftoside (2); the flavonol O-glycosides rutin (L11), isoquercitrin (L12), and astragalin (L17); and the prenylated dihydrostilbenes dihydro-3,5,3',4'-tetrahydroxy-5'-prenylstilbene (L28), dihydro-3,3',4'-trihydroxy-5-O-prenylstilbene (L33), and dihydro-3,5,3',4'-tetrahydroxy-5-O-prenylstilbene.-3,5,3',4'-tetrahydroxy-4,5'-diprenylstilbene (L41), and dihydro-3,5,4'-trihydroxy-4,5'-diprenylstilbene (L44).

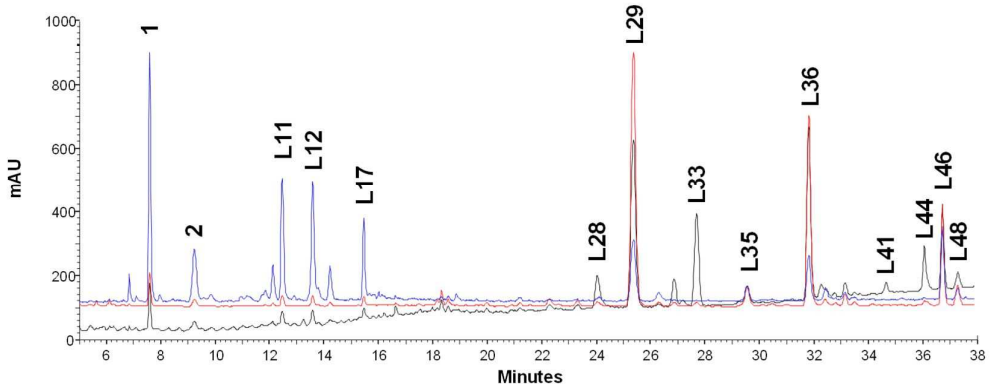

Figure 4.1. *A representative UHPLC-UV profile of* GGL *(GGL-B, HT-2): black line, 220 nm; red line 290 nm; blue line 360 nm.*

These compounds were assumed as GGL markers and quantified in all GGL samples by UHPLC-UV analysis and external calibration method (Table 4.1).

Table 4.1. *Level of the main compounds in GGL according to the harvest time (HT-1, 2, 3) and the production area (GGL-A, B, C).*

		Cultivation site		
Compounds	**Harvest time**	**GGL-A**	**GGL-B**	**GGL-C**
		mg g-1 dry leaves[1,2,3]		
Vincenin-2 (1)	**HT-1**	34.7 ± 2.4^{A,a}	30.0 ± 1.0^{B,b}	13.3 ± 1.1^{C,b}
	HT-2	35.3 ± 0.5^{A,a}	36.3 ± 1.4^{A,a}	20.5 ± 0.5^{B,a}
	HT-3	22.6 ± 1.2^{A,b}	23.2 ± 1.0^{A,c}	9.6 ± 0.8^{B,c}
Iso/shaftoside (2)[4]	**HT-1**	15.4 ± 1.3^{A,a}	15.1 ± 1.5^{A,a}	7.1 ± 0.4^{B,b}
	HT-2	14.9 ± 0.2^{A,a}	15.2 ± 0.7^{A,a}	8.2 ± 0.2^{B,a}
	HT-3	8.1 ± 0.5^{B,b}	10.1 ± 0.9^{A,b}	3.9 ± 0.4^{C,c}
Flavanone C-glycosides (tot)	**HT-1**	50.1 ± 3.6^{A,a}	45.1 ± 2.5^{A,b}	20.4 ± 1.3^{B,b}
	HT-2	50.2 ± 0.7^{A,a}	51.5 ± 2.1^{A,a}	28.7 ± 0.7^{B,a}
	HT-3	30.7 ± 1.0^{A,b}	33.3 ± 1.9^{A,c}	13.5 ± 1.2^{B,c}
Rutin (L11)	**HT-1**	6.7 ± 0.6^{A,a}	6.8 ± 0.4^{A,a}	2.2 ± 0.3^{B,a}
	HT-2	4.5 ± 0.2^{B,b}	5.3 ± 0.2^{A,b}	1.9 ± 0.2^{C,a}
	HT-3	3.4 ± 0.5^{A,c}	2.2 ± 0.3^{B,c}	0.9 ± 0.1^{C,b}
Isoquercitrin (L12)	**HT-1**	4.1 ± 0.3^{A,a}	4.2 ± 0.2^{A,a}	1.5 ± 0.2^{B,a}
	HT-2	2.8 ± 0.2^{B,b}	3.6 ± 0.2^{A,b}	1.7 ± 0.1^{C,a}
	HT-3	2.8 ± 0.2^{A,b}	2.1 ± 0.1^{B,c}	0.8 ± 0.1^{C,b}
Astragalin (L17)[4]	**HT-1**	6.0 ± 0.6^{B,a}	7.5 ± 0.7^{A,a}	2.6 ± 0.3^{C,a}
	HT-2	4.9 ± 0.3^{A,ab}	5.6 ± 0.3^{A,b}	3.1 ± 0.1^{B,b}
	HT-3	4.5 ± 0.5^{A,b}	2.4 ± 0.3^{B,c}	1.1 ± 0.1^{C,c}
Flavonol-O-glycosides (tot)	**HT-1**	16.8 ± 2.4^{A,a}	18.5 ± 1.1^{A,a}	6.3 ± 0.7^{B,a}
	HT-2	12.2 ± 0.6^{B,b}	14.5 ± 0.5^{A,b}	6.6 ± 0.4^{C,a}
	HT-3	10.6 ± 1.0^{A,b}	6.7 ± 0.6^{B,c}	2.8 ± 0.2^{C,b}
Pinocembrin (L29)	**HT-1**	29.2 ± 4.6^{A,b}	23.2 ± 4.4^{A,b}	13.4 ± 1.4^{B,b}
	HT-2	54.5 ± 1.4^{A,a}	51.3 ± 0.6^{B,a}	23.8 ± 1.4^{C,a}
	HT-3	19.9 ± 1.4^{B,c}	33.3 ± 1.9^{A,c}	7.6 ± 0.9^{C,c}
Licoflavanone (L36)	**HT-1**	26.0 ± 4.1^{A,b}	26.7 ± 3.9^{A,b}	14.0 ± 1.5^{B,b}
	HT-2	42.1 ± 0.9^{B,a}	45.6 ± 0.5^{A,a}	22.3 ± 1.3^{C,a}
	HT-3	17.6 ± 1.2^{B,c}	32.0 ± 2.5^{A,b}	4.8 ± 0.7^{C,c}
8,6-prenylnaringenin (L35)[5]	**HT-1**	4.5 ± 0.2^{A,a}	4.8 ± 0.6^{A,a}	1.5 ± 0.1^{B,b}
	HT-2	3.5 ± 0.5^{B,b}	5.4 ± 0.2^{A,a}	2.9 ± 0.2^{B,a}
	HT-3	2.4 ± 0.3^{B,c}	3.2 ± 0.3^{A,b}	1.2 ± 0.1^{C,c}
Glabranin (L46)	**HT-1**	21.8 ± 2.9^{A,b}	16.9 ± 4.1^{A,b}	7.3 ± 0.7^{B,b}
	HT-2	31± 0.5^{A,a}	25.6 ± 0.9^{B,a}	14.4 ± 0.8^{C,a}
	HT-3	7.8 ± 0.5^{B,c}	11.2 ± 1.7^{A,b}	3.8 ± 0.5^{C,c}
Glabranin isomer (L48)[6]	**HT-1**	4.9 ± 1.0^{B,b}	3.5 ± 1.0^{B,c}	7.3 ± 0.5^{A,b}
	HT-2	7.7 ± 0.1^{C,a}	26.6 ± 0.9^{A,a}	14.5 ± 0.9^{B,a}
	HT-3	6.8 ± 0.7^{B,a}	13.7 ± 0.8^{A,b}	4.0 ± 0.3^{C,c}
Flavanones (tot)	**HT-1**	86.4 ± 12.5^{A,b}	75.1 ± 13.2^{A,b}	43.6 ± 2.2^{B,b}
	HT-2	138.7 ± 2.5^{B,a}	154.6 ± 3.0^{A,a}	77.8 ± 4.4^{C,a}
	HT-3	54.5 ± 3.7^{B,c}	93.4 ± 7.0^{A,b}	21.3 ± 1.9^{C,c}
Prenylflavanones (tot)	**HT-1**	57.2 ± 8.1^{A,b}	51.9 ± 9.2^{A,b}	30.2 ± 1.1^{B,b}
	HT-2	84.2 ± 1.2^{B,a}	103.3 ± 2.4^{A,a}	54.0 ± 3.1^{C,a}
	HT-3	34.7 ± 2.3^{B,c}	60.1 ± 5.2^{A,b}	13.7 ± 1.0^{C,c}
dihydro-3,3′,4′-trihydroxy- 5-O-prenylstilbene (L33)	**HT-1**	26.7 ± 3.3^{A,b}	22.1 ± 1.6^{A,b}	9.4 ± 1.0^{B,b}
	HT-2	34.8 ± 1.6^{A,a}	31.4 ± 0.9^{B,a}	15.9 ± 1.0^{C,a}
	HT-3	4.8 ± 0.5^{B,c}	8.6 ± 1.0^{A,c}	1.3 ± 0.2^{C,c}
dihydro-3,5,4'-trihydroxy-4,5'-diprenylstilbene (L44)	**HT-1**	33.2 ± 5.9^{A,a}	27.1 ± 3.9^{A,a}	11.0 ± 0.9^{B,b}
	HT-2	29.6 ± 4.1^{A,a}	26.2 ± 1.7^{AB,a}	19.9 ± 1.0^{B,a}
	HT-3	3.9 ± 0.7^{B,b}	6.5 ± 0.6^{A,b}	1.4 ± 0.2^{C,c}
dihydro-3,5,3',4'-tetrahydroxy-5'-prenylstilbene (L28)[7]	**HT-1**	11.0 ± 0.2^{A,b}	10.5 ± 0.7^{A,a}	3.2 ± 0.2^{B,b}
	HT-2	12.8 ± 0.8^{A,a}	11.7 ± 0.4^{A,a}	5.0 ± 0.4^{B,a}
	HT-3	2.8 ± 0.2^{B,c}	4.2 ± 0.3^{A,b}	1.1 ± 0.1^{C,c}
dihydro-3,5,3′,4′-tetrahydroxy-4,5′-diprenylstilbene (L41)[8]	**HT-1**	17.6 ± 3.3^{A,a}	11.8 ± 2.1^{B,a}	2.8 ± 0.2^{C,b}
	HT-2	8.8 ± 0.3^{A,b}	5.9 ± 0.1^{B,b}	4.3 ± 0.5^{C,a}
	HT-3	0.5 ± 0.1^{B,c}	2.3 ± 0.3^{A,c}	0.3 ± 0.1^{C,c}

Dihydrostilbenes (tot)	**HT-1**	88.6 ± 12.3^{A,a}	71.5 ± .7^{A,a}	26.4 ± 1.2^{B,b}
	HT-2	85.9 ± 3.9^{A,a}	75.2 ± 2^{AB,a}	45.1 ± 2.9^{B,a}
	HT-3	12.0 ± 0.5^{B,b}	21.6 ± 1.2^{A,b}	4.1 ± 0.4^{C,c}

[1]Data are expressed as the mean ± standard deviation of three biological replicates. [2]Uppercase (A, B, C) and lowercase (a, b, c) letters in the same row indicate statistically significant differences (Tukey's HSD test, 95.0%) among cultivation sites and harvest times, respectivley. [4]expressed as vincenin equivalent; [5]expressed as licoflavanone equivalent; [6]expressed as glabranin equivalent; [7]expressed as stilbene L33 equivalent; [8]expressed as stilbene L44.

Calabrian GGL exhibited high levels of specialized metabolites, with total content ranging from 4 to 30 g 100 g-1 dry leaf DM. Figure 4.2 shows the changes in the abundance level of each metabolite class and the most abundant compounds (Pin, Lic, Gla and stilbene L33).

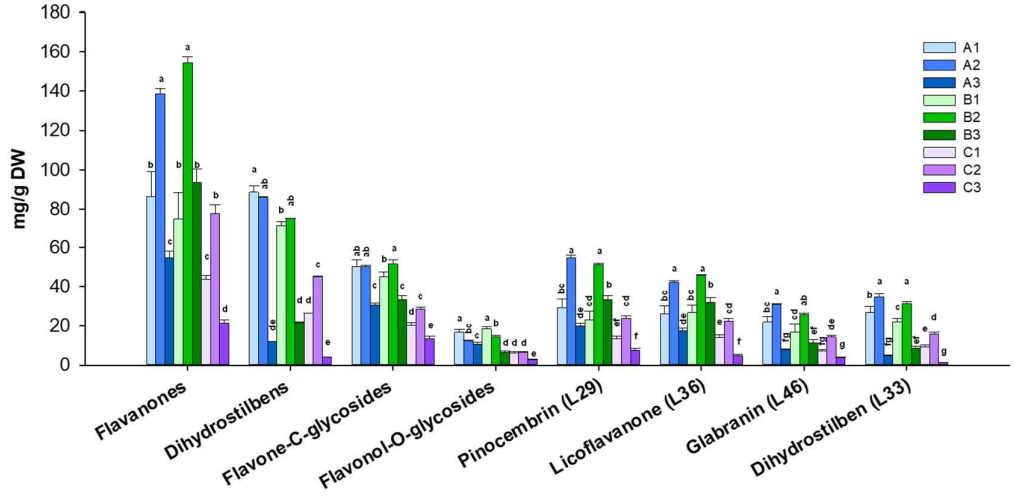

Figure 4.2. *Levels of metabolite classes and the most abundant compounds from three production areas (P) and three harvest times (HT) of* GGL.

Different letters within each metabolite class or compound indicate significant differences between extracts (p ≤ 0.05 by a post-hoc Tukey's HSD test).

Overall, Fs were the most abundant class of secondary metabolites, constituting 33–61% of the total quantified metabolite content, with Pin (L29) and Lic (L36) being the major compounds (each accounting for 11–21% of the total content). Next in order of abundance were prenylated dihydrostilbenes, accounting for 10-37% of the total content, with L33 and L44 being the major compounds, followed by flavone C-glycosides, accounting for 17-32% of the

total content, and flavonol O-glycosides, accounting for 4-10% (Table 4.1 and Figure 4.2).

Quantitative data on GGL phytochemicals revealed significant variations in their content in relation to production areas (P) and harvesting times (HT) (Table 4.1 and Figure 4.2). The levels of each GGL marker and metabolite class were statistically evaluated according to their respective influences of P and HT. Two-way ANOVA analysis showed that both P and HT had a statistically significant effect on the levels of all GGL markers. Additionally, the interaction between P and HT was statistically significant for all analysed compounds and metabolite classes (see Table 4.1 and Table 4.2).

Table 4.2. *F ratios of P and HT and their interaction of GGL compound content*.

Factor	P (2) [b]	HT (2) [b]	PxHT (4)[b]
Flavanones	183 *	239 *	15 *
Dihydrostilbenes	132 *	318 *	21 *
Flavones	417 *	202 *	9 *
Flavonols	294 *	182 *	27 *
L29	210 *	250 *	26 *
L36	211 *	171 *	13 *
L46	101 *	168 *	11 *
L33	216 *	531 *	25 *
TEAC	40 *	114 *	3.4 *

*Values given as F-ratio, * significant at p ≤ 0.001. of Fisher; [b] degrees of freedom in brackets.*

In particular, the variation in the levels of the most abundant compound classes (Fs and prenylated dihydrostilbenes) is predominantly attributed to the dynamic influence of developmental stages (HT), which shape the overall composition of bioactive compounds according to the plant's growth cycle. Conversely, P had a greater impact on the variance for flavone C-glycosides and flavonol O-glycosides (Table 4.2). The effects of P and HT on the content of different metabolite classes are consistent with their distinct localization within the leaf [110], which suggests different biological roles. Specifically, Fs and dihydrostilbenes, which accumulate in the leaf exudate, are likely to be responsible for resistance to pathogens, herbivore attacks and drought stress, while glycosylated flavones and flavonols, which are distributed solely in the inner leaf tissue, may be involved in photoprotection, shielding plant cells from photoxidation [110,126].

Considering the harvesting time, the levels of GGL specialized metabolites differed significantly among the three-time frames (Figure 4.3).

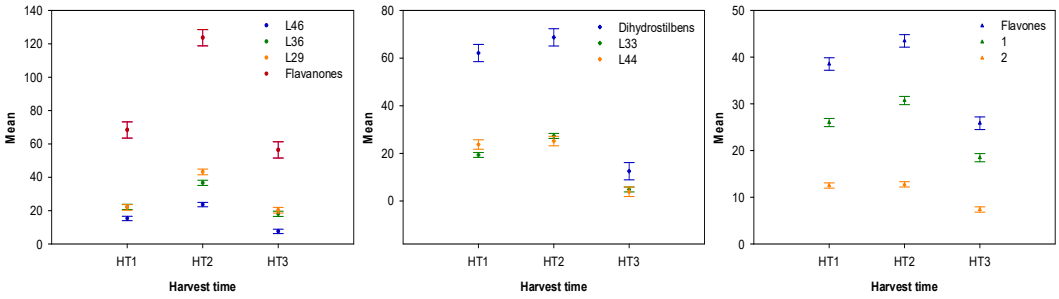

Figure 4.3. *Means plot of metabolite contents of* GGL *according to the harvesting time.*

Bars display the confidence intervals for the level means using themean squared error from the ANOVA ($p < 0.05$).

HT3 exhibited the lowest levels of each compound or metabolite class, regardless of the production area (see Table 4.1 and Figure 4.2). These results can easily be attributed to developmental changes associated with plant growth, particularly leaf senescence and catabolic recycling activities, which are necessary for nutrient remobilization from senescing leaves to sink tissues [126,127]. Notably, different trends in the content of various compound classes were observed, particularly among the most abundant classes. Significant variation in flavanone levels was observed across the three HTs: the total content and major Fs (Pin, Lic and Gla) doubled between HT1 and HT2, before decreasing by 61%, 40%, and 73% in GGL-A, GGL-B, and GGL-C, respectively, in HT3. Conversely, prenylated dihydrostilbenes showed no significant variation between HT1 and HT2 but underwent a drastic reduction ranging from 71% to 91% from HT2 to HT3 in all three production areas (Figure 4.3). Pin, prenylated Fs and dihydrostilbenes accumulate in the sticky exudate covering the surface of GGL [110]. It has been reported that *G. glabra* exudate is responsible for resistance to biotic and abiotic stresses, such as attacks by pathogens and herbivores and drought stress [128]. The well-known antimicrobial and cytotoxic activities of Pin and Lic further support their role in deterring insects and defending against predators [112,129–131]. This is consistent with reports on eucalypt oil glands, where Pin has been identified

as the main component, with antibacterial, antifungal and antifeedant activities that are clearly related to plant defence [132]. Thus, the high levels of Fs and prenylated dihydrostilbenes observed during flowering are most likely part of the licorice plant's defensive strategy [133].

A similar variation in flavone C-glycosides was observed regardless of the production area. However, flavonol-O-glycosides showed a significant decrease in both A and B production areas from HT1 to HT2, whereas their content did not change significantly in C production areas during these two harvesting times (Table 4.1 and Table 4.2). The different behaviour observed in the A, B and C production areas during the three HTs can be attributed to environmental conditions. HT1 and HT2 (from late spring to summer) encompass seasons characterized by high UV light, especially in southern Italy; therefore, the accumulation of these antioxidant compounds is expected to increase. However, our results suggest that plants in areas A and B may experience better shading than those in area C [134]

Our data also highlights significant differences between the production areas. For all quantified compounds, the content of GGL-C was statistically different from that of GGL-A and GGL-B. Conversely, no statistically significant differences were observed between the A and B areas, except for the content of prenylated Fs (Figure 4.4).

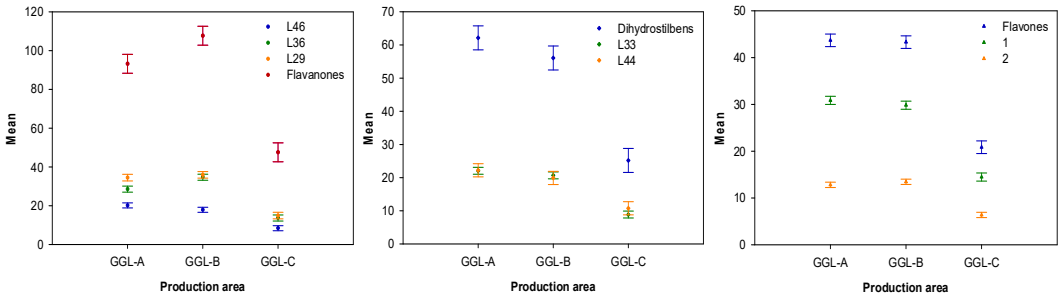

Figure 4.4. *Means plot of metabolite contents of* GGL *according to the production area.*

Bars display the confidence intervals for the level means using the mean squared error from the ANOVA ($p < 0.05$).

Specifically, GGL-A and GGL-B showed the highest metabolite content (10–29 and 15–30 g 100 g^{-1} DM, respectively) at all three harvest times, whereas the

lowest total metabolite content (4–16 g 100 g^{-1} DM) was detected in GGL-C, with a statistically significantly lower content of each analyzed compound observed in these samples compared to the other two (Table 4.1 and Table 4.2). Since it is well-known that pedoclimatic conditions play a crucial role in the accumulation of secondary metabolites by influencing water and nutrient uptake, these results suggest that the significantly lower phytochemical content of GGL-C samples may reflect the different and potentially less favourable growth conditions experienced by *G. glabra* in the Ionian hinterland [135]. Conversely, the phytochemical content of GGL-A and GGL-B extracts was similar and more than double that of GGL-C. Generally, no marked differences were observed among the different metabolite classes.

This analysis revealed that the highest content of secondary metabolites was found in samples from cultivation areas A and B, corresponding respectively to the Ionian Sea coast and the Tyrrhenian coast hinterland, particularly during the pre-flowering and flowering phenological phases.

To achieve a comprehensive valorization of GGL biomass, a quantitative investigation was also extended to *G. glabra* roots (GGR), considering that the harvesting period can similarly influence the content of secondary metabolites and main phytochemical markers, thus contributing to the enhancement of the entire Calabrian licorice production chain. The results obtained from the quantitative analysis of the exhaustive extracts of Calabrian licorice roots (Figure 4.5) are consistent with the data reported in the literature [106,136,137]. The most abundant class of secondary metabolites are saponins, which represent 67-75% of the total content of secondary metabolites quantified in the exhaustive extracts. In root harvesting phase (HT-3), the amount of glycyrrhizic acid (R41), the licorice quality marker, is in line with the requirements established by the production specifications for Calabrian PDO licorice (ecotypes A 2.2% DW; ecotype B 3.3% DW; and C 2.3% DW) (Figure 4.5).

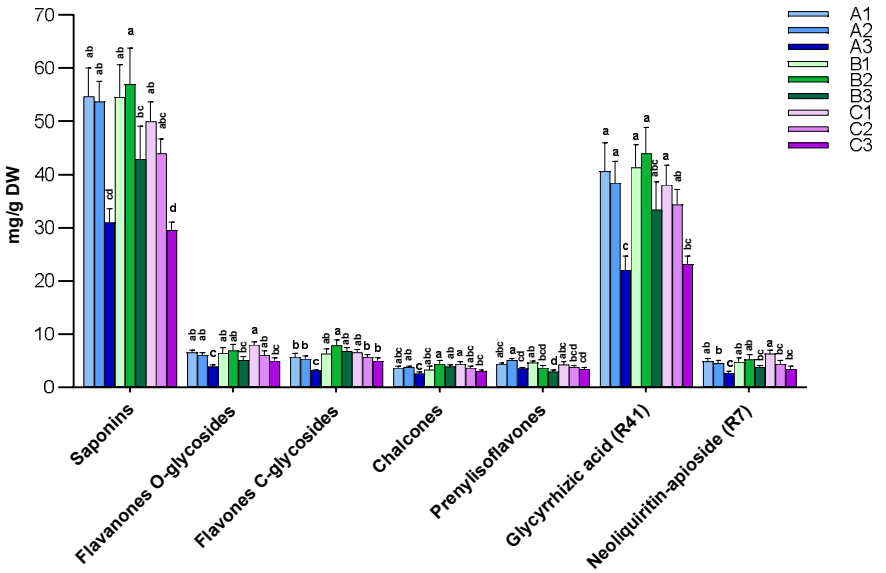

Figure 4.5. *Levels of metabolite classes and the most abundant compounds from three production areas (P) and three harvest times (HT) of* GGR.

Different letters within each metabolite class or compound indicate significant differences between extracts (p ≤ 0.05 by a post-hoc Tukey's HSD test).

All quantified metabolites showed statistically significant differences for both factors examined (P and HT), with the most pronounced variations occurring during the harvesting stages (Table 4.3), particularly for glycyrrhizic acid. Although statistically significant (Table 4.3), these variations are still within a limited concentration range.

Table 4.3. *F ratios of P and HT and their interaction of GGR compound content.*

Factor	P (2) [b]	HT (2) [b]	PxHT (4)[b]
Saponins	11 *	45 *	1.9
Flavanones O-glycosides	3.4	25 *	2.6
Flavones C-glycosides	28 *	12 *	5.5 *
Chalcones	4.5 *	9.5 *	6.3 *
Prenyl-isoflavones	7.7 *	25 *	5.3 *
Glycyrrhizic acid	9 *	33 *	1.5
Neoliquiritin-apioside	3.4	24 *	3.1 *

*Values given as F-ratio, * significant at p ≤ 0.001. of Fisher; [b] degrees of freedom in brackets.*

This observation is probably attributable to the selection over time of the most suitable ecotype in terms of quality and adaptability to the conditions of the

Calabrian territory, as well as to the effectiveness of the application of the PDO regulations, which standardize agricultural practices and the processing of Calabrian licorice.

In detail, the most pronounced effects were found for saponins and flavanone O-glycosydes, the latter representing the most abundant flavonoid class in GGR. The most marked reduction is observed in GGR harvested during the senescence phase of the plant (Figure 4.5), corresponding to the root harvesting period currently defined by the production protocol. Specifically, between stage 2 and stage 3, a reduction in glycyrrhizic acid content of 24-42% and neoliquiritin apioside of 20-40% is observed in the three different ecotypes, with similar values for the different classes of metabolites (flavone-C-glycosides, 12/43%; flavanone-O-glycosides, 17/35%; chalcones, 12/32%; saponins, 27/42%; prenylisoflavones, 8/32%). The reduced secondary metabolite content found in the roots of all ecotypes during the autumn harvest may reflect a seasonal release or translocation of these compounds into the soil, supporting allelopathic or defensive functions, as observed in other perennial herbaceous species [138]. Hence, the optimal root harvesting time coincides with the flowering stage, when the concentrations of bioactive metabolites reach their highest values, while avoiding the operational problems associated with autumn harvesting, such as low temperatures, heavy rainfall, and reduced farmland accessibility.

On this basis, the leaves would shift from waste biomass to a valuable source of sustainable bioactive metabolites, enabling harvesting before their natural senescence and strengthening the entire Calabrian PDO licorice production chain.

4.3. *In vitro* and *in vivo* Antioxidant and Anti-Aging Properties of GGL[1]

In recent years, interest in natural compounds with antioxidant and neuroprotective properties has increased significantly. Oxidative stress plays a key role in the aging process, and neurodegenerative diseases such as Parkinson's disease (PD) are one of the main areas of research for the development of preventive and therapeutic strategies [122,139]. The aging oxidative theory suggests that the loss of function typical of advanced age is associated with the accumulation of structural damage caused by oxidative stress [122]. PD, the second most common neurodegenerative disease, is characterized by the abnormal accumulation of the protein α-synuclein (α-syn), which induces toxicity associated with aggregate formation, leading to vesicular trafficking impairment, increased oxidative stress and mitochondrial dysfunction, reduced lifespan, disturbed calcium signaling, and altered autophagy [140]. Aging and age-related neurodegeneration are among the main challenges in modern medicine [122] and PD affects about 10 million people worldwide [141].

In this section, GGL extracts were first assessed using chemical assays to evaluate their antioxidant potential and subsequently tested on eukaryotic cell model, *Saccharomyces cerevisiae*, engineered for the overexpression of α-syn [142,143]. This model, which reproduces the main pathological features of PD, including reduced vitality, increased ROS, and protein aggregate formation, represents a versatile system confirming the antioxidant activity observed *in vitro* and investigating potential anti-aging effects through lifespan experiments, allowing multiple aspects of the extracts bioactivity to be evaluated in a single organism.

4.3.1. Antioxidant Activity In Vitro and In Vivo of GGL Extract[1]

In order to evaluate how the differences recorded in GGL phytochemical profiles reflect biological properties, the AOC of GGL extracts were evaluated

spectrophotometrically by ABTS *in vitro* assay (Fig. 4.6a). As well, to ascertain which specialized metabolites contribute most to the antioxidant activity, distinctive GGL compounds were tested for their antioxidant potential (Table 4.4). Two-way ANOVA analysis also revealed statistically significant variations in *in vitro* AOC according to the production area (P) and harvesting time, as well as the P x HT interaction (Table 4.2). Antioxidant activity of GGL extracts (Fig. 4.6a) changed according to the quantitative profiles.

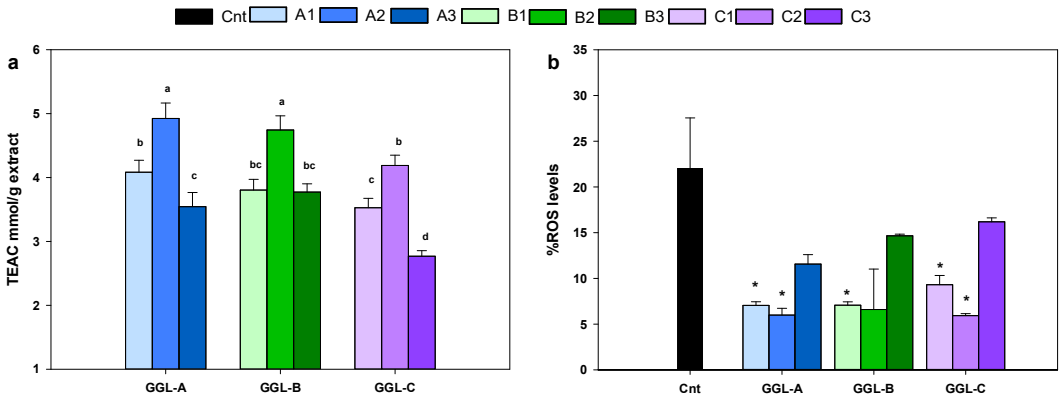

Fig.4.6. *AOC of GGL extracts from three production areas and three harvest times, measured as (a) TEAC equivalents by ABTS assay and (b) ROS content (assayed by DHE staining).*

*a. Different letters indicate significant differences between extracts ($p \leq 0.05$ by Tukey's HSD test); b. *$p < 0.05$ relative to control cells.*

Regarding the harvest time, GGL samples collected in HT2 exhibited significantly higher antioxidant activity than those collected in HT1 and HT3 (Fig. 4.6), which is consistent with the metabolite enrichment characteristic of this growth stage. Conversely, no statistically significant differences were observed between A and B areas (Fig. 4.6). These data further support the optimal harvesting conditions identified by the quantitative analysis of GGL markers, suggesting that these compounds are most likely responsible for antioxidant activity.

AOC of some GGL compounds, including Pin, Lic, Gla, prenylstilbene L33, and prenylstilbene L44, previously purified and characterized from *G. glabra* exudate, were evaluated in ABTS assay. Indeed, as shown in Table 4.4, the tested compounds showed higher antioxidant powers than Trolox, in the

following activity order Lic > isoquercitrin > rutin > stilbene L33> Gla > Pin > stilbene L44 > vincenin 2. Notably, the most abundant compounds (Lic, stilbene L33, Gla and Pin) demonstrated superior or comparable antioxidant activity to the flavonols rutin and isoquercetrin, whose content was distinctly lower in the GGL extracts. Thus, the AOC of GGL may be due to its high content of prenylated Fs and dihydrostilbenes. These results are consistent with what has been reported in previous studies [144–146] on bioactivity of GGL extracts.

Table 4.4. *Antioxidant activity of GGL main compounds by ABTS assay.*

Compound	TEAC (mmol TE/ mmol±SD)
Vincenin 2	1.12 ± 0.01
Rutin	6.00 ± 0.04
Isoquercitrin	6.45 ± 0.03
Pinocembrin	3.21 ± 0.01
Licoflavanone	9.55 ± 0.04
Glabranin	4.08 ± 0.03
Prenylstilbene (L33)	5.09 ± 0.01
Prenylstilbene (L44)	2.50 ± 0.01

Values are expressed ad mean ± DS of three replicates.

Oxidative stress, resulting from the excessive intracellular accumulation of reactive oxygen species (ROS), reactive nitrogen species (RNS), and other free radical species, contributes to the onset and progression of various diseases, including PD [133]. To estimate the ability of GGL extracts to exert an antioxidant response at the cellular level rather than just their radical scavenging capacity, the antioxidant effect of the GGL extracts was evaluated using a *Saccharomyces cerevisiae* yeast model expressing human α-synuclein as shown in Fig. 4.6b. Treatment with GGL extracts was found to remarkably reduce the intracellular ROS levels in exponentially growing yeast cells, with the GGL extracts with the highest phytochemical content (HT-1 and 2) exhibiting significant antioxidant effects. This study highlights that the main metabolites are indeed responsible for the antioxidant effect promoted by GGL, confirming that the biomass can be effectively harvested at the flowering stage to obtain extracts with strong bioactive potential. Moreover, it underlines the importance of validating preliminary chemical screening assays, commonly

used to assess potential bioactivity, through complementary studies that better reproduce physiological conditions. In this regard, the *in vivo* yeast model confirmed the AOC of GGL extracts, supporting the relevance of integrating chemical and biological approaches in the evaluation of natural bioactives.

4.3.2. Anti-aging effects of GGL extracts in yeast cells expressing human α-synuclein[1]

α-Synuclein is a presynaptic protein associated with the pathophysiology of synucleinopathies, including PD [120,147] and budding yeast has been extensively employed in models of synucleinopathies [148,149]. Thus, the effect of GGL extracts on the longevity of yeast cells over-expressing the human α-synuclein was investigated, to evaluate whether GGL extracts could exert anti-aging effects. GGLextracts were added to exponentially growing yeast cells at a concentration of 0.2% in a synthetic minimal medium. Results show that all the extracts prolonged chronological lifespan (CLS) of yeast cells (Figure 4.7), with a significant marked increase in both mean and maximal lifespan. In fact, mean lifespan resulted 2.5 times longer while maximal lifespan increased up to 3 times relative to the control (Figure 4.7b).

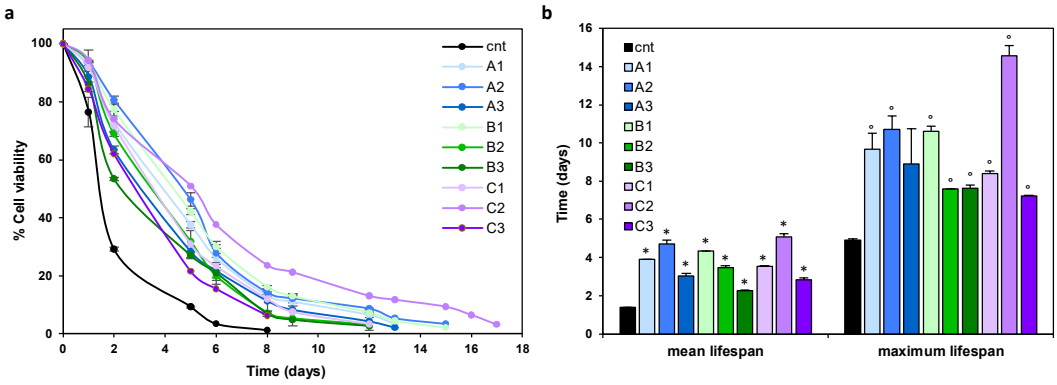

Figure 4.7. *Anti-aging effects of GGL extracts on yeast cells overexpressing α-synuclein: (a) CLS; (b) mean and maximum lifespan of CLS of yeast cells.*

** p < 0.05 for mean lifespan in control cells, ° p < 0.05 for maximum lifespan in control cells.*

The assessment of mean and maximum lifespan provides complementary insights into cell survival. The mean lifespan corresponds to the time point at

which 50% of the cell population remains viable, while the maximum lifespan indicates the time at which viability decreases to 10%. Together, these parameters offer a broader understanding of how treatments influence both average and long-term cell survival. Across all production areas, the senescence stage (HT-3) exhibited the lowest lifespan values, thereby confirming the decline in cellular resilience associated with this developmental phase. In contrast, the pre-flowering and flowering stages (HT1 and HT2) yielded the highest longevity, particularly in samples from areas A and C, while in area B, the pre-flowering stage was the most effective in extending both lifespan parameters.

Overall, the data indicate that GGL extracts can delay cellular senescence by reducing intracellular ROS levels and mitigating α-syn-induced toxicity. Consistently, samples collected during HT1 and HT2, stages associated with the highest metabolite content, also exhibited the most pronounced anti-aging effects.

4.4. Supercritical CO_2 extraction ($scCO_2$) for the selective and sustainable recovery of GGL compounds[2]

The comprehensive phytochemical profiling of GGL revealed a rich diversity of secondary metabolites, including Fs, dihydrostilbenes, and flavonoid glycosides [110]. While the latter are mainly localized within leaf tissues and act as UV-B protectants, the leaf surface predominantly contains prenylated Fs such as Pin, Lic, and Gla [110]. These hydrophobic compounds are closely associated with the plant's defence mechanisms, contributing to resistance against pathogens, herbivores, and drought stress [150], enhancing bioactivity and affinity to biological membranes [115]. Owing to their ecological function and proven antimicrobial, antioxidant activities [112,131], they represent valuable targets for selective recovery. For this reason, this section focused on developing a sustainable extraction strategy aimed at efficiently isolating these bioactive surface metabolites through green and selective supercritical fluid extraction. At present, the recovery of bioactive compounds from natural resources with high potential, often discarded within production chains, cannot be separated from the adoption of advanced, environmentally friendly extraction techniques. In this regard, the extraction processes developed should comply with the principles of Green Chemistry applied to extraction [8]. Among the most promising methods, compressed-fluid-based extraction techniques, including subcritical and supercritical fluids, have proven to be efficient tools for isolating bioactives from natural matrices [151]. These techniques are scalable and offer significant advantages over conventional extraction methods and optimizing their parameters to obtain high-quality extracts can promote the industrial valorization of the selected matrices [151]. SFE stands out for its minimal, or even zero, use of organic solvents. Carbon dioxide (CO_2) is the most widely employed solvent for SFE of natural bioactive compounds, as it fully meets the Green Analytical Chemistry principles. Its supercritical conditions are easily attainable (31.1 °C and 74 bar), it is non-toxic, non-flammable, and recognized as Generally Regarded as Safe (GRAS) for food applications. Under supercritical conditions, CO_2 exhibits high diffusivity, while its solvent power and density can be finely tuned by adjusting

temperature and pressure. One of the main advantages of SFE with $scCO_2$ is the ability to obtain solvent-free extracts: upon depressurization, CO_2 returns to the gaseous state, while the compounds extracted from the matrix precipitate. Although the low polarity of CO_2 may limit its efficiency for polar analytes, this drawback can be easily overcome by adding small amounts of polar modifiers [152]. In this study, however, pure CO_2 was selected due to the hydrophobic nature of the target metabolites.

Method optimization plays a key role in SFE. Several parameters must be considered, including extraction temperature and pressure, type and percentage of modifier (if present), and sample load. The effectiveness and quality of the process depend on optimizing these parameters to maximize the recovery of target compounds, minimize environmental impact, and preserve the natural integrity of the extracts. A careful evaluation of the extract profiles, metabolite levels, and potential co-extracted components is equally essential to ensure high-quality and reproducible results [15].

This section describes the design and optimization of SFE for the sustainable and selective recovery of exudate components from GGL. The technique was tailored to extract the target metabolites using an eco-friendly solvent, with the goal of obtaining enriched extracts characterized by high-grade purity, zero solvent consumption, and minimal co-extraction of non-target components. SFE optimization was performed through RSM, monitoring the qualitative and quantitative composition of the extracts via UHPLC-UV analysis. Optimal conditions were established to maximize the recovery and purity of the main GGL markers, Pin, Lic, and Gla, while minimizing co-extraction during processing. Finally, the performance of SFE was compared with conventional extraction techniques.

4.4.1. Preliminary $scCO_2$ experiments

Preliminary extraction trials were performed prior to setting up the DoE to define key technical parameters, refine the experimental domain, and identify the most relevant factors for chemometric optimization. These preliminary tests helped narrow the operative ranges, reducing unnecessary variables and

enhancing the robustness of the design [68]. All experiments were carried out in duplicate under fixed conditions: a 20 min static phase followed by a 90 min dynamic phase, with aliquots withdrawn at 30-min intervals to monitor extraction progress. A single extraction cycle was performed using a matrix/solvent ratio of 50 g L^{-1}, a CO_2 flow rate of 2 L min^{-1}, and a packing ratio of matrix, glass wool, and glass beads of 1:2:2 (v/v/v). The CO_2 needle heater set at 80 °C. The results were expressed as mg of Pin, Lic, Gla and total Fs per extraction interval determined by UHPLC-UV analysis. These trials were aimed at establishing the operative limits for pressure (150 - 450 bar), temperature (40 - 80 °C), and sample loading (1.2 - 2.4 g, for the 24 mL extraction cell volume).

The temperature range selected for this study was carefully defined based on literature data, which commonly report working intervals between 40 °C, slightly above the critical temperature of CO_2, and 80 °C. For instance, Majdi et al. [153] optimized the supercritical extraction of fatty acids from tobacco seeds using temperatures between 55 °C and 75 °C, while Akanda et al. [154] investigated oil recovery from various plant species within a broader range of 40 - 100 °C. Conversely, milder conditions (40 - 60 °C) are generally adopted for thermolabile compounds such as carotenoids [155] or phenolic molecules structurally related to our target prenylated Fs, like xanthohumol in hop [156]. At constant pressure, the effect of temperature remains controversial. Increasing temperature decreases the density of supercritical CO_2, making the solvent more gas-like and thus reducing its solvating power. On the other hand, higher temperatures enhance diffusivity and solute vapor pressure, improving mass transfer and solvent penetration into the plant matrix [7].

In our case, increasing the temperature from 40 °C to 80 °C at a constant pressure of 300 bar preserved the naturalness of the extract, as shown by the GGL chromatogram enriched exclusively in target compounds (Fig. 4.8a), while improving the overall recovery of Fs by approximately 47 % (Fig.4.8b), confirming that higher temperatures enhance solvent diffusivity, allowing better interaction with the superficial metabolites of the leaves. The upper operational limit of 80 °C was therefore selected as the optimal temperature, since it ensured extract integrity while still enhancing recovery.

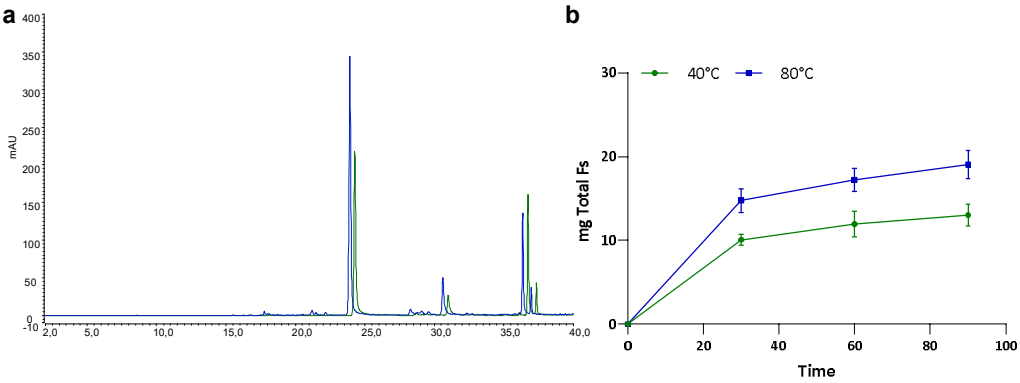

Figure 4.8. *UHPLC-UV chromatograms (290 nm) of GGL-scCO₂ at 300 bar and 80°C(blue) and 40°C (green) (a). Amount (mg) of total Fs at different temperatures (300 bar) as a function of extraction time (90 min) (b).*

Values are expressed ad mean ± DS of two replicates.

The pressure range was selected based on literature data, which report extraction pressures spanning from below 100 bar, used for the recovery of approximately 60% of eugenol [157], up to 450 bar for carotenoids [158] and 350 bar for xanthohumol [156]. In all cases, elevated pressure at constant temperature increased extraction yield, as higher pressures enhance the solvation power of CO_2 by increasing its density and, consequently, its solvent strength. In our study, the selective recovery of target metabolites was investigated within the 150 - 450 bar range at a temperature of 60 °C. At constant temperature and at increasing pressure, CO_2 density increased from 603 kg m^{-3} to 913 kg m^{-3} (Sitography 5). Consistently, the total amount of Fs at 150 bar was ~70% lower than at 450 bar (7.4 – 23.4 mg of total FSs, respectively, Fig. 4.9), confirming the positive effect of higher CO_2 density on solvent strength and extraction performance. However, further increasing the extraction pressure can reduce the selectivity of supercritical CO_2, as the higher density promotes the co-extraction of less soluble matrix components [159]. Additionally, at very high pressures, pump performance becomes less reproducible. For these reasons, the maximum operating pressure was set at 400 bar, ensuring process stability while maintaining efficient and selective metabolite recovery.

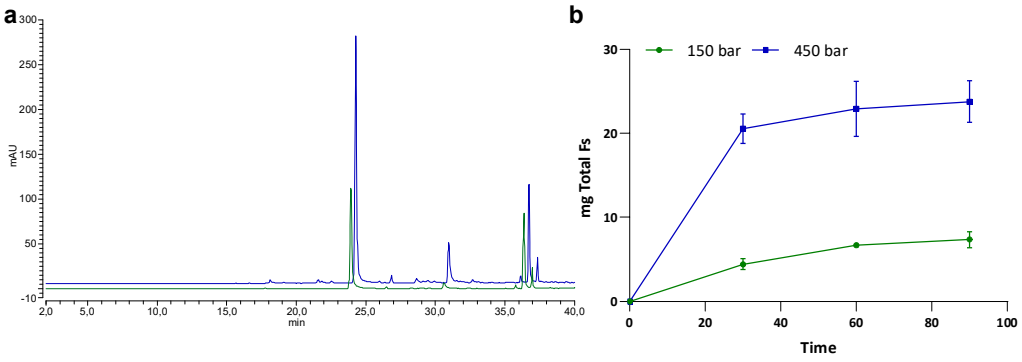

Figure 4.9. *UHPLC-UV chromatograms (290 nm) of GGL-scCO₂ at 60°C and 450 bar (blue) and 150 bar (green) a). Amount (mg) of total Fs at different pressures (60 °C) as a function of extraction time (90 min) (b).*

Values are expressed ad mean ± DS of two replicates.

Concerning matrix amount, 1.2 g and 2.4 g were tested in a 24 mL extraction cell, yielding comparable metabolite contents and extraction efficiencies; therefore, the lower ratio was selected to minimize material consumption. A CO_2 flow rate of 2 L min^{-1} was adopted, ensuring efficient extract release without needle freezing. This flow rate is lower than those reported in similar studies using the same equipment but larger extraction vessels and sample loads [155,160].

4.4.2. Optimization of scCO₂ by RSM

Preliminary experiments confirmed the high effectiveness of $scCO_2$ in selectively recovering the target metabolites (Pin, Lic, and Gla) from GGL. As shown in the chromatograms (Fig. 4.8a-4.9a), no co-extraction of other metabolites typically present in the exhaustive GGL extract (Fig. 4.1) was observed, demonstrating not only the green advantages of solvent-free extraction, but also the intrinsic selectivity of $scCO_2$ toward hydrophobic Fs. Nonetheless, extraction performance strongly depends on operating conditions: temperature provides moderate improvements by enhancing solvent diffusivity, whereas pressure, with the associated increase in CO_2 density, markedly boosts solvent strength and overall extraction efficiency.

Regarding extraction time, preliminary experiments revealed a typical extraction kinetic profile (Fig. 4.8b-4.9b): an initial Constant Extraction Rate (CER) phase (0-30 min), where the linear slope reflects the rapid extraction of the most accessible metabolites, followed by a Falling Extraction Rate (FER) phase and a final diffusion-controlled phase (30-60-90 min), where the decreasing slope indicates increasing mass-transfer limitations within the matrix [161]. These results highlight the need to carefully balance temperature, pressure, and dynamic time to maximize extraction purity. Based on these considerations, $scCO_2$ extraction was optimized using RSM with BBD, evaluating the effects of temperature (A), pressure (B), and dynamic time (C) in the established ranges (Table 4.5).

Table 4.5. *Independent $ScCO_2$ factors and their level.*

Independent factors	Units	Level		
		− 1	**0**	**1**
A. Temperature	°C	40	60	80
B. Pressure	bar	150	275	400
C. Dynamic time	min	30	60	90

Fixed factors: M/S ratio, 50 g L^{-1}; CO_2 flow rate, 2 LPM; needle CO_2 heater, 80 °C; Ratio matrix/ glass wool/ glass beads, 1:2:2.

The response variables included EE (g 100 g^{-1} leaf), extract content of the target metabolites (P, g 100 g^{-1} extract), and overall EY. Greater weight was assigned to the extract content of the three markers to prioritize extract purity in the global desirability function. The results for all these variables, obtained under different BBD experimental conditions (Table 4.6), and confirm the indications from preliminary trials: $scCO_2$ extraction consistently produced an extract enriched in target Fs, approximately threefold compared with exhaustive extraction, while maintaining extraction yields comparable to those reported in the literature for this technique, when using CO_2 without any modifier [162,163] .

Table 4.6. *BBD matrix, target response values and predicted and experimental results obtained under optimal scCO$_2$ conditions*

run	block	A (°C)	B (bar)	C (min)	EE Pinl	EE_Lic (g 100 g^{-1} GGL)	EE_Gla	EE_Tot	P_Pin	P_Lic	P_Gla (g 100 g-1 ext)	P Tot	yield (g 100 g^{-1})
1	1	40	150	60	0.37	0.06	0.08	0.5	14.9	2.3	3.4	21.1	2.1
2	1	60	275	60	0.82	0.20	0.13	1.2	18.7	4.7	3.0	27.2	4.4
3	1	60	275	60	0.78	0.19	0.13	1.3	19.1	4.8	3.3	28.1	4.1
4	1	40	275	30	0.63	0.13	0.09	0.9	18.9	3.8	2.7	26.2	3.3
5	1	40	275	90	0.96	0.28	0.12	1.4	19.7	5.9	2.4	28.8	4.8
6	1	80	275	30	0.64	0.13	0.13	0.9	17.1	3.4	3.5	25.0	3.8
7	1	80	150	60	0.19	0.02	0.06	0.3	8.9	1.0	2.6	13.4	2.2
8	1	60	150	90	0.33	0.05	0.08	0.5	12.5	1.9	3.0	18.2	2.7
9	1	60	150	30	0.15	0.02	0.05	0.2	12.5	1.3	3.7	18.5	1.2
10	1	60	400	90	0.93	0.33	0.12	1.4	18.9	6.7	2.5	28.9	4.9
11	1	40	400	60	0.90	0.30	0.12	1.4	18.7	6.3	2.5	28.3	4.8
12	1	60	275	60	0.85	0.23	0.13	1.3	17.7	4.7	2.6	25.8	4.8
13	1	80	275	90	0.83	0.23	0.15	1.3	14.5	4.1	2.7	22.1	5.7
14	1	60	400	30	0.72	0.15	0.13	1.0	20.8	4.4	3.7	29.9	3.5
15	1	80	400	60	0.84	0.28	0.15	1.3	15.5	5.2	2.7	24.1	5.4
16	1	60	275	60	0.74	0.20	0.12	1.1	16.1	4.3	2.6	23.8	4.6
Optimum		**°C**	bar	min	**EE_Pin**	**EE_Lic**	**EE_Gla**	**EE_Tot**	**P_Pin**	**P_Lic**	**P_Gla**	**P_TOT**	**yield**
Predicted values		**40**	**364**	**30**	0.8	0.2	0.1	1.1	20.7	5.0	2.9	30.3	4.0
95% confidence interval					0.7-0.8	0.1-0.2	0.1-0.1	1.0-1.2	19.3-22.2	4.6-5.5	2.0-3.8	28.4-32.2	3.6-4.5
Desirability			**0.92**		0.8	0.5	0.6	0.7	1.0	0.7	0.5	1.0	0.6
Experimental value (n = 4)					0.7 ± 0.2	0.2 ± 0.1	0.1 ± 0.0	1.1 ± 0.3	19.7 ± 1.4	5.5 ± 1.6	3.4 ± 0.3	28.8 ± 2.5	3.9 ± 0.9
95% confidence interval					0.5-0.9	0.1-0.3	0.1-0.2	0.8-1.4	19.0-19.9	5.1-7.2	3.1-3.6	27.1-31.7	2.8-4.4

ANOVA analysis (Table 4.7) assessed the statistical significance of factors A-C and their interactions, while standardized effects and relative contributions were summarized in the Pareto charts (Fig. 4.10). Experimental factors A-C showed no statistically significant effect on Gla content in the extract; therefore, this response variable was not considered in the subsequent chemometric analysis. The results indicated that pressure (B) and its quadratic term (BB) was the most influential factor for all the responses considered, both in terms of EE (g 100 g^{-1} leaf) and P (g 100 g^{-1} extract). On the other hand, temperature (A) and dynamic time (C) affected only specific variables. Temperature showed a direct effect only on the extract content (P) of Pin, Lic, and total Fs, whereas dynamic time mainly impacted EEs of target metabolites and EY (Table 4.7).

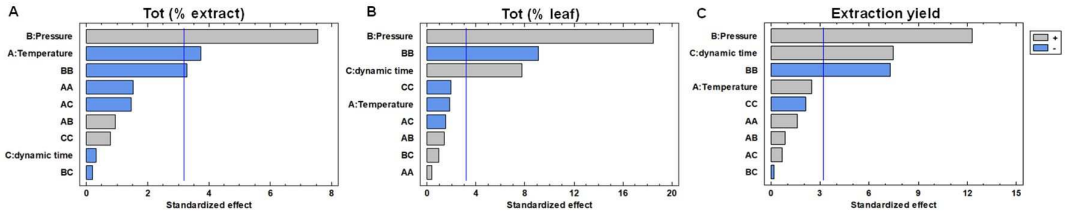

Fig. 4.10 *Pareto charts of standardized effects of $scCO_2$ factors on EE and P of total Fs, and EY.*

The vertical line marks significance at the 95% confidence level.

The regression model equations (Table 4.8) resulting from the removal of statistically no significant terms ($p > 0.05$, 95% confidence level), accurately describe the relationship between the experimental factors and the response variables. All models were highly significant ($p < 0.0001$), indicating that the observed variability in the responses is effectively explained by the experimental factors. Lack-of-fit ($p > 0.05$) further confirmed the adequacy of the models, demonstrating the absence of systematic discrepancies between experimental observations and regression predictions. Model predictivity was robust, R^2 values ranged from 86% to 98%, showing that the response variability was explained by the models, while adjusted R^2 values (82%–97%) supported the overall reliability of the regression models (Table 4.7), providing a solid statistical basis for interpreting the combined effects of $scCO_2$ extraction parameters.

Table 4.7. *Analysis of Variance (ANOVA) for response variables of $scCO_2$.*

	Pin (% leaf)		Lic (% leaf)		Gla (% leaf)		Fs (% leaf)		Pin (% extract)		Lic (% extract)		Gla (% extract)		Fs (% extract)		Extraction yield	
	F-value	*p*-value	*F*-value	*p*-value	*F*-value	*p*-value	*F*-value	*p*-value	*F*-value	*p*-value	*F*-value	*p*-value	*F*-value	*p*-value	*F*-value	*p*-value	*F*-value	*p*-value
A: Temperature	7.1	0.0764	5.04	0.1104	32.00	0.0109	3.45	0.1601	18.34	0.0234	54.03	0.0052	0.33	0.6078	13.94	0.0335	6.18	0.0888
B: Pressure	301.2	0.0004	345.04	0.0003	312.50	0.0004	341.47	0.0003	44.11	0.0070	658.19	0.0001	1.69	0.2849	57.05	0.0048	151.63	0.0012
C: Dyn. time	45.2	0.0067	88.17	0.0026	24.50	0.0158	59.95	0.0045	0.96	0.3999	82.60	0.0028	9.71	0.0526	0.09	0.7824	55.64	0.0050
AA	0.1	0.8479	0.75	0.4502	0.25	0.6514	0.13	0.7393	2.30	0.2266	0.79	0.4387	2.05	0.2475	2.32	0.2249	2.53	0.2099
AB	1.6	0.2989	0.33	0.6042	25.00	0.0154	1.92	0.2595	1.09	0.3733	0.22	0.6682	1.95	0.2572	0.86	0.4215	0.70	0.4639
AC	2.1	0.2398	2.08	0.2446	1.00	0.3910	2.35	0.2228	1.62	0.2931	9.97	0.0510	0.54	0.5158	2.16	0.2384	0.45	0.5509
BB	90.3	0.0025	30.08	0.0119	110.25	0.0018	83.26	0.0028	12.77	0.0374	55.21	0.0050	0.84	0.4262	10.80	0.0464	53.05	0.0053
BC	0.1	0.7745	18.75	0.0227	16.00	0.0280	0.90	0.4126	0.51	0.5285	14.69	0.0313	0.54	0.5158	0.03	0.8637	0.03	0.8777
CC	2.5	0.2152	5.33	0.1041	6.25	0.0877	3.88	0.1433	0.99	0.3938	4.16	0.1340	1.30	0.3376	0.60	0.4939	4.38	0.1274
Lack of fit	0.57	0.6717	1.36	0.4030	7.67	0.0642	0.91	0.5289	0.54	0.6866	0.12	0.9442	1.23	0.4339	0.41	0.7599	1.26	0.43
Lack of fit [a]	0.34	0.8743	1.69	0.2559	5.08	0.1050	0.74	0.6162	1.38	0.3360	2.21	0.2758	-	-	1.31	0.3588	1.28	0.3707
Model		0.0000		0.0000		0.0001		0.0000		0.0000		0.0000		0.2267		0.0000		0.0000
R^2		98.96		98.59		95.30		98.86		94.70		99.62		73.88		95.41		97.59
adjusted R^2		97.41		96.48		88.26		97.15		86.76		99.05		34.71		88.54		93.97
R^2 [a]		96.02		95.90		93.95		96.35		86.16		97.91		-		88.82		92.52
adjusted R^2 [a]		95.03		94.41		89.92		95.43		82.70		96.86		-		86.03		90.65

[a] *not significant terms excluded ($p > 0.05$).*

Table 4.8. *Regression equations of the fitted models and corresponding optimal levels of $scCO_2$ factors*

Response variables (Y)	Regression equation	Optimal factors		
		A	B	C
Pin (g/100 g leaf)	$-1.1936 + 0.010358\times B + 0.00379167\times C - 0.00001456\times B^2$	58	356	90
Lic (g/100 g leaf)	$-0.2314 + 0.001982\times B - 0.000833333\times C - 0.00000304\times B^2 + 0.00001\times B\times C$	60	400	90
Gla (g/100 g leaf)	$-0.0798 - 0.000875\times A + 0.001034\times B + 0.001025\times C + 0.000005\times A\times B - 0.00000168\times B^2 - 0.00000266667\times B\times C$	80	355	90
Tot (g/100 g leaf)	$-1.727 + 0.01458\times B + 0.00625\times C - 0.00002\times B^2$	44	364	90
Pin (g/100 g extract)	$5.32945 - 0.101188\times A + 0.109194\times B - 0.00015288\times B^2$	40	357	65
Lic (g/100 g extract)	$-1.77545 - 0.0288125\times A + 0.038286\times B - 0.00741667\times C - 0.00005272\times B^2 + 0.000113333\times B\times C$	40	400	90
Tot (g/100 g extract)	$7.3919 - 0.123625\times A + 0.148348\times B - 0.00019696\times B^2$	40	377	58
Yield (g/100 g)	$-5.261 + 0.04868\times B + 0.02625\times C - 0.0000696\times B^2$	46	350	90

As highlighted by the response surfaces (Fig. 4.11 and 4.12), pressure is therefore a determining factor for both the extraction yield and selectivity of target metabolite. Increased pressure increases $scCO_2$ density, improving its solvent power and ability to penetrate the pores of the matrix, resulting in increased extraction efficiency [7,161]. However, the quadratic term of pressure showed a negative effect (Fig 4.10): above 350 bar a plateau was observed for all response variables (Table 4.8). This behaviour reflects the fact that, beyond a certain threshold, additional pressure no longer enhances extraction performance: the increased fluid viscosity reduces CO_2 diffusivity, while the higher solvent strength promotes the co-extraction of highly nonpolar leaf components such as waxes and lipids.

As for temperature, its effect is more complex. A linear negative influence was observed on the extract content of Pin and Lic (Fig. 4.11), with 40 °C emerging as the optimal level for all purity-related variables (Table 4.8). This trend is likely attributable to the increased co-extraction of other matrix components at higher temperatures, which reduces the relative proportion of the target Fs in the extract. Conversely, extraction efficiency is not significantly influenced by temperature, except for EE Gla (Fig. 4.11): being the most non-polar metabolite, it benefits from the increase in solute volatility induced by higher temperatures [164].

Dynamic time showed differentiated behaviour: it contributed positively to EY and to the EEs of the Fs (Fig. 4.12), with maximum values reached at 90 minutes (Table 4.8), but it did not significantly influence extract purity (Fig. 4.12).

This outcome is consistent with the localization of the target metabolites, concentrated on the leaf surface. Their selective recovery occurs mainly during the first 30 minutes, as observed in the preliminary experiments (Fig. 4.8-4.9). Extending the dynamic time increases their extraction to some extent but also leads to progressive fluid saturation and enhances the co-extraction of lipophilic matrix components, thereby reducing process selectivity while increasing CO_2 and energy consumption.

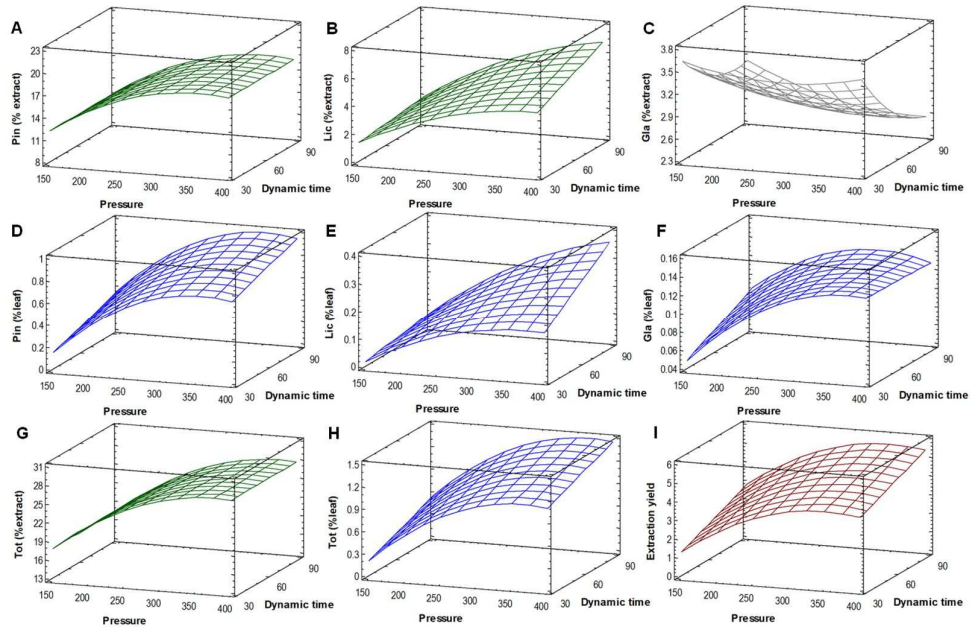

Fig 4.11. *Response surfaces of Pin (A), Lic (B) and Gla (C); EE of Pin (D), Lic (E), and Gla (F); P of Tot (G); EE of Tot (H) and EY (I) as a function of pressure and dynamic time in scCO₂ of GGL.*

Temperature fixed at the center point (°C = 60). Only statistically significant effects are shown.

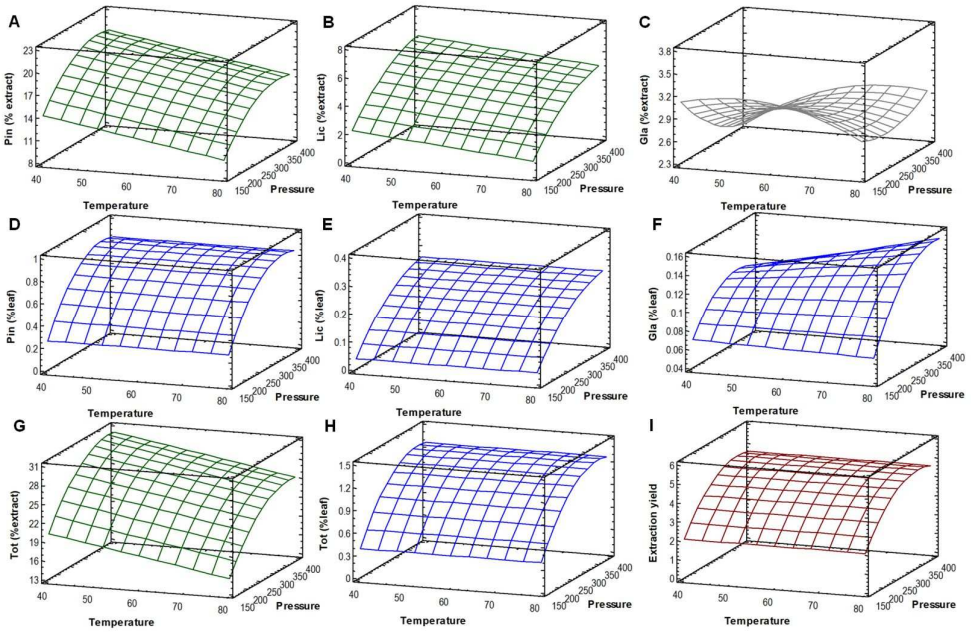

Fig 4.12. *Response surfaces of P of Pin (A), Lic (B) and Gla (C); EE of Pin (D), Lic (E), and Gla (F); P of Tot (G); EE of Tot (H) and EY (I) as a function of temperature and pressure in scCO₂ of GGL.*

The DT was fixed at the center point (min = 60). Only statistically significant effects are shown.

For all the reasons discussed above, a multiple response analysis was applied to simultaneously maximize the recovery of main compounds (EE of Pin, Lic, Gla and Fs) and produce extract enriched in target Fs (P of Pin, Lic and Fs), consequently minimizing the co-extraction of other matrix components. Using the desirability function, the optimal conditions were identified as 40 °C, 370 bar in 90 min, with a desirability index of 0.92. These conditions were experimentally validated (n = 4), collecting extracts at 30-minute intervals. The experimental results indicated a ~25% decrease in compound purities in the 90-min extracts compared to the 30-min ones (Fig. 4.13), with only a modest improvement in the recovery of target Fs (~ 10%).

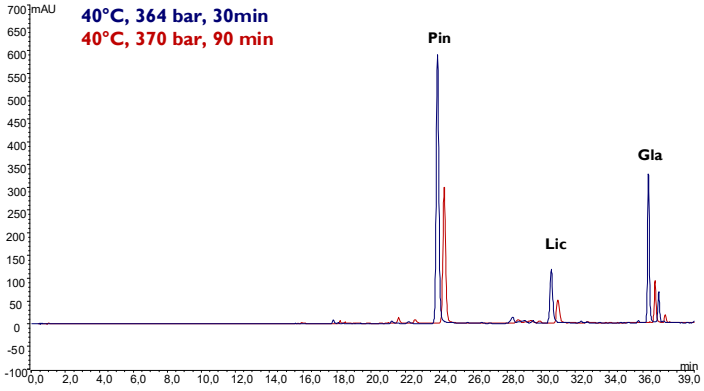

Fig 4.13. *UHPLC-UV profiles at 290 nm of scCO₂ extract obtained at 40°C, 370 bar, 30 min (blue line) and at 40°C, 370 bar, 90 min (red line).*

Since the aim of this work is to obtain enriched extracts of surface metabolites within a sustainable extraction framework, a second optimization step was performed by introducing an additional response variable previously not considered: CO_2 consumption (L min^{-1}). By integrating this response variable, the optimal compromise between purity, recovery, and sustainability was identified at 40°C, 364 bar, 30 min with a desiderability index of 0.94 (Fig. 4.14). These conditions were experimentally validated (n = 4), and the results obtained were fully consistent with the predicted intervals and fell within the confidence range (Table 4.6). Notably, this optimized protocol provides an enriched extract while reducing CO_2 consumption to one third of that required under the initial optimal settings, producing a ready-to-use powder within just 30 minutes.

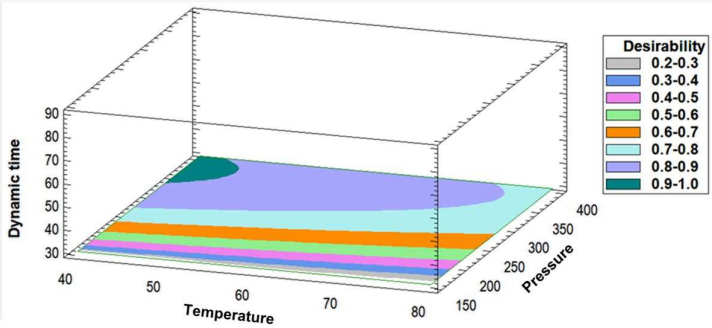

Fig 4.14. *Desiderability plot of $scCO_2$ optimization.*

4.4.3. $ScCO_2$ Performance and Comparison vs conventional methods

After the optimization process, the extraction performance of $scCO_2$ were compared with SLE. Ethanol and aqueous ethanol mixtures were excluded, as they do not provide sufficient selectivity toward exudate-derived Fs. Indeed, alcoholic and hydroalcoholic extraction recovers not only the target Fs but also the entire polar and semipolar metabolite fraction, mainly C-glycosyl flavones and O-glycosyl flavonols, which is not desirable when selective enrichment is the goal. Therefore, to perform a meaningful comparison and to ensure a truly selective recovery of the target Fs, the most appropriate extraction solvents were identified based on their Hildebrand solubility parameters [162]. This parameter, which reflects the cohesive energy of the solvent, is particularly suitable for comparing $scCO_2$ with conventional solvents, as it correctly integrates the density variations of $scCO_2$ at pressure and temperature variation [165]. Using the formula proposed by Marcus [165] for supercritical fluids and the tabulated values of Barton [166]optimized $scCO_2$ (40 °C, 400 bar) has a δ_H of 16.6 $MPa^{1/2}$ a value falling between hexane (δ_H = 14.8) and chloroform (δ_H = 18.8). Therefore, these two solvents were used in this study as a benchmark to evaluate the extraction efficiency, the enrichment capability and the overall sustainability of the $scCO_2$ process.

The extraction variables reported in Table 4.9 showed that, although the three solvents exhibit comparable Hildebrand solubility parameters, their interactions with the target metabolites differ markedly. Supercritical CO_2

displayed the highest selectivity (Fs purity), yielding extracts 3-fold and 16-fold richer in Fs compared with chloroform- and hexane-SLE, respectively (Table 4.9).

Table 4.9. *Extraction performance of optimized $scCO_2$ compared with conventional techniques.*

	$scCO_2$	**SLE-$CHCl_3$**	**SLE-Hexane**
Extract yield (g 100 g^{-1} leaf)	3.9 ± 0.9	34.9 ± 1.9	7.8 ± 0.1
Pin recovery (%)	31.2 ± 7.6	74.2 ± 4.4	2.8 ± 0.1
Lic recovery (%)	12.9 ± 6.1	85.4 ± 5.4	2.8 ± 0.1
Gla recovery (%)	38.2 ± 8.6	85.5 ± 4.6	8.5 ± 0.1
Flavanones purity (%)	28.8 ± 2.5	10.1 ± 0.1	1.9 ± 0.1
Green extraction principle	**$scCO_2$**	**SLE-$CHCl_3$**	**SLE-Hexane**
1. Raw material (g g^{-1} flavanones)	88	28	714
2. Ethanol volume (L g^{-1} flavanones)	0	0.6	14.3
3. Energy consumption (W per extraction cycle)	900	40	40
4. Waste (g g^{-1} extract)	85	19	673
5. Extraction time (h per extraction cycle)	1	24	24
6. Product recovery (%)	25.3 ± 7.3	79.6 ± 4.8	3.2 ± 0.1

Chloroform, despite its higher extraction efficiency (recovery 74-85%) and overall yield (Table 4.9), produced extracts with substantially lower purity than those obtained with $scCO_2$, highlighting the limited selectivity of the solvent and the likely co-extraction of highly non-polar leaf components, such as waxes and lipids. Hexane, whose Hildebrand solubility parameter is closer to that of $scCO_2$, nevertheless showed inferior performance in efficiency, yield, and purity (Table 4.9).

The extraction efficiency, the enrichment capability and the sustainability of $scCO_2$ were evaluated according to the six principles of eco-extraction [8,17] and compared with $CHCl_3$-SLE and Hexan-SLE (Table 4.9). The comparative results, illustrated in the radar chart (Fig. 4.15) show that the values closest to the center of the diagram correspond to greater overall sustainability of the process. Hexane was excluded from the radar chart as its low performance would have rescaled the plot (which normalizes to min-max values), artificially flattening the profiles of both $CHCl_3$-SLE and $scCO_2$. $ScCO_2$ extraction aligns with multiple principles of eco-extraction, beginning with solvent selection.

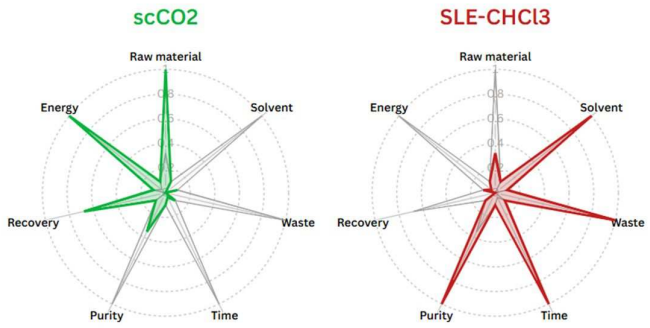

Fig 4.15. *Process assessment of $scCO_2$ and $CHCl_3$-SLE according to the six green extraction principles.*

Data are normalized on a 0–1 scale. Lower values indicate better performance.

Solvent choice must align with the principles of a circular economy, favoring options that are biodegradable, non-persistent, and safe to handle in terms of flammability, odor, and volatility [18]. Chloroform and hexane are classified as hazardous under the CHEM21 guide [167]and pose risks related to toxicity, flammability, and waste management. In contrast, CO_2 offers a more sustainable and safer alternative being non-toxic, non-flammable, cost-effective, and fully reusable, returning to its gaseous state upon depressurization without generating liquid waste streams.

Waste generation is also minimized: in addition to the recyclability of CO_2, the exhausted plant matrix remains dry, solvent-free, and fully reusable to make further extractions aimed at recovering more polar fractions or performing fractional, phase-selective separation by adjusting pressure, temperature, or adding small percentages of co-solvent.

$ScCO_2$ is not time-consuming, under optimized conditions, a high-purity extract is obtained in about 30 min, compared with 24 h typically required for solvent maceration.

Regarding energy and cost, the initial capital cost of supercritical equipment is high, and energy consumption, driven by pumps operating up to 600 bar and heaters reaching up to 300 °C, is higher than conventional maceration (approximately 20-fold higher). However, unlike maceration, $scCO_2$ does not require post-processing steps for solvent removal.

The optimized $scCO_2$ extract is enriched to 28.8% (g 100 g^{-1} extract) in the three target Fs (Pin, Lic and Gla), whereas chloroform and hexane yield extracts containing only ~10% and ~2% (g 100 g^{-1} extract), respectively.

Finally, although $scCO_2$ provides a lower overall EY and 3-fold lower extraction efficiency compared to $CHCl_3$-SLE, this is not a drawback within the scope of this study: the goal was the production of a highly selective and enriched extract, which $scCO_2$ achieves uniquely thanks to its tunable solvent strength and high affinity for non-polar leaf-surface Fs.

Finally, to assess whether in $scCO_2$ extract was retained the biological activity of GGL, intracellular ROS production was evaluated in yeast cells overexpressing α-synuclein, together with the anti-aging effect of $scCO_2$ extract and two of the three main metabolites contained in the extract (Pin and Gla) (Fig. 4.16).

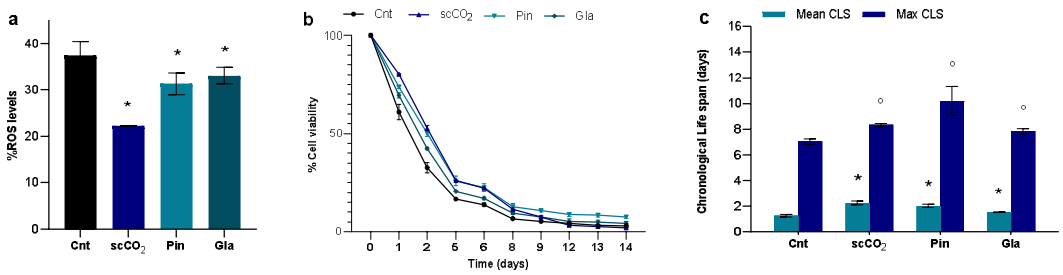

Fig 4.16. *Antioxidant and Antiaging effects of $scCO_2$ and its main compounds: (a) Intracellular ROS level in a yeast model of S. cerevisiae expressing the human α-synuclein, (b) CLS of yeast cells; (c) mean and maximum CLS, (a): *p < 0.05 relative to control cells, (b): *, ° p < 0.05 0.05 relative to control cells.*

$ScCO_2$ resulted in a significant reduction in intracellular ROS content (22.3 ± 0.1 %) compared to the control, although less than the exhaustive extract (13.9 ± 2.1%). This behaviour is consistent with the presence, in the exhaustive extract, of additional flavonoid classes with well-established antioxidant properties. Pin and Gla showed significant but lower reductive activity than $scCO_2$, suggesting that the AOC of the supercritical extract derives from a synergistic effect between the three predominant molecules.

Concerning the anti-aging effect, $scCO_2$ extract and compounds tested prolonged the CLS of yeast, resulting in a significant increase in both average

and maximum lifespan (Fig. 4.16c). In this case, the $scCO_2$ profile indicates that the anti-aging activity is mainly attributable to Pin and Gla, the most abundant metabolites in the extract.

Overall, $scCO_2$ is confirmed as a green, selective, and highly modular technique, retaining the biological activity of GGL and capable of overcoming many of the limitations of conventional extractions, offering high-purity extracts with minimal environmental impact and a good antioxidant activity.

4.5. Conclusions and future perspectives

Research conducted on GGL has highlighted the high potential of this untapped biomass, as a sustainable source of high value-added compounds. Previous studies by the DIFARMA-UNISA Food Chemistry and Analysis Laboratory have described a characteristic phytochemical profile of GGL, mainly constituted by Fs, Pin, Lic, and Gla, followed, in order of abundance, by prenylated dihydrostilbenes, C-glycosylated flavones, and O-glycosylated flavonols.

In the present study, the influence of the harvesting period and the cultivation area on the metabolic content of the leaves of Calabrian PDO licorice was evaluated. UHPLC-HRMS analysis [110] showed similiar qualitative profiles between different production areas and harvesting periods, while these factors significantly influence the content of specialized metabolites. The results show that the highest levels of bioactive compounds, particularly Fs and dihydrostilbenes, were found in the leaves collected in the Ionian coastal areas and the Tyrrhenian hinterland during the pre-flowering and flowering stages, which, even in the roots, correspond to the period with the greatest accumulation of secondary metabolites.This suggests that GGL can be transformed from a crop biomass into a valuable resource and strengthening the entire Calabrian PDO supply chain.

The study also highlighted the antioxidant properties of GGL extracts and their ability to counteract α-synuclein toxicity-induced senescence in a yeast model, supporting the potential functional role of these extracts in age-related diseases.

Based on this evidences, a green extraction strategy using $scCO_2$, selected to ensure sustainable and efficient recovery of leaf exudate compounds, was carrefully optimized. Optimization using RSM and UHPLC-DAD analysis identified pressure as the main parameter affecting selectivity and extraction efficiency. Optimal conditions allowed the production of a fraction enriched in the Fs Pin, Lic, and Gla, minimizing CO_2 consumption and obtaining safe, high-quality extracts.

Compared to conventional methods, $scCO_2$ achieved better performance in terms of selectivity, enrichment capacity, and environmental impact, while preserving the antioxidant properties of the matrix. Ongoing studies will extend the evaluation of neuroprotective *in vivo* potential on *Drosophila melanogaster*, pilot-scale validation and possible industrial exploitation of the Calabrian PDO GGL within a dedicated technological hall.

4.6. Materials and methods

4.6.1 Chemicals and standards

Analytical grade ethanol (EtOH), MS grade formic acid (HCOOH), 6-hydroxy-2,5,7,8- acid tetramethylcroman-2-carboxylic acid (Trolox), 2,2′-azinobis (3-ethylbenzothiazoline-6-sulphonic acid (ABTS), and the reference standards of isoquercitrin and rutin were provided by Merck Chemicals (Milan, Italy). MS grade acetonitrile and water were purchased from Romil (Cambridge, UK). Ultrapure water (18 MΩ) was prepared using a Milli-Q purification system (Millipore, Bedford, USA). Reference standards of liquiritin, isoliquiritin, glycyrrhizin (R41) and isoquercitrin (L12) were supplied by Extrasynthese (Lyon, France) and Sigma-Aldrich. Pinocembrin (L29), licoflavanone (L36), glabranin (L46), dihydro-3,3',4'-trihydroxy-5-O-prenylstilbene (L33) and dihydro-3,5,4′-trihydroxy-4,5′-diprenylstilbene (L44) were purified by RP-HPLC preparative from *G. glabra* exudate and characterized by 1D- and 2D-NMR (purity ≥ 96% from HPLC). Finally, vincenin-2 was previously isolated from natural sources [168].

4.6.2 Sampling and exhaustive extraction

GGL var. *typica* were kindly supplied by Nature Med S.r.l. (Castrovillari (CS), Italy) of the Consortium for Protected Designation of Origin "Liquirizia di Calabria PDO''. The cultivation and harvesting were conducted according to the disciplinary of the "Liquirizia of Calabria PDO". Plant materials were collected in 2022 from 3−4 year old plants in three typical PDO production areas of Calabria region: Villapiana (GG-A), (Cosenza; coordinates (lat, long): 39.810000, 16.470000, elevation: 16 m), Castrolibero (GG-B) (Cosenza; coordinates (lat, long): 39.322460, 16.192634, elevation: 290 m) and Scandale (GG-C) (Crotone; coordinates (lat, long): 39.152599, 17.011761, elevation: 63 m). Root and leaf samples were harvested during three growing phases of 2019: Harvesting Time 1 (HT1), corresponding to the pre-flowering stage, at early May; HT 2, corresponding to the flowering stage, at mid-June; HT 3, corresponding to the senescence stage (root collection), at late October. For

each geographical area at each HT, three representative samples (about 0.5 kg each replicate) were randomly collected. Drying of root and leaf materials (ventilated oven with a temperature of 50 °C) was carried out by Nature Med S.r.l. using standardized procedures in accordance to set rules of PDO disciplinary. Each sample of dried leaves and roots was finely ground using a Grindomix GM 200 knife mill (Retsch, Haan, Germany), operating in short cycles. The ground sample was sieved with a mesh size of 300-600 µm to obtain a sample with a homogeneous particle size distribution.

For $ScCO_2$ studies GGL samples were collected during flowering stage in 2023 from Castrolibero (Cosenza, Italy) PDO production area. The samples were processed as described above.

Exhaustive extraction was carried out in triplicate using ultrasonic-assisted solid–liquid extraction (Labsonic LBS2 ultrasonic thermostatic bath, Treviglio, Italy) with 70% aqueous ethanol (v/v) as the extraction solvent (matrix/solvent ratio 1:20, 25 °C for 30 minutes). The process was repeated three times with fresh solvent, and the exhaustive extraction was monitored by UHPLC-PDA analysis (area of main peaks < 2%). The resulting supernatants were then centrifuged for 10 minutes at 13,000 g pooled, filtered (Whatman No. 1 filter), concentrated under vacuum at 40 °C using a rotary evaporator and freeze-dried (Alpha 1-2 LD freeze dryer, Christ, Germany).

4.6.3. UHPLC-DAD analysis

Quantitative analysis of *G. glabra* extracts was performed using a Platin Blue UHPLC system, (Knauer, Labservice Analytica, Bologna, Italy) consisting of two Ultra High-Pressure Pumps, an autosampler, a column temperature manager and a diode array detector. UHPLC separation was performed using a previously developed method [110]. Briefly, the chromatographic separations were performed using a Kinetex C18 column (2.1 × 100 mm, 1.6 µm; Phenomenex, Bologna, Italy) protected by a C18 Guard Cartridge (2.1 mm I.D.) and thermostated at 25 °C. A binary gradient of H_2O and MeCN, both containing 0.1% of formic acid, at a flow rate of 500 µL min^{-1} (injection volume, 5 µL) was employed. The elution method was as follows: 0-3 min, 2 % B; 3-5

min,2-13% B;5-9min, 13 %B ;9-12 min 13-18 %B; 12-13 18%B ;13-17min,18-30%B ; 17-20 min, 30 % B; 20-30 min, 30-40 % B; 30-38 min, 40-60%B; 38-39 min, 60-98%B; 39-44 min, 98%B; 44-45 min, 98-2%B; 45-50 min, 2%B. UV spectra were acquired in the range of 200-600 nm and three wavelengths were selected for the detection of target analytes based on the maximum absorbance of pure compounds: 220 (prenylated dihydrostilbenes), 290 (flavanones) and 360 (flavones-C-glycosides and flavonols-O-glycosides) nm. External standards method was employed to determine the levels of main compounds in the *G. glabra* extracts. Stock solutions of reference standards for root samples (vincenin 2, liquiritin, isoliquiritin, glycyrrhizic acid e glabridin) and for leaf samples (vincenin 2, rutin, isoquercitrin, pinocembrin, licoflavone, glabrinin, dihydro-3,3',4'-trihydroxy-5-O-prenylstilbene (L33) and dihydro-3,5,4′-trihydroxy-4,5′-diprenylstilbene (L44)) were prepared in MeOH at a concentration of 5 mg mL^{-1} and stored at -20 °C. A mixture of reference standards was prepared at concentration of 1 mg mL^{-1}, and the calibration levels were prepared by appropriate serial dilution with MeOH/H_2O, 1:1 v/v, and analysed in triplicate. The linearity of the calibration curves was evaluated in the concentration range of 6.25 -100 µg mL^{-1} for vincenin 2, rutin and Isoquercitrin, and 12.5 - 200 µg mL^{-1} for the remaining reference compounds. The regression curves were tested with the analysis of variance (ANOVA) and linear model was found appropriate over tested concentration range (R^2 values > 0.999). The samples were analysed after appropriate dilutions, to fall within the dynamic calibration range. The quantification of compounds of *G. glabra* extracts, for which no reference standards were available, was determined using the calibration curves of standards belonging to the same class of secondary metabolites (similar chromophore). The amount of the compounds was expressed as mg per g of dry material (mg/g DM) ± standard deviation (n = 3 biological replicates).

4.6.4. ABTS assay

The antioxidant activities of the exhaustive GGL extracts and the major GGL compounds, vicenin-2, rutin, isoquercitrin, pinocembrin, licoflavanone,

glabranin, dihydro-3,3',4'-trihydroxy-5-O-prenylstilbene (L33) and dihydro-3,5,4′-trihydroxy-4,5′-diprenylstilbene(L44), were evaluated using ABTS assays, performed as described in Section 2.4.4.GGL dried extracts were dissolved in methanol at the concentration of 1 mg/mL and then diluted with with 5 mM PBS (pH 7.4) to provide approximately 20–80% control absorbance. Results were expressed as TEAC per g of extract (mmol TE/g) or per mmol of pure compound (mmol TE/mmol).

4.6.5. Yeast Strains and Media

Yeast strain used to evaluate the biological activity of dried GGL extracts is BY4742 MATα his3Δ1 leu2Δ0 lys2Δ0 ura3Δ0 [pYX242- SNCA] overexpressing human α-synuclein. Cells were grown at 30 °C in minimal medium containing 2% glucose as a carbon source and 0.67% yeast nitrogen base without amino acids and supplemented with 50 mg L^{-1} of required amino acids and bases for which the strain was auxotrophic, with a constant shaking (120 rpm). GGL extracts were resuspended in 150 µL of EtOH 100%, vortexed, incubated in the termomixer at 25 °C for 1 hour, sonicated for 20 minutes and dissolved in the liquid medium at a concentration of 0.2% of the yeast strain and filtered through 0.22 µm filters, as previously reported [122,123].

4.6.6. Chronological Lifespan Experiments (CLS)

Yeast cells were grown in liquid medium until the mid-late exponential phase, centrifugated (13000 rpm, 5 min) and then inoculated at 0.150 OD mL^{-1} (Optical Density mL^{-1}) in flasks containing medium in the absence (negative control) or presence of the extracts (0.2% concentration). Survival was assessed by propidium iodide staining (PI) at the indicated time points with the Cytoflex cytofluorimeter (Beckman Coulter) and analyzed with the Cytoflex software, as previously reported [122,123].

4.6.7. Analysis of Reactive Oxygen Species (ROS) Levels

Analysis of cellular superoxide was performed by DHE (dihydroethidium) staining. Cells were collected after 24 h treatment with 0.2% GGL extracts and 0.2% were resuspended in PBS and stained with 5 µg/mL for 10 min. FACS analyses were performed with Cytoflex cytofluorimeter (Beckman Coulter) and analyzed with the Cytoflex software, as previously reported [122,123]. Results are expressed ad mean and DS of at least two independent experiments

4.6.8 Conventional solid-liquid extraction

Maceration was employed as conventional solid-liquid extraction technique (SLE) using chloroform and hexane as extraction solvents. 5 g of GGL in 100 mL of solvent were subjected to maceration at room temperature for 24 h. After extraction and filtration, the extracts were treated as detailed in section 4.5.2.

4.6.9. Supercritical CO_2 extraction ($scCO_2$)

$ScCO_2$ was performed with Spe-ed Helix supercritical fluid extractor (Applied Separations, Allentown, PA, USA) in static and dynamic extraction mode using 24 mL stainless steel cells and 60 mL collection bottles. Extraction cells, equipped with cellulose filters at both the top and bottom, were loaded with the sample mixed with glass wool and 4 mm glass beads in a 1:2:2 (v/v/v) ratio. The fixed instrumental parameters were set as follows: CO_2 as extraction solvent, CO_2 flow rate of 2 L min^{-1}, CO_2 needle heater set at 80 °C. After each run, a purge step was performed by closing the CO_2 inlet and opening the outlet valve to vent residual CO_2; complete depressurization required approximately 10 min.

For the preliminary experiments, a single extraction cycle with a 20 min static phase was applied, and trials involving variations in pressure and temperature were performed. Under optimal conditions, $ScCO_2$ was performed at a temperature of 40 °C, pressure of 370 bar and 30 min dynamic time, loading 1.2 g of matrix into 24 mL cells. After extraction, the yield was determined, and

an aliquot of the resulting extract was weighed, dissolved, and diluted to a final concentration of 0.5 mg g^{-1} extract for UHPLC analyses.

4.6.10. Experimental design and optimization

$ScCO_2$ conditions were optimized by Response Surface Design using a BBD quadratic model (6 degrees of freedom), consisting of one block replicates of 16 randomized experimental runs and four center points. The experimental design and optimization of operational conditions for each extraction process were performed using Statgraphics Centurion 18 software, provided by Statgraphics Technologies (Adalta snc, Arezzo, Italy). The independent experimental factors considered for each extraction method and their levels (-1, 0, and +1) are reported in Table 4.5. Minimum and maximum levels of the independent factors were selected based on preliminary experiments. EE (g 100 g^{-1} leaf) and P (g 100 g^{-1} extract) of the main GGL compounds (Pin, Lic and Gla) were designated as response variables to be maximized. Furthermore, EY (g extract 100 g^{-1} leaf) and total leaf and extract metabolite content were considered as response variables. The experimental conditions for the design and the corresponding response variable values are listed in Tables 4.6. A second-order polynomial equation was used to fit each dependent variable (Y) as a function of the independent factors (A-C). Mathematical models of the estimated response surfaces were defined after removing the non-significant factors and two-factor interactions identified by ANOVA ($p > 0.05$). Model adequacy and quality were verified through lack-of-fit test and regression coefficients (R2 and adjusted R2), respectively. Subsequently, simultaneous optimization of independent factors was conducted using the desirability function aiming to maximize EEs and Ps of main GGL compounds, with purity being prioritized over extraction efficiency in the desirability weighting. The suggested optimal conditions were experimentally validated by comparing predicted values of response variables with the experimental data of four extraction replicates (95% confidence interval).

4.6.11. Statistical analysis

The quantitative data and TEAC values were subjected to analysis of variance (ANOVA) using Statgraphic Centurion 18 software from Statgraphics Technologies (Arezzo, Italy). A two-way ANOVA (3 production areas × 3 HTs) was applied to each GGL marker, the total of metabolite classes, and TEAC values. The means were separated using the Tukey HSD test only when the F-test for factors and their interaction were significant at the *p*-value < 0.05 probability level.

Regarding the CLS assays and analysis of ROS levels, experiments were performed in duplicate. The results are expressed as mean ± SD (standard deviation). Results were compared using the two-sided Student's *T*-test. Differences were considered statistically significant at $p < 0.05$.

5. Concluding remarks

In the modern era, where sustainability and ecological transition are strategic priorities, the exploitation of natural biomass not fully exploited yet, requires an approach that considers the entire extract life cycle, from raw material selection to final product development. In this perspective, CSL and GGL leaves are two emblematic examples. Both belong to well-established agricultural Italian supply chain, and constitute renewable, yet currently underutilized, biomasses. Their valorization as value-added co-products can therefore generate environmental, economic, and social benefits, aligning with the principles of sustainable resource management and circular bioeconomy. Carob leaves can be collected during fruit harvesting, turning an untapped material into a useful resource. Similarly, licorice, protected by a PDO in Calabria, offers leaves that, if harvested at the appropriate time, prevent waste and support full supply-chain circularity.

Hence, in this research project, CSL and GGL, untapped biomasses with high potential, distinctive chemical profiles, and demonstrated biological activity, confirmed their relevance through the outcomes obtained. Their potential was exploited through the sustainable recovery of secondary metabolites, using two green techniques, PHWE and ScCO2, tailored and carefully optimized for each matrix. Through a chemometric approach, the response variables of the extraction processes were defined and optimized, maximizing efficiency, purity, and selectivity towards the target metabolites and analyzing the effects and the interaction between the fundamental parameters of the techniques used. The optimized green conditions, PHWE for CSL and ScCO2 for GGL, outperformed conventional techniques in terms of extraction yield, selectivity, and preservation (or increase) of biological activity, highlighting the robustness of the adopted sustainable approach and the potential application of the obtained extracts.

The application of the *Path2Green* metric [18] to the two optimized extraction techniques (PHWE for CSL and $ScCO_2$ for GGL) enabled an integrated assessment of their sustainability performance across the 12 principles of green extraction process (Fig. 5.1).

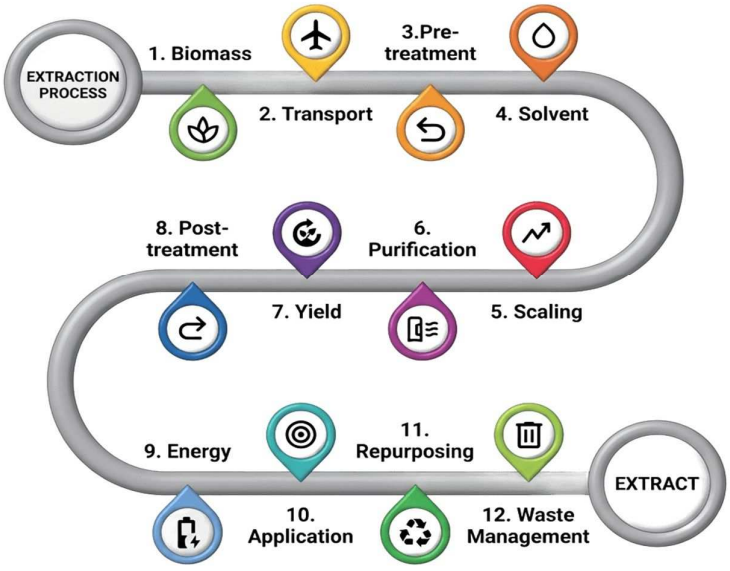

Figure 5.1. *The 12 principles of green extraction process evaluated by Path2Green metric [18].*

Path2Green offers an overview of the environmental, social, and economic sustainability of an extraction approach, providing a nuanced assessment of its overall impact from biomass collection/production to the end of the process. It integrates key factors such as resource depletion, energy consumption, waste generation, and biodiversity preservation.

PHWE and $ScCO_2$ achieved final scores of + 0.334 and + 0.129 (Fig. 5.2), respectively, reflecting a moderately sustainable profile with specific strengths and areas for improvement. Both methods align with green principles thanks to the use of locally sourced and renewable biomass, and safe and renewable solvents (water and CO_2), the absence of solvent-free residues in the final extracts, and the real possibility to recycle CO_2 and auxiliary materials. The techniques used, based on pressurized fluids, are also easily scalable at the pilot level, favoring the industrial adoption of continuous in-flow processes and the production of “ready-to-use” extracts, without additional post-extraction steps.

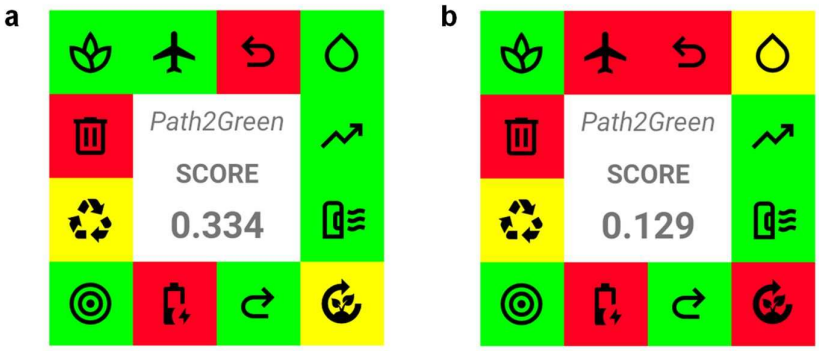

Figure 5.2. *Path2Green pictograms (lab-scale evaluation) of optimized CSL PHWE (a) and GGL ScCO₂ (b).*

The 12 principles of green extraction are visually represented and color-coding indicates the degree of compliance: green (strong), yellow (moderate), and red (requiring improvement). The overall process score is expressed on a scale from − 1.0 (red, poor alignment) to + 1.0 (green, excellent alignment).

Energy assessments show that, although PHWE and $ScCO_2$ require high pressure or temperature operating conditions, the limited extraction time (approximately 30 min) and the future possibility of powering these industrial facilities with renewable energy lower their ecological footprint. The simple, low-impact physical pre-treatment of the matrices further contributes to reducing the environmental impact.

Even the most critical parameters of the metric, such as transport, yield, and waste production, can be mitigated in a real industrial setting by locating the processing units directly within agricultural facilities (“hull technology”) and by fully reusing the residual biomass: in the case of PHWE, wet residue can be valorized as biofuel or biochar; for $ScCO_2$, the dry, unexhausted matrix remains suitable for further recovery cycles of other target metabolites. Therefore, the on-site valorization of biomass through dedicated industrial units would reduce the impact of these factors (Fig. 5.3).

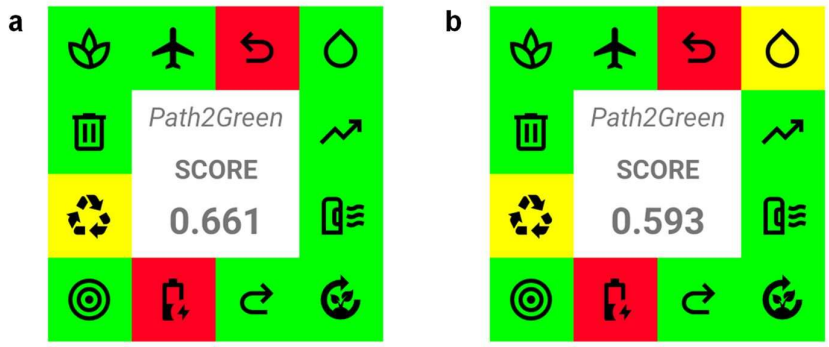

Figure 5.3. *Path2Green pictograms (pilot-scale evaluation) of optimized CSL PHWE (a) and GGL $ScCO_2$ (b).*

Overall, the *Path2Green* metric values reflect a moderately sustainable profile for PHWE and $ScCO_2$ (center value above the neutrality, Fig. 5.1, 5.2), confirming that both techniques, applied to CSL and GGL, are sustainable, efficient extraction processes, fully consistent with current international green transition objectives. At the same time, *in vitro* and *in vivo* studies show that the extracts obtained exhibit interesting antioxidant properties, strong inhibitory ability of a key enzyme in carbohydrate metabolism (CSL) and potential anti-aging effect (GGL), highlighting their real potential for applications in nutraceuticals, food, and human health.

In summary, this study demonstrates how the integration of local agricultural supply chains with advanced extraction techniques, evaluated using quantitative sustainability metrics, pave the way to transform residual biomass into high added-value ingredients, promoting circular, safe production models directed toward human well-being.

References

Bibliography

1 Alexandri, M.; Kachrimanidou, V.; Papapostolou, H.; Papadaki, A.; Kopsahelis, N. Sustainable Food Systems: The Case of Functional Compounds towards the Development of Clean Label Food Products. *Foods* **2022**, *11*, doi: 10.3390/foods11182796.

2. Chemat, F.; Vian, M.A.; Cravotto, G. Green Extraction of Natural Products: Concept and Principles. *Int J Mol Sci* **2012**, *13*, 8615–8627, doi: 10.3390/ijms13078615

3. Chuo, S.C.; Nasir, H.M.; Mohd-Setapar, S.H.; Mohamed, S.F.; Ahmad, A.; Wani, W.A.; Muddassir, M.; Alarifi, A. A Glimpse into the Extraction Methods of Active Compounds from Plants. *Crit Rev Anal Chem* **2022**, *52*, 667–696, doi: 10.1080/10408347.2020.1820851.

4. Atanasov, A.G.; Zotchev, S.B.; Dirsch, V.M.; Orhan, I.E.; Banach, M.; Rollinger, J.M.; Barreca, D.; Weckwerth, W.; Bauer, R.; Bayer, E.A.; et al. Natural Products in Drug Discovery: Advances and Opportunities. *Nat Rev Drug Discov* **2021**, *20*, 200–216, doi: 10.1038/s41573-020-00114-z.

5. Rinaldo John, A.S. Functional Foods: Components, Health Benefits, Challenges, and Major Projects. *DRC Sustainable Future: Journal of Environment, Agriculture, and Energy* **2021**, 61–72, doi:10.37281/drcsf/2.1.7.

6. Anastas, P.T.; W.J.C. *Is Sustainable Energy Development Is Sustainable Energy Development Possible? Possible?*; **1998**;

7. Zia, S.; Khan, M.R.; Shabbir, M.A.; Aslam Maan, A.; Khan, M.K.I.; Nadeem, M.; Khalil, A.A.; Din, A.; Aadil, R.M. An Inclusive Overview of Advanced Thermal and Nonthermal Extraction Techniques for Bioactive Compounds in Food and Food-Related Matrices. *Food Reviews International* **2020**, *38*, 1166–1196, doi: 10.1080/87559129.2020.1772283.

8. Chemat, F.; Abert-Vian, M.; Fabiano-Tixier, A.S.; Strube, J.; Uhlenbrock, L.; Gunjevic, V.; Cravotto, G. Green Extraction of Natural Products. Origins, Current Status, and Future Challenges. *TrAC - Trends in Analytical Chemistry* **2019**, *118*, 248–263, doi: 10.1016/j.trac.2019.05.037.

9. Poletto, P.; Alvarez-Rivera, G.; Torres, T.M.S.; Mendiola, J.A.; Ibañez, E.; Cifuentes, A. Compressed Fluids and Phytochemical Profiling Tools to Obtain and Characterize Antiviral and Anti-Inflammatory Compounds from Natural Sources. *TrAC - Trends in Analytical Chemistry* **2020**, *129*, doi: 10.1016/j.trac.2020.115942.

10. Granato, D.; Barba, F.J.; Bursa´cbursa´c, D.; Kovačevi´c, K.; Lorenzo, J.M.; Cruz, A.G.; Putnik, P. Annual Review of Food Science and Technology Functional Foods: Product Development, Technological Trends, Efficacy Testing, and Safety. *Annual Review ofFood Science and Technology* **2020**, doi:10.1146/annurev-food-032519.

11. Saleem, H.; Yaqub, A.; Rafique, R.; Ali Chohan, T.; Malik, D. e. S.; Tousif, M.I.; Khurshid, U.; Ahemad, N.; Ramasubburayan, R.; Rengasamy, K.R.R. Nutritional and Medicinal Plants as Potential Sources of Enzyme Inhibitors toward the Bioactive Functional Foods: An Updated Review. *Crit Rev Food Sci Nutr* **2024**, *64*, 9805–9828, doi: 10.1080/10408398.2023.2217264.
12. Najmi, A.; Javed, S.A.; Al Bratty, M.; Alhazmi, H.A. Modern Approaches in the Discovery and Development of Plant-Based Natural Products and Their Analogues as Potential Therapeutic Agents. *Molecules* **2022**, *27*, doi: 10.3390/molecules27020349.
13. Mármol, I.; Quero, J.; Ibarz, R.; Ferreira-Santos, P.; Teixeira, J.A.; Rocha, C.M.R.; Pérez-Fernández, M.; García-Juiz, S.; Osada, J.; Martín-Belloso, O.; et al. Valorization of Agro-Food by-Products and Their Potential Therapeutic Applications. *Food and Bioproducts Processing* **2021**, *128*, 247–258, doi:10.1016/j.fbp.2021.06.003.
14. Henderson, K.; Loreau, M. A Model of Sustainable Development Goals: Challenges and Opportunities in Promoting Human Well-Being and Environmental Sustainability. *Ecol Modell* **2023**, *475*, doi:10.1016/j.ecolmodel.2022.110164.
15. López-Salas, L.; Expósito-Almellón, X.; Borrás-Linares, I.; Lozano-Sánchez, J.; Segura-Carretero, A. Design of Experiments for Green and GRAS Solvent Extraction of Phenolic Compounds from Food Industry By-Products - A Systematic Review. *TrAC - Trends in Analytical Chemistry* **2024**, *171*, doi: 10.1016/j.trac.2024.117536.
16. Weremfo, A.; Abassah-Oppong, S.; Adulley, F.; Dabie, K.; Seidu-Larry, S. Response Surface Methodology as a Tool to Optimize the Extraction of Bioactive Compounds from Plant Sources. *J Sci Food Agric* **2023**, *103*, 26–36, doi: 10.1002/jsfa.12121.
17. Herrero, M. Towards Green Extraction of Bioactive Natural Compounds. *Anal Bioanal Chem* **2024**, *416*, 2039–2047, doi:10.1007/s00216-023-04969-0.
18. de Souza Mesquita, L.M.; Contieri, L.S.; e Silva, F.A.; Bagini, R.H.; Bragagnolo, F.S.; Strieder, M.M.; Sosa, F.H.B.; Schaeffer, N.; Freire, M.G.; Ventura, S.P.M.; et al. Path2Green: Introducing 12 Green Extraction Principles and a Novel Metric for Assessing Sustainability in Biomass Valorization. *Green Chemistry* **2024**, *26*, 10087–10106, doi:10.1039/d4gc02512a.
19. Cena, H.& L.M. *Biodiversity and planetary Health: A call for Integrated Action*; www.thelancet.com, 2023; ISBN 9789240070288.
20. Debayo Loss of Biodiversity: The Burgeoning Threat to Human Health. *Ann Ib Postgrad Med* **2019**
21. Negri, S.; Pietrolucci, F.; Andreatta, S.; Chinyere Njoku, R.; Antunes Silva Nogueira Ramos, C.; Crimi, M.; Commisso, M.; Guzzo, F.; Avesani, L. Bioprospecting of Artemisia Genus: From Artemisinin to Other Potentially Bioactive Compounds. *Sci Rep* **2024**, *14*, doi:10.1038/s41598-024-55128-z.
22. Ilyasov, I.R.; Beloborodov, V.L.; Selivanova, I.A.; Terekhov, R.P. ABTS/PP Decolorization Assay of Antioxidant Capacity Reaction Pathways. *Int J Mol Sci* **2020**, *21*, doi: 10.3390/ijms21031131.

23. Shahidi, F.; Ambigaipalan, P. Phenolics and Polyphenolics in Foods, Beverages and Spices: Antioxidant Activity and Health Effects - A Review. *J Funct Foods* **2015**, *18*, 820–897, doi: 10.1016/j.jff.2015.06.018.
24. Alavi, M.; Hamblin, M.; Aghaie, E.; Mousavi, S.A.R.; Hajimolaali, M. Antibacterial and Antioxidant Activity of Catechin, Gallic Acid, and Epigallocatechin-3-Gallate: Focus on Nanoformulations. *Cellular, Molecular and Biomedical Reports* **2023**, *3*, 62–72, doi:10.55705/cmbr.2022.353962.1052.
25. de Jesus, N.Z.T.; de Souza Falcão, H.; Gomes, I.F.; de Almeida Leite, T.J.; de Morais Lima, G.R.; Barbosa-Filho, J.M.; Tavares, J.F.; da Silva, M.S.; de Athayde-Filho, P.F.; Batista, L.M. Tannins, Peptic Ulcers and Related Mechanisms. *Int J Mol Sci* **2012**, *13*, 3203–3228, doi: 10.3390/ijms13033203.
26. ALNasser, M.N.; Alboraiy, G.M.; Alsowig, E.M.; Alqattan, F.M. Cholinesterase Inhibitors from Plants and Their Potential in Alzheimer's Treatment: Systematic Review. *Brain Sci* **2025**, *15*, doi: 10.3390/brainsci15020215.
27. Sanchez-Martinez, J.D.; Bueno, M.; Alvarez-Rivera, G.; Tudela, J.; Ibanez, E.; Cifuentes, A. In Vitro Neuroprotective Potential of Terpenes from Industrial Orange Juice By-Products. *Food Funct* **2021**, *12*, 302–314, doi:10.1039/d0fo02809f.
28. Dos Santos, T.C.; Gomes, T.M.; Pinto, B.A.S.; Camara, A.L.; De Andrade Paes, A.M. Naturally Occurring Acetylcholinesterase Inhibitors and Their Potential Use for Alzheimer's Disease Therapy. *Front Pharmacol* **2018**, *9*, doi: 10.3389/fphar.2018.01192.
29. Berkov, S.; Atanasova, M.; Georgiev, B.; Bastida, J.; Doytchinova, I. The Amaryllidaceae Alkaloids: An Untapped Source of Acetylcholinesterase Inhibitors. *Phytochemistry Reviews* **2022**, *21*, 1415–1443, doi: 10.1007/s11101-021-09790-0.
30. Ghanem, D.M.; Ammar, N.M.; El-Hawary, S.S.; Hamed, A.R.; Hussein, R.A.; El-Desoky, A.H.; Mohamed, D.A.; Mokhtar, F.A.; Okba, M.M. Effect of Carissa Macrocarpa (Eckl.) A. DC. Aerial Parts on Some Non-Communicable Diseases: In Vitro Study and HPLC-QTOF/MS-MS Analysis. *Discover Applied Sciences* **2024**, *6*, doi:10.1007/s42452-024-05899-x.
31. Saci, F.; Bachir bey, M.; Louaileche, H.; Gali, L.; Bensouici, C. Changes in Anticholinesterase, Antioxidant Activities and Related Bioactive Compounds of Carob Pulp (Ceratonia Siliqua L.) during Ripening Stages. *Journal of Food Measurement and Characterization* **2020**, *14*, 937–945, doi:10.1007/s11694-019-00344-9.
32. Murray, A.P.; Faraoni, M.B.; Castro, J.; Alza, N.P.; Cavallaro, V. Natural AChE Inhibitors from Plants and Their Contribution to Alzheimer's Disease Therapy. *Curr Neuropharm*; **2013**,11-4 doi: 10.2174/1570159X11311040004.
33. Tavares, L.; McDougall, G.J.; Fortalezas, S.; Stewart, D.; Ferreira, R.B.; Santos, C.N. The Neuroprotective Potential of Phenolic-Enriched Fractions from Four Juniperus Species Found in Portugal. *Food Chem* **2012**, *135*, 562–570, doi:10.1016/j.foodchem.2012.05.023.

34. Dirir, A.M.; Daou, M.; Yousef, A.F.; Yousef, L.F. A Review of Alpha-Glucosidase Inhibitors from Plants as Potential Candidates for the Treatment of Type-2 Diabetes. *Phytochemistry Reviews* **2022**, *21*, 1049–1079, doi: 10.1007/s11101-021-09773-1.
35. Lam, T.P.; Tran, N.V.N.; Pham, L.H.D.; Lai, N.V.T.; Dang, B.T.N.; Truong, N.L.N.; Nguyen-Vo, S.K.; Hoang, T.L.; Mai, T.T.; Tran, T.D. Flavonoids as Dual-Target Inhibitors against α-Glucosidase and α-Amylase: A Systematic Review of in Vitro Studies. *Nat Prod Bioprospect* **2024**, *14*, doi: 10.1007/s13659-023-00424-w.
36. Cardullo, N.; Muccilli, V.; Pulvirenti, L.; Cornu, A.; Pouységu, L.; Deffieux, D.; Quideau, S.; Tringali, C. C-Glucosidic Ellagitannins and Galloylated Glucoses as Potential Functional Food Ingredients with Anti-Diabetic Properties: A Study of α-Glucosidase and α-Amylase Inhibition. *Food Chem* **2020**, *313*, doi:10.1016/j.foodchem.2019.126099.
37. Lim, J.; Ferruzzi, M.G.; Hamaker, B.R. Structural Requirements of Flavonoids for the Selective Inhibition of α-Amylase versus α-Glucosidase. *Food Chem* **2022**, *370*, 130981, doi:10.1016/j.foodchem.2021.130981.
38. Wang, Y.; Zhang, L.; Xiao, H.; Ye, X.; Pan, H.; Chen, S. Revisiting Dietary Proanthocyanidins on Blood Glucose Homeostasis from a Multi-Scale Structural Perspective. *Curr Res Food Sci* **2024**, *9*, doi: 10.1016/j.crfs.2024.100926.
39. Liu, L.; Jia, W.; Jiang, S.; Zhang, G.; Zhao, J.; Xu, J.; Wang, L.; Wu, D.; Tao, J.; Yue, H.; et al. Inhibitory Activities and Rules of Plant Gallotannins with Different Numbers of Galloyl Moieties on Sucrase, Maltase and α-Amylase in Vitro and in Vivo. *Phytomedicine* **2023**, *120*, doi:10.1016/j.phymed.2023.155063.
40. Celano, R.; Piccinelli, A.L.; Pagano, I.; Roscigno, G.; Campone, L.; De Falco, E.; Russo, M.; Rastrelli, L. Oil Distillation Wastewaters from Aromatic Herbs as New Natural Source of Antioxidant Compounds. *Food Research International* **2017**, *99*, 298–307, doi:10.1016/j.foodres.2017.05.036.
41. Chen, Y.; Geng, S.; Liu, B. Three Common Caffeoylquinic Acids as Potential Hypoglycemic Nutraceuticals: Evaluation of α-Glucosidase Inhibitory Activity and Glucose Consumption in HepG2 Cells. *J Food Biochem* **2020**, *44*, doi:10.1111/jfbc.13361.
42. Dahmani, W.; Elaouni, N.; Abousalim, A.; Akissi, Z.L.E.; Legssyer, A.; Ziyyat, A.; Sahpaz, S. Exploring Carob (Ceratonia Siliqua L.): A Comprehensive Assessment of Its Characteristics, Ethnomedicinal Uses, Phytochemical Aspects, and Pharmacological Activities. *Plants* **2023**, *12*, doi: 10.3390/plants12183303.
43. Brassesco, M.E.; Brandão, T.R.S.; Silva, C.L.M.; Pintado, M. Carob Bean (Ceratonia Siliqua L.): A New Perspective for Functional Food. *Trends Food Sci Technol* **2021**, *114*, 310–322, doi: 10.1016/j.tifs.2021.05.037.
44. Gioxari, A.; Amerikanou, C.; Nestoridi, I.; Gourgari, E.; Pratsinis, H.; Kalogeropoulos, N.; Andrikopoulos, N.K.; Kaliora, A.C. Carob: A Sustainable Opportunity for Metabolic Health. *Foods* **2022**, *11*, doi: 10.3390/foods11142154.

45. Stavrou, I.J.; Christou, A.; Kapnissi-Christodoulou, C.P. Polyphenols in Carobs: A Review on Their Composition, Antioxidant Capacity and Cytotoxic Effects, and Health Impact. *Food Chem* **2018**, *269*, 355–374, doi: 10.1016/j.foodchem.2018.06.152
46. Tomac, I.; Mikušová, V.; Mikuš, P.; Labuda, J. Effective Detection of Antioxidants Using Functional Schemes of Enzyme Inhibition and Competing (Bio)Reactions. *Talanta Open* **2025**, *12*, doi: 10.1016/j.talo.2025.100525.
47. Uysal, S.; Zengin, G.; Aktumsek, A.; Karatas, S. Chemical and Biological Approaches on Nine Fruit Tree Leaves Collected from the Mediterranean Region of Turkey. *J Funct Foods* **2016**, *22*, 518–532, doi:10.1016/j.jff.2016.02.006.
48. Custódio, L.; Patarra, J.; Alberício, F.; Neng, N.R.; Nogueira, J.M.F.; Romano, A. In Vitro Antioxidant and Inhibitory Activity of Water Decoctions of Carob Tree (Ceratonia Siliqua L.) on Cholinesterases, α-Amylase and α-Glucosidase. *Nat Prod Res* **2015**, *29*, 2155–2159, doi:10.1080/14786419.2014.996147.
49. Aboura, I.; Nani, A.; Belarbi, M.; Murtaza, B.; Fluckiger, A.; Dumont, A.; Benammar, C.; Tounsi, M.S.; Ghiringhelli, F.; Rialland, M.; et al. Protective Effects of Polyphenol-Rich Infusions from Carob (Ceratonia Siliqua) Leaves and Cladodes of Opuntia Ficus-Indica against Inflammation Associated with Diet-Induced Obesity and DSS-Induced Colitis in Swiss Mice. *Biomedicine and Pharmacotherapy* **2017**, *96*, 1022–1035, doi:10.1016/j.biopha.2017.11.125.
50. El Sayed, N.S.; Abidar, S.; Nhiri, M.; Hritcu, L.; Ibrahim, W.W. Aqueous Extract of Ceratonia Siliqua L. Leaves Elicits Antioxidant, Anti-Inflammatory, and AChE Inhibiting Effects in Amyloid-B42-Induced Cognitive Deficit Mice: Role of A7-NAChR in Modulating Jak2/PI3K/Akt/GSK-3β/β-Catenin Cascade. *Phytotherapy Research* **2023**, *37*, 2437–2453, doi:10.1002/ptr.7766.
51. Elbouzidi, A.; Taibi, M.; Ouassou, H.; Ouahhoud, S.; Ou-Yahia, D.; Loukili, E.H.; Aherkou, M.; Mansouri, F.; Bencheikh, N.; Laaraj, S.; et al. Exploring the Multi-Faceted Potential of Carob (Ceratonia Siliqua Var. Rahma) Leaves from Morocco: A Comprehensive Analysis of Polyphenols Profile, Antimicrobial Activity, Cytotoxicity against Breast Cancer Cell Lines, and Genotoxicity. *Pharmaceuticals* **2023**, *16*, doi:10.3390/ph16060840.
52. Deans, B.J.; Skierka, B.E.; Karagiannakis, B.W.; Vuong, D.; Lacey, E.; Smith, J.A.; Bissember, A.C. Siliquapyranone: A Tannic Acid Tetrahydropyran-2-One Isolated from the Leaves of Carob (Ceratonia Siliqua) by Pressurised Hot Water Extraction. *Aust J Chem* **2018**, *71*, 702–707, doi:10.1071/CH18265.
53. De Luca, M.; Tuberoso, C.I.G.; Pons, R.; García, M.T.; Morán, M. del C.; Martelli, G.; Vassallo, A.; Caddeo, C. Ceratonia Siliqua L. Pod Extract: From Phytochemical Characterization to Liposomal Formulation and Evaluation of Behaviour in Cells. *Antioxidants* **2023**, *12*, doi:10.3390/antiox12061209.
54. Cerrato, A.; Cannazza, G.; Capriotti, A.L.; Citti, C.; La Barbera, G.; Laganà, A.; Montone, C.M.; Piovesana, S.; Cavaliere, C. A New Software-Assisted Analytical

Workflow Based on High-Resolution Mass Spectrometry for the Systematic Study of Phenolic Compounds in Complex Matrices. *Talanta* **2020**, *209*, doi:10.1016/j.talanta.2019.120573.

55. Correia, P.J.; Pestana, M. Sugars and Phenols in Carob Tree Fruits from Different Producing Countries: A Short Review. *Heliyon* **2024**, *10*, doi: 10.1016/j.heliyon.2024.e30922.
56. Martić, N.; Zahorec, J.; Stilinović, N.; Andrejić-Višnjić, B.; Pavlić, B.; Kladar, N.; Šoronja-Simović, D.; Šereš, Z.; Vujčić, M.; Horvat, O.; et al. Hepatoprotective Effect of Carob Pulp Flour (Ceratonia Siliqua L.) Extract Obtained by Optimized Microwave-Assisted Extraction. *Pharmaceutics* **2022**, *14*, doi:10.3390/pharmaceutics14030657.
57. Ydjedd, S.; Bouriche, S.; López-Nicolás, R.; Sánchez-Moya, T.; Frontela-Saseta, C.; Ros-Berruezo, G.; Rezgui, F.; Louaileche, H.; Kati, D.E. Effect of in Vitro Gastrointestinal Digestion on Encapsulated and Nonencapsulated Phenolic Compounds of Carob (Ceratonia Siliqua L.) Pulp Extracts and Their Antioxidant Capacity. *J Agric Food Chem* **2017**, *65*, 827–835, doi:10.1021/acs.jafc.6b05103.
58. Wojdyło, A.; Nowicka, P. Profile of Phenolic Compounds of Prunus Armeniaca L. Leaf Extract Determined by LC-ESI-QTOF-MS/MS and Their Antioxidant, Anti-Diabetic, Anti-Cholinesterase, and Anti-Inflammatory Potency. *Antioxidants* **2021**, *10*, doi:10.3390/antiox10121869.
59. Rodríguez-Solana, R.; Coelho, N.; Santos-Rufo, A.; Gonçalves, S.; Pérez-Santín, E.; Romano, A. The Influence of in Vitro Gastrointestinal Digestion on the Chemical Composition and Antioxidant and Enzyme Inhibitory Capacities of Carob Liqueurs Obtained with Different Elaboration Techniques. *Antioxidants* **2019**, *8*, doi:10.3390/antiox8110563.
60. Zhu, J.; Chen, C.; Zhang, B.; Huang, Q. The Inhibitory Effects of Flavonoids on α-Amylase and α-Glucosidase. *Crit Rev Food Sci Nutr* **2020**, *60*, 695–708, doi: 10.1080/10408398.2018.1548428.
61. Smyrska-Wieleba, N.; Mroczek, T. Natural Inhibitors of Cholinesterases: Chemistry, Structure–Activity and Methods of Their Analysis. *Int J Mol Sci* **2023**, *24*, doi: 10.3390/ijms24032722.
62. Caesar, L.K.; Cech, N.B. Synergy and Antagonism in Natural Product Extracts: When 1 + 1 Does Not Equal 2. *Nat Prod Rep* **2019**, *36*, 869–888, doi: 10.1039/c9np00011a.
63. Serio, S.; Santoro, V.; Celano, R.; Fiore, D.; Proto, M.C.; Corbo, F.; Clodoveo, M.L.; Tardugno, R.; Piccinelli, A.L.; Rastrelli, L. Carob (Ceratonia Siliqua) Leaves: A Comprehensive Analysis of Bioactive Profile and Health-Promoting Potential of an Untapped Resource. *Food Chem* **2025**, *468*, doi:10.1016/j.foodchem.2024.142392.
64. Granato, D.; Zabetakis, I.; Koidis, A. Sustainability, Nutrition, and Scientific Advances of Functional Foods under the New EU and Global Legislation Initiatives. *J Funct Foods* **2023**, *109*, doi: 10.1016/j.biopha.2023.115155.

65. Amador-Luna, V.M.; Montero, L.; Herrero, M. Compressed Fluids for the Extraction of Bioactive Compounds from Plants, Food by-Products, Seaweeds and Microalgae – an Update from 2019 to 2023. *TrAC - Trends in Analytical Chemistry* **2023**, *169*, doi: 10.1016/j.trac.2023.117410.
66. Plaza, M.; Marina, M.L. Pressurized Hot Water Extraction of Bioactives. *TrAC - Trends in Analytical Chemistry* **2023**, *166*, doi: 10.1016/j.trac.2023.117201.
67. Putnik, P.; Lorenzo, J.M.; Barba, F.J.; Roohinejad, S.; Jambrak, A.R.; Granato, D.; Montesano, D.; Kovačević, D.B. Novel Food Processing and Extraction Technologies of High-Added Value Compounds from Plant Materials. *Foods* **2018**, *7*, doi: 10.3390/foods7070106.
68. Benedetti, B.; Caponigro, V.; Ardini, F. Experimental Design Step by Step: A Practical Guide for Beginners. *Crit Rev Anal Chem* **2020**, *52*, 1015–1028, doi: 10.1080/10408347.2020.1848517.
69. Pinto, D.; Vieira, E.F.; Peixoto, A.F.; Freire, C.; Freitas, V.; Costa, P.; Delerue-Matos, C.; Rodrigues, F. Optimizing the Extraction of Phenolic Antioxidants from Chestnut Shells by Subcritical Water Extraction Using Response Surface Methodology. *Food Chem* **2021**, *334*, doi:10.1016/j.foodchem.2020.127521.
70. García-Marino, M.; Rivas-Gonzalo, J.C.; Ibáñez, E.; García-Moreno, C. Recovery of Catechins and Proanthocyanidins from Winery By-Products Using Subcritical Water Extraction. In Proceedings of the Analytica Chimica Acta; March 23 **2005**; Vol. 563, pp. 44–50, doi: 10.1016/j.aca.2005.10.054.
71. Šafranko, S.; Ćorković, I.; Jerković, I.; Jakovljević, M.; Aladić, K.; Šubarić, D.; Jokić, S. Green Extraction Techniques for Obtaining Bioactive Compounds from Mandarin Peel (Citrus Unshiu Var. Kuno): Phytochemical Analysis and Process Optimization. *Foods* **2021**, *10*, doi:10.3390/foods10051043.
72. Rivera-Tovar, P.R.; Torres, M.D.; Camilo, C.; Mariotti-Celis, M.S.; Domínguez, H.; Pérez-Correa, J.R. Multi-Response Optimal Hot Pressurized Liquid Recovery of Extractable Polyphenols from Leaves of Maqui (Aristotelia Chilensis [Mol.] Stuntz). *Food Chem* **2021**, *357*, doi:10.1016/j.foodchem.2021.129729.
73. Vinatoru, M.; Mason, T.J.; Calinescu, I. Ultrasonically Assisted Extraction (UAE) and Microwave Assisted Extraction (MAE) of Functional Compounds from Plant Materials. *TrAC - Trends in Analytical Chemistry* **2017**, *97*, 159–178, doi: 10.1016/j.trac.2017.09.002.
74. Kumar, K.; Srivastav, S.; Sharanagat, V.S. Ultrasound Assisted Extraction (UAE) of Bioactive Compounds from Fruit and Vegetable Processing by-Products: A Review. *Ultrason Sonochem* **2021**, *70*, doi: 10.1016/j.ultsonch.2020.105325.
75. Rao, M.V.; Sengar, A.S.; C K, S.; Rawson, A. Ultrasonication - A Green Technology Extraction Technique for Spices: A Review. *Trends Food Sci Technol* **2021**, *116*, 975–991, doi: 10.1016/j.tifs.2021.09.006.

76. Yamada, K.; Shimada, T.; Nishimura, M.; Hara-Nishimura, I. A VPE Family Supporting Various Vacuolar Functions in Plants. *Physiol Plant* **2005**, *123*, 369–375, doi: 10.1111/j.1399-3054.2005.00464.x.
77. Ogino, H.; Ishikawa, H. *Enzymes Which Are Stable in the Presence of Organic Solvents*; **2001**; Vol. 91, doi: 10.1016/S1389-1723(01)80051-7.
78. Díaz-de-Cerio, E.; Tylewicz, U.; Verardo, V.; Fernández-Gutiérrez, A.; Segura-Carretero, A.; Romani, S. Design of Sonotrode Ultrasound-Assisted Extraction of Phenolic Compounds from Psidium Guajava L. Leaves. *Food Anal Methods* **2017**, *10*, 2781–2791, doi:10.1007/s12161-017-0836-z.
79. Azwanida NN A Review on the Extraction Methods Use in Medicinal Plants, Principle, Strength and Limitation. *Med Aromat Plants (Los Angel)* **2015**, *04*, doi:10.4172/2167-0412.1000196.
80. Jacotet-Navarro, M.; Rombaut, N.; Deslis, S.; Fabiano-Tixier, A.S.; Pierre, F.X.; Bily, A.; Chemat, F. Towards a “Dry” Bio-Refinery without Solvents or Added Water Using Microwaves and Ultrasound for Total Valorization of Fruit and Vegetable by-Products. *Green Chemistry* **2016**, *18*, 3106–3115, doi:10.1039/c5gc02542g.
81. Vernès, L.; Abert-Vian, M.; El Maâtaoui, M.; Tao, Y.; Bornard, I.; Chemat, F. Application of Ultrasound for Green Extraction of Proteins from Spirulina. Mechanism, Optimization, Modeling, and Industrial Prospects. *Ultrason Sonochem* **2019**, *54*, 48–60, doi:10.1016/j.ultsonch.2019.02.016.
82. Hirondart, M.; Rombaut, N.; Fabiano-Tixier, A.S.; Bily, A.; Chemat, F. Comparison between Pressurized Liquid Extraction and Conventional Soxhlet Extraction for Rosemary Antioxidants, Yield, Composition, and Environmental Footprint. *Foods* **2020**, *9*, doi:10.3390/foods9050584.
83. Granato, D.; Shahidi, F.; Wrolstad, R.; Kilmartin, P.; Melton, L.D.; Hidalgo, F.J.; Miyashita, K.; Camp, J. van; Alasalvar, C.; Ismail, A.B.; et al. Antioxidant Activity, Total Phenolics and Flavonoids Contents: Should We Ban in Vitro Screening Methods? *Food Chem* **2018**, *264*, 471–475, doi:10.1016/j.foodchem.2018.04.012.
84. Ahmad, F.; Leake, D.S. Antioxidants Inhibit Low Density Lipoprotein Oxidation Less at Lysosomal PH: A Possible Explanation as to Why the Clinical Trials of Antioxidants Might Have Failed. *Chem Phys Lipids* **2018**, *213*, 13–24, doi:10.1016/j.chemphyslip.2018.03.001.
85. M Davies, A.; G Holt, A. Why Antioxidant Therapies Have Failed in Clinical Trials. *J Theor Biol* **2018**, *457*, 1–5, doi:10.1016/j.jtbi.2018.08.014.
86. Granato, D. Next-Generation Analytical Platforms for Antioxidant Capacity Assessment: The Urge for Realistic and Physiologically Relevant Methods. *Biomedicine and Pharmacotherapy* **2023**, *165*, doi:10.1016/j.biopha.2023.115155.
87. Brodkorb, A.; Egger, L.; Alminger, M.; Alvito, P.; Assunção, R.; Ballance, S.; Bohn, T.; Bourlieu-Lacanal, C.; Boutrou, R.; Carrière, F.; et al. INFOGEST Static in Vitro

Simulation of Gastrointestinal Food Digestion. *Nat Protoc* **2019**, *14*, 991–1014, doi:10.1038/s41596-018-0119-1.

88. Gericke, B.; Amiri, M.; Naim, H.Y. The Multiple Roles of Sucrase-Isomaltase in the Intestinal Physiology. *Mol Cell Pediatr* **2016**, *3*, 1–6, doi: 10.1186/s40348-016-0033-y.
89. Ramirez-Bermudez, J. Alzheimer's Disease: Critical Notes on the History of a Medical Concept. *Arch Med Res* **2012**, *43*, 595–599, doi: 10.1007/s00204-017-2079-6.
90. Mohammadi, N.; Farrell, M.; O'Sullivan, L.; Langan, A.; Franchin, M.; Azevedo, L.; Granato, D. Effectiveness of Anthocyanin-Containing Foods and Nutraceuticals in Mitigating Oxidative Stress, Inflammation, and Cardiovascular Health-Related Biomarkers: A Systematic Review of Animal and Human Interventions. *Food Funct* **2024**, *15*, 3274–3299, doi:10.1039/d3fo04579j.
91. Cruz, T.M.; Lima, A. dos S.; Silva, A.O.; Mohammadi, N.; Zhang, L.; Azevedo, L.; Marques, M.B.; Granato, D. High-Throughput Synchronous Erythrocyte Cellular Antioxidant Activity and Protection Screening of Phenolic-Rich Extracts: Protocol Validation and Applications. *Food Chem* **2024**, *440*, doi:10.1016/j.foodchem.2023.138281.
92. Massaccesi, L.; Galliera, E.; Corsi Romanelli, M.M. Erythrocytes as Markers of Oxidative Stress Related Pathologies. *Mech Ageing Dev* **2020**, *191*, doi:10.1016/j.mad.2020.111333.
93. Cruz, T.M.; Lima, A. dos S.; Silva, A.O.; Mohammadi, N.; Zhang, L.; Azevedo, L.; Marques, M.B.; Granato, D. High-Throughput Synchronous Erythrocyte Cellular Antioxidant Activity and Protection Screening of Phenolic-Rich Extracts: Protocol Validation and Applications. *Food Chem* **2024**, *440*, 138281, doi:10.1016/j.foodchem.2023.138281.
94. Zhang, L.; Peng, C.Y.; Wang, P.X.; Xu, L.; Liu, J.H.; Xie, X.; Lu, L.; Tu, Z.C. Hypoglycemic and H2O2-Induced Oxidative Injury Protective Effects and the Phytochemical Profiles of the Ethyl Acetate Fraction from Radix Paeoniae Alba. *Front Nutr* **2023**, *10*, doi:10.3389/fnut.2023.1126359.
95. Aquino, R.P.; Mencherini, T.; Mazzei, P.; Esposito, T.; Prete, F. Del; Fortunato, F.; Pepe, G.; Auriemma, G.; Sansone, F. Spray Dried Inulin–Sodium Carboxymethylcellulose Microcarriers with Solid-to-Colloidal Transition: Development for Foliar Delivery of Polyphenol-Rich Extract. *Carbohydrate Polymer Technologies and Applications* **2025**, 101023, doi:10.1016/j.carpta.2025.101023.
96. Sansone, F.; Mencherini, T.; Picerno, P.; D'Amore, M.; Aquino, R.P.; Lauro, M.R. Maltodextrin/Pectin Microparticles by Spray Drying as Carrier for Nutraceutical Extracts. *J Food Eng* **2011**, *105*, 468–476, doi:10.1016/j.jfoodeng.2011.03.004.
97. Sansone, F.; Esposito, T.; Mencherini, T.; Del Prete, F.; Cannoniere, A.L.; Aquino, R.P. Exploring Microencapsulation Potential: Multicomponent Spray Dried Delivery Systems for Improvement of Chlorella Vulgaris Extract Preservation and Solubility. *Powder Technol* **2023**, *429*, doi:10.1016/j.powtec.2023.118882.

98. Zannini, M.; Cattivelli, A.; Nissen, L.; Conte, A.; Gianotti, A.; Tagliazucchi, D. Identification, Bioaccessibility, and Antioxidant Properties of Phenolic Compounds in Carob Syrup. *Foods* **2024**, *13*, doi:10.3390/foods13142196.
99. Goulas, V.; Georgiou, E. Utilization of Carob Fruit as Sources of Phenolic Compounds with Antioxidant Potential: Extraction Optimization and Application in Food Models. *Foods* **2020**, *9*, doi:10.3390/foods9010020.
100. Singh, B.; Mal, G.; Sharma, D.; Sharma, R.; Antony, C.P.; Kalra, R.S. Gastrointestinal Biotransformation of Phytochemicals: Towards Futuristic Dietary Therapeutics and Functional Foods. *Trends Food Sci Technol* **2020**, *106*, 64–77, doi: 10.1016/j.tifs.2020.09.022.
101. Barlow, S.; Chesson, A.; Collins, J.D.; Flynn, A.; Galli, C.L.; Hardy, A.; Jany, K.-D.; Jeger, M.-J.; Knaap, A.; Kuiper, H.; et al. SCIENTIFIC OPINION Guidance on Safety Assessment of Botanicals and Botanical Preparations ** Intended for Use as Ingredients in Food Supplements 1 EFSA Scientific Committee. *EFSA Journal* **2009**, *7*, 1249, doi:10.2093/j.efsa.2009.1249.
102. Haddock, E.A.; Gupta, R.K.; Al-Shafi, S.M.K.; Haslam, E.; Magnolato, D. The Metabolism of Gallic Acid and Hexahydroxydiphenic Acid in Plants. Part 1. Introduction. Naturally Occurring Galloyl Esters. *J Chem Soc Perkin 1* **1982**, 2515–2524, doi:10.1039/P19820002515.
103. Wolfe, K.L.; Rui, H.L. Cellular Antioxidant Activity (CAA) Assay for Assessing Antioxidants, Foods, and Dietary Supplements. *J Agric Food Chem* **2007**, *55*, 8896–8907, doi:10.1021/jf0715166.
104. Docimo, T.; Celano, R.; Lambiase, A.; Di Sanzo, R.; Serio, S.; Santoro, V.; Coccetti, P.; Russo, M.; Rastrelli, L.; Piccinelli, A.L. Exploring Influence of Production Area and Harvest Time on Specialized Metabolite Content of Glycyrrhiza Glabra Leaves and Evaluation of Antioxidant and Anti-Aging Properties. *Antioxidants* **2024**, *13*, doi:10.3390/antiox13010093.
105. Karkanis, A.; Martins, N.; Petropoulos, S.A.; Ferreira, I.C.F.R. Phytochemical Composition, Health Effects, and Crop Management of Liquorice (Glycyrrhiza Glabra L.): A Medicinal Plant. *Food Reviews International* **2018**, *34*, 182–203, doi: 10.1080/87559129.2016.1261300.
106. Pastorino, G.; Cornara, L.; Soares, S.; Rodrigues, F.; Oliveira, M.B.P.P. Liquorice (Glycyrrhiza Glabra): A Phytochemical and Pharmacological Review. *Phytotherapy Research* **2018**, *32*, 2323–2339, doi: 10.1002/ptr.6178.
107. Ceccuzzi, G.; Rapino, A.; Perna, B.; Costanzini, A.; Farinelli, A.; Fiorica, I.; Marziani, B.; Cianci, A.; Rossin, F.; Cesaro, A.E.; et al. Liquorice Toxicity: A Comprehensive Narrative Review. *Nutrients* **2023**, *15*, doi: 10.3390/nu15183866.
108. Russo, M.; Serra, D.; Suraci, F.; Di Sanzo, R.; Fuda, S.; Postorino, S. The Potential of E-Nose Aroma Profiling for Identifying the Geographical Origin of Licorice (Glycyrrhiza

Glabra L.) Roots. *Food Chem* **2014**, *165*, 467–474, doi:10.1016/j.foodchem.2014.05.142.

109. Official Journal of the European Union *Commision Implementing Regulation (EU) No 1072/2011*; **2011**;
110. Celano, R.; Docimo, T.; Piccinelli, A.L.; Rizzo, S.; Campone, L.; Di Sanzo, R.; Carabetta, S.; Rastrelli, L.; Russo, M. Specialized Metabolite Profiling of Different Glycyrrhiza Glabra Organs by Untargeted UHPLC-HRMS. *Ind Crops Prod* **2021**, *170*, doi:10.1016/j.indcrop.2021.113688.
111. Siracusa, L.; Saija, A.; Cristani, M.; Cimino, F.; D'Arrigo, M.; Trombetta, D.; Rao, F.; Ruberto, G. Phytocomplexes from Liquorice (Glycyrrhiza Glabra L.) Leaves - Chemical Characterization and Evaluation of Their Antioxidant, Anti-Genotoxic and Anti-Inflammatory Activity. *Fitoterapia* **2011**, *82*, 546–556, doi:10.1016/j.fitote.2011.01.009.
112. Fan, Y.H.; Ye, R.; Xu, H.Y.; Feng, X.H.; Ma, C.M. Structures and In Vitro Antihepatic Fibrosis Activities of Prenylated Dihydrostilbenes and Flavonoids from Glycyrrhiza Uralensis Leaves. *J Food Sci* **2019**, *84*, 1224–1230, doi:10.1111/1750-3841.14592.
113. Ye, R.; Fan, Y.H.; Ma, C.M. Identification and Enrichment of α-Glucosidase-Inhibiting Dihydrostilbene and Flavonoids from Glycyrrhiza Uralensis Leaves. *J Agric Food Chem* **2017**, *65*, 510–515, doi:10.1021/acs.jafc.6b04155.
114. Qamar, S.; Torres, Y.J.M.; Parekh, H.S.; Robert Falconer, J. Extraction of Medicinal Cannabinoids through Supercritical Carbon Dioxide Technologies: A Review. *J Chromatogr B Analyt Technol Biomed Life Sci* **2021**, *1167*, doi: 10.3390/nu15183866.
115. Chen, X.; Mukwaya, E.; Wong, M.S.; Zhang, Y. A Systematic Review on Biological Activities of Prenylated Flavonoids. *Pharm Biol* **2014**, *52*, 655–660, doi: 10.3109/13880209.2013.853809.
116. Chang, S.K.; Jiang, Y.; Yang, B. An Update of Prenylated Phenolics: Food Sources, Chemistry and Health Benefits. *Trends Food Sci Technol* **2021**, *108*, 197–213, doi: 10.1016/j.tifs.2020.12.022.
117. Wen, L.; Zhou, T.; Jiang, Y.; Gong, L.; Yang, B. Identification of Prenylated Phenolics in Mulberry Leaf and Their Neuroprotective Activity. *Phytomedicine* **2021**, *90*, doi:10.1016/j.phymed.2021.153641.
118. Jo, Y.H.; Lee, S.; Yeon, S.W.; Turk, A.; Lee, J.H.; Hong, S.M.; Han, Y.K.; Lee, K.Y.; Hwang, B.Y.; Kim, S.Y.; et al. Anti-Diabetic Potential of Masclura Tricuspidata Leaves: Prenylated Isoflavonoids with α-Glucosidase Inhibitory and Anti-Glycation Activity. *Bioorg Chem* **2021**, *114*, doi:10.1016/j.bioorg.2021.105098.
119. Song, Y.H.; Cai, H.; Gu, N.; Qian, C.F.; Cao, S.P.; Zhao, Z.M. Icariin Attenuates Cardiac Remodelling through Down-Regulating Myocardial Apoptosis and Matrix Metalloproteinase Activity in Rats with Congestive Heart Failure. *Journal of Pharmacy and Pharmacology* **2011**, *63*, 541–549, doi:10.1111/j.2042-7158.2010.01241.x.
120. Dodel, R.; Csoti, I.; Ebersbach, G.; Fuchs, G.; Hahne, M.; Kuhn, W.; Oechsner, M.; Jost, W.; Reichmann, H.; Schulz, J.B. Lewy Body Dementia and Parkinson's Disease

with Dementia. In Proceedings of the Journal of Neurology; September **2008**; Vol. 255, pp. 39–47, doi: 10.1007/s00415-008-5007-0.

121. Lázaro, D.F.; Pavlou, M.A.S.; Outeiro, T.F. Cellular Models as Tools for the Study of the Role of Alpha-Synuclein in Parkinson's Disease. *Exp Neurol* 2017, *298*, 162–171, doi: 10.1016/j.expneurol.2017.05.007.
122. Tripodi Farida Protective Effect of Vigna Unguiculata Extract against Aging and Neurodegeneration. *Aging* **2020**, doi: 10.18632/aging.104069.
123. Tripodi, F.; Falletta, E.; Leri, M.; Angeloni, C.; Beghelli, D.; Giusti, L.; Milanesi, R.; Sampaio-Marques, B.; Ludovico, P.; Goppa, L.; et al. Anti-Aging and Neuroprotective Properties of Grifola Frondosa and Hericium Erinaceus Extracts. *Nutrients* **2022**, *14*, doi:10.3390/nu14204368.
124. Cheel, J.; Tůmová, L.; Areche, C.; van Antwerpen, P.; Nève, J.; Zouaoui-Boudjeltia, K.; San Martin, A.; Vokřál, I.; Wsól, V.; Neugebauerová, J. Variations in the Chemical Profile and Biological Activities of Licorice (Glycyrrhiza Glabra L.), as Influenced by Harvest Times. *Acta Physiol Plant* **2013**, *35*, 1337–1349, doi:10.1007/s11738-012-1174-9.
125. Ju, Y.; Wang, Y.; Ma, L.; Kang, L.; Liu, H.; Ma, X.; Zhao, D. Comparative Analysis of Polyphenols in Lycium Barbarum Fruits Using UPLC-IM-QTOF-MS. *Molecules* **2023**, *28*, doi:10.3390/molecules28134930.
126. Agati, G.; Brunetti, C.; Fini, A.; Gori, A.; Guidi, L.; Landi, M.; Sebastiani, F.; Tattini, M. Are Flavonoids Effective Antioxidants in Plants? Twenty Years of Our Investigation. *Antioxidants* **2020**, *9*, 1–17, doi: 10.3390/antiox9111098.
127. Li, W.; Zhang, H.; Li, X.; Zhang, F.; Liu, C.; Du, Y.; Gao, X.; Zhang, Z.; Zhang, X.; Hou, Z.; et al. Intergrative Metabolomic and Transcriptomic Analyses Unveil Nutrient Remobilization Events in Leaf Senescence of Tobacco. *Sci Rep* **2017**, *7*, doi:10.1038/s41598-017-11615-0.
128. Chang, H.; Chen, P.; Ma, M. Feeding Preference of Altica Deserticola for Leaves of Glycyrrhiza Glabra and G. Uralensis and Its Mechanism. *Sci Rep* **2020**, *10*, doi:10.1038/s41598-020-58537-y.
129. Frattaruolo, L.; Carullo, G.; Brindisi, M.; Mazzotta, S.; Bellissimo, L.; Rago, V.; Curcio, R.; Dolce, V.; Aiello, F.; Cappello, A.R. Antioxidant and Anti-Inflammatory Activities of Flavanones from Glycyrrhiza Glabra L. (Licorice) Leaf Phytocomplexes: Identification of Licoflavanone as a Modulator of NF-KB/MAPK Pathway. *Antioxidants* **2019**, *8*, doi:10.3390/antiox8060186.
130. Diaz Napal, G.N.; Palacios, S.M. Bioinsecticidal Effect of the Flavonoids Pinocembrin and Quercetin against Spodoptera Frugiperda. *J Pest Sci (2004)* **2015**, *88*, 629–635, doi:10.1007/s10340-014-0641-z.
131. Rasul, A.; Millimouno, F.M.; Ali Eltayb, W.; Ali, M.; Li, J.; Li, X. Pinocembrin: A Novel Natural Compound with Versatile Pharmacological and Biological Activities. *Biomed Res Int* **2013**, *2013*, doi:10.1155/2013/379850.

132. Hanawa, F.; Yamada, T.; Nakashima, T. *Phytoalexins from Pinus Strobus Bark Infected with Pinewood Nematode, Bursaphelenchus Xylophilus*; **2001**, doi: 10.1016/s0031-9422(00)00514-8.
133. Hermann, S.; Orlik, M.; Boevink, P.; Stein, E.; Scherf, A.; Kleeberg, I.; Schmitt, A.; Schikora, A. Biocontrol of Plant Diseases Using Glycyrrhiza Glabra Leaf Extract. *Plant Dis* **2022**, *106*, 3133–3144, doi:10.1094/PDIS-12-21-2813-RE.
134. Wang, P.; Chen, S.; Gu, M.; Chen, X.; Chen, X.; Yang, J.; Zhao, F.; Ye, N. Exploration of the Effects of Different Blue Led Light Intensities on Flavonoid and Lipid Metabolism in Tea Plants via Transcriptomics and Metabolomics. *Int J Mol Sci* **2020**, *21*, 1–18, doi:10.3390/ijms21134606.
135. Cornara, L.; Sgrò, F.; Raimondo, F.M.; Ingegneri, M.; Mastracci, L.; D'Angelo, V.; Germanò, M.P.; Trombetta, D.; Smeriglio, A. Pedoclimatic Conditions Influence the Morphological, Phytochemical and Biological Features of Mentha Pulegium L. *Plants* **2022**, *12*, doi:10.3390/plants12010024.
136. Rizzato, G.; Scalabrin, E.; Radaelli, M.; Capodaglio, G.; Piccolo, O. A New Exploration of Licorice Metabolome. *Food Chem* **2017**, *221*, 959–968, doi:10.1016/j.foodchem.2016.11.068.
137. Song, W.; Qiao, X.; Chen, K.; Wang, Y.; Ji, S.; Feng, J.; Li, K.; Lin, Y.; Ye, M. Biosynthesis-Based Quantitative Analysis of 151 Secondary Metabolites of Licorice to Differentiate Medicinal Glycyrrhiza Species and Their Hybrids. *Anal Chem* **2017**, *89*, 3146–3153, doi:10.1021/acs.analchem.6b04919.
138. Van der Putten, W.H.; Bardgett, R.D.; Bever, J.D.; Bezemer, T.M.; Casper, B.B.; Fukami, T.; Kardol, P.; Klironomos, J.N.; Kulmatiski, A.; Schweitzer, J.A.; et al. Plant-Soil Feedbacks: The Past, the Present and Future Challenges. *Journal of Ecology* **2013**, *101*, 265–276, doi:10.1111/1365-2745.12054.
139. Calabresi, P.; Mechelli, A.; Natale, G.; Volpicelli-Daley, L.; Di Lazzaro, G.; Ghiglieri, V. Alpha-Synuclein in Parkinson's Disease and Other Synucleinopathies: From Overt Neurodegeneration Back to Early Synaptic Dysfunction. *Cell Death Dis* **2023**, *14*, doi: 10.1038/s41419-023-05672-9.
140. Tripodi, F.; Lambiase, A.; Moukham, H.; Spandri, G.; Brioschi, M.; Falletta, E.; D'Urzo, A.; Vai, M.; Abbiati, F.; Pagliari, S.; et al. Targeting Protein Aggregation Using a Cocoa-Bean Shell Extract to Reduce α-Synuclein Toxicity in Models of Parkinson's Disease. *Curr Res Food Sci* **2024**, *9*, doi:10.1016/j.crfs.2024.100888.
141. Oliveira, L.M.A.; Gasser, T.; Edwards, R.; Zweckstetter, M.; Melki, R.; Stefanis, L.; Lashuel, H.A.; Sulzer, D.; Vekrellis, K.; Halliday, G.M.; et al. Alpha-Synuclein Research: Defining Strategic Moves in the Battle against Parkinson's Disease. *NPJ Parkinsons Dis* **2021**, *7*, doi: 10.1038/s41531-021-00203-9.
142. Fruhmann, G.; Seynnaeve, D.; Zheng, J.; Ven, K.; Molenberghs, S.; Wilms, T.; Liu, B.; Winderickx, J.; Franssens, V. Yeast Buddies Helping to Unravel the Complexity of

Neurodegenerative Disorders. *Mech Ageing Dev* **2017**, *161*, 288–305, doi: 10.1016/j.mad.2016.05.002.

143. Tenreiro, S.; Franssens, V.; Winderickx, J.; Outeiro, T.F. Yeast Models of Parkinson's Disease-Associated Molecular Pathologies. *Curr Opin Genet Dev* **2017**, *44*, 74–83, doi: 10.1016/j.gde.2017.01.013.
144. Biondi, D.M.; Rocco, C.; Ruberto, G. Dihydrostilbene Derivatives from Glycyrrhiza Glabra Leaves. *J Nat Prod* **2005**, *68*, 1099–1102, doi:10.1021/np050034q.
145. Biondi, D.M.; Rocco, C.; Ruberto, G. New Dihydrostilbene Derivatives from the Leaves of Glycyrrhiza Glabra and Evaluation of Their Antioxidant Activity. *J Nat Prod* **2003**, *66*, 477–480, doi:10.1021/np020365s.
146. Trombetta, D.; Giofrè, S. V; Tomaino, A.; Raciti, R.; Saija, A.; Cristani, M.; Romeo, R.; Siracusa, L.; Ruberto, G. *Selective COX-2 Inhibitory Properties of Dihydrostilbenes from Liquorice Leaves-In Vitro Assays and Structure/Activity Relationship Study*; **2014**, 1761-4.
147. Van Den Eeden, S.K.; Tanner, C.M.; Bernstein, A.L.; Fross, R.D.; Leimpeter, A.; Bloch, D.A.; Nelson, L.M. Incidence of Parkinson's Disease: Variation by Age, Gender, and Race/Ethnicity. *Am J Epidemiol* **2002**, *157*, 1015–1022, doi:10.1093/aje/kwg068.
148. Sampaio-Marques, B.; Burhans, W.C.; Ludovico, P. Yeast at the Forefront of Research on Ageing and Age-Related Diseases. In *Progress in Molecular and Subcellular Biology*; Springer Science and Business Media Deutschland GmbH, **2019**; Vol. 58, pp. 217–242, doi: 10.1007/978-3-030-13035-0_9.
149. Sampaio-Marques, B.; Guedes, A.; Vasilevskiy, I.; Gonçalves, S.; Outeiro, T.F.; Winderickx, J.; Burhans, W.C.; Ludovico, P. α-Synuclein Toxicity in Yeast and Human Cells Is Caused by Cell Cycle Re-Entry and Autophagy Degradation of Ribonucleotide Reductase 1. *Aging Cell* **2019**, *18*, doi:10.1111/acel.12922.
150. Yazaki, K.; Sasaki, K.; Tsurumaru, Y. Prenylation of Aromatic Compounds, a Key Diversification of Plant Secondary Metabolites. *Phytochemistry* **2009**, *70*, 1739–1745, doi: 10.1016/j.phytochem.2009.08.023.
151. Gallego, R.; Bueno, M.; Herrero, M. Sub- and Supercritical Fluid Extraction of Bioactive Compounds from Plants, Food-by-Products, Seaweeds and Microalgae – An Update. *TrAC - Trends in Analytical Chemistry* **2019**, *116*, 198–213, doi: 10.1016/j.trac.2019.04.030
152. Herrero, M.; Castro-Puyana, M.; Mendiola, J.A.; Ibañez, E. Compressed Fluids for the Extraction of Bioactive Compounds. *TrAC - Trends in Analytical Chemistry* **2013**, *43*, 67–83, doi: 10.1016/j.trac.2012.12.008.
153. Majdi, S.; Barzegar, M.; Jabbari, A.; Aghaalikhani, M. *Supercritical Fluid Extraction of Tobacco Seed Oil and Its Comparison with Solvent Extraction Methods*; **2012**; Vol. 14.
154. Akanda, M.J.H.; Sarker, M.Z.I.; Ferdosh, S.; Manap, M.Y.A.; Rahman, N.N.N.A.; Kadir, M.O.A. Applications of Supercritical Fluid Extraction (SFE) of Palm Oil and Oil from Natural Sources. *Molecules* **2012**, *17*, 1764–1794, doi: 10.3390/molecules17021764.

155. Gilbert-López, B.; Mendiola, J.A.; van den Broek, L.A.M.; Houweling-Tan, B.; Sijtsma, L.; Cifuentes, A.; Herrero, M.; Ibáñez, E. Green Compressed Fluid Technologies for Downstream Processing of Scenedesmus Obliquus in a Biorefinery Approach. *Algal Res* **2017**, *24*, 111–121, doi:10.1016/j.algal.2017.03.011.

156. Pinto, M.B.C.; Vardanega, R.; Náthia-Neves, G.; de França, P.R.L.; Kurozawa, L.E.; Meireles, M.A.A.; Schmidt, F.L. Novel Brazilian Hop (Humulus Lupulus L.) Extracts through Supercritical CO2 Extraction: Enhancing Hop Processing for Greater Sustainability. *Food Research International* **2023**, *172*, doi:10.1016/j.foodres.2023.113169.

157. Guan, W.; Li, S.; Yan, R.; Tang, S.; Quan, C. Comparison of Essential Oils of Clove Buds Extracted with Supercritical Carbon Dioxide and Other Three Traditional Extraction Methods. *Food Chem* **2007**, *101*, 1558–1564, doi:10.1016/j.foodchem.2006.04.009.

158. Kassama, L.S.; Shi, J.; Mittal, G.S. Optimization of Supercritical Fluid Extraction of Lycopene from Tomato Skin with Central Composite Rotatable Design Model. *Sep Purif Technol* **2008**, *60*, 278–284, doi:10.1016/j.seppur.2007.09.005.

159. Ivanovic, J.; Ristic, M.; Skala, D. Supercritical CO2 Extraction of Helichrysum Italicum: Influence of CO2 Density and Moisture Content of Plant Material. *Journal of Supercritical Fluids* **2011**, *57*, 129–136, doi:10.1016/j.supflu.2011.02.013.

160. Sánchez-Camargo, A. del P.; Pleite, N.; Mendiola, J.A.; Cifuentes, A.; Herrero, M.; Gilbert-López, B.; Ibáñez, E. Development of Green Extraction Processes for Nannochloropsis Gaditana Biomass Valorization. *Electrophoresis* **2018**, *39*, 1875–1883, doi:10.1002/elps.201800122.

161. Rovetto, L.J.; Aieta, N. V. Supercritical Carbon Dioxide Extraction of Cannabinoids from Cannabis Sativa L. *Journal of Supercritical Fluids* **2017**, *129*, 16–27, doi:10.1016/j.supflu.2017.03.014.

162. Cheah, E.L.C.; Heng, P.W.S.; Chan, L.W. Optimization of Supercritical Fluid Extraction and Pressurized Liquid Extraction of Active Principles from Magnolia Officinalis Using the Taguchi Design. *Sep Purif Technol* **2010**, *71*, 293–301, doi:10.1016/j.seppur.2009.12.009.

163. Gallo-Molina, A.C.; Castro-Vargas, H.I.; Garzón-Méndez, W.F.; Martínez Ramírez, J.A.; Rivera Monroy, Z.J.; King, J.W.; Parada-Alfonso, F. Extraction, Isolation and Purification of Tetrahydrocannabinol from the Cannabis Sativa L. Plant Using Supercritical Fluid Extraction and Solid Phase Extraction. *Journal of Supercritical Fluids* **2019**, *146*, 208–216, doi:10.1016/j.supflu.2019.01.020.

164. Bimakr, M.; Rahman, R.A.; Taip, F.S.; Ganjloo, A.; Salleh, L.M.; Selamat, J.; Hamid, A.; Zaidul, I.S.M. Comparison of Different Extraction Methods for the Extraction of Major Bioactive Flavonoid Compounds from Spearmint (Mentha Spicata L.) Leaves. *Food and Bioproducts Processing* **2011**, *89*, 67–72, doi:10.1016/j.fbp.2010.03.002.

165. Marcus, Y. Solubility Parameter of Carbon Dioxide-an Enigma. *ACS Omega* **2018**, *3*, 524–528, doi:10.1021/acsomega.7b01665.
166. Barton, A.F.M.. *CRC Handbook of Solubility Parameters and Other Cohesion Parameters : Second Edition*; Taylor and Francis, **2017**; ISBN 0849301769.
167. Prat, D.; Wells, A.; Hayler, J.; Sneddon, H.; McElroy, C.R.; Abou-Shehada, S.; Dunn, P.J. CHEM21 Selection Guide of Classical- and Less Classical-Solvents. *Green Chemistry* **2016**, *18*, 288–296, doi:10.1039/c5gc01008j.
168. Piccinelli, A.L.; Mesa, M.G.; Armenteros, D.M.; Alfonso, M.A.; Arevalo, A.C.; Campone, L.; Rastrelli, L. HPLC-PDA-MS and NMR Characterization of C-Glycosyl Flavones in a Hydroalcoholic Extract of Citrus Aurantifolia Leaves with Antiplatelet Activity. *J Agric Food Chem* **2008**, *56*, 1574–1581, doi:10.1021/jf073485k.

Sitography

S1:https://www.un.org/sustainabledevelopment/news/communications-material/

S2: https://www.actaplantarum.org/

S3: https://www.who.int/publications/b/74273

S4:https://rivistafrutticoltura.edagricole.it/featured/avocado-carrubo-ficodindia-al-posto-dellolivo-nelle-aree-colpite-da-xylella/

S5:https://webbook.nist.gov/cgi/fluid.cgi?TUnit=C&PUnit=bar&DUnit=mol%2Fl&HUnit=kJ%2Fmol&WUnit=m%2Fs&VisUnit=uPa*s&STUnit=N%2Fm&Type=IsoTherm&RefState=DEF&Action=Page&ID=C124389

Scientific contributions

Full papers

Docimo, T., Celano, R., Lambiase, A., Di Sanzo, R., Serio, S., Santoro, V., & Piccinelli, A.L. Exploring Influence of Production Area and Harvest Time on Specialized Metabolite Content of Glycyrrhiza glabra Leaves and Evaluation of Antioxidant and Anti-Aging Properties. *Antioxidants* (2024). https://doi.org/10.3390/antiox13010093

Serio, S., Santoro, V., Celano, R., Fiore, D., Proto, M.P., Corbo, F., Clodoveo, M.L., Tardugno, R., Piccinelli, A.L., Rastrelli, L.. Carob (Ceratonia siliqua) leaves: A comprehensive analysis of bioactive profile and health-promoting potential of an untapped resource. *Food Chemistry* (2025). https://doi.org/10.1016/j.foodchem.2024.142392

Serio, S., Santoro, V., Piccinelli, A.L., Celano, R., and Rastrelli, L. Advanced extraction techniques for sustainable recovery of health-promoting compound from Carob leaves. *Ultrasonics Sonochemistry* (2026). https://doi.org/10.1016/j.ultsonch.2025.107710

Poster presentation

Celano R., Docimo T., Serio S., Carabetta S., Di Sanzo R., Russo M., Piccinelli A.L., Rastrelli L., Metabolic plasticity in Glycyrrhiza glabra leaves shapes development and environment. 13th National Congress on Food Chemistry, Messina (TP), Italy, May 29-31, 2023.

Rizzo S., Celano R., Serio S., Santoro V., Russo M.T., Rastrelli L., Piccinelli A.L., Target screening method for the quantitative determination of 118 pyrrolizidine alkaloids in food supplements, herbal infusions, honey, and teas by liquid chromatography coupled to quadrupole Orbitrap mass spectrometry. 13th National Congress on Food Chemistry, Messina (TP), Italy, May 29-31, 2023.

Serio S., Santoro, V., Celano R., Piccinelli A.L., Rastrelli L., Bioactivity screening of Italian flora plants by high throughput in vitro assay: evaluation of potential biological activities for the treatment of non-communicable diseases. National Biodiversity Forum, Palermo (PA), Italy, May 20-21, 2024.

Serio, S., Santoro, V., Celano, R., Piccinelli, A.L., Rastrelli, L. Green vs. Conventional Extraction: Toward Sustainable Bioactive Recovery. National Biodiversity Forum, Milano (MI), Italy, May 19-21, 2025.

Serio, S., Santoro, V., Celano, R., Piccinelli, A.L., Rastrelli, L. Optimization of green extraction techniques of Ceratonia siliqua leaves compounds. 73rd International Congress and Annual meeting of the Society for Medicinal Plant and Natural Product Research (GA), Napoli (NA), Italy, August 31- September 3, 2025.

Oral presentations

Serio S., Santoro V., Celano R., Tardugno R., Corbo F., Clodoveo M.L., Rastrelli L., Piccinelli A.L., Ceratonia siliqua L. leaves: an unexplored source of bioactive compounds. 30th Peruvian congress of chemistry and the 30th SILAE, Lima, Perú, October 16-20, 2023.

Serio, S., Santoro, V., Celano, R., Piccinelli, A.L., Rastrelli, L. Enhancing green extraction strategies of Ceratonia siliqua leaves compounds. 13th National Congress on Food Chemistry, Milano (MI), Italy, July 9-11, 2025.

Partecipation in courses and schools

27th mass spectrometry course, Pontignano (SI), Italy, March 13-17,2023.

School of metabolomics in natural product research- from biomarker discovery to deep metabolome analysis targeted isolation of bioactive compounds, Catania, Italy, September 21-22, 2023.